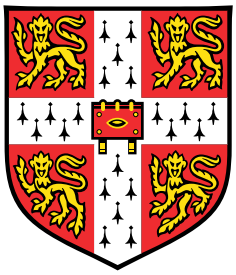

Multifield inflation in random potentials and the rapid-turn limit

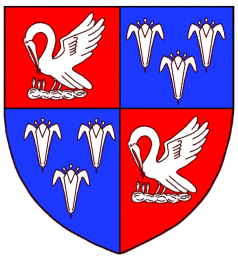

Theodor Björkmo

Department of Applied Mathematics and Theoretical Physics
University of Cambridge

This dissertation is submitted for the degree of
Doctor of Philosophy

Corpus Christi College September 2019

Declaration

I hereby declare that except where specific reference is made to the work of others, the contents of this dissertation are original and have not been submitted in whole or in part for consideration for any other degree or qualification in this, or any other university. This dissertation is my own work and contains nothing which is the outcome of work done in collaboration with others, except as specified in the text and Acknowledgements. This dissertation contains fewer than 65,000 words including appendices, bibliography, footnotes, tables and equations and has fewer than 150 figures.

Theodor Björkmo
September 2019

Abstract

Multifield inflation in random potentials and the rapid-turn limit

Theodor Björkmo

Cosmological inflation is a simple, and observationally well-supported, mechanism for generating a flat, spatially homogeneous universe with the statistical correlations in the cosmic microwave background we see today. Determining precisely how inflation happened, and how many fields were involved, are some of the main challenges of modern cosmology.

The first part of the thesis, consisting of Chapters 2 and 3, addresses this question by looking at what future measurements of local non-Gaussianity will tell us. Local non-Gaussianity has been proposed as a key observable for distinguishing between single- and multifield inflation, as a large value of this parameter would rule out the former. However, a small value would not necessarily rule out the latter. Using a new technique for generating random functions with Gaussian random fields, which we also prove the validity of, we generate random potentials for as many as 100 fields for inflation. We look at the observables of these models and in particular compute the local non-Gaussianity. An overwhelming majority of these models give local non-Gaussianity compatible with single-field inflation, despite significant multifield effects on superhorizon scales, indicating that this observable may not be sufficient to distinguish between these types of models.

The second part of the thesis, consisting of Chapters 4 and 5, addresses another aspect of this question by looking at other types of inflationary solutions than slow-roll, slow-turn. Slow-roll, slow-turn is an easily realised solution, but requires a very flat potential over large distances in field-space. The fine-tuning needed for this remains an Achilles heel of the inflationary paradigm. However, there are inflationary solutions which can be realised in steep potentials. 'Hyperinflation' is a particularly interesting one of these, and we investigate this solution in detail. Using the techniques developed to study hyperinflation, we then show that there exists a new, completely general two-field attractor solution that is characterised by rapidly turning fields. This 'rapid-turn attractor' does not require any particular background geometry, and explains how several recently studied two-field inflation models are related to each other.

Acknowledgements

I would like to acknowledge my supervisors, Dr. David Marsh and Professor Anne-Christine Davis, for their advice, guidance, and support throughout the completion of this degree. Chapters 2, 3, and 4 are based on work done in collaboration with David Marsh, published in [39–41]. Chapter 5 is based both on work undertaken alone, published in [37], and work done in collaboration with David Marsh and Ricardo Zambujal Ferreira [38].

I would also like to thank my family and friends for their unwavering support through these years as a graduate student. In particular my parents Malin and Ola, my brother Ulrik, Bogdan, Shayan, and Tegan deserve thanks (more than can be adequately described in an acknowledgements section) for all the help and moral support they provided over the last few years.

Table of contents

List of figures **xiii**

1 Introduction **1**
1.1 Inflation . . . 3
1.1.1 FRW cosmology . . . 4
1.1.2 Scalar fields in FRW space-times . . . 6
1.1.3 Slow-roll inflation . . . 7
1.1.4 Rapid-turn inflation . . . 9
1.2 Inflationary perturbation theory . . . 10
1.2.1 Field perturbations and vielbeins . . . 12
1.2.2 Quantisation and primordial perturbations . . . 13
1.2.3 Observables in multifield inflation . . . 15
1.3 Inflation and high-energy physics . . . 18

2 Inflation in Gaussian random field potentials **21**
2.1 Introduction . . . 21
2.2 Gaussian random fields for inflation . . . 25
2.2.1 High-dimensional GRFs as random multifield scalar potentials . 26
2.2.2 A new, efficient, local construction of GRFs . . . 29
2.2.3 Physical properties of GRF potentials . . . 32
2.2.4 The statistical ensembles of models . . . 40
2.2.5 Method: background . . . 43
2.2.6 Method: perturbations . . . 43
2.3 Result I: Planck compatibility is not rare, but future experiments may rule out this class of models . . . 47
2.3.1 Background evolution in GRF inflation . . . 48
2.3.2 Smooth and simple power spectra from complex inflationary models 52
2.3.3 Distributions of n_s and α_s . . . 54

2.3.4 Substantial superhorizon evolution, but also decaying isocurvature 59
2.4 Result II: At large $N_{\rm f}$, GRF and RMT models largely agree 62
2.4.1 Comparison of DBM and GRF potentials 63
2.4.2 Comparison of DBM and GRF predictions 65
2.5 Result III: $f_{\rm NL} \sim \mathcal{O}(1)$ is very rare in manyfield inflation 68
2.5.1 Why so small? 71
2.6 Conclusions 72

3 Gaussian random fields 75
3.1 Introduction 75
3.2 A new method for generating realisations of a GRF 77
3.2.1 Motivational example 79
3.2.2 All orders proof 81
3.2.3 Summary 88
3.3 Applications 89
3.3.1 Random, high-dimensional potential energy landscapes 89
3.3.2 Model selection for Gaussian process regression 90
3.4 Conclusions 93

4 Hyperinflation 95
4.1 Introduction 95
4.2 Hyperbolic geometry and hyperinflation 97
4.2.1 Hyperinflation 98
4.3 Generalising hyperinflation 100
4.3.1 Two-field covariant formulation 101
4.3.2 Generalised hyperinflation 102
4.3.3 Hyperinflation in random potentials 105
4.3.4 Multifield generalisation 105
4.4 Linear stability 107
4.4.1 The two-field case 107
4.4.2 Perturbations in the general multifield case 109
4.5 Examples 109
4.5.1 Example 1: hyperinflation in the Poincare patch 110
4.5.2 Examples 2 & 3: the non-symmetric hyperinflation attractor and 'geometric destabilisation' 110
4.5.3 Example 4: small-field hyperinflation 112
4.5.4 Example 5: multifield hyperinflation 114

4.6 Hyperinflation and the swampland . . . 115
4.6.1 Hyperinflation and the weak gravity conjecture . . . 115
4.6.2 Observational predictions for generalised hyperinflation . . . 116
4.6.3 Small-field hyperinflation in steep potentials and reheating . . . 117
4.7 Conclusions . . . 119

5 The rapid-turn attractor 121
5.1 Introduction . . . 121
5.2 Rapid-turn inflation . . . 122
5.2.1 Finding the attractor solution . . . 123
5.2.2 Perturbations and stability . . . 125
5.2.3 Rapid-turn inflation and the swampland . . . 126
5.3 Examples of rapid-turn attractors . . . 127
5.3.1 Hyperinflation . . . 128
5.3.2 A flat field-space model . . . 128
5.3.3 Side-tracked inflation . . . 129
5.3.4 Angular inflation . . . 130
5.4 Primordial perturbations . . . 131
5.5 Non-Gaussianity and perturbativity . . . 134
5.5.1 The 4-point correlator . . . 137
5.5.2 The general n-point correlator . . . 139
5.6 Conclusions . . . 141

6 Conclusions 143

References 147

Appendix A Extra material for Chapter 2 159
A.1 Numerical method . . . 159
A.2 Ensembles of models . . . 161
A.3 A single-field toy model . . . 162
A.4 The DBM construction of random manyfield potentials . . . 166
A.5 Case studies and a modified GRF potential . . . 168
A.5.1 A 100-field model . . . 168
A.5.2 A 25-field model giving large non-Gaussianity . . . 169
A.5.3 Manyfield inflation in uplifted potentials . . . 171

Appendix B Perturbations in rapid-turn inflation models **173**
B.1 Linear perturbations 173
B.2 Hyperinflation 175
B.2.1 Multifield extension to hyperinflation 176
B.3 Primordial perturbations 177
B.4 Power spectra and mode functions in $c_s^2 < 0$ theories 181

List of figures

2.1 An example of a GRF potential with $N_{\rm f} = 2$ and $n_{\rm max} = 175$. Here $\phi \in [-4\Lambda_{\rm h},\ 4\Lambda_{\rm h}]^2$ and inflation is supported near $\phi = 0$. The red circle delineates the region in which a potential truncated at fifth order approximates the full potential to per cent level accuracy. 27

2.2 Schematic illustration of the relevant energy scales of the GRF potentials. The light blue shaded region indicates the equilibrium spectrum of the Hessian; the darker region corresponds to our chosen 'flat spectrum' initial condition. 39

2.3 The value of the potential as a function of the field displacement (left), and the evolution of multiple components of the fields (right) in a random 100-field GRF model. 48

2.4 Eigenvalue evolution of the Hessian in a 100-field example, starting from a flat spectrum. 49

2.5 Histogram of the e-fold distribution of the baseline model (cf. equation (2.2.44)), and the dependence of the mean and standard deviation on the hyperparameters in one-parameter variations from the baseline. Each data point is generated from an ensemble of 2000 inflationary models. 51

2.6 Examples of power spectra from 15 randomly generated models of GRF inflation for $N_{\rm f} = 10$ (left) and $N_{\rm f} = 50$ (right). Hyperparameters other than $N_{\rm f}$ are as in the baseline case, cf. equation (2.2.44). 53

2.7 The distribution of n_s and α_s for 25,000 inflation models spanning values of $N_{\rm f}$ between 5 and 50, with the 68% and 95% confidence contours from Planck (TT+TE+lowP+lensing) [10]. 55

2.8 The spectral index and its running as functions of the smoothness of the potential in one-parameter variations from the baseline hyperparameters. The blue regions indicate the 68% c.l. from Planck (TT+lowP+lensing) [10]. 56

2.9 The distribution of ($N^{\rm end}$, n_s) at the end of inflation (left) and the change of the spectral index on superhorizon scales, $\Delta n_s = n_s^{\rm end} - n_s^\star$, (right), for about 19,000 inflation models with uniform mass spectra, again spread over values of $N_{\rm f}$ varying between 5 and 50 (the same models as in Figure 2.7, but without the compressed spectra models). The black curve in the left graph shows the prediction of the single-field model discussed in Appendix A.3. 58

2.10 The spectral index and its running as a function of $N_{\rm f}$ in one-parameter variations from the baseline together with the 68% c.l. from Planck [10]. 59

2.11 Superhorizon evolution of the mode exiting the horizon 55 e-folds before the end of inflation for the flat initial spectrum (left) and the compressed spectrum (right), cf. equation (2.2.42). Boxes indicate first and third quartile, together with the median; 'whiskers' indicate 1st and 99th percentile. The left graph shows a one-parameter variation from the baseline; the right shows models with $\Lambda_{\rm h} = 0.4$, $\epsilon_{\rm i} = 10^{-10}$ and $\eta_{\rm i} = -10^{-4}$. 60

2.12 Isocurvature-to-curvature ratio at the end of inflation for flat (left) and compressed (right) initial spectra. Other hyperparameters as in Figure 2.11. 62

2.13 The total number of e-folds and n_s as functions of $\eta_{\rm i}$, with other parameters as in the baseline and together with the 68% c.l. from Planck [10]. 67

2.14 Values for $f_{\rm NL}$ and n_s for 25,000 random inflation models, spanning values of $N_{\rm f}$ between 5 and 50 (the same as in Figure 2.7). The black line in the right plot indicates the single-field consistency condition: $f_{\rm NL} = \frac{5}{12}(n_s - 1)$. NB: the graph on the right excludes six points with $|f_{\rm NL}| > 1$. 69

2.15 Superhorizon evolution and surviving isocurvature for the same models as in Figure 2.14. 70

3.1 An example of a GRF with $d = 2$ and $n_{\rm max} = 175$. Here $\mathbf{x} \in [-4l,\ 4l]^2$. 76

3.2 Likelihood contours for the hyperparameters at the 68% and 95% confidence levels obtained from random realisations of the GRF. The true hyperparameter values are $(h, \ell) = (1.22, 0.33)$ as indicated by the black dot, and we have fixed $\bar{f} = 0$. 93

4.1 The analytical predictions from hyperinflation (green) and slow-roll inflation (purple) together with a numerical realisation of Example 2 (blue). The momenta are quickly attracted to the slow-roll solution, but then destabilise and approach the hyperinflation attractor. 111
4.2 Three graphs for the antisymmetric hyperinflation model of Example 3. The top figure shows five trajectories in field space converging to the hyperinflation attractor. The left figure shows how the momenta π_v and π_w converge to the correct values in one example. The right figure shows how slow-roll with a small velocity in the w-direction quickly becomes unstable for $\pi_{w,i}/\pi_{v,i} = 10^{-2}, \ldots, 10^{-10}$. 113
4.3 The convergence of π_{w1}^2 (orange), π_{w2}^2 (purple) and their sum (blue) to the analytic hyperinflation solution (green) of Example 5 with $N_{\rm f} = 3$. 114

5.1 RMS fractional differences over a few oscillation cycles between the predicted $\hat{\pi}_v$ (left), $\hat{\pi}_w$ (right) and numerically calculated field momenta π_v, π_w in the flat field-space model as the solutions converge. 129
5.2 The turn rate ω in the side-tracked example (green), and the fractional difference between the numerical and predicted values (blue). 130
5.3 Comparison between predicted growth and numerically calculated values, computed using the methods of appendix B.3. The graph on the left has $\xi = 0$ fixed and the one on the right has $\omega = 90$. 134
5.4 The four-point correlation function gets a contribution from a scalar exchange diagram, corresponding to two insertions of the cubic interaction Hamiltonian. 136

A.1 Multifield aspects of the 100-field example. 168
A.2 Multifield effects in the 25-field model with large non-Gaussianity. . . 170
A.3 Eigenvalue evolution for a 20-field model with uplifted potential (left) and comparison of predictions for spectral index computed from ensembles of 1000 models (right). 171

Chapter 1

Introduction

The last few decades have seen significant advances in the field of cosmology. Measurements of the expansion of the universe indicate that the universe is almost exactly spatially flat, that it is dominated by dark energy, and that the majority of its matter content is dark matter, which seemingly does not interact with Standard Model particles. This is the so called ΛCDM model. Although there is very strong observational evidence for this model, and the parameters have been measured to a high precision [12], there are several aspects of it that are not well understood, such as the nature of dark matter and dark energy, and why the universe is so flat.

More recently, experimental attention has been focused on the cosmic microwave background (CMB), with the aim of learning as much as possible about the initial conditions of our universe. The CMB consists of photons released 380 000 years after the Big Bang [12], when the temperature dropped low enough for electrons to be bound to protons, letting the photons propagate freely. This is as far back in time as we see directly with any telescope-based experiments. The CMB has a black body spectrum, so by measuring the wavelengths of the light coming in, one can deduce the temperature, and hence energy density, of the universe when and where the photons were released. A striking feature of the CMB is just how uniform it is. Across all directions, the fractional variation is just 1 part in 100 000, even though it extends far beyond scales which would be in causal contact in a naive Big Bang cosmology. What is even more remarkable is that there are in fact *correlations* in the fluctuations on these scales, suggesting that they must have been in causal contact at some point in the early universe.

To explain the origin of these correlations, and why the universe is so flat, homogeneous, and isotropic, one can add a new phase of exponential expansion in the early universe, which is called inflation. During inflation, scalar fields give the universe a

slowly varying vacuum energy, causing an exponential expansion which flattens and homogenises the universe. However, quantum fluctuations of the scalar fields during this expansion also give rise to small, correlated fluctuations in energy density, explaining the variations we see in the CMB. The power spectrum of the CMB fluctuations is near scale-invariant, with a slight red tilt, which is the natural prediction of most inflation models, and the non-Gaussian three-point correlations functions have been constrained to be small, which is again what most inflation models predict [15].

Beyond these 'scalar' density fluctuations, during inflation quantum fluctuations also generate gravitational waves, known as 'tensor' fluctuations. If these were to be detected, they would provide direct evidence for inflation, and their amplitude would tell us the exact energy scale of inflation. As of yet, these have not been discovered, but the gravitational wave amplitudes that have been ruled out thus far only correspond to inflation models that would require significant fine-tuning.

The inflationary paradigm is well supported by experimental observations, but with the information currently available it is not possible to determine exactly *how* inflation happened, i.e. the form and scale of the potential or the number of fields involved. This is one of the main challenges of modern cosmology. Determining precisely how inflation happened is not likely to be easy, but if it were to be done successfully, it would reveal information about physics we could never dream of testing in a particle accelerator. The energy scale of inflation can be as large as 10^{16} GeV [14], far beyond the 10 TeV scale currently probed in the LHC. Since scalar fields are ubiquitous in low energy effective field theories of string theory and in supersymmetric extensions of the Standard Model, and there is no indication that terrestial experiments will ever probe these theories, inflation may be our chance to get insight into these high-energy phenomena.

While CMB has given us very accurate measurements of the primordial power spectrum, primordial non-Gaussianity remains insufficiently constrained for us to be able to start ruling out inflation models in earnest [15], and future CMB experiments are unlikely to change this. To make progress, therefore, experimental attention is shifting to the large-scale strucutre (LSS) of the universe, where one uses the galaxy distribution to infer the statistics of the initial, primordial perturbations. This has the advantage of giving a much larger, three-dimensional data set, compared to the two-dimensional data set from the CMB, but involves the highly non-trivial task of taking into account the non-linear gravitational evolution. LSS experiments are expected to come in with results over the coming decades, and in the next ten or twenty years we should have sufficiently accurate measurements of 'local' non-Gaussianity for

us to ask preliminary questions about how inflation happened. Accurate measurements of other types of non-Gaussianity are however likely to be further away in time, but if measured, they could distinguish between different types of multifield inflation models.

In the near future, until we start getting very accurate measurements from LSS surveys, we will not be able to determine the exact inflationary mechanism of the early universe, but there are more modest goals that may be achievable with measurements of local non-Gaussianity. An initial question we may want to answer is whether inflation was driven by one field or more. As single- and multifield theories of inflation behave very differently, and can produce distinct observational signatures, this is a question we may be able to make progress with. Similarly, in the multifield case we may also hope to distinguish between models with straight and curved trajectories. There are also various theoretical issues with inflation that deserve attention. A common criticism against inflation is that it requires a very flat potential, but this is not the case for all inflationary solutions, and there are attractor solutions beyond the standard 'slow-roll' solution which can avoid this issue. More generally, there is also the question of how inflation may be embedded into quantum gravity or other UV theories, which is far from completely understood. The former is also connected to the cosmological constant problem, which is the issue of how the vacuum energy of our universe came to be so small and positive. The smallness is problematic from a generic naturalness point of view, but the positivity is surprising because string theory, our only currently workable theory of quantum gravity, significantly favours negative energy vacua, and the construction of positive energy vacua is challenging.

It was within this experimental and theoretical context that the research presented in this thesis was conducted, and the rest of this introduction will give the theoretical background that underpins the later chapters.

1.1 Inflation

In this thesis we are primarily concerned with inflationary theories involving two or more fields, and this introductory section will review how these theories work on both the background and perturbation levels. To start, we give a brief review of FRW cosmology, and present some of the main theoretical motivation for inflation. After that, we will introduce the basic ingredients needed for inflation, and also give a brief overview of inflationary perturbation theory, as it is crucial for both the computation of observables and the study of the stability of various solutions. Part of the thesis will also be concerned with Gaussian random fields (GRF), but as they are only a

means to an end here, their discussion will be contained to the first part of the thesis, in Chapters 2 and 3.

1.1.1 FRW cosmology

As far as we can tell, gravity in our universe is described by Einstein's theory of General Relativity, which is governed by the Einstein equation

$$G_{\mu\nu} = 8\pi G T_{\mu\nu}. \tag{1.1.1}$$

Observations tell us that the universe is homogeneous and isotropic, so one can make the ansatz that the metric should be given by

$$ds^2 = -dt^2 + a(t)^2 \left(\frac{dr^2}{1 - kr^2} + r^2 d\Omega^2 \right), \tag{1.1.2}$$

where we allow for a non-flat background; $k > 0$ corresponds to positive curvature and $k < 0$ corresponds to negative curvature, i.e. hyperbolic curvature, and $k = 0$ corresponds to a flat universe. $a(t)$ is the scale factor which relates coordinate distances to physical distances, and it describes the expansion of the universe in time. With this ansatz, the Einstein equation reduces to

$$\frac{\dot{a}^2}{a^2} = \frac{8\pi G\rho}{3} - \frac{k}{a^2} \tag{1.1.3}$$

$$\frac{\ddot{a}}{a} = -\frac{4\pi G}{3}(\rho + 3P), \tag{1.1.4}$$

where $\rho \equiv -T^0_0$ is the energy density and $P \equiv T^i_i/3$ is the pressure. From now on we will also use the definition $H \equiv \dot{a}/a$, where H is referred to as the Hubble rate. The ratio of the pressure to density is also defined to be $w \equiv P/\rho$. The energy density for each component evolves as

$$\dot{\rho} = -3H(\rho + P) = -3(1 + w)H\rho, \tag{1.1.5}$$

which is derived from the continuity equation $\nabla_\mu T^{\mu 0} = 0$.

Our universe is well described by the ΛCDM-model, where we have matter ($w = 0$, $\rho \propto a^{-3}$), radiation ($w = 1/3$, $\rho \propto a^{-4}$), and dark energy ($w = -1$, $\rho = \text{const}$), but no spatial curvature ($k = 0$). In the early universe, when a is small, matter and radiation dominate since they scale as a^{-3} and a^{-4} respectively, so one can deduce from equation 1.1.3 and the fact that $\dot{a} > 0$ that at some point in the past there must have been a

singularity where $a = 0$. This singularity is the so called 'Big Bang', which by current estimates occured approximately 13.8 billion years ago [12].

The particle horizon, which is the maximum comoving distance between points at time t that could have been in causal contact, is generally given by

$$\chi_{\rm ph} = \int_{t_i}^{t} \frac{dt'}{a(t')} = \frac{2H_0^{-1}}{1+3w}\left(a^{(1+3w)/2} - a_i^{(1+3w)/2}\right), \tag{1.1.6}$$

where we write $a(t) = a$, $a(t_i) = a_i$. The CMB was released at a point up to which radiation was dominant, so we can take $w = 1/3$. Letting $a_i \to 0$, we find a finite answer, which is about 30,000 times smaller than the comoving radius of the CMB. However, despite this, the CMB is not only almost exactly homogeneous and isotropic, but there are in fact *correlations* in the temperature fluctuations on scales much larger than the particle horizon. We therefore need to explain how these fluctuations came to be in causal contact. This is called the horizon problem.

To solve this we note that if $w < -1/3$, $\chi_{\rm ph}$ actually diverges as $a_i \to 0$. If we therefore add a phase with $w < -1/3$ in the early universe, we can make $\chi_{\rm ph}$ sufficiently large for the CMB to be within the particle horizon, and thus in causal contact. However, it is not enough that the points should be in causal contact - the intial conditions need to homogenise before the rest of the evolution begins, which is a stronger condition than having a particle horizon larger than the comoving CMB radius.

This can be formulated in terms of the so called 'Hubble horizon', $(aH)^{-1}$, which is the comoving distance which can be traversed in one Hubble time, H^{-1}. The particle horizon defines which points in space-time may have been in causal contact, but the Hubble horizon defines which points can be in causal contact over one Hubble time. The horizon problem is solved if at some point in the past the Hubble horizon contained all of the visible universe. This requires a prolonged phase with a decreasing Hubble horizon, which like $w < -1/3$ corresponds to a phase of accelerating expansion, $\ddot{a}/a > 0$, as can be deduced from equation 1.1.4. This condition can equivalently be written as

$$\epsilon \equiv -\frac{\dot{H}}{H^2} < 1. \tag{1.1.7}$$

The condition that the observable universe today must have been contained inside the Hubble horizon during inflation requires about 60 e-folds of expansion. For this to

happen, ϵ must not only be small, but also slowly varying. This demands that

$$\eta \equiv \frac{\dot{\epsilon}}{H\epsilon}, \tag{1.1.8}$$

which charactarises the rate of increase of ϵ, satisfies

$$|\eta| \ll 1. \tag{1.1.9}$$

1.1.2 Scalar fields in FRW space-times

To realise this phase of accelerated, near-exponential, expansion we need to introduce some form of energy density which approximately mimics dark energy, but then eventually decays into the matter fields we observe around us today, at which point standard ΛCDM cosmology resumes. This turns out to be remarkably easy to do. All we need is some number of scalar fields displaced from the vacuum, rolling down their potential, but as we shall see there is also a remarkable amount of depth in this framework.

The dynamics of some number of scalar fields minimally coupled to gravity is governed by the action

$$\mathcal{S} = \int d^4x\sqrt{-g}\left[\frac{1}{16\pi G}R - \frac{1}{2}G_{ab}\partial^\mu\phi^a\partial_\mu\phi^b - V(\phi)\right], \tag{1.1.10}$$

where G_{ab} is the field-space metric, which we allow to be non-trivial. By varying the scalar field part of the action with respect to the metric one can deduce that the stress tensor is given by

$$T_{\mu\nu} = G_{ab}\partial_\mu\phi^a\partial_\nu\phi^b - g_{\mu\nu}\left(\frac{1}{2}G_{ab}\partial_\alpha\phi^a\partial^\alpha\phi^b + V(\phi)\right). \tag{1.1.11}$$

For cosmology we make the ansatz that the field is spatially homogeneous, meaning that $\partial_i\phi^a = 0$. Consequently, we find that the energy density and pressure are given by

$$\rho \equiv -T^0{}_0 = \frac{1}{2}G_{ab}\dot{\phi}^a\dot{\phi}^b + V(\phi), \qquad P \equiv \frac{1}{3}T^i{}_i = \frac{1}{2}G_{ab}\dot{\phi}^a\dot{\phi}^b - V(\phi). \tag{1.1.12}$$

based on this we see that for $w \equiv P/\rho < -1/3$ to be satisfied, we need to be in a regime where the potential energy dominates.

Rather than working with the two Friedmann equations, for scalar fields we will substitute the second one with the scalar field equations of motion, and thus work with

$$\mathcal{D}_t\dot{\phi}^a = -3H\dot{\phi}^a - V^{;a} \tag{1.1.13}$$

$$H^2 = \frac{\frac{1}{2}\dot{\phi}_a\dot{\phi}^a + V}{3M_{\rm P}^2}, \tag{1.1.14}$$

where $\mathcal{D}_t X^a \equiv \dot{X}^a + \Gamma^a_{bc}\dot{\phi}^b X^c$ and $M_{\rm P} \equiv 1/\sqrt{8\pi G}$ is the reduced Planck mass. The second Friedmann equation can be recovered from these two.

Using the equations of motion, one finds that ϵ is given by

$$\epsilon = \frac{\frac{1}{2}\dot{\phi}^2}{H^2M_{\rm P}^2} = 3\frac{\frac{1}{2}\dot{\phi}^2}{\frac{1}{2}\dot{\phi}^2 + V}. \tag{1.1.15}$$

To have a small value for ϵ we therefore require $\frac{1}{2}\dot{\phi}^2 \ll V$, just as deduced earlier. Differentiating the above expression, we also straightforwardly find that η is given by

$$\eta = 2\frac{\dot{\phi}_a\mathcal{D}_t\dot{\phi}^a}{H\dot{\phi}^2} + 2\epsilon, \tag{1.1.16}$$

which in turn requires $|\dot{\phi}_a\mathcal{D}_t\dot{\phi}^a| = \frac{1}{2}|\mathcal{D}_t\dot{\phi}^2| \ll H\dot{\phi}^2$. Inflation therefore requires the energy density of the universe to be dominated by the potential energy of the scalar fields, and for it to last the kinetic energy of the fields must also vary slowly.

The latter condition has a unique interpretation in single-field inflation: it must necessarily be the case that $\ddot{\phi} \ll H\dot{\phi}$. For multifield inflation, there are now however two options. Either we have $|\mathcal{D}_t\dot{\phi}^a| \ll H\dot{\phi}$, leading to the standard slow-roll, slow-turn scenario, or $\mathcal{D}_t\dot{\phi}^a$ is nearly orthogonal to $\dot{\phi}^a$. Slow-roll models have been very thoroughly studied, but the latter much less so. Models where the acceleration of the fields is orthogonal to the velocity are so called rapid-turn models, which will be the topic of Chapters 4 and 5.

1.1.3 Slow-roll inflation

In slow-roll (slow-turn) inflation we assume that $\mathcal{D}_t\dot{\phi}^a \ll H\dot{\phi}^a$. We then drop this term from equations of motion, and moreover assume that $\dot{\phi}^2 \ll V$, to find that the

equations simplify to

$$\dot{\phi}^a = -V^{;a}/3H \tag{1.1.17}$$

$$H^2 = \frac{V}{3M_{\rm P}^2}. \tag{1.1.18}$$

The evolution of the system thus turns into a gradient flow. This does not always admit analytic solutions, but it is generally straightforward to solve numerically.

To see when this is a good approximation, we need to see when ϵ and η are small when the equations of motion take the above form. We find that they can be written

$$\epsilon = \epsilon_V, \qquad \eta = 4\epsilon_V - 2\eta_{\parallel} \tag{1.1.19}$$

where the parameters ϵ_V and $\eta_{\parallel}$ are given by

$$\epsilon_V = \frac{M_{\rm P}^2 V_{;a} V^{;a}}{2V^2}, \qquad \eta_{\parallel} = \frac{M_{\rm P}^2 n^a V_{;ab} n^b}{V}, \tag{1.1.20}$$

and $n^a = \dot{\phi}^a/\sqrt{\dot{\phi}^b\dot{\phi}_b}$ is the unit vector in the direction of motion. In single-field inflation one often writes $\eta_{\parallel}$ as η_V, but in multifield inflation the latter is often taken to be $\eta_V = M_{\rm P}^2 \min(\mathrm{eig}(V_{;ab}))/V$. For slow-roll inflation to happen, the potential must be flat and the second derivative of it in the direction of motion must also be small with respect $M_{\rm P}$.

These conditions are not expected to be satisfied at generic points in a potential. In an EFT with a cut-off Λ smaller than the Planck-scale, one would expect to have $\epsilon_V \sim M_{\rm P}^2/\Lambda^2$ and $\eta_V \sim M_{\rm P}^2/\Lambda^2$, which for $\Lambda < M_{\rm P}$ are both greater than 1. If, on the other hand Λ were much greater than $M_{\rm P}$ this problem would be trivial, but how an EFT with a cut-off beyond $M_{\rm P}$, the scale of quantum gravity, could exist is unclear. However, a caveat to the above is that these are 'naturalness' arguments, similar to the kind which incorrectly argued that new physics had to appear at CERN at the 10 TeV scale, and so should perhaps be taken with a grain of salt. Moreover, the fact that we only expect inflation to happen at particular points in a potential is not necessarily a problem in itself, as we do not know anything at all about the initial conditions for the field position and velocity, or more precisely their joint probability density, and even less about the probability density for subsequent phase space positions.

Notwithstanding the above, the theories we shall look at next are interesting because they can avoid some of these problems.

1.1.4 Rapid-turn inflation

As mentioned before, $\mathcal{D}_t\dot{\phi}^a$ does not need to be much smaller than $H\dot{\phi}^a$ as long as the two are more or less orthogonal. In this thesis we shall primarily be intersted in these models when there are exactly two fields.

To analyse these models, we first define two very useful vectors:

$$n^a = \dot{\phi}^a/\sqrt{\dot{\phi}^b\dot{\phi}_b}, \qquad s^a = \mathcal{D}_t n^a/\sqrt{\mathcal{D}_t n^b \mathcal{D}_t n_b}. \tag{1.1.21}$$

Not only will we use them to understand the background solution, but they will come up again (and be generalised) in the perturbation theory, where n^a corresponds to the adiabatic direction and s^a corresponds to the isocurvature direction. Moreover, the crucial turn rate ω is now defined through

$$\omega \equiv s_a \mathcal{D}_N n^a. \tag{1.1.22}$$

The (dimensionless) turn rate tells us how strongly the inflationary motion deviates from being a geodesic – for values $\omega \gtrsim \mathcal{O}(1)$ the motion would be considered to be highly non-geodesic.

To see how inflation with a large turn rate works, we begin by projecting the equations of motion onto the n^a, s^a basis:

$$\ddot{\phi} = -3H\dot{\phi} - V_n \tag{1.1.23}$$

$$\omega H\dot{\phi} = -V_s, \tag{1.1.24}$$

where we defined $V_n \equiv n^a V_{;a}$, $V_s \equiv s^a V_{;a}$, and $\dot{\phi} = \sqrt{\dot{\phi}^a\dot{\phi}_a}$. So far everything remains rather abstract, and we will only solve the equations properly later in the thesis. To do so we are going to have to reformulate the equations of motion in another vielbein basis, but we are already in a position to show one of the reasons why these theories are interesting. From equation 1.1.23 and the definition of η one can show

$$V_n = -H\dot{\phi}(3 - \epsilon + \eta/2). \tag{1.1.25}$$

Together with 1.1.24 and using the fact that $V_n^2 + V_s^2 = |\nabla V|^2$, one can then show that when ϵ and η are small, ϵ_V can be written [112]

$$\epsilon_V = \frac{M_{\rm P}^2}{2}\frac{V_n^2 + V_s^2}{V^2} \simeq \epsilon\left(1 + \frac{\omega^2}{9}\right). \tag{1.1.26}$$

When the turn-rate is large, ϵ gets suppressed relative to ϵ_V, and if ω is sufficently large it is possible to have inflation even where ϵ_V is too big for slow-roll, slow-turn inflation. Since one of the main criticisms against inflation is that it requires a very flat potential to work, this is a very interesting avenue to explore.

These solutions are however not quite as straightforward to construct as slow-roll, but this is something we will investigate in this thesis. These solutions, which have mainly been studied in the context of two-field inflation, are very interesting in and of themselves, and what if anything links the known solutions together was very much an open question at the start of this PhD. As we shall see, they can in fact be described by a general attractor solution, which will be derived in Chapter 5.

1.2 Inflationary perturbation theory

Our universe is of course not completely homogeneous, so we also need to consider perturbations around the inflationary background solutions. Here we will give a brief review of the linear inflationary perturbation theory. Some second-order perturation theory will be used in one of the chapters in the context of the slow-roll approximation, however the results from the δN formalism will only be stated.

In slow-roll, the perturbation theory is rather straightforward, as one can generally assume that the field perturbations are canonically normalised and that they are only weakly coupled. In rapid-turn inflation this is not at all the case. To understand the perturbation theory of these models, which is crucial, we need a more sophisticated mathematical machinery, which we will give an introduction to here.

The perturbation theory is not just necessary for understanding what primordial perturbations these models generate, but also for understanding the stability of various solutions. In hyperbolic field spaces, for example, slow-roll can in fact be destablised, with the fields ending up in rapid-turn solutions [37, 41, 45, 165].

To perturb around the flat FRW metric $ds^2 = -dt^2 + a^2\delta_{ij}dx^i dx^j$ one can make the general ADM ansatz

$$ds^2 = -N^2dt^2 + h_{ij}(dx^i + N^i dt)(dx^j + N^j dt). \tag{1.2.1}$$

However, this has some redundant degrees of freedom, and we need to choose a gauge for the perturbations. A very useful gauge, that we shall use almost exclusively, is the spatially flat gauge, where in the absence of tensor perturbations we have $h_{ij} = a^2\delta_{ij}$, $N = 1 + \alpha$, and $N^i = \beta^i$. By expanding the action to second order, and solving for α

and β, one finds (after tedious algebra that we will not cover) that the spatially-flat gauge quadratic action for the inflationary perturbations is given by [107, 110, 172]:

$$\mathcal{S}_{(2)} = \frac{1}{2}\int \frac{d^3k}{(2\pi)^3} dt a^3 \left[G_{ab}\mathcal{D}_t\delta\phi^a_{\mathbf{k}}\mathcal{D}_t\delta\phi^b_{-\mathbf{k}} - \left(\frac{k^2}{a^2}G_{ab} + M_{ab}\right)\delta\phi^a_{\mathbf{k}}\delta\phi^b_{-\mathbf{k}}\right], \tag{1.2.2}$$

where M_{ab} is the effective mass matrix given by

$$M_{ab} = V_{;ab} - R_{acdb}\dot{\phi}^c\dot{\phi}^d + (3-\epsilon)\frac{\dot{\phi}_a\dot{\phi}_b}{M_{\rm P}^2} + \frac{\dot{\phi}_a V_{,b} + V_{,a}\dot{\phi}_b}{HM_{\rm P}^2}, \tag{1.2.3}$$

and where $V_{;ab}$ is the second covariant derivative of the potential on the target space, given by $V_{;ab} = V_{,ab} - V_{,c}\Gamma^c_{ab}$. Varying this action one straightforwardly finds that the equations of motion for the perturbations are

$$\mathcal{D}_t\mathcal{D}_t\delta\phi^a + 3H\mathcal{D}_t\delta\phi^a + \frac{k^2}{a^2}\delta\phi^a + M^a{}_b\delta\phi^b = 0. \tag{1.2.4}$$

To compute non-Gaussianity, one also needs to keep the cubic-order terms in the action. This expression is however large, messy and largely uninformative, and as such we omit it here, but it can for example be found in [79]. In this thesis we will only be computing local non-Gaussianity in the slow-roll approximation. This can be computed in a much more straightforward way using the δN formalism [132, 135, 172, 185].

The field perturbations here are gauge-dependent quantities. To relate these perturbations to late-time observables, we need to introduce the gauge-invariant curvature perturbation ζ, which in the spatially flat gauge is given by

$$\zeta = -\frac{\delta\rho}{H\dot{\rho}} + \mathcal{O}(\delta\rho^2). \tag{1.2.5}$$

This can be expressed in the particularly convenient form [75, 82]

$$\zeta = -\frac{n_a\delta\phi^a}{\sqrt{2\epsilon}M_{\rm P}} + \mathcal{O}(\delta\phi^2). \tag{1.2.6}$$

On superhorizon scales, $k \ll aH$, one can show that its superhorizon evolution is completely generally given by

$$\mathcal{D}_N\zeta = -\frac{2\omega s_a\delta\phi^a}{\sqrt{2\epsilon}M_{\rm P}} + \mathcal{O}(\delta\phi^2). \tag{1.2.7}$$

This expression vanishes identically for single-field inflation, where ζ is consequently conserved, or more generally when $\omega = 0$. In these theories the value of ζ freezes out when it leaves the Hubble-horizon at $k = aH$, and it suffices to compute its subhorizon evolution. For multifield theories, however, this expression is in general non-zero, and so this evolution must be computed explicitly.

What we actually observe are the statistical two- and three-point correlation functions, the power spectrum $P_\zeta(k)$,

$$\langle \zeta(\mathbf{k}_1)\zeta(\mathbf{k}_2)\rangle = (2\pi)^3\delta^{(3)}(\mathbf{k}_1+\mathbf{k}_2)\frac{2\pi^2}{k^3}P_\zeta(k) \tag{1.2.8}$$

and bispectrum $B_\zeta(k_1, k_2, k_3)$,

$$\langle \zeta(\mathbf{k}_1)\zeta(\mathbf{k}_2)\zeta(\mathbf{k}_3)\rangle = (2\pi)^3\delta^{(3)}(\mathbf{k}_1+\mathbf{k}_2+\mathbf{k}_3)B_\zeta(k_1,k_2,k_3), \tag{1.2.9}$$

which are both evaluated at the end of inflation. However, observational limits are usually given in terms of the spectral index n_s, its running α_s, and the non-linearity parameter $f_{\rm NL}$, which are given by [139]

$$n_s = 1 + \frac{d\ln P_\zeta}{d\ln k}, \qquad \alpha_s = \frac{dn_s}{d\ln k}, \qquad -\frac{6}{5}f_{\rm NL} = \frac{\prod_i k_i^3}{\sum_i k_i^3}\frac{B_\zeta}{4\pi^4 P_\zeta^2}. \tag{1.2.10}$$

In addition to these, an important observable is the power spectrum of primordial gravitational waves, but these have not yet been observed.

Inflation generically produces a near scale invariant power spectrum, and nearly all inflation models so far constructed can produce a power spectrum compatible with current observations. To distinguish between models of inflation we therefore will need information from the bispectrum.

In the next section we will explore how these observables, and in particular the power spectrum, arise from the quantum fluctuations of the inflaton fields during inflation. A comprehensive introduction is beyond the scope of this thesis, especially since the two different parts of the thesis take this material in two very different directions, but the aim will be to provide the base on which later chapters will be built.

1.2.1 Field perturbations and vielbeins

The form of the quadratic action above in equation 1.2.2 is not ideal for quantisation. The appearance of the field-space metric makes the interpretation, and comparison of, the various field fluctuations harder. To get around this problem, it is useful

to introduce a vielbein basis $\delta\phi^I = e^I_a \delta\phi^a$, where the e^I_a are constructed such that $e^I_a e^a_J = \delta^I_J$ and $e^I_a e^b_I = \delta^a_b$. The idea is to work with field fluctuations projected onto this basis, $\delta\phi^I \equiv e^I_a \delta\phi^a$.

As a starting point, we define a covariant derivative on the vielbein basis

$$\mathcal{D}_t X^I \equiv \dot{X}^I + Y^I{}_J \, X^J, \tag{1.2.11}$$

where $Y^I{}_J \equiv e^I_a \mathcal{D}_t e^a_J$. With this definition, the covariant derivative satisfies

$$\mathcal{D}_t X^a = e^a_I \mathcal{D}_t X^I, \qquad \mathcal{D}_t \mathcal{D}_t X^a = e^a_I \mathcal{D}_t \mathcal{D}_t X^I, \tag{1.2.12}$$

and the action for the $\delta\phi^I$ becomes

$$\mathcal{S}_{(2)} = \frac{1}{2}\int \frac{d^3k}{(2\pi)^3} dt a^3 \left[\delta_{IJ}\mathcal{D}_t\delta\phi^I_{\mathbf{k}}\mathcal{D}_t\delta\phi^J_{-\mathbf{k}} - \left(\frac{k^2}{a^2}\delta_{IJ} + M_{IJ}\right)\delta\phi^I_{\mathbf{k}}\delta\phi^J_{-\mathbf{k}}\right]. \tag{1.2.13}$$

This action is going to be very useful for us in Chapters 4 and 5 when we are interested in the stability of various background solutions.

1.2.2 Quantisation and primordial perturbations

To quantise these perturbations, we change time variable to $d\tau = dt/a$, and define the new fields $v^I = a\delta\phi^I$. This gives the action

$$\mathcal{S}_{(2)} = \frac{1}{2}\int \frac{d^3k}{(2\pi)^3} d\tau \left[\delta_{IJ}\mathcal{D}_\tau v^I_{\mathbf{k}}\mathcal{D}_\tau v^J_{-\mathbf{k}} - \left((k^2 - (\mathcal{H}^2 + \mathcal{H}'))\delta_{IJ} + a^2 M_{IJ}\right) v^I_{\mathbf{k}} v^J_{-\mathbf{k}}\right]. \tag{1.2.14}$$

This action gives the form of the equations of motion that are most easily integrated, but to find the correct initial conditions for quantisation one has to match the deep sub-horizon behaviour with the canonically normalised variables. These are related to the original matrices through a rotation, giving [7, 8]

$$v^I = \mathcal{T}\exp\left[-\int_{\tau_i}^{\tau} Y(\tau)^I_J\right] u^J \qquad \Rightarrow \qquad \mathcal{D}_\tau u^I = \partial_\tau u^I. \tag{1.2.15}$$

The u^I fields have a completely canonical kinetic term, at the cost of a rotating mass matrix. However, deep inside the horizon it will be negligible compared to the k^2 term.

In the simple case of single-field slow-roll, where we for simplicity also neglect the effective mass, which is $\mathcal{O}(\epsilon)$, the mode function satisfies

$$v_k'' + \left(k^2 - \frac{2}{\tau^2}\right) v_k = 0. \tag{1.2.16}$$

Deep inside the horizon it must also match with the Bunch-Davies initial condition

$$\lim_{k\tau\to-\infty} v_k = \frac{e^{-ik\tau}}{\sqrt{2k}}, \tag{1.2.17}$$

and so one finds the general solution to be

$$v_k = \frac{e^{-ik\tau}}{\sqrt{2k}}\left(1 - \frac{i}{k\tau}\right). \tag{1.2.18}$$

This tells us that the power spectrum of the field fluctuations on superhorizon scales is given by

$$P_{\delta\phi}(k) = \frac{k^3}{2\pi^2}|\delta\phi_k|^2 = \frac{k^3}{2\pi^2}\frac{|v_k|^2}{a^2} \overset{-k\tau\ll 1}{=} \left.\frac{H^2}{4\pi^2}\right|_{k=aH}. \tag{1.2.19}$$

From the definition of the curvature perturbation, $\zeta = \delta\phi/\sqrt{2\epsilon}M_{\rm P}$, it then follows that the power spectrum for single-field slow-roll is given by

$$P_\zeta(k) = \left.\frac{H^2}{8\pi^2\epsilon M_{\rm P}^2}\right|_{k=aH}. \tag{1.2.20}$$

From $\ln k = N + \ln H$ one can straightforwardly show that up to $\mathcal{O}(\epsilon)$ corrections, $d\ln k \simeq dN$, and one then finds that the spectral index and its running are given by

$$n_s - 1 = -2\epsilon - \eta, \qquad \alpha_s = -2\epsilon\eta - \eta\xi, \tag{1.2.21}$$

where in this context $\xi \equiv d\ln\eta/dN$. As such, single-field inflation naturally predicts a small negative value for the spectral index and an even smaller, $\mathcal{O}((n_s-1)^2)$, value for its running. This is very much in agreement with measurements of the CMB power spectrum from Planck, which give $n_s = 0.9649 \pm 0.0042$ and $\alpha_s = -0.0045 \pm 0.0067$ (68 % CL) [14].

Similarly, one can show that the tensor power spectrum turns out to be

$$P_t(k) = \left.\frac{2H^2}{\pi^2 M_{\rm P}^2}\right|_{k=aH}. \tag{1.2.22}$$

Its amplitude relative to the scalar power spectrum, and its spectral index are then found to be

$$r \equiv \frac{P_\zeta}{P_t} = 16\epsilon, \qquad n_t \equiv \frac{d\ln P_t}{d\ln k} = -2\epsilon. \tag{1.2.23}$$

If primordial tensor modes were to be observed, we would get a direct measurement of the energy scale of inflation, and by checking if $r/n_t = -8$, we could immediately test single-field inflation. Any deviation from this relation would rule out single-field inflation. Tensor modes have not yet been discovered, however, and the current bound on the tensor-scalar ratio from Planck is given by $r < 0.064$ (95 % CL) [14].

It is perhaps not surprising that the tensor power spectrum has not been observed. For a monotonically increasing ϵ, one can show that the field excursion satisfies

$$d\phi = \sqrt{2\epsilon} M_{\rm P} dN, \quad \Rightarrow \quad \Delta\phi > \sqrt{2\epsilon_\star} N M_{\rm P}, \tag{1.2.24}$$

where the subscript $\star$ here, as elsewhere in the thesis, denotes that the quantity is evaluated as CMB scales exist the horizon, ~ 60 e-folds before the end of inflation. This expression immediately implies [133]

$$r < \frac{16}{N^2}\left(\frac{\Delta\phi}{M_{\rm P}}\right)^2. \tag{1.2.25}$$

With $N \approx 60$, required to explain the homogeneity of the CMB, one sees that $r \geq \mathcal{O}(0.01)$ requires a super-Planckian field excursion, which in EFT contexts would be problematic.

The last observable that needs to be mentioned in this context is local non-Gaussianity, that is non-Gaussianity in the configuration, $k_1 \ll k_2, k_3$. By expanding the action to cubic order and performing a very tedious calculation, one can show that in single-field inflation one has [139]

$$f_{\rm NL}^{\rm loc} = \frac{5}{12}(n_s - 1). \tag{1.2.26}$$

Any deviation from this relation would also rule out single-field inflation.

1.2.3 Observables in multifield inflation

When more than one field is involved, however, the situation is not quite so simple. In slow-roll with multiple fields this is due to the evolution of the curvature perturbation on superhorizon scales. In rapid-turn inflation, where the perturbations are strongly

coupled, there is generally interesting behaviour in the power spectrum as it crosses the horizon. In this subsection we will briefly review these two phenomena.

In multifield slow-roll inflation, the power spectrum is no longer conserved on superhorizon scales. Since the background evolution is a first order gradient flow, we can use the separate-universe picture to evolve the field perturbations as perturbations of the background flow [155],

$$\mathcal{D}_N \delta\phi^a = -M_{\rm P}^2 G^{ad} \left((\ln V)_{;db} \delta\phi^b + (\ln V)_{;dbc} \delta\phi^b \delta\phi^c + \dots \right) \tag{1.2.27}$$

Assuming that all the fields are light, with $m < 3H/2$, their correlation functions at horizon crossing are given by

$$\langle \delta\phi_\star^a(\mathbf{k}_1) \delta\phi_\star^b(\mathbf{k}_2) \rangle = (2\pi)^3 \delta^{(3)}(\mathbf{k}_1 + \mathbf{k}_2) \frac{2\pi^2}{k^3} \frac{H^2(N_\star)}{4\pi^2} G_\star^{ab} \tag{1.2.28}$$

The curvature perturbation can also be written as an expansion in the field perturbations $\delta\phi^a$ (the momentum perturbations can be ignored), which can be evolved forward from horizon crossing to the end of inflation. Since isocurvature perturbations source the curvature perturbation, but are not themselves sourced by it, the power spectrum at the end of inflation can be written [162]

$$P_\zeta = \left(1 + \|T_{\zeta\mathcal{S}}\|^2 \right) P_\zeta^\star, \tag{1.2.29}$$

where $T_{\zeta\mathcal{S}}$ is the transfer vector from the light isocurvature modes at horizon crossing to the curvature perturbation at the end of inflation, and we used the fact that the power spectrum in each field direction is equal at horizon crossing. This tells us that the scalar power spectrum can only increase after the end of inflation, so the tensor-scalar ratio can be suppressed below 16ϵ in multifield inflation. Moreover, to compute the spectral index and its running one now also needs to take into account the $N_\star$-dependence of $T_{\zeta\mathcal{S}}$.

To discuss non-Gaussianity we need to go beyond linear order. In slow-roll, the curvature perturbation at the end of inflation can be written as an expansion of horizon-crossing field perturbations

$$\zeta(\mathbf{x}) = N_a \delta\phi_\star^a(\mathbf{x}) + \frac{1}{2} N_{ab} \delta\phi_\star^a(\mathbf{x}) \delta\phi_\star^b(\mathbf{x}) + \dots, \tag{1.2.30}$$

where the N_a and N_{ab} coefficients can be calculated with the δN formalism [132, 135, 172, 185]. In terms of these, $\|T_{\zeta\mathcal{S}}\| = \|(\delta_b^a - n^a n_b) N^b / N_c n^c\|$. When the second-order

term is large, which can happen if the power spectrum grows significantly during inflation, local non-Gaussianity gets an enhancement from the term [136]

$$-\frac{6}{5}f_{\rm NL}^{\rm loc} \supset \frac{N_a N_b N^{ab}}{(N^c N_c)^2}. \tag{1.2.31}$$

Exactly what conditions are required for this term to be large, and how generic that is, are two questions which we set out to answer in the first part of the thesis. Future large-scale structure (LSS) experiments hope to measure whether $f_{\rm NL}^{\rm loc}$ is smaller than 1, and an important question to answer is what models could be ruled out if this turns out to be the case. Single-field inflation has non-Gaussianity given by equation 1.2.26, which is $\mathcal{O}(\epsilon)$, so a large value of $f_{\rm NL}^{\rm loc}$ would rule out single-field inflation. However, a small value of $f_{\rm NL}^{\rm loc}$ would not necessarily rule out multifield inflation, and to see what we can hope to learn from future observations we want to know how generically multifield inflation gives large non-Gaussianity.

In rapid-turn two-field inflation, the kinetic coupling between the two fields in the term changes the dynamics significantly on subhorizon scales. Working with the kinematic basis, $e_I^a = (n^a, s^a)$, one finds that the kinetic term in the action now becomes

$$\frac{1}{2}\mathcal{D}_\tau v_I \mathcal{D}_\tau v^I = \frac{1}{2}(v_n' - \mathcal{H}\omega v_s)^2 + \frac{1}{2}(v_s' + \mathcal{H}\omega v_n)^2. \tag{1.2.32}$$

These theories can often be approximated by single-field models with a modified speed of sound, which have the action [4, 53, 98]

$$\mathcal{S}_{(2)}^{\rm eff} = \int \frac{d^3k}{(2\pi)^3} d\tau a^2 \epsilon M_{\rm P}^2 \left[\frac{\zeta'^2}{c_s^2} - k^2\zeta^2\right], \tag{1.2.33}$$

where

$$c_s^{-2}(k) = 1 + \frac{4\omega^2}{(k/aH)^2 + M_{ss}/H^2 - \omega^2}. \tag{1.2.34}$$

If $M_{ss}/H^2 > \omega^2$ these theories have a positive, but reduced, speed of sound, and are among other things characterised by large equilateral non-Gaussianity, $f_{\rm NL}^{\rm eq} \propto c_s^{-2}$. If however $M_{ss}/H^2 < \omega^2$, the speed of sound becomes imaginary. These rather unusual theories can see an exponential amplification of the power spectrum during horizon crossing, and we will be investigating these in the second part of the thesis.

1.3 Inflation and high-energy physics

Inflation provides a simple explanation for the universe we see around us, but it cannot be viewed as a single model; countless different potentials can give us enough e-folds of expansion with a more or less correct power spectrum. This is in one way a strength of the inflationary paradigm, but it also makes it very hard to determine how exactly it happened. However, we do know that inflation would have happened at energy scales beyond those currently probed in the LHC, and it could therefore give us a view into physics at energy scales we could never hope to test in any other way. It therefore makes sense to look to string theory, supergravity, and other models for quantum gravity and GUT-scale physics for inspiration in understanding how inflation could have happened.

One generic feature of compactifications of string theory is the presence of a large number of light (Kähler) moduli fields. A natural question to ask therefore is if there are any observational signatures characteristic to inflation models with large numbers of fields. This is the question that the first part of the thesis is concerned with. There are however two particularly important obstacles to answering this question. The first is that we do not have a prior for what the potential should look like; we have poor theoretical control over the string landscape and no accurate idea of what the potentials look like near saddle-points. The second is that even if we did know this, we could not compute the cosmological observables with this information only. This is because when you have more than one light field, the curvature perturbation is no longer conserved, so the observables need to be explicitly evolved forward until inflation ends or the isocurvature modes are sufficiently suppressed.

To answer this question we first need to make some assumption about what the potentials may look like. A reasonably minimal assumption, which also has computational advantages, is to let the potentials follow the distribution of a Gaussian random field (GRF). We will do so with a Gaussian covariance function, and prove some algebraic results that let us vastly simplify the generation of these potentials. This will let us study inflation in random potentials, and in particular we will be able to compute the local non-Gaussianity in models with as many as 100 fields, which had never been done before.

Previously, the 'manyfield' limit of inflation was studied most effectively with Dyson Brownian motion (DBM) potentials [77, 78, 142]. In this construction, the Hessian of the potential undergoes a random walk in field space along the trajectory. This allows for a computationally efficient modelling of random potentials with large numbers of

fields, and interestingly it was found that in the limit of many fields the observables become remarkably simple and compatible with observations. An interesting question to ask is therefore if this is a generic feature of manyfield potentials, and we will investigate this with the GRF construction. A problem with the DBM models is that the Hessian is almost surely not differentiable as a function of field space position, and the third derivatives are therefore not well definied. This prohibits the study of local non-Gaussianity, which we will be able to study with GRF inflation.

Another common feature of string compactifications is negatively curved field spaces. Inflation models in hyperbolic field spaces can exhibit really interesting behaviours, and the second part of the thesis will begin by trying to understand hyperinflation, one of these models that was proposed recently. Hyperinflation is interesting because it can take place in potentials that are far too steep for slow-roll, and unlike many other models in hyperbolic field spaces, the solution is described well algebraically. This made it an ideal context for developing a better mathematical and physical understanding of rapid-turn inflation models.

Using the mathematical framework developed for studying hyperinflation we then find that there is a unique, general two-field rapid-turn attractor solution. Chapter 5 will show how this solution can be found and discuss its properties. Using this solution hyperinflation can easily be recovered, and we will show how side-tracked inflation and other models also arise in this context.

There has been a lot of interest recently in this type of models because they can be compatible with the (controversial) 'swampland conjectures'. Irrespective of whether one takes these conjectures seriously, these models are very interesting because they can arise in potentials with large values of the derivatives. A common criticism against slow-roll inflation is that the gradient and eigenvalues of Hessian need to take (from and EFT perspective) unnaturally small values over large regions in field-space, but this is not necessary for rapid-turn inflation models. However, what they gain in robustness against the background potential they lose in mathematical simplicity, and in particular the perturbation theory of these models is rather non-trivial. We also discuss this aspect of rapid-turn attractors, and in particular investigate the exponential growth that the perturbations undergo at horizon crossing if the sound speed is imaginary.

Chapter 2

Inflation in Gaussian random field potentials

2.1 Introduction

Inflation provides a rather simple explanation of the origin of the primordial density perturbations and successfully resolves the flatness and homogeneity problems of the standard hot big bang cosmology. However, little is known about the microscopic origin of inflation and, in particular, what degrees of freedom it involved. Inflation may have probed energies far above those accessible by terrestrial experiments, and is sensitive to physics beyond the Standard Model of particle physics. Models of inflation with only a single additional scalar field can be compatible with all current observations, but so may models with multiple fields. Additional scalar fields are common in extensions of the Standard Model that address the gauge hierarchy problem, and ubiquitous in ultraviolet completions realised in string theory. Determining the field content relevant in the early universe is a fundamental challenge of modern cosmology.

Primordial non-Gaussianity of the local type has been proposed as a key observable to observationally distinguish between multifield and single-field models of inflation. In single-field inflation, the levels of local non-Gaussianity can be related to the deviation from scale invariance of the primordial power spectrum [64, 139],[1] which is very small [10]. Multiple-field effects can significantly enhance the levels of non-Gaussianity, and amplitudes of the order of $f_{\rm NL} \sim 1$ are realised in some models.[2] Current constraints from Planck observations of the Cosmic Microwave Background give $f_{\rm NL} = 0.9 \pm 5.1$

[1] This rule applies under some assumptions, which can be violated in special models [55, 150].

[2] In this chapter, we focus on non-Gaussianities of the local type, and denote $f_{\rm NL}^{\rm loc} = f_{\rm NL}$ without superscript.

(68% c.l.) [15], and future surveys of the Large-Scale Structure of the universe are expected to reach a sensitivity of $\sigma(f_{\rm NL}) \sim \mathcal{O}(1)$ [17, 26, 66, 74, 92, 146, 176], probing some subset of models of multiple-field inflation. It is now pressing to assess what we realistically can hope to learn about fundamental physics from these experiments.

The conditions under which large non-Gaussianity is generated during and after inflation have been studied before by many authors (for a review, see [47]). However, direct investigations tend to be hampered by the computational complexity of multi-field systems, and most studies have been restricted to models with two or a few fields, or models with greatly restricting symmetry structures [31, 87, 160, 162, 164, 175, 183]. For a more complete understanding of multifield inflation, it is necessary to go beyond these simplifying assumptions, and allow both for more fields and for non-trivial interactions. This is crucial for understanding what models of inflation can be ruled out if $f_{\rm NL}$ is constrained to be less than one, or what types of inflationary models are favoured if $f_{\rm NL}$ of order one is measured. Addressing this question is one of the main aims of this chapter.

Multifield inflation models with generic interactions between the fields have large numbers of free parameters. In a low-energy effective theory for $N_{\rm f}$ fields valid below the cut-off scale Λ, these are the Wilson coefficients, $c_{a_1 \ldots a_n}$, of all operators that may be important during inflation, e.g.

$$V(\phi_1, \ldots, \phi_{N_{\rm f}}) = \Lambda^4 \sum_{n=0}^{n_{\rm max}} c_{a_1 \ldots a_n} \frac{\phi^{a_1}}{\Lambda} \ldots \frac{\phi^{a_n}}{\Lambda} \,. \tag{2.1.1}$$

Unfortunately, the relevant values (or distribution of values) of these parameters are not known from fundamental physics. One approach, pursued here, is then to search for properties that are rather insensitive to the details of the parameter distribution, and that depend only on a few effective parameters. The widespread appearance of emergent universality in complex physical and mathematical systems suggests that such robustness may be found as the number of fields, $N_{\rm f}$, becomes large [72, 90, 124, 189]. Motivated by this, we pursue a statistical approach: we generate ensembles of multifield scalar potentials $V(\phi_1, \ldots, \phi_{N_{\rm f}})$ randomly, and determine the distribution of observables as $N_{\rm f} \gg 1$.

To access the interesting regime of multiple light fields with non-trivial interactions, the potentials need to be mathematically simple enough to be computationally tractable. One such class of potentials, recently studied in [32, 77, 78, 97, 142, 159, 186], can be constructed using non-equilibrium random matrix theory techniques. According to the prescription of [142], the computational difficulties of multifield inflation can be

substantially mitigated by realising $V(\phi_1, \ldots, \phi_{N_\mathrm{f}})$ only locally along the field trajectory (while being undetermined elsewhere in field space), and by postulating that the Hessian matrix evolves according to Dyson Brownian motion (DBM) along the inflationary path. The local Taylor coefficients to quadratic order, defined patch-wise along the path, evolve non-trivially during inflation and implicitly capture the effects of higher-order interaction terms. This method remains computationally efficient up to very large N_f, making it possible to determine the observational predictions[3] in models of inflation with up to a hundred interacting fields [77, 78]. In reference [77], it was shown that the predictions of these 'DBM models' become simpler and sharper as the number of fields is increased, and very complicated models with many fields are commonly compatible with Planck constraints on the primordial power spectrum [78].

However, the random matrix theory method of [142] is not suitable to investigate the generation of primordial non-Gaussianities during inflation: the Brownian motion of the eigenvalues of the Hessian matrix is continuous but not differentiable, and the third derivatives of the potential, required for the computation of the three-point correlation function, are not well-defined in the continuum limit.[4]

Manyfield inflation from Gaussian random fields

An alternative approach is to generate random multifield potentials using Gaussian random fields (GRFs). This was first done in [94, 95] by expanding $V(\phi_1, \ldots, \phi_{N_\mathrm{f}})$ in a set of Fourier modes for potentials with $N_\mathrm{f} \leq 6$ and $\Lambda > M_\mathrm{P}$ (see also [179] for $N_\mathrm{f} = 1$). However, the interesting regime of multiple-field inflation in potentials with structure on sub-Planckian distances in field space remained intractable.

To access the regime with $\Lambda < M_\mathrm{Pl}$, reference [23] proposed to generate the potential only locally in field space, e.g. by gluing together multiple patches along a path in field space, or by generating the Taylor coefficients of the potential to a sufficiently high order at a single point. These models have well-defined higher derivatives and are arguably simpler than the DBM potentials, but a significant limitation arises from the need to explicitly specify a very large number of Taylor coefficients, which are not statistically independent. For example, a model with $N_\mathrm{f} = 100$ fields and the potential expanded up to fifth order around a single point involves 96,560,546 independent

[3] This method is limited to observables that can be inferred from information about the potential up to second order in derivatives as expanded around any point along the field trajectory. As we will review in section 2.2.6, this includes quantities computed from the two-field correlators such as the primordial power spectrum, including its spectral index and its running.

[4] This obstacle may be overcome by regularisation, or by modifying the rules governing the stochastic evolution (cf. [32] for one suggestion).

Taylor coefficients. The probability distribution of these coefficients involves the inverse covariance matrix which has 4.7×10^{15} independent, and in general non-vanishing, elements. Naively generating such a matrix numerically is computationally prohibitive, making explicit studies impractical or impossible.

In this chapter, we explain how one can overcome these obstacles and generate multifield GRFs to explicitly study the manyfield limit of inflation in general potentials. We construct models with up to 100 fields by generating the potential locally around an 'approximate saddle-point' up to fifth order in the fields, and we use an adaptation of the 'transport method' [79, 81, 153, 174] to compute cosmological observables from the two-field and three-field correlation functions. To make this possible, we identify drastic algebraic simplifications for GRFs with a Gaussian covariance function, and we use these to obviate the need for extremely heavy numerics. This key advance allows us to study the generation of local non-Gaussianities in random manyfield models of inflation, and assess what levels of $f_{\rm NL}$ are generated.

There are three particularly important results in this chapter:

1. Planck compatible power spectra are not rare for these models: even for highly complicated manyfield models with millions of non-vanishing interaction terms, the spectral index commonly falls within the observationally allowed range. Interestingly, these models make a sharp statistical prediction for the running of the spectral index, $\alpha_s = \mathrm{d}n_s/\mathrm{d}\ln k$, which can be ruled out by future experiments.

2. At large $N_{\rm f}$, the observational predictions of our GRF models agree well with, but are sharper than, recent predictions derived from DBM potentials. As these two constructions are fundamentally different and independent, this suggests the existence of a 'universality class' of large-$N_{\rm f}$ models for which the observables are largely insensitive to the details of the underlying potential.

3. The amplitude of local non-Gaussianities is typically very small, $|f_{\rm NL}| \ll 1$. Even when the power spectrum undergoes significant superhorizon evolution, indicative of multifield effects being important, $f_{\rm NL}$ is typically highly suppressed, and even approximately follows the single-field consistency relation: $f_{\rm NL} = \frac{5}{12}(n_s - 1)$. Moreover, in the rare cases where $f_{\rm NL} \sim \mathcal{O}(1)$, isocurvature modes remain unsuppressed at the end of inflation, and a detailed modelling of the reheating dynamics is required to extract reliable predictions. We conclude that constraining $f_{\rm NL}$ to be smaller than order unity would not rule out manyfield inflation, but a measurement of a large value for $f_{\rm NL}$ would point to rather special inflationary dynamics.

We expect that the predictions of this class of models may extend also to other constructions of small-field, slow-roll models of approximate saddle-point inflation. However, distinct classes of multifield models (such as large-field models, or models with sharp features in the potential) may well lead to different predictions for some observables.

This chapter is organised as follows: in section 2.2, we review how GRFs can be used as models for multifield inflationary potentials, and we illustrate the key simplifications that allow us to access the manyfield regime. We furthermore discuss the natural energy scales intrinsic to GRF potentials, their possible interpretation as physical effective field theory potentials, and we critically discuss the tuning required to use these potentials to study multifield inflation. We finally present the ensembles of potentials that we study explicitly, and our method for computing cosmological observables. In sections 2.3–2.5 we discuss the three main results of this chapter. We conclude and discuss further directions in section 2.6. A number of additional details, including illustrative case studies, can be found in the Appendix A.

Throughout this chapter we set the reduced Planck mass to one, $M_{\rm Pl} = 2.4 \times 10^{18}\,{\rm GeV} = 1$, but we occasionally reinstate factors of $M_{\rm Pl}$ for clarity.

2.2 Gaussian random fields for inflation

In this section we explain how we use Gaussian random fields (GRFs) to study random multifield inflation.[5] The basic idea is to construct the potential locally in field-space as a truncated Taylor series with randomly generated coefficients. By going to sufficiently high order in the Taylor expansion, one can obtain a well-approximated potential in a domain containing the inflaton trajectory. This makes GRFs a powerful tool for studying the observational signatures of generic large-$N_{\rm f}$ inflation models.

We begin by briefly reviewing the statistical properties of Gaussian random fields and how the probability distribution function (PDF) for the Taylor coefficients is obtained. This PDF involves the inverse of the covariance matrix and is unfortunately of very limited practical use when $N_{\rm f}$ is large. However, we find that for a Gaussian covariance function for the random field, there is a drastic simplification which allows us to generate explicit potentials even when $N_{\rm f} \gg 1$.

[5]Previous work on inflation in random potentials include [1, 29, 30, 34, 89, 94, 111, 126, 130, 131, 140, 144, 145, 158, 179**?** –181]. References [19, 20, 108] studied the impact of randomness on particle production during inflation, and references [11, 76, 147] investigated random compactification effects in brane inflation in string theory.

We go on to present the class of random inflation models discussed in this chapter. Specifically, we discuss the relevant mass-scales of the potentials, and how the GRFs under certain conditions admit an interpretation as proxies for physical effective field theories (EFTs). However, we also point out a challenge for using GRFs to study multifield inflation: the typical mass-splitting of the fields tend to exceed the Hubble parameter, leading to single-field dynamics. We then describe how we choose the initial conditions to generate large ensembles of potentials with multifield dynamics during inflation. We close this section by briefly explaining the methods used to calculate the background trajectory and the superhorizon evolution of the field perturbations.

2.2.1 High-dimensional GRFs as random multifield scalar potentials

A Gaussian random field has a mean value $\bar{V}$ and a covariance function,

$$\langle (V(\phi_1) - \bar{V})(V(\phi_2) - \bar{V}) \rangle = C(\phi_1, \phi_2)\,, \tag{2.2.1}$$

where the ϕ_i are position vectors in field space (with components ϕ_i^a), which we take to be flat $\mathbb{R}^N$. Furthermore, we take the GRF to be stationary and isotropic with mean zero[6] so that

$$C(\phi_1, \phi_2) = C(\phi_1 - \phi_2) = C(|\phi_1 - \phi_2|)\,. \tag{2.2.2}$$

The covariances for the derivatives are given by the derivatives of the covariance function:

$$\left\langle \frac{\partial^{n_1} V(\phi_1)}{\partial \phi_1^{a_1} \dots \partial \phi_1^{a_{n_1}}} \frac{\partial^{n_2} V(\phi_2)}{\partial \phi_2^{b_1} \dots \partial \phi_2^{b_{n_2}}} \right\rangle = \frac{\partial^{n_1+n_2} C(\phi_1, \phi_2)}{\partial \phi_1^{a_1} \dots \partial \phi_1^{a_{n_1}} \partial \phi_2^{b_1} \dots \partial \phi_2^{b_{n_2}}}\,. \tag{2.2.3}$$

All non-vanishing elements have either n_1 and n_2 both odd, or both even. To simplify notation, we will from now on write derivatives as

$$\frac{\partial^n V(\phi)}{\partial \phi_1^{a_1} \dots \partial \phi_1^{a_n}} \equiv V_{a_1 \dots a_n}(\phi)\,. \tag{2.2.4}$$

In this chapter, we create random multifield potentials by generating Taylor coefficients at a single point in field space. The joint probability distribution of the Taylor

[6] In the bulk of this chapter, we focus exclusively on this simplest class of GRFs. However, in Appendix A.5 we briefly discuss a modified GRF that includes a large field-independent cosmological constant, cf. $\bar{V} \gg 1$.

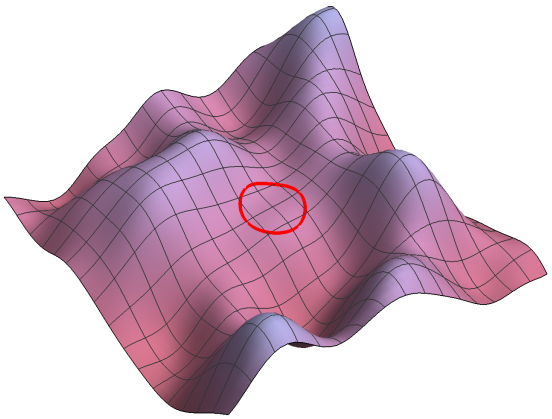

Fig. 2.1 An example of a GRF potential with $N_{\rm f} = 2$ and $n_{\rm max} = 175$. Here $\phi \in [-4\Lambda_{\rm h},\ 4\Lambda_{\rm h}]^2$ and inflation is supported near $\phi = 0$. The red circle delineates the region in which a potential truncated at fifth order approximates the full potential to per cent level accuracy.

coefficients is a multivariate normal distribution with a covariance matrix given by the derivatives of the covariance function at $\phi_1 = \phi_2$. Of course, not all the derivatives are independent, so we only generate the derivatives $V_{abc\ldots}$ with indices ordered such that $a \geq b \geq c$ et cetera. This ensures that all the unique, independent derivatives are included exactly once. If we collectively denote the independent Taylor coefficients of the potential (which includes V, V_a, V_{ab} et cetera) by V_α, where α runs over all the ordered sets of indices for the derivatives we include, the multivariate probability density function is given by

$$P(V_\alpha) = \frac{\exp\left(-\frac{1}{2}(V_\alpha - \mu_\alpha)(\Sigma^{-1})_{\alpha\beta}(V_\beta - \mu_\beta)\right)}{\sqrt{\det(2\pi\Sigma)}}\,, \tag{2.2.5}$$

where $\mu_\alpha = \langle V_\alpha \rangle$ is the expectation value vector and $\Sigma_{\alpha\beta} = \langle V_\alpha V_\beta \rangle$ is the covariance matrix.

Throughout this chapter (and just as in [23]), we will be working with a Gaussian covariance function,

$$C(\phi_1, \phi_2) = \Lambda_{\rm v}^8 e^{-(\phi_1 - \phi_2)^2/2\Lambda_{\rm h}^2}\,. \tag{2.2.6}$$

Here $\Lambda_{\rm v}$ sets the 'vertical energy scale' of the potential and the 'horizontal scale', $\Lambda_{\rm h}$, sets the correlation length of the potential. We are interested in studying models in which the potentials have structure on sub-Planckian scales, so we take $\Lambda_{\rm h} < M_{\rm P}$.

In section 2.2.3, we will discuss the physical interpretation of $\Lambda_{\rm v}$ and $\Lambda_{\rm h}$, and how potentials with the covariance function (3.1.2) may be regarded as proxies for Wilsonian effective field theories.

Schematically, our procedure for studying manyfield inflation in GRF potentials is as follows: we generate the potential locally in a domain of size $\Lambda_{\rm h}$ around $\phi = 0$,

$$V(\phi) = \sum_{n=0}^{n_{\rm max}} V_{a_1\ldots a_n} \frac{1}{n!}\phi^{a_1}\ldots\phi^{a_n} = \sum_{n=0}^{n_{\rm max}} \Lambda_{\rm v}^4 \tilde{V}_{a_1\ldots a_n} \frac{1}{n!}\frac{\phi^{a_1}}{\Lambda_{\rm h}}\ldots\frac{\phi^{a_n}}{\Lambda_{\rm h}}\,, \tag{2.2.7}$$

up to some order $n_{\rm max}$. Throughout this chapter we take $n_{\rm max} = 5$, unless otherwise specified. This ensures that the third derivatives of the potential, which are required to compute non-Gaussianities, are well-approximated and non-trivial within the domain.[7]

If all Taylor coefficients are chosen randomly according to the PDF of equation (3.2.3), the potential is typically much too steep to support inflation. However, by choosing a subset of the Taylor coefficients, V, V_{a_1} and $V_{a_1a_2}$, by hand and generating the remaining coefficients through the corresponding conditional PDF, we can construct multifield scalar potentials that are suitable for slow-roll inflation around $\phi = 0$, but have the random structure of a Gaussian random field away from this point. For example, with $N_{\rm f} = 100$ and $n_{\rm max} = 5$, we specify the $1 + 100 + 5,050 = 5,151$ first Taylor coefficients by hand, and generate the remaining 96,555,395 coefficients randomly by using the constrained PDF obtained from equation (3.2.3). We will refer to scalar potentials generated by this method as 'GRF potentials'.[8]

As we will discuss in detail in section 2.2.4, we choose the parameters V, V_{a_1} and $V_{a_1a_2}$ so that $\phi = 0$ is an approximately saddle-point of the potential with multiple fields with $m^2 \leq H^2$. The 'horizontal scale', $\Lambda_{\rm h}$, and the number of fields, $N_{\rm f}$, both have important effects on the generated model. Finally, $\Lambda_{\rm v}$ can be fixed from the normalisation of the primordial perturbations for each model. We will refer collectively to the set $(V, V_{a_1}, V_{a_1a_2}, N_{\rm f}, \Lambda_{\rm h})$ as the 'hyperparameters' of the GRF potentials.

For each of the potentials that we construct, we study how the fields evolve from the approximate saddle-point, assuming that the field initially 'rolls' slowly. Due

[7]With the covariance function given in (3.1.2), the dimensionless coefficients $\tilde{V}_\alpha$ at order n have rms-values ranging between 1 (all indices different) and $\sqrt{(2n-1)!!}$ (all indices the same). Since these increase slower than $n!$, the Taylor series converges as $n_{\rm max} \to \infty$. By going to high orders in the series, one can therefore construct a large potential landscape, cf. Figure 3.1. In this chapter, we focus on the inflationary phase in models with small field excursions (see below), for which an expansion to $n_{\rm max} = 5$ suffices.

[8]By the use of this phrase, we do not suggest that our class of models is unique: other covariance functions or field space geometries can lead to distinct ensembles of models. For the ease of presentation however, we will in this chapter refer to our models as 'the' GRF models.

to the randomness of the potentials, models with the same hyperparameters but different higher-order Taylor coefficients give rise to different inflationary trajectories, and consequently different numbers of e-folds of inflation. For models supporting at least 60 e-folds of inflation, we compute the evolution of the two-field and three-field correlation functions for the perturbations during inflation using the 'transport method' [79, 81, 153, 174], and we evaluate the predictions for observables of the models at the end of inflation (for the two-point statistics, our approach is exactly that of [77]).

By generating large numbers of inflationary models for each fixed set of hyperparameters that we are interested in, we can study the statistical predictions for the generation of cosmological observables in manyfield models of inflation. In particular, we compute the power spectrum of the primordial curvature perturbation, and, upon finding that it is typically well-fitted by a power-law over the scales that are constrained by observations of the Cosmic Microwave Background (CMB), we compute the values of the spectral index n_s and its running $\alpha_s = \mathrm{d}n_s/\mathrm{d}\ln k$, and in addition, the tensor-to-scalar ratio, r. Furthermore, from the two-field correlators, we study the co-evolution of the isocurvature and curvature perturbations during inflation. Finally, using the standard δN formula [31, 135, 172, 177, 183] and the three-point function of the fields, we compute the local non-Gaussianity parameter $f_{\mathrm{NL}} = f_{\mathrm{NL}}^{\mathrm{loc}}$.

We emphasise that we only study the generation of observables *during* the inflationary period, and we defer the study of the post-inflationary approach to the final vacuum and the reheating process to future studies.

2.2.2 A new, efficient, local construction of GRFs

Given the probability density function of equation (3.2.3), it might seem straightforward to just start generating the Taylor coefficients. However, the appearance of the inverse covariance matrix presents a significant complication which has curtailed previous attempts to the single-field or effectively single-field regimes [23, 144, 145]. Even with a sparse covariance matrix, as it is in our case, the inverse covariance matrix is in general hard to diagonalise, and grows rapidly in size as the number of fields is increased.

We here identify an algebraic property of the covariance matrix which allows us to circumvent this computational hurdle: Gaussian random fields with a Gaussian covariance function have the elegant property that if we know all the derivatives of the same type (even or odd) to some order, then the conditional covariance matrix for the Taylor coefficients at the next order of the same type is diagonal. This result holds to all orders and for any number of fields. This means that all the Taylor coefficients can be generated in a step-by-step fashion as a set of *independent* Gaussian random

variables, without inverting or diagonalising any matrices at all. In practice, the only large matrices that need to be constructed explicitly are those that are used to calculate shifts in the expectation values of higher-order derivatives, caused by fixing the lower-order derivatives. These matrices are sparse and require little memory to be used. All together, this makes it rather easy to construct the GRF potentials even for a very large number of fields, e.g. $N_{\rm f} = 100$. In fact, this method shifts the computational bottle-neck for studying manyfield inflation in GRF potentials from generating the potential to solving the equations of motions during inflation.

To provide some practical intuition for this method, we here illustrate it by looking at the covariance matrices in the case of $N_{\rm f} = 2$. It is straightforward to check that the covariances vanish between odd and even derivatives for any stationary, isotropic covariance function. The covariance matrix then becomes block diagonal, and we can treat the odd and even derivatives separately. We will therefore look at the potential, Hessian, and fourth derivatives in this case, which is the simplest non-trivial example.

Suppose we have a collection of non-independently distributed Gaussian random variables, Z. If we split them into two parts, they follow the distribution

$$\begin{bmatrix} Z_1 \\ Z_2 \end{bmatrix} \sim N\left(\begin{bmatrix} \mu_1 \\ \mu_2 \end{bmatrix}, \begin{bmatrix} \Sigma_{11} & \Sigma_{12} \\ \Sigma_{21} & \Sigma_{22} \end{bmatrix} \right) , \tag{2.2.8}$$

where (μ_1, μ_2) is the mean vector and Σ_{ij} are block components of the covariance matrix. In our construction, Z_1 will correspond to lower-order Taylor coefficients, and Z_2 to higher-order coefficients in an iterative way which we will make clear below. We may fix the lower-order coefficients by hand (as we will do for the hyperparameters $\tilde{V}$, $\tilde{V}_{a_1}$ and $\tilde{V}_{a_1 a_2}$ in our construction of inflationary potentials), or by randomly generating them from their marginal probability distribution (as we will do for Taylor coefficients of order three or more). The latter case is greatly simplified by the Gaussianity of the distribution: the marginal probability distribution of a subsystem of Gaussian variables (cf. the lower-order coefficients) is simply obtained by truncating the full covariance matrix and mean vector to the variables of the subsystem. For example, the marginal probability distribution of Z_1 obtained from equation (2.2.8) is simply $Z_1 \sim N(\mu_1, \Sigma_{11})$. If we then fix $Z_1 = z_1$, the conditional probability distribution for the remaining variables Z_2 is another multivariate Gaussian distribution given by

$$Z_2 \sim N\left(\mu_2 + \Sigma_{21}\Sigma_{11}^{-1}(z_1 - \mu_1), \Sigma_{22} - \Sigma_{21}\Sigma_{11}^{-1}\Sigma_{12}\right) . \tag{2.2.9}$$

We now want to write down the covariance matrices for the potential and its second and fourth derivatives at $\phi = 0$. For convenience, we here work with the dimensionless fields, $\phi/\Lambda_{\mathrm{h}}$, and the dimensionless potential, V/Λ_{v}^4. By taking the appropriate derivatives of the covariance function, we find that the covariance matrix for the potential, second and fourth derivatives is given by

$$\Sigma = \left(\begin{array}{c|cccc|ccccc} 1 & -1 & 0 & -1 & 3 & 0 & 1 & 0 & 3 \\ \hline -1 & 3 & 0 & 1 & -15 & 0 & -3 & 0 & -3 \\ 0 & 0 & 1 & 0 & 0 & -3 & 0 & -3 & 0 \\ -1 & 1 & 0 & 3 & -3 & 0 & -3 & 0 & -15 \\ \hline 3 & -15 & 0 & -3 & 105 & 0 & 15 & 0 & 9 \\ 0 & 0 & -3 & 0 & 0 & 15 & 0 & 9 & 0 \\ 1 & -3 & 0 & -3 & 15 & 0 & 9 & 0 & 15 \\ 0 & 0 & -3 & 0 & 0 & 9 & 0 & 15 & 0 \\ 3 & -3 & 0 & -15 & 9 & 0 & 15 & 0 & 105 \end{array}\right), \tag{2.2.10}$$

where the first row/column is for the potential, the following three are for the $(1,1)$, $(2,1)$ and $(2,2)$ components of the Hessian, and the final five are for the components of the fourth derivatives in the order $(1,1,1,1)$, $(2,1,1,1)$, et cetera.

Fixing the zeroth order Taylor coefficient $\tilde{V}$ and using equation (2.2.9), the covariance matrix for the remaining variables becomes

$$\Sigma' = \left(\begin{array}{ccc|ccccc} 2 & 0 & 0 & -12 & 0 & -2 & 0 & 0 \\ 0 & 1 & 0 & 0 & -3 & 0 & -3 & 0 \\ 0 & 0 & 2 & 0 & 0 & -2 & 0 & -12 \\ \hline -12 & 0 & 0 & 96 & 0 & 12 & 0 & 0 \\ 0 & -3 & 0 & 0 & 15 & 0 & 9 & 0 \\ -2 & 0 & -2 & 12 & 0 & 8 & 0 & 12 \\ 0 & -3 & 0 & 0 & 9 & 0 & 15 & 0 \\ 0 & 0 & -12 & 0 & 0 & 12 & 0 & 96 \end{array}\right), \tag{2.2.11}$$

where we note that the 3-by-3 block matrix in the upper-left corner, corresponding to the three independent components of $\tilde{V}_{a_1 a_2}$, has become diagonal. This is the conditional covariance matrix for the second derivatives. Fixing $\tilde{V}_{ab}$ (either by hand or randomly, by generating three independent Gaussian variables) in addition to $\tilde{V}$, we

find that the covariance matrix for the fourth derivatives is given by

$$\Sigma'' = \begin{pmatrix} 24 & 0 & 0 & 0 & 0 \\ 0 & 6 & 0 & 0 & 0 \\ 0 & 0 & 4 & 0 & 0 \\ 0 & 0 & 0 & 6 & 0 \\ 0 & 0 & 0 & 0 & 24 \end{pmatrix}, \tag{2.2.12}$$

which again is diagonal. Generating the fourth derivatives randomly now simply involves generating five independent Gaussian random numbers. Note in particular that to construct the Taylor coefficients up to fourth order, we are never required to invert or diagonalise the full covariance matrix. This is the key realisation that allows us to commence the study of manyfield inflation in GRF potentials.

The method illustrated here extends to arbitrary $N_{\rm f}$ and to all orders in the Taylor expansion. The general formulae for these covariance matrices and the matrices that shift the expectation values can be found in Chapter 3, where the details and a general proof of this method will be presented separately.

2.2.3 Physical properties of GRF potentials

It is important to note that physical effective field theories supporting manyfield inflation may differ substantially in many details from the mathematically simple GRF models that we study. For example, EFTs with many light fields may reflect the imprints of broken symmetries, such as supersymmetry or axionic shift symmetries for some of the fields. It then appears reasonable to expect that some of the GRF estimates (e.g. of the fine-tuning of manyfield inflationary models) may differ from that of a physically motivated manyfield theory. However, it is still possible for GRF models of manyfield inflation to be sufficiently complex to capture non-trivial multifield dynamics, and can provide access to 'universal' or robust aspects of manyfield models, if they exist. Motivated by this, our approach here is to engineer manyfield models of slow-roll saddle-point inflation using GRFs, and to search for mechanisms that determine the distribution of observables.

To understand the properties of the class of potentials that we study, it is important to characterise the various energy scales that are associated with them. In this subsection, we discuss the distribution of the slow-roll parameters and the typical scale of higher-order terms in the potential. We furthermore discuss the conditions under which GRF potentials may be interpreted as proxies for physical effective field theories.

Finally, we point out that the mass distribution of GRF potentials is broad compared to the Hubble scale. This raises an additional challenge for using these potentials to study multifield inflation.

Distributions of the parameters of the potential

The value of the potential:

The GRF potentials have mean zero and typically take values in the 1σ range between $-\Lambda_{\rm v}^4$ and $\Lambda_{\rm v}^4$. For the models of inflation that we consider in the bulk of this chapter, we take the dimensionless parameter $\tilde{V} = 1$, so that $V = \Lambda_{\rm v}^4\,(1 + \mathcal{O}(\phi/\Lambda_{\rm h}))$. The hyperparameter $\Lambda_{\rm v}$ then sets the energy scale of inflation. During slow-roll inflation close to the approximate saddle-point at $\phi = 0$, the square of the Hubble parameter is then given by

$$H^2 = \frac{1}{3}\frac{\Lambda_{\rm v}^4}{M_{\rm P}^2}\,. \tag{2.2.13}$$

The gradient:

The typical magnitude of the gradient vector is most easily characterised in terms of the inflationary slow-roll parameter,

$$\epsilon_V = \frac{M_{\rm P}^2}{2}\frac{\partial^a V \partial_a V}{V^2} = \frac{1}{2}\frac{M_{\rm P}^2}{\Lambda_{\rm h}^2}\tilde{V}^a\tilde{V}_a\,. \tag{2.2.14}$$

For the theory defined by equation (3.1.2), the covariance of the dimensionless Taylor coefficients $\tilde{V}_a$ is given by

$$\langle \tilde{V}_a \tilde{V}_b \rangle = \delta_{ab}\,, \tag{2.2.15}$$

so the typical value of the slow-roll parameter ϵ_V is given by

$$\langle \epsilon_V \rangle = 2N_{\rm f}\left(\frac{M_{\rm P}}{\Lambda_{\rm h}}\right)^2 \gg 1\,. \tag{2.2.16}$$

At a typical point in field space, the potential is then too steep to support slow-roll, slow-turn inflation. Since the Taylor coefficients $\tilde{V}_a$ are $N_{\rm f}$ independent Gaussian variables, the probability of ϵ_V being no larger than some value $\epsilon_\star$ is given by [23],

$$P(\epsilon_V \leq \epsilon_\star) = \frac{1}{(\sqrt{2\pi})^{N_{\rm f}}}\int_{|\mathbf{x}|\leq\sqrt{2\epsilon_\star}\Lambda_{\rm h}/M_{\rm P}} d^{N_{\rm f}}x\, e^{-x^2/2} \simeq \frac{2}{N_{\rm f}\,\Gamma(\frac{N_{\rm f}}{2})}\left(\sqrt{\epsilon_\star}\frac{\Lambda_{\rm h}}{M_{\rm P}}\right)^{N_{\rm f}}\,. \tag{2.2.17}$$

Obtaining a small ϵ_V parameter requires tuning of the slope of the potential, and this tuning becomes more severe as $\Lambda_{\rm h}$ is decreased from $M_{\rm P}$. Note however that equation (2.2.17) gives the probability of a randomly chosen point having a small ϵ_V parameter, not the probability that a point with a small ϵ_V parameter exists in the field space. The latter probability depends on the volume of field space, which we do not model in this chapter.

The Hessian matrix:

The Hessian matrix, V_{ab}, determines the curvature of the potential and its eigenvalues are the squared masses of the fields. From the covariance function (3.1.2) it is easy to see that the dimensionless Hessian has zero mean and a covariance given by

$$\langle \tilde{V}_{ab}\tilde{V}_{cd}\rangle = \Big(\delta_{ab}\delta_{cd} + \delta_{ac}\delta_{bd} + \delta_{ad}\delta_{bc}\Big)\,. \tag{2.2.18}$$

The probability distribution for the Hessian (with all other Taylor coefficients marginalised over), can then be obtained by inverting the covariance matrix $\Sigma_{(ab)(cd)} \equiv \langle \tilde{V}_{ab}\tilde{V}_{cd}\rangle$ to find

$$\left(\Sigma^{-1}\right)_{(ab)(cd)} = -\frac{1}{2(N_{\rm f}+2)}\delta_{ab}\delta_{cd} + \delta_{ac}\delta_{bd} - \frac{1}{2}\delta_{ad}\delta_{bc}\,. \tag{2.2.19}$$

The marginal probability distribution is then given by [44]

$$P(\tilde{V}_{ab}) = C_{\rm n}\exp\left(-\frac{1}{4}\left(\tilde{V}_{ab}\tilde{V}_{ba} - \frac{1}{N_{\rm f}+2}(\tilde{V}_{aa})^2\right)\right). \tag{2.2.20}$$

Here $C_{\rm n}$ is a normalisation factor.

To elucidate the consequences of this probability distribution, it is useful to consider the large-$N_{\rm f}$ limit in which an eigenvalue density can easily be derived. We will denote the physical squared masses by m_a^2 and work with the dimensionless eigenvalues λ_a of $\tilde{V}_{ab}$:

$$m_a^2 = \frac{\Lambda_{\rm v}^4}{\Lambda_{\rm h}^2}\,\lambda_a\,. \tag{2.2.21}$$

To derive the eigenvalue density, we change variables from $\tilde{V}_{ab}$ to its eigenvalues and eigenvectors, and integrate out the latter. Importantly, the probability distribution of the eigenvalues involves the Vandermonde determinant arising from the change of measure,

$$\prod_{a\leq b} d\tilde{V}_{ab} \sim \prod_{a<b}|\lambda_a - \lambda_b| \prod_{a=1}^{N_{\rm f}} d\lambda_a\,. \tag{2.2.22}$$

The Vandermonde determinant encodes the 'eigenvalue repulsion' which is the key driver behind the large-$N_{\rm f}$ universality encountered in random matrix theory (see e.g. [72, 90, 124]). The appearance of the Vandermonde determinant in the probability distribution for the Hessian matrix of GRF potentials is indicative of the close connection between random function theory and random matrix theory. We will return to this connection towards the end of this section, and then again in section 2.4.

By using the eigenvalue density function,

$$\rho(\lambda) = \frac{1}{N_{\rm f}} \sum_{a}^{N_{\rm f}} \delta(\lambda - \lambda_a)\,, \tag{2.2.23}$$

the probability distribution for the eigenvalues can be expressed as

$$P(\rho) = C_{\rm n} \exp\Bigg[-\frac{N_{\rm f}}{4}\bigg(\int d\lambda \lambda^2 \rho(\lambda) - \bigg(\int d\lambda \lambda \rho(\lambda) \bigg)^2 \bigg) + \frac{{N_{\rm f}}^2}{2} \int d\lambda d\lambda' \rho(\lambda)\rho(\lambda') \ln(|\lambda - \lambda'|) \Bigg]\,. \tag{2.2.24}$$

The typical distribution of the eigenvalues of the dimensionless Hessian matrix can be found from saddle-point evaluation of equation (2.2.24). This gives [44]

$$\rho_{sc}(\lambda) = \frac{1}{2\pi N_{\rm f}} \sqrt{4N_{\rm f} - (\lambda - \bar{\lambda})^2}\,. \tag{2.2.25}$$

For $\bar{\lambda} = 0$, this spectrum is precisely a Wigner semi-circle, i.e. the spectrum of the Gaussian Orthogonal Ensemble (GOE) of random symmetric matrices with independent, Gaussianly distributed entries. For $\bar{\lambda} \neq 0$, the semi-circle is rigidly shifted to be centred at $\bar{\lambda}$ [44].

To properly understand the significance of the shift $\bar{\lambda}$, it is instructive to calculate the conditional probability distribution of the Hessian, given that the potential has a certain value, say $V = V_\star$. The Hessian matrix and the value of the potential are correlated, and upon using equation (2.2.9) for the conditional probability distribution, we find the moments [23, 44]

$$\langle \tilde{V}_{ab} \rangle \Big|_{V=V_\star} = -\frac{V_\star}{\Lambda_{\rm v}^4}\, \delta_{ab}\,, \tag{2.2.26}$$

$$\langle \tilde{V}_{ab} \tilde{V}_{cd} \rangle \Big|_{V=V_\star} - \big(\langle \tilde{V}_{ab} \rangle \langle \tilde{V}_{cd} \rangle \big) \Big|_{V=V_\star} = \Big(\delta_{ac}\delta_{bd} + \delta_{ad}\delta_{bc} \Big)\,. \tag{2.2.27}$$

According to equation (2.2.27), every unique element of the Hessian is now statistically independent of the others, and we can write the Hessian as [23]

$$V_{ab} = \frac{\Lambda_{\rm v}^4}{\Lambda_{\rm h}^2}\left(-\frac{V_\star}{\Lambda_{\rm v}^4}\,\delta_{ab} + R_{ab}\right)\,, \tag{2.2.28}$$

where R_{ab} is a random matrix in the Gaussian Orthogonal Ensemble (GOE). The spectrum of the dimensionless Hessian is then given by,

$$\rho_{sc}(\lambda) = \frac{1}{2\pi N_{\rm f}}\sqrt{4N_{\rm f} - (\lambda + V_\star/\Lambda_{\rm v}^4)^2}\,. \tag{2.2.29}$$

Clearly, for points with vanishing vacuum energy, $V_\star = 0$, the spectrum of the Hessian is precisely that captured by the Wigner semi-circle. For $V_\star > 0$, which is the case relevant for inflation, the typical spectrum is a semi-circle rigidly shifted downwards, making comparatively more eigenvalues tachyonic. However, for $V_\star = \Lambda_{\rm v}^4$ and $N_{\rm f} \gg 1$, this shift is small: the endpoints of the semi-circle spectrum of R_{ab} are located at $\pm 2\sqrt{N_{\rm f}}$, and the spectrum of V_{ab} is a shifted semi-circle with endpoints at $(\pm 2\sqrt{N_{\rm f}} - 1)\Lambda_{\rm v}^4/\Lambda_{\rm h}^2$.

We define the slow-roll η_V parameter as

$$\eta_V = M_{\rm P}^2\frac{m_{\rm min}^2}{V}\,, \tag{2.2.30}$$

with $m_{\rm min}^2$ denoting the smallest eigenvalue of the Hessian matrix. An immediate consequence of equation (2.2.28) is that η_V tends to be very large and negative for the typical, slightly shifted semi-circle spectrum [23]:

$$\eta_V = -(2\sqrt{N_{\rm f}} + 1)\left(\frac{M_{\rm P}}{\Lambda_{\rm h}}\right)^2\,. \tag{2.2.31}$$

Smaller magnitudes of η_V can be obtained if the spectrum of the Hessian is in a rare configuration in which no eigenvalue is very tachyonic. Given equation (2.2.28) for $V = V_\star$, the probability of $|\eta_V|$ being no larger than $|\eta_\star|$ is given by

$$P\left(|m_{\rm min}^2| < |\eta_\star|\frac{V_\star}{M_{\rm P}^2}\right) = P_{\rm GOE}\left(\lambda_{\rm min} > 1 + \eta_\star\frac{\Lambda_{\rm h}^2}{M_{\rm P}^2}\right)\,, \tag{2.2.32}$$

where $\lambda_{\rm min}$ denotes the smallest eigenvalue of the GOE matrix R, and $P_{\rm GOE}$ denotes its probability distribution. For $N_{\rm f} \gg 1$, the radius of the typical semi-circle configuration

is $2\sqrt{N_{\rm f}} \gg 1$, so that

$$P_{\rm GOE}\left(\lambda_{\rm min} > 1 + \eta_\star \frac{\Lambda_{\rm h}^2}{M_{\rm P}^2}\right) \approx P_{\rm GOE}\left(\lambda_{\rm min} > 1\right) = \exp\left(-c\, {N_{\rm f}}^2\right) , \tag{2.2.33}$$

where $c = \frac{1}{108}\left(35 + 16\sqrt{7} + 27\ln(18) - 54\ln\left(\sqrt{7}-1\right)\right) \approx 1.19$. In the last step we have used the fluctuation probability computed for the subset of 'fluctuated spectra' of the GOE with no negative eigenvalue [71]. Hence, small slow-roll parameters are very infrequent in GRF potentials with many fields.

We close this section by noting that the tight connection between our GRF models and random matrix ensembles also has strong implications for the distribution of vacua [23, 44]. Metastability of Minkowski and de Sitter critical points requires $m_{\rm min}^2 > 0$. According to the RMT analysis, such points are exceedingly rare:

$$P(m_{\rm min}^2 > 0 | V \geq 0) \leq P_{\rm GOE}(\lambda_{\rm min} \geq 0)\,. \tag{2.2.34}$$

The rarity of metastable de Sitter vacua is a common feature also of other classes of random potentials, such as random supergravity theories [23, 25, 141].

Equation (2.2.34) implies that the fraction of metastable de Sitter vacua in our GRF potentials is bounded from above by the probability of large fluctuations of one of the simplest random matrix ensembles. As a consequence, the frequency of metastable de Sitter vacua scales with $N_{\rm f}$ like $\ln(P_{\rm GOE}) \sim -{N_{\rm f}}^2$. Recently however, the authors of [88] (see also [23]) found that vacua in GRF potentials comprise a fraction of $\sim \exp\left(-\alpha N_{\rm f}\right)$ of all critical points of GRFs (for some constant α), which far exceeds the metastability estimate of (2.2.34). This apparent discrepancy is resolved by noting that the vast majority of the metastable vacua found in [88] are located deep down in the potential, at $V \lesssim -2\sqrt{N_{\rm f}}\Lambda_{\rm v}^4$, in our mean-zero GRF models.[9] For such large and negative values of the potential, the semi-circle spectrum is rigidly shifted upwards so that metastability is common. Due to the simple relation of equation (2.2.28) (and its generalisation for other covariance functions), any carefully phrased question about the vacuum statistics in GRF models map into precise questions about the eigenvalue statistics of random matrices.

[9] The analogous result in random supergravities is that most metastable de Sitter vacua realised in the 'approximately supersymmetric' regime [23, 141]. Note however, that known constructions of de Sitter string compactifications tend to rely on non-random 'structures' to enhance the probability of metastability (see e.g. [6, 42, 63, 84, 91, 100, 113, 143, 171, 188]). Thus it is certainly possible that the simple GRF models may capture some rather robust aspects of manyfield inflation in fundamental theory, but fail to accurately describe their vacuum structure.

Cubic and higher-order terms:

GRF potentials have non-trivial, randomly generated interaction terms at cubic and higher orders. At order n, these are of the order of

$$V_{a_1 \ldots a_n} \sim \frac{\Lambda_{\rm v}^4}{\Lambda_{\rm h}^n} \,. \tag{2.2.35}$$

In particular, each of the cubic order terms are then of the order of

$$V_{abc} \sim \frac{\Lambda_{\rm v}^4}{\Lambda_{\rm h}^3} \sim \frac{H^2 M_{\rm P}^2}{\Lambda_{\rm h}^3} \sim \left(\frac{\Lambda_{\rm v}}{\Lambda_{\rm h}}\right)^2 \left(\frac{M_{\rm P}}{\Lambda_{\rm h}}\right) H \,. \tag{2.2.36}$$

The vertical scale $\Lambda_{\rm v}$ factors out of the evolution equations for both the background and the perturbations and only serves as a normalisation factor for the scale of the scalar perturbations. We find in all cases that $(\Lambda_{\rm v}/\Lambda_{\rm h})^2 < \Lambda_{\rm h}/M_{\rm P}$, and the cubic terms of equation (2.2.36) tend to be smaller than H in the models that we consider. However, since $\Lambda_{\rm v}$ does not affect the field equations, it also does not affect our predictions for the spectral index, its running, or the local non-Gaussianity parameter, $f_{\rm NL}$. Consequently, the predictions of our models also apply to models in which $V_{abc} \approx H$, but for which the amplitude of the scalar perturbations is larger than the observationally inferred value.[10]

GRF potentials and physical effective field theories

Gaussian random fields provide a mathematically convenient construct, but are not directly derived as effective field theories (EFTs) from particle physics or string theory.[11] In this section, we discuss how the GRF potentials exhibit some 'EFT-like' properties with important consequences for the cosmology. Relatedly, we note that these potential naturally have spread-out mass spectra, and additional tuning is required to construct models with non-trivial multifield dynamics.

In quantum field theory, unprotected dimensionful operators are naturally large. For the UV cutoff Λ, the potential is typically of the order of $V \sim H^2 M_{\rm P}^2 \sim \Lambda^4$, and the scalar masses are of order $m^2 \sim \Lambda^2 \sim H M_{\rm P} \gg H^2$ (cf. equation (2.1.1)). In the GRF potentials considered in this chapter, cf equation (2.2.7), the scale Λ is replaced

[10] Another way to achieve a relative enhancement of the cubic terms with respect to the Hubble parameter is to set the zeroth order Taylor coefficient much below its rms value: $\tilde{V} \ll 1$. This however makes the fine-tuning required to achieve small slow-roll parameters more severe.

[11] Simple GRFs can under certain assumptions be related to the potentials of multi-axion theories [24].

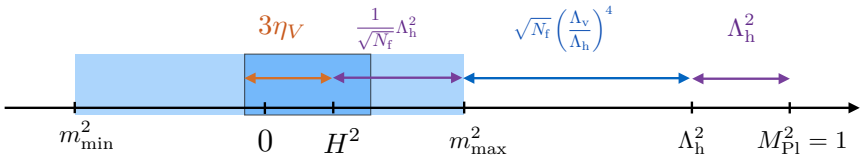

Fig. 2.2 Schematic illustration of the relevant energy scales of the GRF potentials. The light blue shaded region indicates the equilibrium spectrum of the Hessian; the darker region corresponds to our chosen 'flat spectrum' initial condition.

by the two parameters Λ_v and Λ_h. The horizontal scale Λ_h sets the coherence length of the potentials, and can be interpreted as the UV-cutoff of the theory. Since all operators are suppressed by the same cut-off scale, sharp features over distances $\ll \Lambda_h$ are very rare. We expect this to be a general feature of models with generic interactions suppressed by a single, common cut-off scale.

The parameter Λ_v sets the natural energy scale of the GRF models. During inflation, a consistent EFT interpretation requires $H^2 \ll \Lambda_h^2$. If reheating proceeds rapidly after the end of inflation, the stronger condition of $V \sim \Lambda_v^4 \sim T_{rh}^4 \ll \Lambda_h^4$ applies. By taking $\Lambda_v < \Lambda_h$, even the latter condition is generically satisfied. A Wilsonian EFT is obtained by integrating out states more massive than the UV cutoff, leaving only states with $m^2 \leq \Lambda^2$. Consequently, in the context of GRF potentials, we expect the eigenvalues of the Hessian matrix to be no larger than $\sim \Lambda_h^2$. For $\Lambda_v < \Lambda_h$, this condition is satisfied unless N_f is very large:

$$\frac{m^2_{max}}{\Lambda_h^2} \approx \left(2\sqrt{N_f} - 1\right) \frac{\Lambda_v^4}{\Lambda_h^4} \,. \tag{2.2.37}$$

Figure 2.2 illustrates the relevant energy scales of GRF potentials discussed in this chapter.

We now note a serious obstacle for using GRF potentials to study multifield inflation: the mass spectrum is generically spread out over energy scales $\gg H$. This is immediately evident from the width of the (shifted) Wigner semi-circle distribution, which predicts a typical eigenvalue spacing for the Hessian of

$$\frac{\frac{1}{N_f}\left(m^2_{max} - m^2_{min}\right)}{H^2} = 12 \frac{1}{\sqrt{N_f}} \left(\frac{M_P}{\Lambda_h}\right)^2 \,. \tag{2.2.38}$$

For $\Lambda_h < M_P$, this then implies that only systems with a very large number of fields, $N_f \gtrsim (M_P/\Lambda_h)^4$, can be expected to exhibit non-trivial multiple field effects. This large spread in the masses explains why recent attempts at using GRFs to study multiple-field inflation [144] have only captured single-field dynamics. To use these

models to study non-trivial multifield dynamics, one has to further tune the initial conditions.

The particular $N_{\rm f}$ dependence of equation (2.2.38) follows from the form of the covariance function, cf. equation (3.1.2). The width of the eigenvalue distribution may be changed by modifying the covariance function, e.g. to $C(\phi_1-\phi_2) = N_{\rm f}\Lambda_{\rm v}^8 e^{-(\phi_1-\phi_2)^2/2N_{\rm f}\Lambda_{\rm h}^2}$, which gives an $N_{\rm f}$ independent eigenvalue distribution of the Hessian, and an additional suppression by $1/\sqrt{N_{\rm f}}$ in equation (2.2.38). However, such a modified covariance function enhances the effective coherence length of the potential to $\sqrt{N_{\rm f}}\Lambda_{\rm h}$, which becomes super-Planckian for large $N_{\rm f}$.[12]

The broad spread in the distribution of masses of GRF potentials is not surprising as these models do not incorporate protective approximate symmetries (e.g. broken supersymmetry, or approximate shift-symmetries), which can lower the natural scale of dimensionful operators, and make inflation less fine-tuned. It would be interesting to extend our method to construct manyfield models of inflation in random supergravity models with spontaneously broken supersymmetry, following the ideas proposed in [23, 25, 141].

2.2.4 The statistical ensembles of models

As discussed in section 2.2.1, the hyperparameters of our GRF potentials are:

$$(\tilde{V}, \tilde{V}_a, \tilde{V}_{ab}, N_{\rm f}, \Lambda_{\rm h}, \Lambda_{\rm v})\,. \tag{2.2.39}$$

An understanding of pre-inflationary physics in fundamental theory could potentially provide us with prior probability distributions on these parameters. Lacking such priors, we compute the observational predictions for certain ranges of the hyperparameters, and investigate how these predictions change as hyperparameters are varied.

Specifically, we construct ensembles of manyfield models of inflation as follows: First, we set $\tilde{V}$ to its rms value, $\tilde{V} = 1$, so that $\Lambda_{\rm v}$ sets the scale of the potential at $\phi = 0$. In slow-roll inflation, the parameter $\Lambda_{\rm v}$ has no effect on the equations of motion for either the background field or the perturbations around it. We exploit this by evolving each model with a fiducial value of $\Lambda_{\rm v}$ and, for each model yielding

[12] This lesson applies somewhat more generally: the width of the mass spectrum relative H^2 is controlled by $C^{(4)}(0)/C(0)$. Compressing the spectrum requires decreasing this ratio, but for many covariance functions $C^{(p)}(0)/C(0) \sim (C^{(4)}(0)/C(0))^{p/4}$, and an overall suppression of these ratios translates directly into an increased coherence length. Compressing the mass scale while keeping the coherence scale associated with the interaction terms fixed then requires covariance functions with multiple scales. We will not consider such modifications further in this chapter.

a sufficiently long period of inflation, rescale $\Lambda_{\rm v}$ at the end of inflation so that the amplitude of the primordial curvature perturbation at the 'pivot scale' is consistent with the value determined by the Planck experiment [10].[13] This fixes $\Lambda_{\rm v}$ separately for each model.

To obtain sufficiently flat potentials that support inflation, the gradient and Hessian have to be tuned. We set $\tilde{V}_a$ so that ϵ_V is sufficiently small that models with at least 60 e-folds of inflation are not too infrequent. This leads us explore values of ϵ_V in the range of 2×10^{-8} to 10^{-11}. We henceforth take

$$\epsilon_{\rm i} \equiv \epsilon_V\Big|_{\phi=0} , \tag{2.2.40}$$

to parameterise the magnitude of the gradient vector. The vector $\tilde{V}_a$ obviously also has a direction, and we explore the effect of its alignment relative to the eigenvectors of $\tilde{V}_{ab}$, as we now discuss.

We have seen in section 2.2.3 that the curvature of the potential needs to be tuned to give rise to sustained inflation and multifield dynamics. In particular, the smallest eigenvalue of the Hessian, which we parametrise by

$$\eta_{\rm i} \equiv \eta_V\Big|_{\phi=0} , \tag{2.2.41}$$

must be close to zero. We numerically investigate values of $\eta_{\rm i}$ in the range -10^{-1} to -10^{-4}. To explore the non-generic spectra relevant for multifield inflation, we consider two (non-random) initial conditions for the spectrum of V_{ab}:

$$\begin{array}{lll} \text{Flat spectrum :} & m_a^2\big|_{\phi=0} : & \text{Uniformly distributed in } \left(3\eta_{\rm i}H^2,\ \tfrac{9}{4}H^2\right) , \\ \text{Compressed spectrum :} & m_a^2\big|_{\phi=0} : & \text{Uniformly distributed in } \left(3\eta_{\rm i}H^2,\ -3\eta_{\rm i}H^2\right) . \end{array} \tag{2.2.42}$$

Field perturbations with an effective squared mass greater than $9H^2/4$ are exponentially suppressed already at horizon exit.[14] This motivates the upper bound of the 'flat spectrum'. The (extremely) compressed, nearly degenerate spectrum is specifically chosen to maximise the chances of non-trivial multifield effects, and is included for

[13] To identify the precise e-fold at which the pivot scale crossed the horizon during inflation requires a detailed modelling of the reheating phase (cf. [134] for a review). For the baseline parameters, we find that the pivot scale exited the horizon $58 - N_{\rm rh}$ e-folds before the end of inflation, where $N_{\rm rh}$ parametrises the expansion between the end of inflation and the onset of the hot big bang. For concreteness, we will assume throughout this chapter that the pivot scale crossed the horizon 55 e-folds before the end of inflation.

[14] More precisely, the effective squared masses of the perturbations are the eigenvalues of the matrix $M_{ab} = V_{ab} - \frac{1}{a^3}\partial_t\left(a^3\frac{\dot{\phi}_a\dot{\phi}_b}{H}\right)$ [58, 152] .

reasons that will become apparent in section 2.5. We note that these initial spectra will 'relax' to the generic spectrum for a GRF over distances of $\sim \mathcal{O}(\Lambda_{\rm h})$. During most of inflation, the field is slowly rolling and this relaxation is very slow in e-fold 'time', but we will see that towards the end of inflation, multiple fields develop tachyonic masses, $m_a^2 < 0$.

We now return to the question of the relative alignment of V_a with the eigenvectors of V_{ab}. In a Gaussian random field the gradient and Hessian are uncorrelated, $\langle V_a V_{ab}\rangle = 0$, and generically, V_a has support along all eigenvectors of V_{ab}. However, slow-roll inflation makes the field follow the gradient descent along the potential, which tends to quickly align V_a with the smallest eigenvalue direction of the Hessian matrix, which we will denote by '1' (for a more detailed discussion on this, see e.g. [78]). Motivated by this, we consider two classes of orientations of V_a:

$$\begin{aligned} &\text{Random}: && V_a\Big|_{\phi=0} \sim \sqrt{2\epsilon_{\rm i}}\,\tfrac{\Lambda_{\rm v}^4}{M_{\rm P}}\,\text{Uniform}\left(S^{N_{\rm f}-1}\right)\,, \\ &\text{Aligned}: && V_a\Big|_{\phi=0} = \sqrt{2\epsilon_{\rm i}}\,\tfrac{\Lambda_{\rm v}^4}{M_{\rm P}}\,\delta_{a\,1}\,. \end{aligned} \tag{2.2.43}$$

With the initial conditions $(\tilde{V}, \tilde{V}_a, \tilde{V}_{ab})$ fixed, we generate the higher-order Taylor coefficients randomly using the conditional PDFs derived as discussed in section 2.2.2.

Finally, we explore the numerically accessible a range of values for the remaining hyperparameters $N_{\rm f}$ and $\Lambda_{\rm h}$: for $N_{\rm f}$ very large or $\Lambda_{\rm h}$ small, inflation is only supported if the slow-roll parameters are highly tuned, which can cause numerical accuracy problems.[15] A summary of the hyperparameter choices that we explore in this chapter can be found in Appendix A.2. Some of our results are best illustrated for a fixed choice of parameter. We take as our baseline model

$$\textbf{Baseline:}\ N_{\rm f} = 10\,,\quad \Lambda_{\rm h} = 0.4 M_{\rm P}\,,\quad \epsilon_{\rm i} = 2\times 10^{-9}\,,\quad \eta_{\rm i} = -10^{-4}\,, \tag{2.2.44}$$

with the flat spectrum of the Hessian, cf. equation (2.2.42), and a randomly directed gradient vector. For this choice of hyperparameters, obtaining at least 60 e-folds of inflation is not uncommon, and $N_{\rm f}$ is sufficiently large for multifield effects to be clearly manifest.

[15] The computations reported in this chapter did not require supercomputer capabilities, but potentials with $N_{\rm f} \gg 1$ places some restrictions on memory access. Our largest simulations ran on a computing system with 144 CPUs and 516 GB RAM.

2.2.5 Method: background

Given a randomly generated multifield potential, we evolve the fields numerically using the coupled Klein-Gordon and Friedmann-Robertson-Walker equations,

$$\ddot{\phi}^a + 3H\dot{\phi}^a = -\partial^a V \ , \quad H^2 = \frac{\frac{1}{2}\dot{\phi}^a\dot{\phi}_a + V}{3M_{\rm P}^2} \, . \tag{2.2.45}$$

In the slow-roll approximation that we use throughout this chapter, these equations become

$$3H\dot{\phi}^a = -\partial^a V \ , \quad H^2 = \frac{V}{3M_{\rm P}^2} \, . \tag{2.2.46}$$

Expressed with respect to the number of e-folds, N, the slow-roll Klein-Gordon equation is simply given by

$$\frac{d\phi^a}{dN} = -\partial^a \ln V \, . \tag{2.2.47}$$

Equation (2.2.47) makes it clear that the vertical scale, $\Lambda_{\rm v}$, has no impact on the background field evolution in slow-roll.

2.2.6 Method: perturbations

To calculate the observational predictions of the manyfield models of inflation, we use the 'transport method' [79, 81, 153, 174] (see also [21, 83, 154, 170, 173]). This formalism allows us to evolve the two-field and three-field correlators on superhorizon scales from horizon crossing to the end of inflation.[16] Analytic solutions for this method exist for certain potentials, just like in the δN formalism, but the main advantage of it is that it allows for accurate and efficient numerical solutions, regardless of the form of the potential. In this subsection, we briefly review the key elements of the transport method. We furthermore recall how multifield dynamics can cause the curvature perturbation to evolve on superhorizon scales, and we define the isocurvature and curvature correlators. We close this section by briefly reviewing the δN formula for the non-Gaussianity amplitude $f_{\rm NL}$.

[16] The transport method can be applied to both slow-roll and non-slow-roll systems, and also on sub-horizon scales [153]. For our purposes, it suffices to consider the superhorizon evolution of the field perturbations during slow-roll inflation.

The transport method

In the spatially flat gauge, we can write the perturbations at the end of inflation as an expansion in the perturbations at horizon exit:

$$\delta\phi^a = \Gamma^a{}_b \delta\phi^b_\star + \frac{1}{2}\Gamma^a{}_{bc}\delta\phi^b_\star\delta\phi^c_\star + ... \tag{2.2.48}$$

where the horizon exit perturbations have been marked with a $\star$. Using the separate-universe approach [132, 185], we expand the slow-roll, slow-turn equations of motion, equation (2.2.47), around the background trajectory to obtain evolution equations for $\delta\phi^a$. It is then easy to see that the 'propagators' $\Gamma^a{}_b$ and $\Gamma^a{}_{bc}$ must obey the differential equations

$$\frac{d\Gamma^a{}_b}{dN} = u^a{}_c\Gamma^c{}_b\,, \tag{2.2.49}$$

$$\frac{d\Gamma^a{}_{bc}}{dN} = u^a{}_d\Gamma^d{}_{bc} + u^a{}_{de}\Gamma^d{}_b\Gamma^e{}_c\,, \tag{2.2.50}$$

where

$$u^a{}_b = -\partial^a\partial_b \ln V\,, \tag{2.2.51}$$

$$u^a{}_{bc} = -\partial^a\partial_b\partial_c \ln V\,, \tag{2.2.52}$$

with the derivatives evaluated on the background trajectory. These differential equations have the following formal solutions:

$$\Gamma^a{}_b(N) = \Gamma^a{}_b(N, N^\star) = \mathcal{P}\,\exp\left(\int_{N^\star}^{N} dN' u^a{}_b(N')\right)\,, \tag{2.2.53}$$

$$\Gamma^a{}_{bc}(N) = \Gamma^a{}_{bc}(N, N^\star) = \int_{N^\star}^{N} dN' \Gamma^a{}_\mu u^\mu{}_{\nu\rho}(N')\Gamma^\nu{}_b\Gamma^\rho{}_c\,, \tag{2.2.54}$$

where $\mathcal{P}$ is a path ordering operator. In equation (2.2.54), we have used Greek indices as a short-hand for propagators evolving to or from N', e.g. $\Gamma^\nu{}_b = \Gamma^\nu{}_b(N', N^\star)$.

Once the field perturbations at the end of inflation, $\delta\phi^a_{\rm end}$, are known, the curvature perturbation is given by a gauge transformation:

$$\zeta = \zeta_a\delta\phi^a_{\rm end} + \frac{1}{2}\zeta_{ab}\delta\phi^a_{\rm end}\delta\phi^b_{\rm end} + ..., \tag{2.2.55}$$

where the coefficients N_a and N_{ab} are given by [153]

$$\zeta_a = \frac{1}{\sqrt{2\epsilon}} \frac{V_a}{\sqrt{V^b V_b}}\,, \tag{2.2.56}$$

$$\zeta_{ab} = \frac{V V_{ab}}{V^c V_c} + \frac{V_a V_b}{V^c V_c}\left(1 + 2\frac{V}{(V^e V_e)^2} V^f V_{fd} V^d\right) - \frac{V}{(V^c V_c)^2}\left(V_a V_{bc} V^c + V_b V_{ac} V^c\right)\,. \tag{2.2.57}$$

The curvature perturbation

We write the field two-point correlator as

$$\langle \delta\phi^a_\star(\mathbf{k}_1)\delta\phi^b_\star(\mathbf{k}_2)\rangle = (2\pi)^3\delta^{(3)}(\mathbf{k}_1+\mathbf{k}_2)\frac{2\pi^2}{k^3}\Sigma^{ab}_\star\,. \tag{2.2.58}$$

In slow-roll and with a slowly turning field trajectory at horizon crossing, we can take the initial condition of the field correlators to be given by

$$\Sigma^{ab}_\star = \frac{H^2(N^\star)}{4\pi^2}\,\delta^{ab}\,. \tag{2.2.59}$$

In [78], it was shown that this approximation works well for manyfield models of approximate saddle-point inflation. The curvature power spectrum at some later time, N, is then given by

$$P_\zeta(N,k) = \zeta_a(N)\zeta_c(N)\,\Gamma^a{}_b(N,N_\star)\,\Gamma^c{}_d(N,N_\star)\,\Sigma^{bd}_\star\,. \tag{2.2.60}$$

Isocurvature perturbations

To linear order in the field perturbations, the curvature perturbation of equation (2.2.55) is given by field fluctuations along the instantaneous background trajectory,

$$\zeta = \frac{1}{\sqrt{2\epsilon_V}}\delta\phi_\parallel\,, \tag{2.2.61}$$

where $\delta\phi_\parallel = v_a\delta\phi^a$ for $v_a = V_a/|V_b|$. Field perturbations along the $N_{\rm f}-1$ perpendicular directions give rise to 'entropic' or 'isocurvature' perturbations. We can decompose the field fluctuations as

$$\delta\phi^a \equiv \delta\phi_\parallel\, v^a + \delta\phi^j_\perp\, w^a_j\,, \tag{2.2.62}$$

where $w^a_j(N)$ denotes a generic orthonormal frame of basis vectors in directions perpendicular to V_a. Here a is a vector index a and with $j = 1,\ldots,N_{\rm f}-1$. In analogy to

ζ (and just as in [78]), we define the isocurvature $\mathcal{S}^i$ as

$$\mathcal{S}^i \equiv \frac{1}{\sqrt{2\epsilon_V}}\delta\phi^i_\perp \,. \tag{2.2.63}$$

In slow-roll and on superhorizon scales, the curvature and isocurvature evolve as [78, 110]

$$\zeta' = 2\left(v^a \frac{V_{ab}}{V} w^b_i\right)\mathcal{S}^i \,, \tag{2.2.64}$$

$$(\mathcal{S}^i)' = (v^a \frac{V_{ab}}{V} v^b - 2\epsilon_V)\mathcal{S}^i - w^a_i \frac{V_{ab}}{V}\, w^b_k\, \mathcal{S}^k \,. \tag{2.2.65}$$

Equations (2.2.64) and (2.2.65) reflect the well-known fact that isocurvature can source superhorizon evolution of the curvature perturbation ζ, but the curvature perturbation does not source isocurvature [102, 107].

The isocurvature correlations are then given by

$$\langle \mathcal{S}^i(\mathbf{k}_1)\mathcal{S}^j(\mathbf{k}_2)\rangle = (2\pi)^3\delta^{(3)}(\mathbf{k}_1+\mathbf{k}_2)\frac{k^3}{2\pi^2}P^{ij}_{\rm iso}(N) \,, \tag{2.2.66}$$

with

$$P^{ij}_{\rm iso}(N) = \frac{1}{2\epsilon_V} w^i_a\, \Sigma^{ab}\, w^j_b \,. \tag{2.2.67}$$

We refer to the total isocurvature power spectrum (without indices) as

$$P_{\rm iso} = \delta_{ij}P^{ij}_{\rm iso}. \tag{2.2.68}$$

Non-Gaussianity

Equation (2.2.55) is related to the commonly used 'δN' formulas, which involve the field perturbation at horizon crossing, by

$$N_a = \zeta_b \Gamma^b{}_a \,, \tag{2.2.69}$$

$$N_{ab} = \zeta_c \Gamma^c{}_{ab} + \zeta_{cd}\Gamma^c{}_a\Gamma^d{}_b \,. \tag{2.2.70}$$

To compute the parameter $f_{\rm NL}$, we use the δN-formalism expression, which is given by [183][17]

$$-\frac{6}{5}f_{\rm NL} = \frac{r}{16}(1+f) + \frac{N^a N^b N_{ab}}{(N_c N^c)^2}, \tag{2.2.71}$$

[17] We adopt the sign convention of [183] for $f_{\rm NL}$.

where $0 \leq f \leq 5/6$ is momentum dependent, and r is the tensor-scalar ratio. In the small-field inflation models studied in this chapter, $r \ll 10^{-3}$, and the first term is negligible.

While the calculation of the power spectrum typically is insensitive to small numerical errors, $f_{\rm NL}$ is not. The dominant, second term of equation (2.2.71) can itself be expressed as the sum of two terms,

$$-\frac{6}{5} f_{\rm NL} = \frac{N^a N^b N_{ab}}{(N_c N^c)^2} = \frac{\zeta_c \Gamma^{ca} \zeta_d \Gamma^{db} (\zeta_{ef} \Gamma^e{}_a \Gamma^f{}_b + \zeta_e \Gamma^e{}_{ab})}{(\zeta_g \Gamma^g{}_i \zeta_h \Gamma^{hi})^2} \,. \tag{2.2.72}$$

Quite commonly, both these terms can be large (say $\mathcal{O}(10)$), but cancel each other to a very high degree (say down to $\mathcal{O}(10^{-2})$). This delicate cancellation calls for high precision of the numerical evaluation of the background and the Γ coefficients. We briefly discuss our numerical implementation of the evolution of the perturbations in Appendix A.1.

2.3 Result I: Planck compatibility is not rare, but future experiments may rule out this class of models

We are now ready to discuss the results of our simulations of manyfield models of inflation in random potentials. In this section we focus on observables related to the two-point correlation function, such as the primordial power spectra of curvature and isocurvature perturbations. Our first key result is that despite multifield effects typically being non-negligible, power spectra tend to be very smooth, and observational compatibility is not rare in these models.

This section is organised as follows: we first discuss the evolution of the classical background, and we highlight and explain the particularly strong 'eigenvalue repulsion' effect on the smallest eigenvalue of the Hessian in GRF models. We then discuss the primordial perturbations of these models: we validate that the power spectra are well-approximated by approximately scale-invariant power laws over the scales relevant for the CMB. We then note that essentially all models predict small deviations from the strict power-law form, and we compute the predictions for the spectral tilt, n_s and its running, α_s, as functions of the hyperparameters. This leads us to establish a surprisingly robust prediction of these models, which makes it possible to rule them

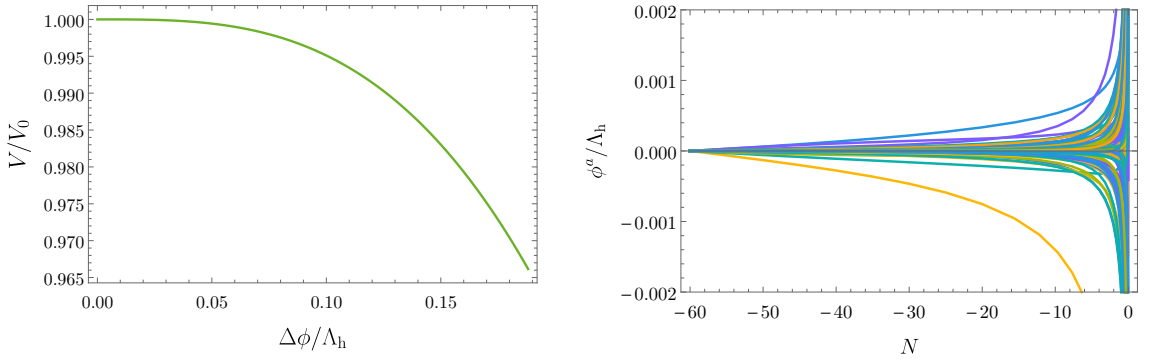

Fig. 2.3 The value of the potential as a function of the field displacement (left), and the evolution of multiple components of the fields (right) in a random 100-field GRF model.

out with future experiments. We furthermore find that multifield effects are typically important, but that, importantly, isocurvature tends to decay during inflation.

Several of the results found in this section are directly analogous to results recently observed in models of manyfield inflation in DBM potentials [78], while others differ substantially. In section 2.4 we compare these setups in detail.

2.3.1 Background evolution in GRF inflation

We first briefly discuss some key elements of the evolution of the inflationary background in the GRF potentials. To get an intuition for these models, it is instructive to first consider an example. We here take a randomly generated 100-field model as our case-study. This model was generated from the hyperparameters $\Lambda_h = 0.4$, $\epsilon = 5 \times 10^{-10}$, $\eta_i = -10^{-4}$, a flat spectrum, cf. equation (2.2.42), and a randomly directed gradient vector at $\phi = 0$. This particular model gives a total number of e-folds $N^{\text{end}} = 80.6$ over a total field displacement of $\Delta\phi = 0.187\Lambda_h$.

The left plot of Figure 2.3 shows the normalised value of the potential energy as a function of $\Delta\phi$. The potential along the descending inflationary trajectory is very smooth and featureless. Since ϵ_V is initially very small and $|\dot{\phi}| = \sqrt{2\epsilon_V}$, the field rolls very slowly initially, but accelerates super-exponentially towards the end of inflation. Figure 2.3 shows how multiple components of the field evolve during inflation, and indicates that the inflationary trajectory turns as the field descends the potential.

The eigenvalues of the Hessian matrix are not constant in a general inflationary model, and we expect the eigenvalues of the GRF models to relax from the fine-tuned initial configuration to the (slightly off-centred) semi-circle spectrum. Figure 2.4 shows

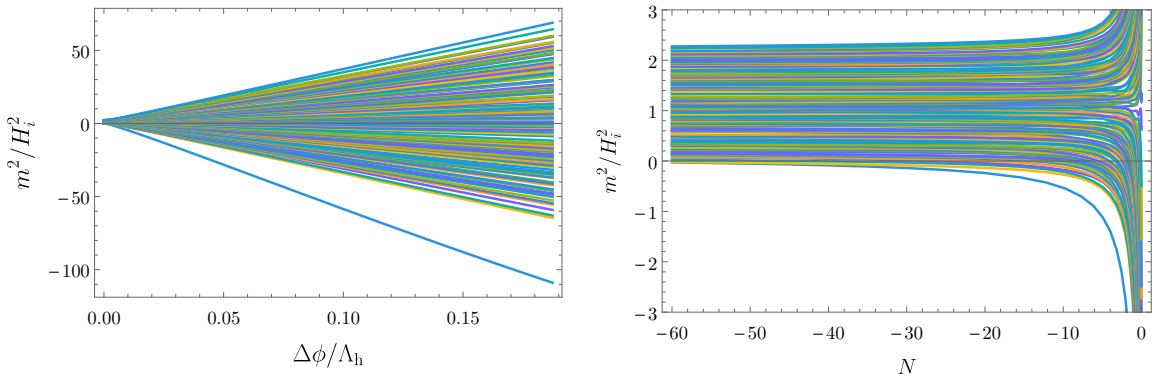

Fig. 2.4 Eigenvalue evolution of the Hessian in a 100-field example, starting from a flat spectrum.

the evolution of the squared masses as a function of the field displacement during inflation (left plot), and as a function of the number of e-folds (right plot) for our 100-field example. Indeed, as the fields evolve from $\phi = 0$, the spectrum spreads out. Half of the fields, initially heavier than the others, tend to become even more massive during inflation, and are not very important for either the background evolution or the spectrum of the perturbations. By contrast, the lighter half of the fields become even lighter, and many even go tachyonic: with small variations over all the models we have considered, almost precisely half the fields have $m^2 < 0$ at the end of inflation.[18] When plotted as a function of $\Delta\phi$, the bundle of eigenvalues is conical, which is indicative of the dominance of the cubic terms in the potential.

The 'straying' smallest mass-squared

Figure 2.4 also illustrates a curious and important feature of these models: the smallest eigenvalue decreases more rapidly than the others, and 'strays' from the conical bundle towards more tachyonic values. This 'straying' behaviour of the smallest eigenvalue has to our knowledge not been discussed previously in the literature, but appears for large N_f in essentially all inflationary models that we have studied. In sections 2.3.4 and 2.5, we will see that it contributes to some of the most interesting predictions of the inflationary GRF models.

While the rapid evolution of the smallest eigenvalue of the Hessian may appear surprising, it has a simple explanation in terms of the properties of the GRF potentials, and the dynamics of multifield slow-roll inflation. In our inflationary models, the initial

[18] On approach to the final vacuum configuration after inflation, these eigenvalues will again become positive.

values of both the gradient and the Hessian matrix are very small. This means that after a short field excursion, which typically involves some turn, the gradient and Hessian become dominated by the third-order terms. Without loss of generality, we may take the '1'-axis to be aligned with the field excursion at this point, with $\phi^1 > 0$. We then have

$$V_a(\phi) \simeq \frac{1}{2} V_{a11} (\phi^1)^2 \,, \qquad\qquad V_{ab}(\phi) \simeq \frac{1}{2} V_{ab1} \phi^1 \,. \tag{2.3.1}$$

With the initial gradient set to be small, the third derivatives are drawn from a distribution with a mean that is very close to zero and variances given by

$$\mathrm{Var}(\tilde{V}_{abc}) = \begin{cases} 6 & \text{if all indices are equal} \\ 2 & \text{if only two are equal} \\ 1 & \text{if none are equal.} \end{cases} \tag{2.3.2}$$

We then see that the magnitude of $V_1(\phi)$ is expected to be larger than the other components of the gradient. Furthermore, since $\phi_1 > 0$, we expect that $\dot{\phi}_1 \propto -V_1(\phi) > 0$, in which case V_{111} must be be negative. We can therefore expect $V_{11}(\phi) = V_{111}\phi_1$ to be larger than the other elements of the Hessian matrix, and negative. Moreover, since $\mathrm{Var}(V_{a11}) > \mathrm{Var}(V_{ab1})$ for $b \neq 1$ (and $a \neq b$) the off-diagonal row-vector V_{1a} is expected to be larger in magnitude than the other row vectors. This will typically lead to a large negative mass-squared eigenvalue with an eigenvector approximately aligned with the gradient direction. This is precisely what we observe through the 'straying' smallest eigenvalue of the Hessian.

This evolution of the squared masses importantly affect the inflationary evolution of the field perturbations (as we will discuss in section 2.3.4), and also the background dynamics. In slow-roll inflation, the acceleration of the field is given by

$$(\phi^a)'' = \sqrt{2\epsilon_V} \left(\frac{V^a_{\ b}\, v^b}{V} - 2\epsilon_V v^a \right) . \tag{2.3.3}$$

We see that if $v_a \approx -\delta^1_a$, the acceleration tends to be large and positive in the '1'-direction. This will make the trajectory 'straighten' during this phase, and v_a will become closer and closer aligned with the direction of the smallest eigenvalue of the Hessian matrix.

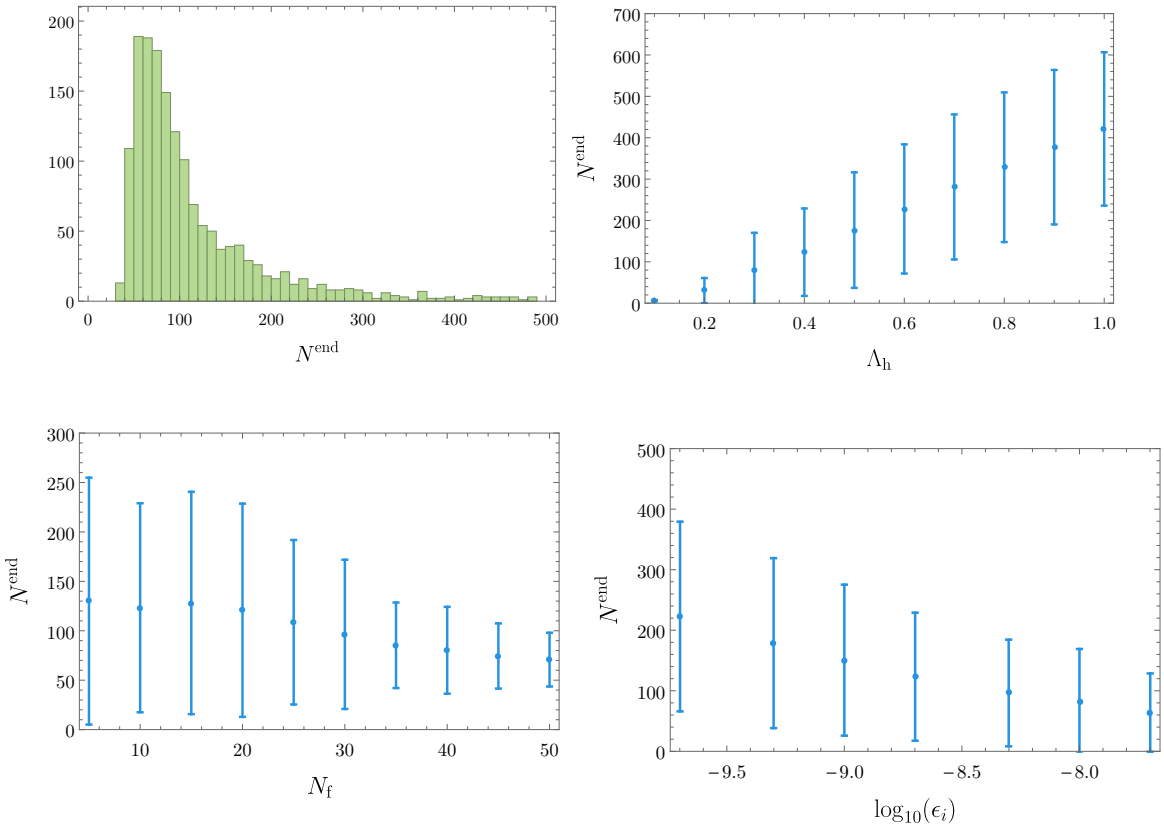

Fig. 2.5 Histogram of the e-fold distribution of the baseline model (cf. equation (2.2.44)), and the dependence of the mean and standard deviation on the hyperparameters in one-parameter variations from the baseline. Each data point is generated from an ensemble of 2000 inflationary models.

The e-fold distribution of GRF models

An important factor influencing the observables is the distribution of the number of e-folds of inflation. Figure 2.5 shows the mean values and standard deviations of this distribution for various one-parameter variations from the baseline parameter choice of equation (2.2.44).

Unsurprisingly, flatter spectra lead to more e-folds of inflation. As the number of fields is increased, the e-fold distribution slowly shift to lower values, but the dependence is not very strong. For a given choice of hyperparameters, the distribution of the number of e-folds typically exhibits a broad peak and a 'heavy', polynomially decreasing tail corresponding to models with a large number of e-folds.

2.3.2 Smooth and simple power spectra from complex inflationary models

We now turn to observables generated by these models, focussing in this section on the power spectrum of the curvature perturbation, $P_\zeta(k)$. While many of the simplest models of single-field or few-field inflation naturally generate very simple, almost scale-invariant power spectra, there is no guarantee that highly complicated and random manyfield models should also do so. Turns of the field trajectory or bumps in the potential could generate strong deviations from scale-invariance, and highly featured power spectra. Quite remarkably however, we here find that even random models involving several dozens of fields and millions of interaction terms typically produce extremely smooth and simple power spectra.

A sense of the typical properties of the generated power spectra can be inferred from Figure 2.6, which shows the power spectra for 15 randomly generated models with 10 (left) and 50 (right) fields. The top row shows the power spectra evaluated over the full range of scales exiting the horizon within the last sixty e-folds of inflation, while the plots of the bottom row zooms in on the 10 e-fold range centred at the 'pivot scale' corresponding to modes exiting the horizon 55 e-folds before the end of inflation. All plotted power spectra are evaluated at the end of inflation, $P_\zeta(N_{\rm end}, k) = P_\zeta(k)$, and normalised at the pivot scale $k_\star$.

Over the full range of scales spanning 60 e-folds, the power spectra show strong deviations from scale-invariance, with rapidly decreasing power spectra for very small-scale modes. This drop in power is related to the rapid growth of the slow-roll parameter ϵ_V towards the end of inflation, which causes a speed-up of the field and a suppression of the power of the curvature perturbation. On zooming in on the scales most relevant for

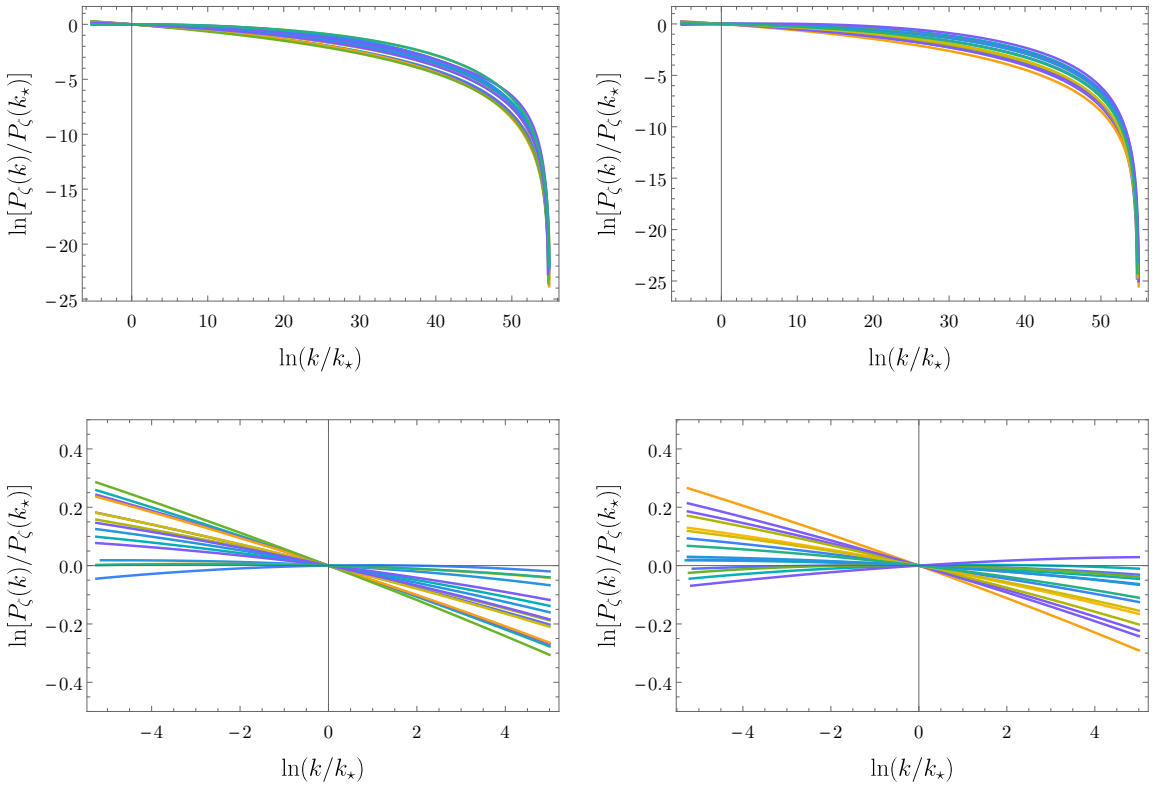

Fig. 2.6 Examples of power spectra from 15 randomly generated models of GRF inflation for $N_\mathrm{f} = 10$ (left) and $N_\mathrm{f} = 50$ (right). Hyperparameters other than N_f are as in the baseline case, cf. equation (2.2.44).

CMB observations, the generated power-spectra are very simple, and of an approximate power-law form. This simple form of the power spectra is common to all GRF models we have studied, independent of the precise choice of hyperparameters. We will now discuss the dependence of the detailed predictions of the models on the hyperparameter choices.

2.3.3 Distributions of n_s and α_s

The simple form of the power spectra around the pivot scales justifies fitting them by an approximate power-law,

$$P_\zeta(k) = A_s \left(\frac{k}{k_\star}\right)^{n_s-1} , \tag{2.3.4}$$

where we allow for a non-vanishing running of the spectral index, $\alpha_s = \mathrm{d}n_s/\mathrm{d}\ln k|_{k=k_\star}$.

Figure 2.7 shows the aggregated values of (n_s, α_s) for 25,000 models of GRF inflation with N_f ranging between 5 and 50, and for varying values of the other hyperparameters.[19] The distribution for n_s indicates that the power spectra are approximately scale-invariant, and that the spectra are more commonly red than blue (around 85% were red). For these values of the hyperparameters, the distribution for n_s is broader than current Planck constraints, but Planck-compatible values are not rare.

The statistical prediction for the running of the spectral index, α_s, is remarkably sharp. A small and negative running is vastly favoured (especially among the models with Planck-compatible spectral indices), and these models could be ruled out should future experiments infer a positive or substantially negative running of the spectral index. Indeed, over 99% of these models, and all of those in the Planck 68% c.l. for n_s, fall in the range $-0.004 < \alpha_s < 0$. For the baseline hyperparameters, cf. equation (2.2.44), we find $n_s = 0.970 \pm 0.018$ and $\alpha_s = -0.00143 \pm 0.00034$. Normalising the amplitude of scalar perturbations fixes Λ_v, for the baseline models we find $\Lambda_\mathrm{v} = 9.6\,(\pm 1.7) \times 10^{-5}$.

The tensor-to-scalar ratio is very small in all models we have constructed. For the baseline parameters, we find $r = 3.07\,(\pm 0.28) \times 10^{-8}$. Since the total field displacement during inflation is $\Delta\phi = 0.36\,(\pm 0.04)\,\Lambda_\mathrm{h}$ for these parameters, we see that the 'Lyth bound' [133] is far from saturated: in single-field models of inflation,

$$r = 16\epsilon_V < 8 \left(\frac{1}{N_\mathrm{exit}}\right)^2 \left(\frac{\Delta\phi}{M_\mathrm{Pl}}\right)^2 , \tag{2.3.5}$$

[19] This aggregate consists of all models in the tables 'varying N_f' and '$N_\mathrm{f} = 50$' in Appendix A.2.

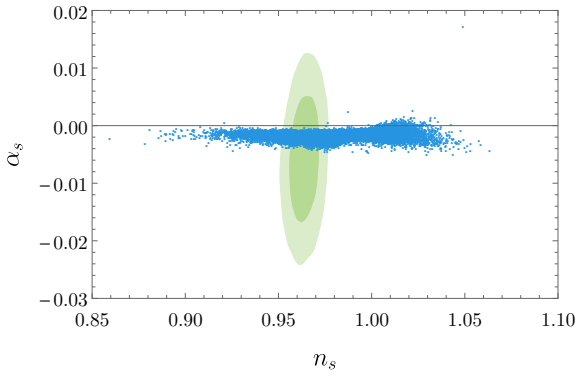

Fig. 2.7 The distribution of n_s and α_s for 25,000 inflation models spanning values of $N_{\rm f}$ between 5 and 50, with the 68% and 95% confidence contours from Planck (TT+TE+lowP+lensing) [10].

if ϵ_V is constant or monotonically increasing, $N_{\rm exit}$ denotes the e-fold when the pivot scale crossed the horizon (in our case $N_{\rm exit} = 55$), and $\Delta\phi$ denotes the total field displacement during inflation. Thus, for the mean-value base-line parameters, we find the bound $r < 5.5 \times 10^{-5}$. There are two reasons for the non-saturation of the Lyth bound. First, the field initially evolves very slowly, but speeds up super-exponentially towards the end of inflation. Second, we will see in section 2.3.4 that isocurvature modes tend to enhance the amplitude of the scalar perturbation, but leave the tensor perturbations untouched. This further suppresses the tensor-to-scale ratio r.

Figure 2.7 shows that manyfield GRF models can be compatible with current observational constraints on the power spectrum, but provide a sharp prediction for its running, and can be ruled out by future experiments. We now investigate how these predictions depend on the hyperparameters.

Figure 2.8 shows the dependence of n_s and α_s of $\epsilon_{\rm i}$ and $\Lambda_{\rm h}$. All data points are based on at least 1000 models except those with $\Lambda_{\rm h} \leq 0.3$ or $\epsilon_i \geq 10^{-8}$ where fewer models gave sufficient number of e-folds, and the data points are determined from several hundred realisations. We first note that taking $\Lambda_{\rm h}$ large or $\epsilon_{\rm i}$ small both have the effect of 'flattening' the potential, either globally or locally around $\phi = 0$. Figure 2.8 indicates that such a flattening makes the spectrum more red, and the statistical predictions for n_s and α_s become sharper. For large $\Lambda_{\rm h}$, this reddening of the spectra make the models significantly discrepant with current observational bounds on n_s, making it possible to rule out this particular region of hyperparameter space with current observations (however, by increasing $\epsilon_{\rm i}$, the spectral indices at large $\Lambda_{\rm h}$ can be made compatible with Planck again). The distribution of the running of the spectral index is, by comparison, remarkably robust under changes to the hyperparameters. All

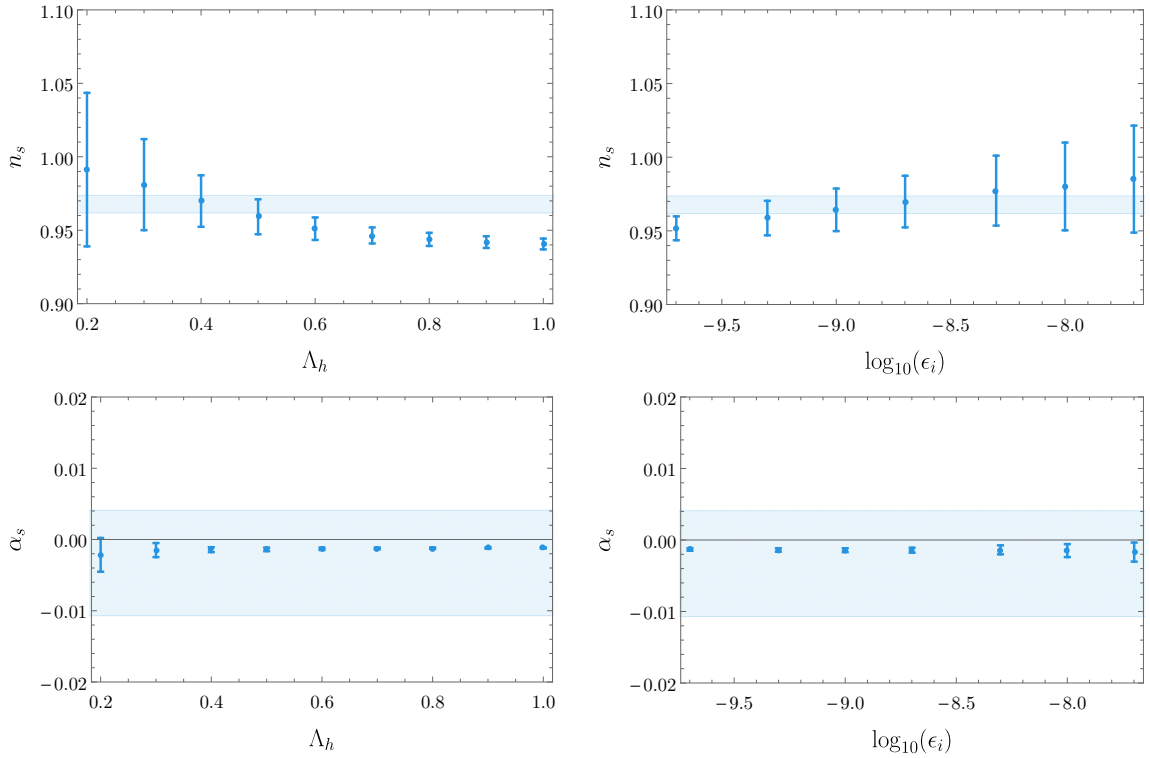

Fig. 2.8 The spectral index and its running as functions of the smoothness of the potential in one-parameter variations from the baseline hyperparameters. The blue regions indicate the 68% c.l. from Planck (TT+lowP+lensing) [10].

sampled models are compatible with current constraints on α_s, and the prediction of a small negative running remains sharp as either $\epsilon_{\rm i}$ is decreased or $\Lambda_{\rm h}$ is increased.

The observed relation between a flatter potential and a redder spectral index may appear surprising at first, as flatter potentials commonly give rise to more scale-invariant spectra. There is however a rather simple explanation of this empirical relation. The spectral index of the perturbations depends not only on the flatness of the potential, but also on its curvature. In a general multifield model,[20] the spectral index at the end of inflation is given by [83],

$$n_s - 1 = -2\left(\epsilon^\star + e^a\, u^\star_{ab}\, e^b\right) = 2\frac{e^a V^\star_{ab} e^b}{V^\star} - 2\left(\epsilon^\star + \frac{e^a V^\star_a V^\star_b e^b}{V^\star}\right), \tag{2.3.6}$$

where the $\star$ subscript denotes quantities evaluated at horizon crossing, the symmetric tensor u_{ab} is defined as in equation (2.2.51), and the unit vector e_a, which encodes the

[20] Assuming that at horizon crossing $\Sigma_{ab} = \delta_{ab}\, H^2_\star/2$, as we do throughout this chapter.

possible superhorizon evolution of the spectral index, is defined as,

$$e_a = \frac{\zeta_b \Gamma^b{}_a}{|\zeta_c \Gamma^c{}_d|} \,. \tag{2.3.7}$$

Physically, it relates the adiabatic perturbation at the end of inflation to field perturbations at horizon crossing. If there is no superhorizon evolution, e^a is aligned with the tangent vector of the field trajectory at $N^\star$ (i.e. $e_a \propto \partial_a V(\phi_\star)$). However, if the spectral index evolves on superhorizon scales, e^a becomes misaligned, typically towards the most tachyonic directions.

In the approximate saddle-point models that we consider, the potentials need to be very flat around $\phi = 0$ in order to support sufficiently long periods of inflation, cf. Figure (2.5). The spectral index will therefore be dominated by the term involving the Hessian.

In inflationary realisations giving not much more than 60 e-folds of inflation, the pivot scale exits the horizon relatively early during inflation. At this point, the masses will not have had time to spread out much, and the gradient will in general not be aligned with the most tachyonic direction. The curvature perturbation will then typically undergo some evolution on superhorizon scales, and the vector e_a will develop components in both the adiabatic direction (at $N^\star$) and the more tachyonic directions.[21] A wide distribution of the spectral index is therefore expected in this case.

By contrast, in models supporting $\gg 60$ e-folds of inflation, the pivot scale typically exits the horizon when the gradient is dominated by the third-order coefficient in the Taylor series. In this case, the masses will have spread out more and both the gradient vector at $N^\star$ and e_a will, to good approximations, be aligned with the direction of the smallest eigenvalue of the Hessian. This results in a redder power spectrum, since the smallest mass eigenvalue has had time to decrease further. Moreover, the variance of the spectral index is smaller in these models, since the direction of e_a is much less random. These effects are visible in Figure 2.9.

The relation between flatter potentials and redder power spectra is now easy to understand. With all else the same, a flatter potential generates more e-folds of inflation so that the horizon crossing of the pivot scale, 55 e-folds before the end of inflation, happens correspondingly later (in e-fold time) after the field has left $\phi = 0$. As per the discussion above, we then expect to see redder power spectra with smaller variances, which is precisely what we see when $\epsilon_{\rm i}$ is decreased or $\Lambda_{\rm h}$ is increased.

[21] This also explains why the spectral index becomes redder due to superhorizon evolution, cf. Figure 2.9.

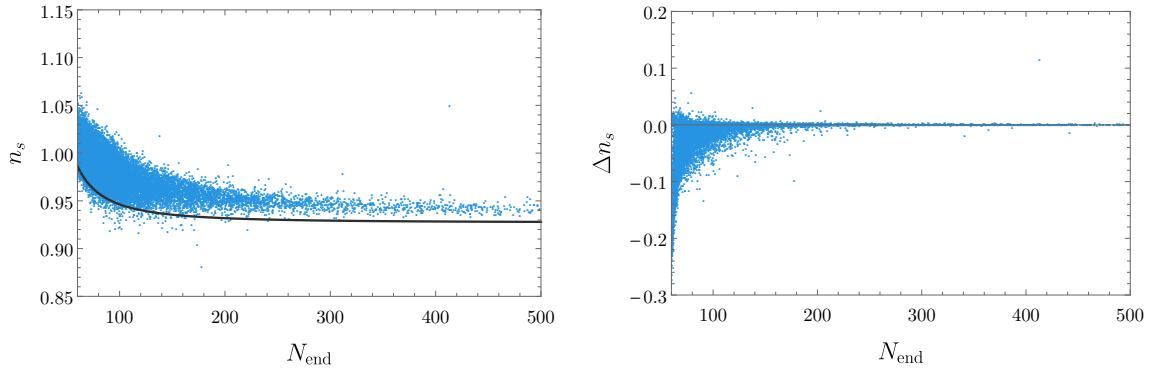

Fig. 2.9 The distribution of ($N^{\rm end}$, n_s) at the end of inflation (left) and the change of the spectral index on superhorizon scales, $\Delta n_s = n_s^{\rm end} - n_s^\star$, (right), for about 19,000 inflation models with uniform mass spectra, again spread over values of $N_{\rm f}$ varying between 5 and 50 (the same models as in Figure 2.7, but without the compressed spectra models). The black curve in the left graph shows the prediction of the single-field model discussed in Appendix A.3.

We now turn to the effects of the number of fields, $N_{\rm f}$, on the power spectrum. Figure 2.10 shows the how the mean values and standard deviations of n_s and α_s are weakly dependent on $N_{\rm f}$. First, we note that as $N_{\rm f}$ is increased, the spectra become less red and the variance of the spectral index also increases, albeit slowly. This may again be explained by the correlation between n_s and the total number of e-folds of inflation: as the number of fields is increased, the models tend to give fewer e-folds of inflation, cf. Figure 2.5, which leads to e_a developing non-vanishing components along multiple directions in field space.

In sum, we have found that the distribution for the spectral index in our GRF models tends to favour red, approximately scale-invariant spectra. Some regions of the parameter space lead to sharp predictions of excessively red spectra, and can be ruled out already with current observations. However, large regions of hyperparameter space are compatible with current constraints from the Planck experiment. More importantly, we have found that these models predict, sharply and robustly, a small negative running of the spectral index. The Planck experiment has constrained the running of the spectral index to $\alpha_s = -0.005 \pm 0.013$ [14], but future experiments may reach a sensitivity of $\sigma(\alpha_s) = 10^{-3}$ [163]. A future observation of $\alpha_s \gtrsim 0$ or $\alpha_s \lesssim -0.004$ would rule out all Planck-compatible models that we have constructed.

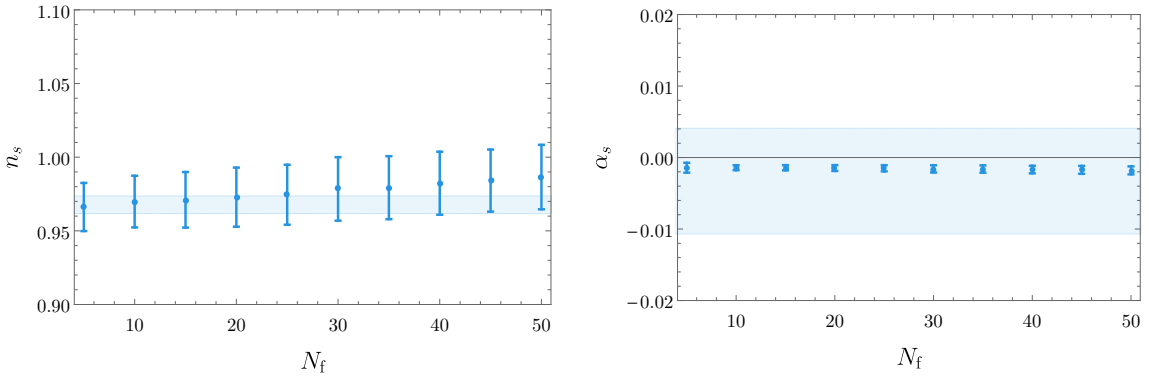

Fig. 2.10 The spectral index and its running as a function of N_f in one-parameter variations from the baseline together with the 68% c.l. from Planck [10].

2.3.4 Substantial superhorizon evolution, but also decaying isocurvature

We have seen in section 2.3.3 that the predictions from the random GRF models are remarkably simple, despite the underlying potentials being highly non-trivial functions of many fields. Indeed, the prediction of an approximate scale-invariant power spectrum with a small running of the spectral index agree with two of the 'generic' predictions of *single-field* models of slow-roll inflation. In this section, we investigate to what extend multifield dynamics is important for the predictions of the manyfield GRF models.

We begin by considering the superhorizon evolution of the pivot-scale modes exiting the horizon 55 e-folds before the end of inflation. We first recall that to linear order in the field perturbations (and upon suppressing the k dependence), the modes at the end of inflation are related to the modes at horizon exit by the transfer equation [18, 50, 184],

$$\begin{pmatrix} \zeta \\ \mathcal{S}^i \end{pmatrix}_\mathrm{end} = \begin{pmatrix} 1 & T_{\zeta\mathcal{S}^j} \\ 0 & T_{\mathcal{S}^i\mathcal{S}^j} \end{pmatrix} \begin{pmatrix} \zeta \\ \mathcal{S}^j \end{pmatrix}_\star . \tag{2.3.8}$$

For $\Sigma^*_{ab} \propto \delta_{ab}$ (as we assume in this chapter, cf. equation (2.2.59)), the superhorizon evolution of the curvature perturbation is given by,

$$\frac{P_\zeta(N_\mathrm{end}, k)}{P_\zeta(N_\star, k)} = 1 + \sum_{i=1}^{N_\mathrm{f}-1} T^2_{\zeta\mathcal{S}^i} , \tag{2.3.9}$$

so that, under these assumptions, superhorizon evolution can only lead to a net increase in the power of the curvature perturbation. If $P_\zeta(N_\mathrm{end}, k)/P_\zeta(N_\star, k) - 1 \lesssim 10^{-3}$ for a range of k modes, the observational predictions of the model can be regarded as safely

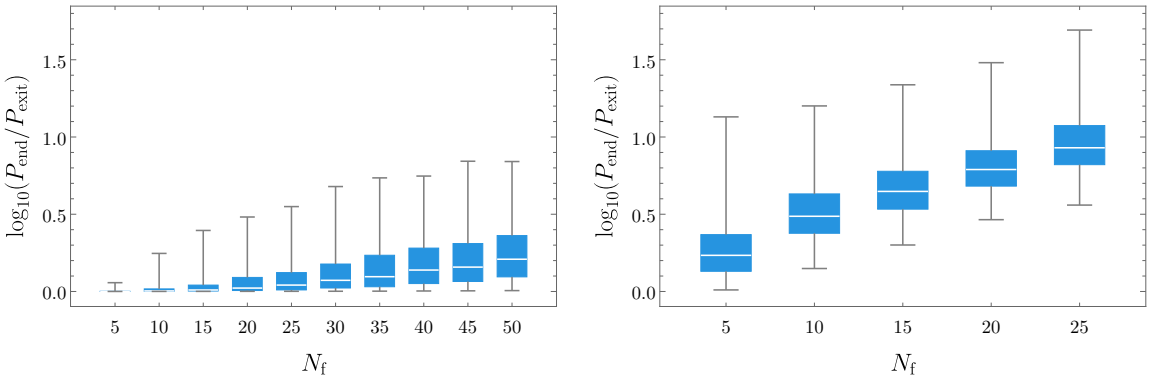

Fig. 2.11 Superhorizon evolution of the mode exiting the horizon 55 e-folds before the end of inflation for the flat initial spectrum (left) and the compressed spectrum (right), cf. equation (2.2.42). Boxes indicate first and third quartile, together with the median; 'whiskers' indicate 1st and 99th percentile. The left graph shows a one-parameter variation from the baseline; the right shows models with $\Lambda_{\rm h} = 0.4$, $\epsilon_{\rm i} = 10^{-10}$ and $\eta_{\rm i} = -10^{-4}$.

independent of multifield effects, and the horizon crossing power spectrum determines the observational predictions for e.g. n_s and α_s. This rarely happens in manyfield models of inflation in GRF potentials.

The box plots in Figure 2.11 show the effects of varying $N_{\rm f}$ on the distributions of $\log_{10}(P_\zeta(N_{\rm end}, k_\star)/P_\zeta(N_\star, k_\star))$ for both the flat (left) and compressed (right) spectra. Each box is generated from over 1000 inflationary models, except for $N_{\rm f} = 20$ and 25 for the compressed spectrum, which were generated from 600 and 200 models, respectively. Unsurprisingly, models with more fields and more compressed initial spectra exhibit larger superhorizon evolution. However, even for the flat spectrum, models with more than 5 fields tend to evolve substantially on superhorizon scales, so that the predictions at horizon crossing do not automatically give the predictions for observables at the end of inflation. Evidently, multi-field effects are important in manyfield inflation in GRF potentials.

In multifield models of inflation, the curvature perturbation may evolve well past the end of inflation, through the reheating phase. In many models of multifield inflation in the literature, this problem is dealt with by ensuring that the fields enter an approximately single-field 'adiabatic limit' in which all but a single mode are very massive (i.e. $m^2 > H^2$) and the isocurvature modes decay exponentially. Once the isocurvature perturbations have decayed, the curvature perturbation ceases to evolve and the predictions are expected to become insensitive to the details of the reheating phase. As illustrated by Figure 2.4, the spectrum of the Hessian matrix of the GRF

models we consider typically contains multiple tachyonic eigenvalues at the end of inflation so that, clearly, no standard adiabatic limit is reached. However, we will now see that isocurvature still becomes exponentially suppressed during inflation.

At horizon crossing, $\Sigma_{ab} \propto \delta_{ab}$ and $P_{\rm iso}/P_\zeta = (N_{\rm f} - 1)$, cf. equation (2.2.68). Figure 2.12 shows the mean values and standard deviations of the ratio $P_{\rm iso}/P_\zeta$ evaluated at the end of inflation in our ensembles of models. Strikingly, the power in the isocurvature mode evolves during inflation from dominating over the curvature perturbation to becoming exponentially suppressed. For the flat initial spectrum and $N_{\rm f} = 5$, the ratio $P_{\rm iso}/P_\zeta$ falls below the numerical accuracy of our simulations. For larger $N_{\rm f}$, this ratio typically remains exponentially suppressed. Models with the highly compressed initial spectrum feature larger levels of isocurvature at the end of inflation, but even in this extreme case, the superhorizon evolution suppresses the isocurvature perturbations by several orders of magnitude.

The suppression of the isocurvature despite multiple tachyonic directions can be understood as a consequence of the inflationary slow-roll dynamics, as discussed in [78]. To see this, we may re-express the components of the transfer matrix (2.3.8) in terms of the transport coefficients $\Gamma_{ab}(N, N_\star)$, using the decomposition of the fluctuations into instantaneous adiabatic and entropic fluctuations, cf. equation (2.2.62):

$$1 = \left(\frac{\epsilon_\star}{\epsilon_N}\right)^{1/2} v_a(N)\, \Gamma^a{}_b\, v^b(N_\star)\,, \tag{2.3.10}$$

$$T_{\zeta \mathcal{S}^i} = \left(\frac{\epsilon_\star}{\epsilon_N}\right)^{1/2} v_a(N)\, \Gamma^a{}_b\, w_i^b(N_\star)\,, \tag{2.3.11}$$

$$T_{\mathcal{S}^i \mathcal{S}^j} = \left(\frac{\epsilon_\star}{\epsilon_N}\right)^{1/2} w_a^i(N)\, \Gamma^a{}_b\, w_j^b(N_\star)\,. \tag{2.3.12}$$

Here $\epsilon_N = \epsilon(N)$ and equation (2.3.10) follows from the conservation of ζ in the absence of entropic perturbations. The appearance of multiple negative eigenvalues of the Hessian matrix leads to multiple growing field perturbations (and multiple eigenvalues of $\Gamma^{\rm T}\Gamma$ that are greater than 1). In slow-roll inflation, the field velocity tends to align with the smallest eigenvalue of the Hessian matrix, cf. equation (2.3.3). This makes the adiabatic field perturbation grow faster than the each of the less tachyonic entropic perturbations. However, from equation (2.3.10) we see that the growth of the adiabatic field perturbation (in the absence of additional sourcing from entropic modes) is directly related to the growth of $\epsilon(N)$.

For entropic modes that grow slower than the adiabatic perturbation, the decaying prefactor $\sqrt{\epsilon_\star/\epsilon_N}$ cause a net suppression of isocurvature during inflation. This explains

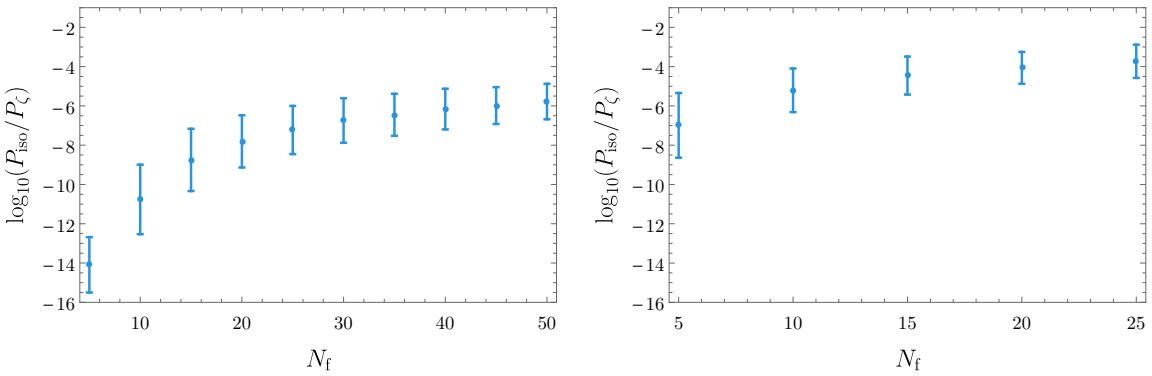

Fig. 2.12 Isocurvature-to-curvature ratio at the end of inflation for flat (left) and compressed (right) initial spectra. Other hyperparameters as in Figure 2.11.

why the isocurvature $\mathcal{S}$ can decay during inflation, despite the presence of multiple tachyonic fields.

This discussion also makes it clear that the 'straying' behaviour of the smallest eigenvalue of the Hessian, discussed in section 2.3.1, leads to a further suppression of isocurvature modes during inflation. Furthermore, the associated 'straightening' of the field trajectory leads to fewer opportunities for the isocurvature to source the curvature perturbation through turns in field space, cf. equation (2.2.64).

In sum, in this subsection we have seen that multifield effects are typically important in manyfield inflation, but that entropic perturbations tend to decay. While no single-field 'adiabatic limit' is reached during inflation in theses models, the large suppression of isocurvature may shield observables from subsequent superhorizon evolution during the post-inflationary reheating phase. It would be interesting to apply our construction of GRF potentials to investigate the evolution of the adiabatic and entropic perturbations in reheating models with many interacting fields in more detail.

2.4 Result II: At large $N_{\rm f}$, GRF and RMT models largely agree

A key motivation behind this work is to use mathematically simple constructions of manyfield systems to search for mechanisms that may drive observables to simple and robust predictions. Identifying such mechanisms could prove very helpful in analysing more complicated manyfield models motivated by fundamental theory. However, even for a given class of mathematically simple models, it can be hard to separate its particularities from the properties that may be more broadly applicable. It is therefore

important to test the predictions of any class of models by comparing to the predictions of independent constructions. To make such comparisons useful, the different classes of models should share some rough similarities, but be fundamentally different in their details. For our purposes, we are interested in models of small-field, slow-roll, saddle-point inflation with many interacting fields. Fortunately, our construction of GRF models in this chapter and the construction of random DBM potentials of [78, 142] now provide two such classes of theories, thus allowing the first critical tests of possible 'universal' predictions of random manyfield models of inflation.

In this section, we first briefly review the differences and similarities between the DBM models and our GRF models in section 2.4.1. Our discussion highlights the differences in the evolution of the Hessian matrix, but also clarifies the context of recent discussions on the equilibrium spectra of single-field and effectively single-field GRF models [144, 145]. In section 2.4.2, we then provide a first detailed comparison between the observational predictions of the DBM and GRF models. A brief review of the DBM construction can be found in Appendix A.4. We refer the reader to references [78, 142] for a more detailed discussion on the properties of DBM potentials.

2.4.1 Comparison of DBM and GRF potentials

The DBM construction of [142] led to the first explicit studies of models of inflation with many interacting fields in random potentials. As we mentioned in section 2.1 however, this prescription differs from GRF models in that the cubic and higher-order terms of the potential are regulator-dependent. In this section, we will discuss how some properties the Hessian matrices differ between the GRF and DBM potentials. For the purpose of clarity, we first compare the *'equilibrium spectra'* of the models, i.e. the eigenvalue distribution of the Hessian matrix at some randomly chosen point in field space, and we then turn to the *evolution* of the Hessian, e.g. from a fine-tuned initial configuration to the equilibrium.

The equilibrium spectra of GRF and DBM models

In equation (2.2.28), we saw that the Hessian matrix in the GRF models consists of a GOE matrix and shift, proportional to the unit matrix times the negative of the value of the potential. We also noted that for $N_{\rm f} \gg 1$ and typical values of the potential, this shift had a very small effect on the spectrum of the GRF. This way, the spectrum of the simplest GRF models is very similar to that of the simplest DBM model, which omits the shift entirely. In the light of this, it may appear surprising that a recent study

claimed that the equilibrium spectrum constitutes a fundamental difference between the GRF and DBM models [144]. We here provide the context for these claims.

First, the variance of the GOE matrix in the simplest GRF model is fixed by the choice of covariance function. For equation (3.1.2), this leads to a width of the Wigner semi-circle spectrum of $4\sqrt{N_{\rm f}}$, cf. equation (2.2.25). In the DBM model, the variance is a free parameter which is typically chosen so that the spectrum has an $N_{\rm f}$-independent width. This choice makes it convenient to compare systems with different number of fields within a fixed mass-range, but other choices are possible, and clearly, the width of the equilibrium eigenvalue spectrum can hardly be described as a fundamental difference between the DBM and GRF constructions.

Second, one can try to make the shift of the spectrum more important even during inflation. To do so, one may attempt to inflate near the bottom of the potential, where the semi-circle spectrum is significantly 'up-shifted' from the centred Wigner semi-circle law. However, for the mean zero GRF models, any upward shift of spectrum only occurs for negative values of the potential, making inflation impossible. To construct models in which the shift is important, one may add to the mean-zero GRF a large, field-independent cosmological constant of size $\mathcal{O}(2\sqrt{N_{\rm f}}\Lambda_{\rm v}^4)$.[22] The uplifted potential will then have a typical, 1σ range of $(2\sqrt{N_{\rm f}}\pm 1)\Lambda_{\rm v}^4$, as opposed to $\pm\Lambda_{\rm v}^4$ for the mean-zero GRF. By construction, the equilibrium spectrum for small values of the potential is now a Wigner semi-circle with the left edge shifted to zero, and no tachyonic eigenvalues. We briefly discuss manyfield inflation in this class of potentials in Appendix A.5.

The substantially shifted spectrum of the Hessian of the modified GRF potential is (by construction) discrepant with the centred Wigner semi-circle, and thereby the equilibrium spectrum of the standard DBM model. This was key to the argument of reference [144], which proposed this discrepancy as a fundamental difference between DBM and GRF models. However, due to the simplicity of equation (2.2.28), it is straightforward to modify the DBM model to capture the spectrum of any such modified GRF model.[23] Thus, it appears challenging to use simplistic arguments based on the equilibrium spectra of the DBM and GRF models to identify fundamental differences between these constructions.

[22]The addition of a large field-independent cosmological constant may appear ad-hoc, and to our knowledge, lacks a clear physical motivation. For example, sources of energy density in string compactifications tend to be moduli-dependent in the Einstein frame.

[23]For example, in direct analogy with equation (2.2.28), one may take $v_{ab}^{\rm tot} = v_{ab}^{\rm DBM} + \delta_{ab} f_{\rm shift}(v_0)$, where only $v_{ab}^{\rm DBM}$ undergoes Dyson Brownian Motion, and the new term encodes the desired shift of the spectrum.

The evolution of the Hessian matrix

The *evolution* of the Hessian matrix as the field traverses some path in field space constitutes a fundamental difference between the DBM and GRF constructions, even if the equilibrium spectra coincide. This difference is evident in the relaxation of the eigenvalues of the Hessian from an atypical initial configuration to the equilibrium configuration, as can bee seen by comparing the 100-field DBM model of Figure 4 of reference [78] to our 100-field GRF model of Figure 2.4. The spectra of the GRF models relax in a much more linear, regular fashion. Moreover, in section 2.3.1 we showed that the statistical properties of the cubic terms in GRF potentials lead to 'straying' smallest eigenvalues in slow-roll inflation. This phenomenon has no counterpart in DBM models.

In sum, while DBM and GRF models for multifield inflation potentials share several mathematical features, the two constructions are independent and the differences lead to noticeably different behaviour in the solutions. Thus, by comparing the predictions of these two classes of models, we may search for robust and model-independent signatures of many-field dynamics during inflation.

2.4.2 Comparison of DBM and GRF predictions

In this section, we assess the robustness of the predictions from manyfield models of inflation by comparing our results derived in this chapter to those derived from DBM models in [78]. The three key common features that both constructutions have are

1. **Manyfield inflation is not single-field inflation.** One immediate aspect of multifield models of inflation is that they typically contain several fields with masses not much larger than the Hubble parameter. Such 'light' fields cannot be integrated out, and commonly contribute to multifield effects that impact observables. In this sense, manyfield models of inflation are clearly not identical to single-field models.

   In [142] however, it was shown that some aspects of the DBM models at large $N_{\rm f}$ (such as the distribution of e-folds), could be modelled by a single-field model. Reference [97] elaborated on this single-field model to estimate the spectral index of the large-$N_{\rm f}$ DBM models, however this single-field estimate was discrepant with the actual distribution computed from the DBM multifield models [77, 78]. Thus, single-field models have had a limited success in describing the properties of manyfield DBM models. Moreover, intrinsically multifield effects

such as superhorizon evolution of the curvature perturbation are common in DBM models, which indicates that manyfield inflation differ from single-field inflation.

We have seen that in manyfield GRF models, multifield effects are also common: the field explores multiple directions in field space, isocurvature modes can be important, and the curvature perturbation typically evolves on superhorizon scales. These effects cannot be captured by a single-field model so that, evidently, manyfield inflation is different from single-field inflation.[24] It can still be interesting to explore how well a simple single-field model can capture the results of the GRF manyfield models. In Appendix A.3, we construct such a single-field model and show that its predictions qualitatively (but not quantitatively) agree with the more complicated GRF models.

2. **Despite tachyons, isocurvature modes generally decay.** In section 2.3.4, we found that despite the presence of multiple tachyons, isocurvature tends to decay during inflation in GRF models. This suppression of isocurvature was previously observed in DBM models in [78], and was there similarly explained as a dynamical consequence of multi-field slow-roll inflation. Comparing our Figure 2.12 to Figure 17 of [78], we see that dependence of the end-of-inflation values of $P_{\rm iso}(k_\star)/P_\zeta(k_\star)$ on $N_{\rm f}$ qualitatively agree between DBM and GRF models: for small $N_{\rm f}$, the suppression is most severe, but it remains exponential for large $N_{\rm f}$.

   Our work provides suggestive evidence for a rather model-independent suppression of isocurvature perturbations in small-field slow-roll inflation. This is non-trivial, as no single-field 'adiabatic limit' is reached in these models, which typically contain many tachyons.

3. **Eigenvalue repulsion drives the predictions.**

   A key finding of reference [142] was that 'eigenvalue repulsion' sharply reduces the duration of inflation near a critical point of the DBM potentials: even if the curvature of the potential is fine-tuned to be small at the critical point, small cross-couplings in the Hessian cause the curvature to grow in the neighbourhood of the critical point. As the field evolves from $\phi = 0$ in DBM models, the

[24] Recently, reference [144] studied a GRF-motivated 'multifield' system with one light and many heavy fields, finding that this model gives rise to single-field dynamics. As we are interested in inflation with many dynamically important fields, our assumptions for the initial configuration differ from that of [144], and the question that we explore here – whether manyfield systems can be effectively described as single-field models – also differ significantly from whether an effectively single-field system is well-described by a single-field system.

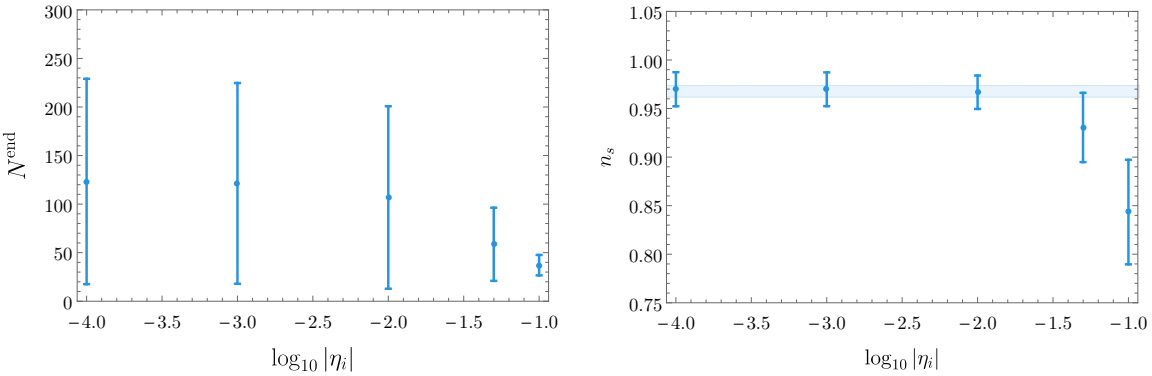

Fig. 2.13 The total number of e-folds and n_s as functions of $\eta_{\rm i}$, with other parameters as in the baseline and together with the 68% c.l. from Planck [10].

eigenvalues of the Hessian matrix relax towards the equilibrium configuration, and quickly spoil any initial fine-tuning of the η_V parameter. As a consequence, it was shown in [142] that the number of e-folds becomes independent of $\eta_{\rm i}$ for $|\eta_{\rm i}| \lesssim 0.01$. Reference [78] furthermore showed that also the spectral index and its running are independent of $|\eta_{\rm i}|$, if similarly small.

As discussed in section 2.4.1, the evolution of the Hessian matrix in the DBM and GRF models differ significantly, and the $\eta_{\rm i}$-dependence of the predictions of the GRF models provides a non-trivial test of the robustness of the DBM results. This is particularly interesting as reference [144] recently used an effectively single-field system motivated by uplifted GRF potentials to propose that the 'steepening' responsible for the $\eta_{\rm i}$ independence is absent in GRF models.[25]

For the GRF models studied in this chapter, Figure 2.13 settles this question. For $-\eta_{\rm i} \gtrsim 0.01$, the predictions depend strongly on $\eta_{\rm i}$, as the initial curvature of the potential curbs the duration of inflation. By contrast, for $-\eta_{\rm i} \lesssim 0.01$ the predictions become independent of the precise value of $\eta_{\rm i}$, as the initial fine-tuning of the Hessian matrix is quickly spoiled when the field moves away from the saddle-point. The distribution of the number of e-folds and the predictions for n_s then stabilise, and become independent of $\eta_{\rm i}$. The running, α_s, while not plotted, is independent of $\eta_{\rm i}$ whenever n_s is. Thus, while the evolution of the Hessian matrix differ between GRF and DBM models, the prediction of $\eta_{\rm i}$ independence (for sufficiently small $\eta_{\rm i}$) holds for both constructions. This strongly suggests that in models in which the eigenvalue spectrum relaxes from an initial, fine-tuned

[25] The authors of references [144, 145] also state that this 'steepening' leads to strong deviations from scale-invariance in DBM models of inflation, but the power spectra of these models are commonly consistent with small deviations from scale invariance [77, 78].

spectrum to a more generic spectrum that includes some tachyonic eigenvalues, the predictions become independent of the initial curvature of the potential for small $|\eta_{\rm i}|$.

In DBM models, several of the predictions at large $N_{\rm f}$ can be explained by eigenvalue repulsion [77, 78, 142]. In particular, the non-generic spectrum in the initial patch quickly relaxes towards the Wigner semi-circle distribution as a consequence of eigenvalue repulsion. This relaxation explains the independence on $\eta_{\rm i}$, the tendency towards red spectral indices, the negative running, and the observed regularity of the power spectra for large $N_{\rm f}$.

In GRF models, the eigenvalues of the Hessian repel in a linear fashion over small field-space distances, leading to the cone of eigenvalue trajectories observed in Figure 2.4. In section 2.3.1, we showed that the statistical properties of the cubic terms of GRF potentials lead to a 'straying' behaviour of the smallest eigenvalue in slow-roll inflation, which is then repelled to tachyonic values at a faster rate than other eigenvalues. Also for the GRF models, we have been able to relate the predictions of the model to properties of the relaxation of the spectrum from a fine-tuned initial configuration to the (slightly shifted) semi-circle. Thus, also for the GRF models, eigenvalue repulsion drives the predictions.

Overall, we find that the only situation for which the predictions differ involves the properties of the models for small $N_{\rm f}$, in which the details of the constructions evidently are very important. For $N_{\rm f} \gg 1$, the predictions of these very different constructions agree, which may be indicative of an emergent limit of inflation in which disparate classes of potentials make the same 'universal' predictions.

2.5 Result III: $f_{\rm NL} \sim \mathcal{O}(1)$ is very rare in manyfield inflation

We are now ready to discuss the main result of this chapter: the levels of primordial non-Gaussianities (NGs) generated in models of manyfield inflation with random potentials. Upcoming cosmological experiments are set to target $f_{\rm NL} \equiv f_{\rm NL}^{\rm local}$, and are expected to reach a sensitivity of $\sigma(f_{\rm NL}) \sim \mathcal{O}(1)$ over the next decade or two [17, 26, 66, 74, 92, 146, 176]. The results presented in this section provide important insights into what we can realistically hope to learn from these experiments.

In inflationary models with multiple canonically normalised fields, the level of non-Gaussianity at horizon exit is commonly very small [31, 183]. Substantial amplitudes

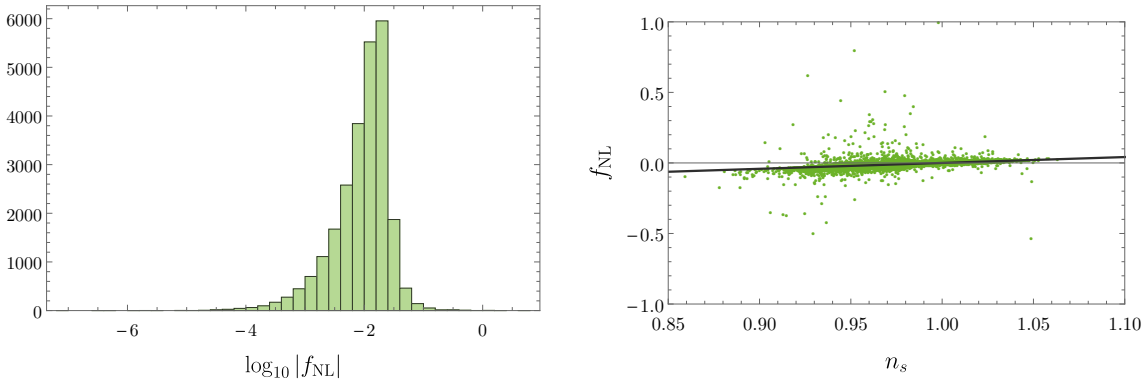

Fig. 2.14 Values for $f_{\rm NL}$ and n_s for 25,000 random inflation models, spanning values of $N_{\rm f}$ between 5 and 50 (the same as in Figure 2.7). The black line in the right plot indicates the single-field consistency condition: $f_{\rm NL} = \frac{5}{12}(n_s - 1)$. NB: the graph on the right excludes six points with $|f_{\rm NL}| > 1$.

of local NG, i.e. $f_{\rm NL} \sim \mathcal{O}(1)$, can be generated through superhorizon evolution of the curvature perturbation, either during inflation or after the end of inflation (cf. e.g. [28, 31, 35, 36, 167, 168, 183, 187] and [47] for a review). In this section, we use the transport method and δN formalism to compute $f_{\rm NL}$ in our ensembles of randomly generated models of manyfield inflation.

The main result of this section is illustrated by Figure 2.14: here n_s and $f_{\rm NL}$ are plotted for an aggregate of 25,000 random inflation models, spanning values of $N_{\rm f}$ between 5 and 50, with both flat and compressed initial mass spectra, cf. equation (2.2.42). The levels of non-Gaussianity is generally very small for these models, with the vast majority having $f_{\rm NL} \sim \mathcal{O}(0.01)$. Out of the 25,000 models, only six had values of $|f_{\rm NL}| > 1$ (these fall outside the boundaries of the right plot of Figure 2.14). Moreover, most realisations even approximately follow the single-field consistency condition between $f_{\rm NL}$ and n_s. For the baseline ensemble of 1000 models (with parameters as in equation (2.2.44)), we find $f_{\rm NL} = -0.012 \pm 0.008$ (at 68% confidence level).

Single-field inflation generates only small levels of NG, and multifield effects are necessary for large $f_{\rm NL}$. However, multifield effects do not suffice to ensure $|f_{\rm NL}| \sim \mathcal{O}(1)$. The left plot of Figure 2.15 shows the relation between $f_{\rm NL}$ and the superhorizon evolution, as given by $\log_{10}\left(P_\zeta(N_{\rm end})/P_\zeta(N_\star)\right)$, for these 25,000 models of inflation. Large values of $f_{\rm NL}$ are only observed in models with some level of superhorizon evolution, but many models with a large ratio of $P_\zeta(N_{\rm end})/P_\zeta(N_\star)$ produce low levels of non-Gaussianity.

There is however a stronger relation between large $f_{\rm NL}$ and the amount of surviving power in the isocurvature modes at the end of inflation, as the right plot of Figure 2.15

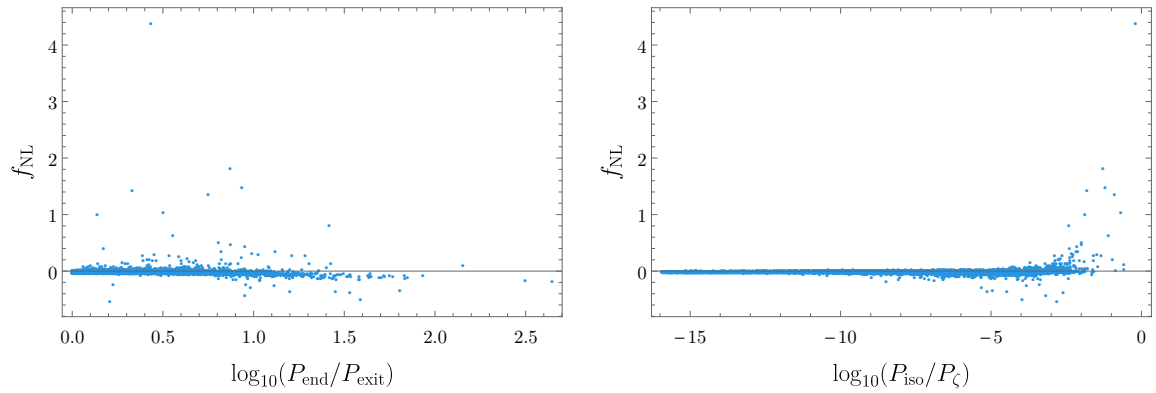

Fig. 2.15 Superhorizon evolution and surviving isocurvature for the same models as in Figure 2.14.

shows. All the cases with large $f_{\rm NL}$ have a ratio of isocurvature modes to adiabatic modes (at $k = k_\star$) of at least $\mathcal{O}(0.01)$. In these models, the curvature perturbation may continue to evolve after the end of inflation, and it is necessary to model the reheating phase to determine the final value of $f_{\rm NL}$ relevant for CMB and Large Scale Structure (LSS) experiments. Only in a handful instances with the highly compressed initial mass spectrum did $f_{\rm NL}$ increase to $\mathcal{O}(1)$ during inflation, but decrease again by the end of it. In Appendix A.5, we provide case studies of a typical 100-field model (with small $f_{\rm NL}$) and one of the rare cases of a 25-field model yielding $f_{\rm NL} \sim \mathcal{O}(1)$.

The statistical prediction of small $f_{\rm NL}$ is robust under changes to the hyperparameters. The number of fields, $N_{\rm f}$, has no noticeable effect on $f_{\rm NL}$: large NGs are rare for all values we have considered. We find a weak dependence on the flatness of the potential: when the potential becomes very flat and the superhorizon evolution decreases (cf. our discussion in section 2.3.3), the values of $f_{\rm NL}$ follow the single-field consistency relation very closely, and large values of $f_{\rm NL}$ become more rare. We find that $f_{\rm NL}$ is independent of $|\eta_{\rm i}|$, except the largest values of $|\eta_{\rm i}|$ we investigate, for which large values of $f_{\rm NL}$ become slightly more common.

The initial mass spectrum at $\phi = 0$ does however have a clear impact on the levels of $f_{\rm NL}$ generated. For the flat spectrum with the eigenvalues of the Hessian uniformly distributed between $3\eta H^2$ and $9H^2/4$, large values of $f_{\rm NL}$ are exceedingly rare: in 19,000 examples with values of $N_{\rm f}$ varying between 5 and 50 we found only one model with large $f_{\rm NL}$ (see Appendix A.5). By contrast, with the (rather extremely) compressed initial spectrum where the masses are spread between $3\eta H^2$ and $-3\eta H^2$, we saw 5 in a sample of around 6,000. Thus, while large values of $f_{\rm NL}$ are still rare, near-degenerate initial spectra appear to make large NGs more frequent.

2.5.1 Why so small?

We have found that in randomly generated models of inflation involving many coupled fields, large values of $f_{\rm NL}$ are very rare. In this section, we discuss the main reasons for this suppression of non-Gaussianities.

The smallness of $f_{\rm NL}$ in our class of models resonates with previous results on the generation of non-Gaussianity through non-derivative interactions during multifield inflation. Reference [31] derived an analytic formula for $f_{\rm NL}$ in multifield models of inflation with sum-separable potentials (thereby generalising the two-field result of [183]), and found that large non-Gaussianities are very rare in slow-roll models with $N_{\rm f}$ free fields. In particular, $f_{\rm NL}$ was found not to be enhanced as $N_{\rm f}$ was increased, consistent with our findings. Moreover, two-field models generating large non-Gaussianities during inflation tend to require substantial levels of fine-tuning, cf. [47–49, 160, 178].

To understand the smallness of $f_{\rm NL}$ in these random manyfield models, it is illuminating to consider the re-expression of the δN formula for $f_{\rm NL}$ derived in [160, 162]. In our notation, generating large $f_{\rm NL}$ in slow-roll, slow-turn models of multifield inflation requires a large contribution from the term

$$f_{\rm NL} \supset \frac{5}{6}\sqrt{2\epsilon_\star}\,\frac{T^2_{\zeta\mathcal{S}}}{\left(1+T^2_{\zeta\mathcal{S}}\right)^2}\,h^i\partial^*_i T_{\zeta\mathcal{S}}\,. \tag{2.5.1}$$

Here $T_{\zeta\mathcal{S}} \equiv \left(\sum_i T^2_{\zeta\mathcal{S}_i}\right)^{1/2}$, and $h^i = e^b\,w^i_b(N^*)/|e^c\,w^j_c(N^*)|$, cf. equations (2.2.62), (2.3.7) and (2.3.11). Here also, ∂^*_i denotes a derivative with respect to the field-space position of the trajectory at horizon crossing in an entropic direction. Equation (2.5.1) has two important consequences: first, to generate large NG, some superhorizon evolution of the curvature perturbation is necessary ($T_{\zeta\mathcal{S}} \neq 0$). However, too much superhorizon evolution suppresses $f_{\rm NL}$. Second, large $f_{\rm NL}$ is only possible if the level of superhorizon evolution of P_ζ is a very sensitive function of the initial conditions, so that $|h^j\partial^*_j T_{\zeta\mathcal{S}}| \gtrsim \mathcal{O}(1/\sqrt{\epsilon_\star})$.

In our GRF models, $T_{\zeta\mathcal{S}}$ is commonly $\mathcal{O}(1)$, and the factor $T^2_{\zeta\mathcal{S}}/(1+T^2_{\zeta\mathcal{S}})^2$ does not strongly suppress $f_{\rm NL}$. However, the amount of superhorizon evolution is rarely a highly sensitive function of the initial conditions: trajectories separated by some small, initial perturbations $|\delta\phi^*_\perp| \ll \Lambda_{\rm h}$ tend to follow very similar paths in field space, and do not generate drastically different $T_{\zeta\mathcal{S}}$. Consequently, $|h^j\partial^*_j T_{\zeta\mathcal{S}}|$ is typically not large enough to generate appreciable levels of NGs.

The decay of isocurvature in multifield, saddle-point models of inflation (cf. our discussion in section 2.3.4) contributes to the typical smallness of $f_{\rm NL}$. When the entropic perturbations $\mathcal{S}^i$ have decayed sufficiently, $T_{\zeta\mathcal{S}}$ ceases to be sourced, and no additional initial condition dependence is induced. This way, the decay of $\mathcal{S}^i$ limits the period during which large NGs could be generated. We also note that $T_{\zeta\mathcal{S}}$ tends to be sensitive to the initial conditions precisely when entropic, off-trajectory perturbations are important. This provides a heuristic explanation for why the isocurvature tends to be large in the few examples we found with $f_{\rm NL} \sim \mathcal{O}(1)$.

We close this section by noting how large $f_{\rm NL}$ may be more frequent in modifications of our construction. Models with very sharp turns or in which nearby classical background trajectories rapidly diverge can lead to substantial non-Gaussianities (see e.g. [8, 54]). In our construction of the potentials, cf. equation (2.2.7), all terms in the potential are suppressed by the same 'UV cut-off scale' $\Lambda_{\rm h}$, which makes features or sharp turns on scales $\ll \Lambda_{\rm h}$ very rare, even if the interaction terms are random. Large $f_{\rm NL}$ may be more common in multi-scale potentials with features on small scales, at least if these appear along the trajectory before the isocurvature has decayed.

Finally, our results do not preclude large values of $f_{\rm NL}$ being generated after inflation, during the reheating phase, as is the case in many 'spectator' models, cf. [69, 129, 137, 138, 151]. However, in models with general interactions and exponentially suppressed isocurvature at the end of inflation, generating large $f_{\rm NL}$ through reheating dynamics may remain challenging.

2.6 Conclusions

In this chapter, we have studied inflation in models with multiple fields subject to randomly generated interaction terms. We have used Gaussian random fields (GRFs) with a Gaussian covariance function to model the scalar potentials locally around an approximate saddle-point in field space. These potentials admit an interpretation as proxies for physical effective field theories, and exhibit structure over field space distances of $\Lambda_{\rm h} < M_{\rm P}$. By identifying and systematically applying algebraic simplifications to the covariance matrix of the Taylor coefficients, we have for the first time been able to use this method to construct explicit scalar potentials with many interacting fields. Our examples include 100-field models involving 97 million independent, randomly generated couplings.

We used these potentials to construct models of slow-roll inflation with many dynamically important fields, i.e. models of manyfield inflation. By using the transport

method and the δN formalism, we computed the primordial perturbations generated during inflation, including the curvature and isocurvature modes, and the amplitude of local non-Gaussianity, $f_{\rm NL}$. These studies led to several novel results.

Summary of findings

As the fields evolve from the approximate saddle-point where the mass spectrum is fine-tuned, the eigenvalues of the Hessian 'relax' towards a shifted semi-circle distribution. This relaxation is, over short distances, driven by the cubic terms in the potential. We have shown that a combination of the statistical properties of Gaussian random fields and the dynamics of multifield slow-roll inflation lead to a particularly fast relaxation of the smallest eigenvalue of the Hessian, making it 'stray' from the other eigenvalues. This 'straying' has important consequences for the observational predictions of the models.

The generated power spectra of the GRF models are very simple, close to scale-invariant and well-described by an approximate power law. We have shown that large regions of the (hyper-)parameter space are compatible with current observational constraints on the spectral index. However, some regions, in particular those describing very flat potentials, are already ruled out by the Planck experiment.

These models make a robust prediction for the running of the spectral index. A small negative running is vastly preferred, and a future observation of α_s outside the range $-0.004 \leq \alpha_s \leq 0$ would, together with existing Planck constraints, rule out all models that we have constructed. For our baseline 10-field model (cf. equation (2.2.44)), we find $\alpha_s = -0.00143 \pm 0.00034$ (the latter being the standard deviation).

A striking aspect of these models is that while several fields go tachyonic during inflation and the curvature perturbation commonly evolves significantly on superhorizon scales, the power in the isocurvature modes decays during inflation. We have explained this phenomenon, also observed in [78], as a consequence of multifield slow-roll dynamics, in which the adiabatic mode tends to align with the most rapidly growing field perturbation. The suppression is further enhanced by the 'straying' of the smallest eigenvalue of the Hessian matrix. The exponential suppression of isocurvature during multifield slow-roll inflation makes the predictions less sensitive to the details of the reheating phase, and could make models involving large numbers of dynamically important fields comfortably compatible with CMB constraints on isocurvature.

We have furthermore critically assessed the similarities and differences between our models and those recently constructed using the random matrix theory 'DBM' technique [77, 78, 142]. We have argued that these constructions provide fundamentally

different descriptions for the evolution of the eigenvalues of the Hessian matrix,[26] yet strikingly, despite the differences in the constructions the predictions of these models agree very well, with the only difference being related to properties of the models at small $N_{\rm f}$. This suggests that, at large $N_{\rm f}$, these very different constructions may fall in the same 'universality class' of inflationary models.

Finally, we computed the level of local non-Gaussianity (NG) generated by multifield effects on superhorizon scales and found that, typically, it is very small, with $|f_{\rm NL}| \ll 1$. For the baseline parameters we found $f_{\rm NL} = -0.012 \pm 0.008$. The smallness of $f_{\rm NL}$ is largely independent of the choice of hyperparameters, and constitutes a robust statistical prediction of these models. We found that $f_{\rm NL}$ is typically small even in models in which multifield effects are important and in which the superhorizon evolution of the perturbations is substantial. In a handful of models, we found $f_{\rm NL} \sim \mathcal{O}(1)$. However, all models with large $f_{\rm NL}$ that we found also have comparatively large levels of isocurvature remaining at the end of inflation, which may affect the predictions of the models through the reheating phase. We have argued that the suppression of $f_{\rm NL}$ is a consequence of the robustness of the multifield evolution to small modifications of the initial conditions, and the decay of isocurvature during inflation.

Our results indicate that multifield models of inflation do not generically predict $f_{\rm NL} \sim \mathcal{O}(1)$, and that large classes of models including the slow-roll, saddle-point GRF models we have constructed, typically yield $|f_{\rm NL}| \ll 1$. This suggests that a future detection of $f_{\rm NL}$ of order unity would point to rather special, non-random inflationary dynamics.

The method developed in this chapter opens a new window towards general models of inflation with many fields subject to non-trivial interactions. Our findings speak for the robustness of the inflationary paradigm: adiabatic, approximate scale-invariant and nearly Gaussian perturbations are commonly regarded as the 'generic predictions' of single-field slow-roll inflation. In this chapter, we have shown that even highly complex models of manyfield inflation produce very similar predictions. We anticipate that these results can be useful in interpreting the outcomes of future cosmological observations.

[26] By contrast, the equilibrium spectra of these models only differ superficially, and are easily rendered compatible. Our discussion in sections 2.2.3 and 2.4 may be useful for readers interested in the context of some recent results comparing GRF and RMT models [88, 144, 145].

Chapter 3

Gaussian random fields

3.1 Introduction

In Chapter 2 we saw how Gaussian random fields (GRFs) can be used to generate random potentials for inflation, but this simple class of random functions also has many other important applications in mathematics, computer science, and the natural sciences.

In this chapter we provide the proof of the result used in Chapter 2, that if a GRF with a Gaussian covariance function is generated order by order as a Taylor series, the covariance matrices of the conditional distributions will always be diagonal. This results holds in any number of dimensions and up to any order. We will also discuss some potential applications of this result beyond random potentials for inflation.

A real-valued and stationary GRF, $f(\mathbf{x})$: $\mathbb{R}^d \to \mathbb{R}$, is a random function that is completely described statistically by its mean value $\bar{f}$ and the covariance function $C(\mathbf{x}_1, \mathbf{x}_2) = C(\mathbf{x}_1 - \mathbf{x}_2)$:

$$\langle (f(\mathbf{x}_1) - \bar{f})(f(\mathbf{x}_2) - \bar{f}) \rangle = C(\mathbf{x}_1 - \mathbf{x}_2)\,. \tag{3.1.1}$$

If we sample the values of $f(\mathbf{x})$ at a set of points $\mathbf{x}_1, \ldots, \mathbf{x}_M$ in $\mathbb{R}^d$, the values follow a multivariate Gaussian distribution with covariances between the points given by the covariance functions, $\Sigma_{ij} = C(\mathbf{x}_i, \mathbf{x}_j)$, and mean $\bar{f}$.

One can use this property to generate values of the GRF at a discrete set of points, but for our purposes, where we need continuous and well defined derivatives, this is not enough. A common, alternative approach is instead to generate f through its Fourier coefficients, which are statistically independent. This method can be efficient even for a wide range of scales, but it is not well-suited for all problems. In particular, it does

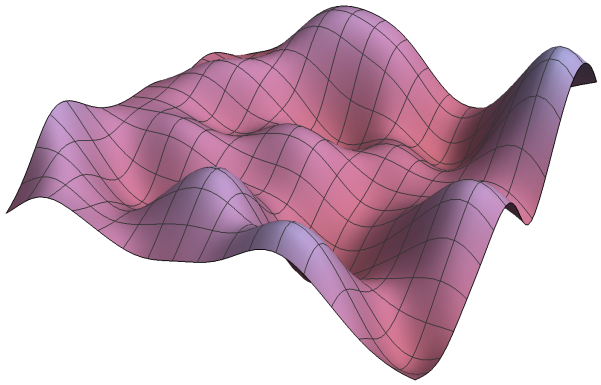

Fig. 3.1 An example of a GRF with $d = 2$ and $n_{\max} = 175$. Here $\mathbf{x} \in [-4l,\ 4l]^2$.

not easily generalise to the conditional problem of generating f given that $f(\mathbf{x}_\star)$ has some special properties (e.g. is a maximum, minimum or a saddle-point).

In this chapter, we present a novel method for addressing these problems for the special but frequently considered case in which the GRF is stationary, isotropic and with a Gaussian (or squared exponential) covariance function:

$$C(\mathbf{x}_1 - \mathbf{x}_2) = h^2 \exp\left(-\tfrac{(\mathbf{x}_1-\mathbf{x}_2)^2}{2\ell^2}\right) . \tag{3.1.2}$$

The hyperparameters of this covariance function are h and ℓ; we take $\bar{f} = 0$ but our results generalise straightforwardly to $\bar{f} \neq 0$. Our method is local, and we construct the explicit realisation of f through its Taylor expansion up to the order $n_{\max}$ around a single point $\mathbf{x}_\star \in \mathbb{R}^d$. By specifying some of the coefficients by hand, this method can be used to conditionally generate f given that it has e.g. a maximum, minimum or saddle point at $\mathbf{x}_\star$, but is otherwise random (there is a slight caveat here that will be covered in Section 3.3.1).

The key simplification of our method is that the covariance matrix becomes exactly diagonal through a sequential, order-by-order use of the marginal and conditional probability distributions for the Taylor coefficients. This dispenses with the need to numerically invert the covariance matrix, which makes our method efficient even for large d or $n_{\max}$.

We expect this method to be particularly useful when one is interested in generating explicit GRFs within a moderately small region in $\mathbb{R}^d$ (say, extending at most a few units of ℓ from $\mathbf{x}_\star$). In Chapter 2 we showed that this method enables explicit studies

of cosmic inflation in models with a large number of fields interacting through a potential energy modelled by a GRF (for related work, see [23, 43, 94, 95, 144, 179]). For $n_{\max} = 5$ a model with $d = 100$ fields involves 96,560,546 interaction terms, and explicitly generating the potential naively involves diagonalising a covariance matrix with $\mathcal{O}(10^{15})$ independent entries. Our method trivialises the inversion of the covariance matrix, and it furthermore makes it very straightforward to condition the GRF on being locally suitable for inflation. Our method is also efficient for moderate d but $n_{\max} \gg 1$, as illustrated by an example in Figure 3.1.

Finally, we also note that this result is also useful in the (niche) inverse problem, where we have a GRF in terms of the Taylor coefficients and want to infer the hyperparameters h and ℓ.

This chapter is rather different from the other in this thesis, as we are not directly concerned with cosmology. Moreover, the proof is rather involved and will require specialised notation that will only be used here. To make the proof easier to understand, we first demonstrate the logic in a few simple examples before tackling the proof in general.

3.2 A new method for generating realisations of a GRF

In this section, we first review some relevant properties of GRFs and establish our notation. We then exemplify our method by considering $d = 2$ and $n_{\max} = 4$, before turning to the general, inductive proof of the method.

A standard result, which will be our starting point, is that the covariances for the derivatives of f are given by the derivatives of the covariance function,

$$\left\langle \frac{\partial^{n_1} f(\mathbf{x}_1)}{\partial x_1^{a_1} \dots \partial x_1^{a_{n_1}}} \frac{\partial^{n_2} f(\mathbf{x}_2)}{\partial x_2^{b_1} \dots \partial x_2^{b_{n_2}}} \right\rangle = \frac{\partial^{n_1+n_2} C(\mathbf{x}_1 - \mathbf{x}_2)}{\partial x_1^{a_1} \dots \partial x_1^{a_{n_1}} \partial x_2^{b_1} \dots \partial x_2^{b_{n_2}}} \,. \tag{3.2.1}$$

The indices a and b take values between 1 and d. The expectation values of the derivatives are given by the derivatives of the expectation value, which we take to be zero. To simplify notation, we will from now on write the derivatives of f as:

$$\frac{\partial^n f(\mathbf{x})}{\partial x^{a_1} \dots \partial x^{a_n}} \equiv f_{a_1 \dots a_n}(\mathbf{x}) \,. \tag{3.2.2}$$

In this chapter we create the random functions by generating Taylor coefficients, $f_{a_1 \dots a_n}$, at a single point, $\mathbf{x}_\star$. Their joint probability distribution is just a multivariate

normal distribution with a covariance matrix given by the derivatives of the covariance function at $\mathbf{x}_1 = \mathbf{x}_2 = \mathbf{x}_\star$. Of course, not all the derivatives are algebraically independent, so we only consider the coefficients $f_{a_1 \ldots a_n}$ with indices ordered such that $a_1 \geq \ldots \geq a_n$. This ensures that all the unique coefficients are included exactly once.

We will consider Taylor expansions that are truncated at a finite order, $n \leq n_{\max}$. To simplify our notation, we denote the unique, ordered Taylor coefficients for any $0 \leq n \leq n_{\max}$ indices by f_α. The multivariate probability density function for the algebraically independent Taylor coefficients is then given by:

$$p(f_\alpha) = \frac{\exp\left(-\frac{1}{2}(f_\alpha - \mu_\alpha)(\Sigma^{-1})_{\alpha\beta}(f_\beta - \mu_\beta)\right)}{\sqrt{\det(2\pi\Sigma)}}\,, \tag{3.2.3}$$

where $\mu_\alpha = \langle f_\alpha \rangle$ is the expectation value vector and $\Sigma_{\alpha\beta} = \langle (f_\alpha - \mu_\alpha)(f_\beta - \mu_\beta) \rangle$ is the covariance matrix. Here repeated indices are a short-hand for the double-sum over n and the ordered indices for each n.

The key obstacle for generating realisation of the GRF from the multivariate probability distribution of equation (3.2.3) is the need to invert the covariance matrix. When the number of independent coefficients becomes very large, numerical inversion becomes prohibitively costly. The purpose of this chapter is to show how such an inversion can be circumvented for GRFs with the covariance function (3.1.2) by sequential application of the marginal and conditional probability distributions for the Taylor coefficients.

In general, if the vectors Z_1 and Z_2, are randomly distributed according to the multivariate normal distribution,

$$\begin{bmatrix} Z_1 \\ Z_2 \end{bmatrix} \sim N\left(\begin{bmatrix} \mu_1 \\ \mu_2 \end{bmatrix}, \begin{bmatrix} \Sigma_{11} & \Sigma_{12} \\ \Sigma_{21} & \Sigma_{22} \end{bmatrix} \right)\,, \tag{3.2.4}$$

where (μ_1, μ_2) is the mean vector and Σ_{ij} are block components of the covariance matrix, then the probability distribution for Z_1 obtained when marginalising over Z_2 is

$$Z_1 \sim N(\mu_1, \Sigma_{11})\,. \tag{3.2.5}$$

The conditional probability distribution for the vector Z_2 obtained after fixing $Z_1 = z_1$ is the multivariate normal distribution with expectation values and covariance given

by:

$$\mathrm{E}[Z_2|z_1] = \mu_2 + \Sigma_{21}\Sigma_{11}^{-1}(z_1 - \mu_1)\,, \tag{3.2.6}$$

$$\mathrm{Cov}[Z_2|z_1] = \Sigma_{22} - \Sigma_{21}\Sigma_{11}^{-1}\Sigma_{12}\,. \tag{3.2.7}$$

By using these expressions, and the fact that we can factorise a general multivariate probability density function for a collection of random variables Z_i as

$$p(z_1, z_2, \ldots, z_n) = p(z_1|z_2, \ldots, z_n)p(z_2|z_3, \ldots z_n)\ldots p(z_n), \tag{3.2.8}$$

we will be able to vastly simplify the joint probability density function by writing it in terms of much simpler conditional densities (which themselves are also Gaussian).

We now give a simple example showing how these expressions simplify the generation of the Taylor coefficients.

3.2.1 Motivational example

To illustrate the main point of our method, it is convenient to initially absorb the hyperparameters h and ℓ of equation (3.1.2) into f and $\mathbf{x}$. The covariance function is then given by

$$\langle f(\mathbf{x}_1)f(\mathbf{x}_2)\rangle = e^{-(\mathbf{x}_1-\mathbf{x}_2)^2/2}\,, \tag{3.2.9}$$

and the covariances of the first few derivatives of f at $\mathbf{x}_\star$ are:

$$\langle ff\rangle = 1\,, \quad \langle ff_a\rangle = 0\,, \quad \langle ff_{ab}\rangle = -\delta_{ab}\,, \tag{3.2.10}$$

$$\langle f_a f_b\rangle = \delta_{ab}\,, \quad \langle f_a f_{bc}\rangle = 0\,, \quad \langle f_{ab}f_{cd}\rangle = \delta_{ab}\delta_{cd} + \delta_{ac}\delta_{bd} + \delta_{ad}\delta_{bc}\,. \tag{3.2.11}$$

Note that we may obtain the covariances between derivatives of different orders by changing which field the derivatives act on; each time this is done, we pick up a minus sign. All covariances between even and odd derivatives vanish since the covariance function is even.

The above covariances are symmetric in all the indices, and for any given set of indices it is easy to write down the value of the covariance according to the following combinatoric rules: If any index appears an odd number of times, the covariance is zero. For an index appearing n (even) times we get a factor of $(n-1)!!$, which is the number of unique ways they can be put together in Kroenecker deltas. The total covariance for a given set of indices is then given by the product of such factors for each index

appearing in the indices. The overall sign is set by half the difference of number of indices of the two sets. For example, $\langle f_{555221} f_{995221} \rangle = (-1)^{(6-6)/2}(4!!)^2(2!!)^2 = 256$.

We now specialise to the case of $d = 2$. Since the covariances between Taylor coefficients with an even and an odd number of indices vanishes, the full covariance matrix is block diagonal. We here consider the covariance matrix for the Taylor coefficients with an even number of indices, which for the variables f, $f_{a_1 a_2}$, and $f_{a_1 \dots a_4}$ is given by

$$\Sigma = \left(\begin{array}{c|ccc|ccccc} 1 & -1 & 0 & -1 & 3 & 0 & 1 & 0 & 3 \\ \hline -1 & 3 & 0 & 1 & -15 & 0 & -3 & 0 & -3 \\ 0 & 0 & 1 & 0 & 0 & -3 & 0 & -3 & 0 \\ -1 & 1 & 0 & 3 & -3 & 0 & -3 & 0 & -15 \\ \hline 3 & -15 & 0 & -3 & 105 & 0 & 15 & 0 & 9 \\ 0 & 0 & -3 & 0 & 0 & 15 & 0 & 9 & 0 \\ 1 & -3 & 0 & -3 & 15 & 0 & 9 & 0 & 15 \\ 0 & 0 & -3 & 0 & 0 & 9 & 0 & 15 & 0 \\ 3 & -3 & 0 & -15 & 9 & 0 & 15 & 0 & 105 \end{array}\right), \tag{3.2.12}$$

where the first row/column is for f, the following three are for the $(1,1)$, $(2,1)$ and $(2,2)$ components of $f_{a_1 a_2}$, and the final five are for the $(1,1,1,1)$, $(2,1,1,1)$, etc. components of $f_{a_1 \dots a_4}$.

The marginal distribution for f is simply given by $f \sim N(0,1)$. Fixing f, the conditional covariance matrix for $f_{a_1 a_2}$ and $f_{a_1 a_2 a_3 a_4}$ is obtained from equation (3.2.7):

$$\Sigma = \left(\begin{array}{ccc|ccccc} 2 & 0 & 0 & -12 & 0 & -2 & 0 & 0 \\ 0 & 1 & 0 & 0 & -3 & 0 & -3 & 0 \\ 0 & 0 & 2 & 0 & 0 & -2 & 0 & -12 \\ \hline -12 & 0 & 0 & 96 & 0 & 12 & 0 & 0 \\ 0 & -3 & 0 & 0 & 15 & 0 & 9 & 0 \\ -2 & 0 & -2 & 12 & 0 & 8 & 0 & 12 \\ 0 & -3 & 0 & 0 & 9 & 0 & 15 & 0 \\ 0 & 0 & -12 & 0 & 0 & 12 & 0 & 96 \end{array}\right). \tag{3.2.13}$$

We note that the 3×3 block matrix in the upper left corner is now diagonal, and the probability distribution for $f_{a_1a_2}$ given f is now given by

$$(f_{a_1a_2}|f) \sim N\left(\begin{bmatrix}-f\\0\\-f\end{bmatrix}, \begin{bmatrix}2&0&0\\0&1&0\\0&0&2\end{bmatrix}\right). \tag{3.2.14}$$

Clearly, the second order derivatives are now independent Gaussian random numbers.

Finally, fixing $f_{a_1a_2}$ in addition to f, we find that the conditional probability distribution for $f_{a_1a_2a_3a_4}$ is given by

$$(f_{a_1a_2a_3a_4}|f_{a_1a_2},\, f) \sim N\left(\begin{bmatrix}-3(f+2f_{11})\\-3f_{21}\\-f-f_{11}-f_{22}\\-3f_{21}\\-3(f+2f_{22})\end{bmatrix}, \begin{pmatrix}24&0&0&0&0\\0&6&0&0&0\\0&0&4&0&0\\0&0&0&6&0\\0&0&0&0&24\end{pmatrix}\right). \tag{3.2.15}$$

Since the covariance matrix again is diagonal, the fourth order Taylor coefficients can also be generated as independent Gaussian random numbers, without the need to diagonalise the original covariance matrix (3.2.12).

3.2.2 All orders proof

In this section, we show that the method of section 3.2.1 applies for arbitrary d and $n_{\max}$. That is, we will show that the conditional covariance matrix for the k:th order Taylor coefficients is diagonal, given all lower-order Taylor coefficients of the same type (even or odd).

Additional notation

It is convenient to introduce some additional notation that will allow us to prove our main result simultaneously for the cases of even and odd number of indices. The covariance matrix is again block-diagonal, and each block further consists of the covariances of Taylor coefficients of increasingly high order, up to order $n_{\max}$ or $n_{\max} - 1$. We collectively refer to the orders in the even and odd case as 'levels', i, where $i = n/2 + 1$ in the even case and $i = (n+1)/2$ in the odd case. For each level, the index α_i runs over the ordered set of indices (we may replace α with any lower case

Greek index). The n_i indices within a set α_i will be labelled by the corresponding lower case Latin letters and a number, e.g. $a_1, a_2, \ldots$. An unordered set will be denoted α_i^u.

For example, for even derivatives $i = 1$ corresponds to f (so that $n_1 = 0$), $i = 2$ to $f_{a_1 a_2}$ ($n_2 = 2$), etc. and for odd derivatives $i = 1$ corresponds to f_{a_1} ($n_1 = 1$), $i = 2$ to $f_{a_1 a_2 a_3}$ ($n_2 = 3$).

It is also convenient to write the covariances as:

$$\langle f_{\alpha_i} f_{\beta_j} \rangle = C_{\alpha_i \beta_j} \,. \tag{3.2.16}$$

Each $C_{\alpha_i \beta_j}$ will consist of a sum over Kronecker deltas that 'connect' indices in α_i with indices in β_j, or with other indices in α_i. We will find it convenient to consider modified covariances, $C^k_{\alpha_i \beta_j}$, which are obtained from $C_{\alpha_i \beta_j}$ by removing all terms with Kronecker deltas connecting either n_1, n_2, ..., or n_k indices from α_i with the same number of indices from β_j (remaining indices are connected internally). We will also write

$$C^{i-1}_{\alpha_i \beta_i} = D_{\alpha_i \beta_i} \,, \tag{3.2.17}$$

for which all indices in α_i are connected with indices in β_i, so that $D_{\alpha_i \beta_i}$ is only non-vanishing if $\alpha_i = \beta_i$, and hence, $D_{\alpha_i \beta_i}$ is a diagonal matrix. For example, in the even case we have:

$$C^1_{\alpha_2 \beta_2} = D_{\alpha_2 \beta_2} = \delta_{a_1 b_1} \delta_{a_2 b_2} + \delta_{a_1 b_2} \delta_{a_2 b_1} \,. \tag{3.2.18}$$

The diagonal matrix can further be written as,

$$D_{\alpha_i \beta_i} = \delta_{\alpha_i \beta_i} \mathrm{Comb}(\alpha_i), \tag{3.2.19}$$

where $\mathrm{Comb}(\alpha_i)$ is a combinatorial factor determined by the values of the indices in α_i, and it is the number of ways the numbers in the set can be paired up with the same numbers in an identical set. If we denote the number of times an index value a appears in α_i by k_a, we then have:

$$\mathrm{Comb}(\alpha_i) = \prod_{a=1}^{d} k_a! \,. \tag{3.2.20}$$

As an example, the set $\{3, 3, 1, 1, 1\}$ can be paired up with an identical ordered set in $2! \times 3! = 12$ ways. We also note that the total number of permutations of a set of indices α_i is given by:

$$\mathrm{Perms}(\alpha_i) = \frac{n_i!}{\mathrm{Comb}(\alpha_i)} \,. \tag{3.2.21}$$

Using the same example as before, one can easily see that the set has 10 permutations, which agrees exactly with $5!/2!3! = 10$.

Finally, we will write the conditional covariance matrix for the Taylor coefficients with levels from k through n, given values for the lower levels 1 through $k-1$ as $\Sigma^{k-1}_{k,n}$.

From the first to the second level

We now want to prove that if we specify levels 1 through k, then the covariance matrix of conditional probability distributions for level $k+1$ will be diagonal. As a starting point, we write down the covariance matrix for levels 1 through n for some $n > k$:

$$\Sigma_{1,n} = \begin{pmatrix} C_{\alpha_1\beta_1} & C_{\alpha_1\beta_2} & C_{\alpha_1\beta_3} & \dots & C_{\alpha_1\beta_{n-1}} & C_{\alpha_1\beta_n} \\ C_{\alpha_2\beta_1} & C_{\alpha_2\beta_2} & C_{\alpha_2\beta_3} & \dots & C_{\alpha_2\beta_{n-1}} & C_{\alpha_2\beta_n} \\ C_{\alpha_3\beta_1} & C_{\alpha_3\beta_2} & C_{\alpha_3\beta_3} & \dots & C_{\alpha_3\beta_{n-1}} & C_{\alpha_3\beta_n} \\ \vdots & \vdots & \vdots & & \vdots & \vdots \\ C_{\alpha_{n-1}\beta_1} & C_{\alpha_{n-1}\beta_2} & C_{\alpha_{n-1}\beta_3} & \dots & C_{\alpha_{n-1}\beta_{n-1}} & C_{\alpha_n\beta_n} \\ C_{\alpha_n\beta_1} & C_{\alpha_n\beta_2} & C_{\alpha_n\beta_3} & \dots & C_{\alpha_n\beta_n} & C_{\alpha_n\beta_n} \end{pmatrix}. \tag{3.2.22}$$

This can be for either the odd or the even case. For the even case $C_{\alpha_1\beta_1} = D_{\alpha_1\beta_1} = \langle f f \rangle = 1$, which can be thought of as a diagonal matrix in the set α_1 (which only takes the value $\emptyset$). For the odd case $C_{\alpha_1\beta_1} = D_{\alpha_1\beta_1} = \langle f_{a_1} f_{b_1} \rangle = \delta_{a_1 b_1}$, which again is diagonal. Thus, the lowest order Taylor coefficients can always be fixed as independent Gaussian random variables.

Now suppose we fix f_{α_1}. From equation (3.2.7), we then obtain the following distribution for the remaining levels:

$$\begin{aligned} \Sigma^1_{2,n} = &\begin{pmatrix} C_{\alpha_2\beta_2} & C_{\alpha_2\beta_3} & \dots & C_{\alpha_2\beta_{n-1}} & C_{\alpha_2\beta_n} \\ C_{\alpha_3\beta_2} & C_{\alpha_3\beta_3} & \dots & C_{\alpha_3\beta_{n-1}} & C_{\alpha_3\beta_n} \\ \vdots & \vdots & & \vdots & \vdots \\ C_{\alpha_{n-1}\beta_2} & C_{\alpha_{n-1}\beta_3} & \dots & C_{\alpha_{n-1}\beta_{n-1}} & C_{\alpha_n\beta_n} \\ C_{\alpha_n\beta_2} & C_{\alpha_n\beta_3} & \dots & C_{\alpha_n\beta_n} & C_{\alpha_n\beta_n} \end{pmatrix} - \\ &- \begin{pmatrix} C_{\alpha_2\gamma_1} \\ C_{\alpha_3\gamma_1} \\ \vdots \\ C_{\alpha_{n-1}\gamma_1} \\ C_{\alpha_n\gamma_1} \end{pmatrix} (D^{-1})_{\gamma_1\epsilon_1} \begin{pmatrix} C_{\epsilon_1\beta_2} & C_{\epsilon_1\beta_3} & \dots & C_{\epsilon_1\beta_{n-1}} & C_{\epsilon_1\beta_n} \end{pmatrix}. \end{aligned} \tag{3.2.23}$$

Again, repeated indices are summed over. In more compact notation, this can be written as:

$$(\Sigma^1_{2,n})_{\alpha_i\beta_j} = C_{\alpha_i\beta_j} - C_{\alpha_n\gamma_1}(D^{-1})_{\gamma_1\epsilon_1}C_{\epsilon_1\beta_j}\,, \tag{3.2.24}$$

where $(\Sigma^1_{2,n})_{\alpha_i\beta_j}$ is the conditional covariance between f_{α_i} and f_{β_j}, given f_{α_1}.

In both the odd and even cases, $D_{\gamma_1\epsilon_1}$ is diagonal and in fact just given by $\delta_{\gamma_1\epsilon_1}$ as described above, so we find:

$$(\Sigma^1_{2,n})_{\alpha_i\beta_j} = C_{\alpha_i\beta_j} - C_{\alpha_n\gamma_1}C_{\gamma_1\beta_j}\,. \tag{3.2.25}$$

This is really just the original covariance, with all the terms mixing n_1 indices from α_j with indices from β_j dropped. To make this obvious, we write out these terms explicitly:

$$(\Sigma^1_{2,n})_{\alpha_i\beta_j} = \begin{cases} \langle f_{a_1\ldots a_{2i-2}} f_{b_1\ldots b_{2j-2}}\rangle - \langle f_{a_1\ldots a_{2i-2}} f\rangle\langle f f_{b_1\ldots b_{2j-2}}\rangle & \text{even case}\,, \\ \langle f_{a_1\ldots a_{2i-1}} f_{b_1\ldots b_{2j-1}}\rangle - \langle f_{a_1\ldots a_{2i-1}} f_{c_1}\rangle\langle f_{c_1} f_{b_1\ldots b_{2j-1}}\rangle & \text{odd case}\,. \end{cases} \tag{3.2.26}$$

In the even case, the second term subtracts from the first all terms where the a_i and b_i indices do not mix, i.e. those terms with $n_1 = 0$ indices from each set in mixed Kronecker deltas. In the odd case, the second term subtracts from the first all terms where only one of the a_i indices and one of the b_i indices are in a Kronecker delta together, i.e. those terms with $n_1 = 1$ indices from each set in mixed Kronecker deltas. It then follows that we have

$$(\Sigma^1_{2,n})_{\alpha_2\beta_2} = C^1_{\alpha_2\beta_2} = D_{\alpha_2\beta_2} = \delta_{\alpha_2\beta_2}\mathrm{Comb}(\alpha_2)\,. \tag{3.2.27}$$

Equation (3.2.27) implies that the second order coefficients of the conditional probability distribution are statistically independent, and can be generated without explicitly inverting a non-trivial covariance matrix (when marginalising over higher levels).

To further illustrate equation (3.2.27), we see that in the even case it explicitly corresponds to:

$$(\Sigma^1_{2,n})_{\alpha_2\beta_2} = \langle f_{a_1a_2} f_{b_1b_2}\rangle - \langle f_{a_1a_2} f\rangle\langle f f_{b_1b_2}\rangle = \delta_{a_1b_1}\delta_{a_2b_2} + \delta_{a_1b_2}\delta_{a_2b_1}\,, \tag{3.2.28}$$

which follows from $\langle f_{a_1a_2} f\rangle = -\delta_{a_1a_2}$. In the odd case, we have

$$\begin{aligned}(\Sigma^1_{2,n})_{\alpha_2\beta_2} &= \langle f_{a_1a_2a_3} f_{b_1b_2b_3}\rangle - \langle f_{a_1a_2a_3} f_{c_1}\rangle\langle f_{c_1} f_{b_1b_2b_3}\rangle \\ &= \delta_{a_1b_1}\delta_{a_2b_2}\delta_{a_3b_3} + \delta_{a_1b_1}\delta_{a_2b_3}\delta_{a_3b_2} + \delta_{a_1b_2}\delta_{a_2b_1}\delta_{a_3b_3} + \delta_{a_1b_2}\delta_{a_3b_2}\delta_{a_3b_1} \\ &\quad + \delta_{a_1b_3}\delta_{a_2b_2}\delta_{a_3b_1} + \delta_{a_1b_3}\delta_{a_3b_2}\delta_{a_2b_3}\,. \end{aligned} \tag{3.2.29}$$

Here we have used

$$\langle f_{a_1a_2a_3} f_{c_1}\rangle = -\delta_{a_1a_2}\delta_{a_3c_1} - \delta_{a_1a_3}\delta_{a_2c_1} - \delta_{a_2a_3}\delta_{a_1c_1}\,, \tag{3.2.30}$$

and a similar expression for $\langle f_{c_1} f_{b_1b_2b_3}\rangle$. The second term of the top line of equation (3.2.29) will cancel out the terms where only one delta contains an index each from both sets, and since every term must have either one or three such deltas (there are three indices in each set), it follows that the only terms that remain are those in which all the indices are mixed.

For pedagogical reasons: from the second to the third level

To illustrate the structure of our general inductive proof, we here consider the less trivial step of the conditional covariance after fixing both f_{α_1} and f_{α_2}. The covariance matrix for the higher levels is then given by

$$(\Sigma^2_{3,n})_{\alpha_i\beta_j} = C^1_{\alpha_i\beta_j} - C^1_{\alpha_i\gamma_2}(D^{-1})_{\gamma_2\epsilon_2}C^1_{\epsilon_2\beta_j}, \tag{3.2.31}$$

with $3 \leq i, j \leq n$. Now, using the expression for the diagonal matrix given in equation (3.2.19), we can write this as

$$(\Sigma^2_{3,n})_{\alpha_i\beta_j} = C^1_{\alpha_i\beta_j} - \sum_{\gamma_2} C^1_{\alpha_i\gamma_2}C^1_{\gamma_2\beta_j}/\mathrm{Comb}(\gamma_2)\,, \tag{3.2.32}$$

where the sum is over ordered sets of indices.

To generalise the argument of the previous section, we first rewrite this in terms a sum over unordered indices. This will overcount the index sets by a factor of how many permutations there are of them, so in every term we need to divide by the number of

permutations:

$$\begin{aligned}(\Sigma^2_{3,n})_{\alpha_i\beta_j} &= C^1_{\alpha_i\beta_j} - \sum_{\gamma_2^u} C^1_{\alpha_i\gamma_2^u} C^1_{\gamma_2^u\beta_j}/(\mathrm{Comb}(\gamma_2)\mathrm{Perms}(\gamma_2)) \\ &= C^1_{\alpha_i\beta_j} - \sum_{\gamma_2^u} C^1_{\alpha_i\gamma_2^u} C^1_{\gamma_2^u\beta_j}/n_2!\,, \end{aligned} \tag{3.2.33}$$

where in the last step we used equation (3.2.21). We recall that $C^1_{\alpha_i\gamma_2^u}$ includes no terms with n_1 indices connecting α_i and γ_2^u. Since these cannot be connected by fewer than n_1 indices (recall that $n_1^{\mathrm{even}} = 0$ and $n_1^{\mathrm{odd}} = 1$), they must be connected by more than n_1 indices. More generally, $C^k_{\alpha_i\beta_j}$ only contains terms in which $n \in \{n_{k+1}, n_{k+2}, ...\}$ indices from two sets α_i and β_j are paired up in Kronecker deltas. This is because there must be even numbers of indices left in the sets α_i and β_j, and all the n_l differ by multiples of two. E.g. for the odd case α_3 has $n_3 = 5$ indices and only $n_1 = 1$, $n_2 = 3$ or $n_3 = 5$ indices from α_3 can be paired up with indices from another set in $C_{\alpha_5\beta_j}$. This then tells us that in $C^1_{\alpha_i\gamma_2^u}$, all n_2 of the indices from the set γ_2^u are together in deltas with some indices from α_i.

Note also that the terms in the $C^1_{\alpha_i\beta_j}$ may be negative, but the relative sign between the two terms in equation (3.2.33) is always the same: the sign in front of the Kronecker deltas in $C^1_{\alpha_i\beta_j}$ is $(-1)^{i-j}$ and in $C^1_{\alpha_i\gamma_2}C^1_{\gamma_2\beta_j}$ it is $(-1)^{i-1}(-1)^{1-j} = (-1)^{i-j}$. This obviously also holds if we replace 1 with any other index k.

Now consider a subset of α_i containing n_2 indices. In $C^1_{\alpha_i,\gamma_2^u}$ the indices in this subset will be paired together with the indices in γ_2^u into deltas in $n_2!$ different ways. The same applies for any given subset of β_j containing n_2 indices in $C^1_{\gamma_2^u,\beta_j}$. When these two terms are multiplied together, each combination of the α_i subset and γ_2^u indices will multiply the β_j subset in all combinations with the γ_2^u indices, giving all $n_2!$ combinations of the α_i and β_j subsets paired into deltas. Every combination will therefore appear $n_2!$ times when all the terms are added together, cancelling out the factor of $1/n_2!$ in equation (3.2.33). The second term of equation (3.2.33) will then subtract off all the terms with n_2 indices from each set α_i and β_j mixed in deltas. What remains is then the initial covariance matrix minus the terms connecting n_1 or n_2 indices from the different sets. We thus have

$$(\Sigma^2_{3,n})_{\alpha_i\beta_j} = C^2_{\alpha_i\beta_j}\,, \tag{3.2.34}$$

from which it immediately follows that:

$$(\Sigma^2_{3,n})_{\alpha_3\beta_3} = C^2_{\alpha_3\beta_3} = D_{\alpha_3\beta_3}\,. \tag{3.2.35}$$

The third level coefficients therefore become statistically independent random variables if all the lower level coefficients are known.

Proof by induction

We may now inductively show that the above procedure and the diagonalisation of the conditional covariance matrix hold to any level. We first assume that

$$(\Sigma^{k-1}_{k,n})_{\alpha_i\beta_j} = C^{k-1}_{\alpha_i\beta_j}\,, \tag{3.2.36}$$

where, again, the superscript $k-1$ on the $C^{k-1}_{\alpha_i\beta_j}$ means that terms connecting n_1, n_2, ... or n_k indices between α_i and β_j are not present in the covariances. Equation (3.2.36) holds for $k = 2$ (cf. equation (3.2.27)) and $k = 3$ (cf. equation (3.2.34)). We would now like to show that equation (3.2.36) holds for $k \to k+1$.

Upon fixing $f_{\alpha_k\beta_k}$ (as well as the lower levels), the conditional covariance matrix for the higher levels is given by

$$\begin{aligned}(\Sigma^{k}_{k+1,n})_{\alpha_i\beta_j} &= C^{k-1}_{\alpha_i\beta_j} - C^{k-1}_{\alpha_i\gamma_k}(D^{-1})_{\gamma_k\epsilon_k}C^{k-1}_{\epsilon_k\beta_j} \\ &= C^{k-1}_{\alpha_i\beta_j} - \sum_{\gamma_k} C^{k-1}_{\alpha_i\gamma_k}C^{k-1}_{\gamma_k\beta_j}/\mathrm{Comb}(\gamma_k) \\ &= C^{k-1}_{\alpha_i\beta_j} - \sum_{\gamma^u_k} C^{k-1}_{\alpha_i\gamma^u_k}C^{k-1}_{\gamma^u_k\beta_j}/n_k!, \end{aligned} \tag{3.2.37}$$

where we have taken precisely the same steps that led us to equation (3.2.33).

The superscript $k-1$ on the $C^{k-1}_{\alpha_i\gamma^u_k}$ indicates that it contains no terms with n_1, n_2, ... n_{k-1} deltas with one index each from α_i and one from γ^u_k. No term can have fewer than n_1 indices connecting α_i and γ^u_k, and since there are n_k indices in γ^u_k it then follows that they all must be connected with an index in α_i.

We now consider a subset of α_i containing n_k indices. In $C^{k-1}_{\alpha_i,\gamma^u_k}$ the indices in this subset will be paired together with the indices in γ^u_k into deltas in $n_k!$ different ways. The same applies for any given subset of β_j containing n_k indices in $C^{k-1}_{\gamma^u_k,\beta_j}$. When these two terms are multiplied together, each combination of the α_i subset and γ^u_k indices will multiply the β_j subset in all combinations with the γ^u_k indices, giving all $n_k!$ combinations of the α_i and β_j subsets paired into deltas. Every combination will therefore appear $n_k!$ times when all the terms are added together, cancelling out the factor of $1/n_k!$ in equation (3.2.37). The second term in equation (3.2.37) will then subtract off all the terms with n_k indices from each set α_i and β_j mixed in deltas. What remains is then the initial covariance matrix connecting at least n_{k+1} indices

from the sets α_i and β_j. That is, we have:

$$(\Sigma^k_{k+1,n})_{\alpha_i\beta_j} = C^k_{\alpha_i\beta_j}\,. \tag{3.2.38}$$

We conclude that this expression holds for any level. In particular, this implies that

$$(\Sigma^k_{k+1,n})_{\alpha_{k+1}\beta_{k+1}} = C^k_{\alpha_{k+1}\beta_{k+1}} = D_{\alpha_{k+1}\beta_{k+1}} = \delta_{\alpha_{k+1}\beta_{k+1}}\,\mathrm{Comb}(\alpha_{k+1})\,, \tag{3.2.39}$$

from which it follows that the $(k+1)$:st level Taylor coefficients can be generated as statistically independent Gaussian variables if all the the lower level coefficients are known.

The expectation values

The only thing that remains to do now is calculate how the expectation values shift as we fix the Taylor coefficients level by level. This just involves evaluating equation (3.2.6) in the general case. If we fix f_{α_k}, then the expectation values for the higher levels ($i > k$) are changed by

$$\mu_{\alpha_i} \to \mu_{\alpha_i} + C^{k-1}_{\alpha_i\beta_k}(D^{-1})_{\beta_k\gamma_k}(f_{\gamma_k} - \mu_{\gamma_k})\,, \tag{3.2.40}$$

where μ_{γ_k} will have been determined by earlier measurements. The elements of the 'shift matrix' matrix,

$$E_{\alpha_i\beta_k} = C^{k-1}_{\alpha_i\gamma_k}(D^{-1})_{\gamma_k\beta_k} = C^{k-1}_{\alpha_i\beta_k}\mathrm{Comb}(\beta_k)^{-1}\,, \tag{3.2.41}$$

can be deduced with combinatorics.

We start by considering $C^{k-1}_{\alpha_i\beta_k}$. Again, every index in β_k must be connected with an index in α_i, and as before, we are dealing with ordered sets of indices. For a given α_i and β_k, $C^{k-1}_{\alpha_i\beta_k}$ will be given by the product of two numbers: the number of ways we can pair up indices in α_i with those β_k, and the number of ways the remaning indices can be paired up with each other, with an overall sign given by $(-1)^{i-k}$. To get $E_{\alpha_i\beta_k}$ one then just divides by $\mathrm{Comb}(\beta_k)$.

3.2.3 Summary

In sum, we have shown that realisations of the Taylor coefficients of the Gaussian random field with the covariance function (3.2.9) can be generated sequentially, in an order-by-order fashion, as independent Gaussian random numbers with the diagonal

covariance matrix:

$$(\Sigma^k_{k+1,n})_{\alpha_{k+1}\beta_{k+1}} = C^k_{\alpha_{k+1}\beta_{k+1}} = D_{\alpha_{k+1}\beta_{k+1}} \tag{3.2.42}$$

This obviates the need to numerically invert large covariance matrices.

The effect of the non-vanishing covariances the different orders is here encoded in the mean values, which shift at each step by

$$\mu_{\alpha_i} \to \mu_{\alpha_i} + E_{\alpha_i\beta_k}(f_{\beta_k} - \mu_{\beta_k})\,, \tag{3.2.43}$$

for $i > k$, where k corresponds to the order of the generated Taylor coefficients, and with $E_{\alpha_i\beta_k}$ defined in equation (3.2.41). The elements of the matrices $D_{\alpha_i\beta_i}$ and $E_{\alpha_i\beta_k}$ are simple combinatorial factors that depend on the set of indices.

3.3 Applications

In this section, we briefly present two applications of our construction. An accompanying Mathematica notebook with examples is available at https://doi.org/10.17863/CAM.22859.

3.3.1 Random, high-dimensional potential energy landscapes

The first application of our method is the efficient generation of random functions locally around a point $\mathbf{x}_\star \in \mathbb{R}^d$. The statistical independence of the Taylor coefficients when generated order-by-order allows for the study of $d \gg 1$ or $n_{\max} \gg 1$. This way our method can be competitive with other ways of generating explicit GRFs (e.g. through the generation of independent Fourier coefficients) when the explicit function is only needed in a moderately small neighbourhood around $\mathbf{x}_\star$, and the covariance function is Gaussian. Moreover, a key benefit of our method is that it permits the generation of the function around special points: for example, one may fix the Taylor coefficients up to second order, i.e. f, f_a, f_{ab}, to permit the generation of random potentials around minima, maxima, and saddle-points with specific properties (the generation of completely random critical points is different, and will be discussed shortly). Our method can also be used to study potentials over distances of a few $\Lambda_{\rm h}$ by taking $n_{\max} \gg 1$ (as illustrated in Figure 3.1). This provides novel opportunities to address a rich class of problems involving multifield dynamics in random potential energy landscapes.

Generating random critical points

There is a subtlety that must be taken into account when generating random critical points with appropriate weights. If we want to generate a potential conditional on $\mathbf{x}_\star$ being a critical point, rather than conditional on some Taylor coefficients taking particular values, there is in fact a dependence of the Hessian on the gradient of the potential which changes the conditional distribution of the former (after the latter has been fixed) away from its Gaussian form.

As is explained in [27], the condition $-\delta/2 < f_a < \delta/2$ taking $\delta \to 0$ gives a conditional probability density for the higher-order Taylor coefficients with the property that critical points with small or zero-valued second derivatives have larger weight than those with large second derivatives. This is because the condition will be satisfied in larger regions around these points. To account for this effect, one should use the condition that there is a critical point in a region of size δ, and then let $\delta \to 0$. In doing so, the probability density of the higher-order coefficients becomes

$$p(f, f_{ab}, \ \ldots | \text{critical point}) \propto |\det f_{ab}| p(f, f_a = 0, f_{ab}, \ \ldots). \tag{3.3.1}$$

The marginal distributions for all the variables other than f_{ab} are unaffected by this, but to generate f_{ab} one must resort to other methods (e.g. MCMC). Once the Hessian is fixed, one may proceed to generate the other coefficients as described earlier in this chapter.[1]

3.3.2 Model selection for Gaussian process regression

The results derived in this chapter can also be useful when training Gaussian random processes with square exponential covariance functions. More specifically, it can be applied to simplify the regression problem mentioned in the introduction: given training data in the form of Taylor coefficients of f at $\mathbf{x}_\star$ to order $n_{\max}$, we may determine the hyperparameters h, ℓ and $\bar{f}$ by maximising the log likelihood. In this section, we show in detail how the log likelihood can be written as a sum over levels, thereby making it possible to constrain the hyperparameters without inverting the covariance matrix.

[1] The generation of third derivatives and higher as described earlier is not affected by this. The reason for this is that while each critical point must be assigned equal probability when the rest of the potential is generated on the condition that $\mathbf{x}_\star$ is a critical point, in the earlier example we were just interested in generating potentials satisfying certain properties. That is, we are conditioning on the event that each f_α is in some range $(f^\star_\alpha - \delta/2, f^\star_\alpha + \delta/2)$, and then take $\delta \to 0$ when computing the conditional density. This is done irrespective of whether the f_α was generated randomly or fixed by hand.

The log marginal likelihood is given by:

$$\ln p(f_\alpha|h,\ell,\bar{f}) = -\frac{1}{2} f_\alpha \Sigma^{-1}_{\alpha\beta} f_\beta - \frac{1}{2}\ln|2\pi\Sigma|\,. \tag{3.3.2}$$

In general, this is a very complicated function of h, ℓ and $\bar{f}$, but we can simplify it substantially by using the algebraic properties proven in this chapter. First, we can use the definition of conditional probabilities to write:

$$p(f_\alpha) = \left[\left(\prod_{i=2}^{n} p(f_{\alpha_i}|f_{\alpha_{i-1}},..)\right) p(f_{\alpha_1})\right]_{\text{even}} \times \left[\left(\prod_{i=2}^{n} p(f_{\alpha_i}|f_{\alpha_{i-1}},..)\right) p(f_{\alpha_1})\right]_{\text{odd}}\,, \tag{3.3.3}$$

where we for simplicity of notation have suppressed the dependence on the hyperparameters. From equation (3.2.39), the conditional probability densities can be further simplified to

$$p(f_{\alpha_i}|f_{\alpha_{i-1}},..) = \frac{1}{\sqrt{|2\pi h^2 \ell^{-2n_i} D_{\alpha_i\beta_i}|}} \exp\left(-\frac{1}{2} h^{-2}\ell^{2n_i}(f_{\alpha_i}-\mu_{\alpha_i}) D^{-1}_{\alpha_i\beta_i}(f_{\beta_i}-\mu_{\beta_i})\right)\,, \tag{3.3.4}$$

where μ_{α_i} is a function of f_{α_j} for $j<i$ as discussed towards the end of §3.2.2. Denoting the number of independent derivatives at level i by d_i, we find

$$\begin{aligned}\ln p(f_{\alpha_i}|f_{\alpha_{i-1}},..) = &-\frac{1}{2} h^{-2}\ell^{2n_i}(f_{\alpha_i}-\mu_{\alpha_i}) D^{-1}_{\alpha_i\beta_i}(f_{\beta_i}-\mu_{\beta_i}) \\ &- d_i(\ln h - n_i \ln \ell) - \frac{d_i}{2}\ln(2\pi) - \frac{1}{2}\operatorname{Tr}\ln(D_{\alpha_i\beta_i})\,.\end{aligned} \tag{3.3.5}$$

The log marginal likelihood is then given by the simple sum

$$\begin{aligned}\ln p(f_\alpha|h,\ell,\bar{f}) = \sum_{\substack{i=1\\ \text{even, odd}}}^{i_{\max}} \Bigg[&-\frac{1}{2} h^{-2}\ell^{2n_i}(f_{\alpha_i}-\mu_{\alpha_i}) D^{-1}_{\alpha_i\beta_i}(f_{\beta_i}-\mu_{\beta_i}) \\ &- d_i(\ln h - n_i \ln \ell) - \frac{d_i}{2}\ln(2\pi) - \frac{1}{2}\operatorname{Tr}\ln(D_{\alpha_i\beta_i})\Bigg],\end{aligned} \tag{3.3.6}$$

which runs over both even and odd derivatives. The remaining complication of (3.3.6) is the mean values μ_{α_i}, which are determined iteratively as:

$$\mu_{\alpha_i} = \sum_{j=1}^{i-1} \ell^{n_j-n_i} E_{\alpha_i\alpha_j}(f_{\alpha_j}-\mu_{\alpha_j})\,, \tag{3.3.7}$$

with $\mu_{\alpha_1} = \bar{f}$ in the even case and $\mu_{\alpha_1} = 0$ in the odd case. The shift matrix $E_{\alpha_i\alpha_j}$ was defined in equation (3.2.41). Using this expression, the expectation values μ_{α_i} can be determined without inverting any matrix, which makes numerical evaluations fast. Derivatives of the mean values are given recursively by

$$\frac{\partial\mu_{\alpha_i}}{\partial\ell} = \sum_{j=1}^{i-1}\left[(n_j - n_i)\ell^{n_j-n_i-1}E_{\alpha_i\alpha_j}(f_{\alpha_j} - \mu_{\alpha_j}) - \ell^{n_j-n_i}E_{\alpha_i\alpha_j}\frac{\partial\mu_{\alpha_j}}{\partial\ell}\right], \tag{3.3.8}$$

$$\frac{\partial\mu_{\alpha_i}}{\partial\bar{f}} = \sum_{j=1}^{i-1} -\ell^{n_j-n_i}E_{\alpha_i\alpha_j}\frac{\partial\mu_{\alpha_j}}{\partial\bar{f}}\,. \tag{3.3.9}$$

The mean values μ_{α_i} do not depend on h. The only non-zero starting value at first order is $\partial\mu_{\alpha_1}/\partial\bar{f} = 1$ in the even case.

To find the Bayesian best-fit parameters, we optimise the log marginal likelihood with respect to all the hyperparameters:

$$\begin{aligned}\frac{\partial}{\partial\ell}\ln p(f_\alpha|h,\ell,\bar{f}) = \sum_i \Bigg[&- n_i h^{-2}\ell^{2n_i-1}(f_{\alpha_i} - \mu_{\alpha_i})D^{-1}_{\alpha_i\beta_i}(f_{\beta_i} - \mu_{\beta_i}) \\ &+ h^{-2}\ell^{2n_i}(f_{\alpha_i} - \mu_{\alpha_i})D^{-1}_{\alpha_i\beta_i}\frac{\partial\mu_{\beta_i}}{\partial\ell} + d_i n_i \ell^{-1}\Bigg]\end{aligned} \tag{3.3.10}$$

$$\frac{\partial}{\partial h}\ln p(f_\alpha|h,\ell,\bar{f}) = \sum_i \left[h^{-3}\ell^{2n_i}(f_{\alpha_i} - \mu_{\alpha_i})D^{-1}_{\alpha_i\beta_i}(f_{\beta_i} - \mu_{\beta_i}) - d_i h^{-1}\right] \tag{3.3.11}$$

$$\frac{\partial}{\partial\bar{f}}\ln p(f_\alpha|h,\ell,\bar{f}) = \sum_i h^{-2}\ell^{2n_i}(f_{\alpha_i} - \mu_{\alpha_i})D^{-1}_{\alpha_i\beta_i}\frac{\partial\mu_{\beta_i}}{\partial\bar{f}}. \tag{3.3.12}$$

Evidently, the only matrices that appear in this problem are the diagonal $D_{\alpha_i\beta_i}$ and the shift matrix $E_{\alpha_i\beta_j}$, but these are easy to compute from combinatorics, cf. equations (3.2.19) and (3.2.41). Moreover, once computed for a given d and $n_{\max}$, they can be re-used for any training data set. This model selection problem is controlled by the mean values μ_{α_i} and their derivatives, and requires no inversion of large matrices.

We illustrate the application of this method for randomly generated data in Figure 3.2. The hyperparameters h and ℓ can be determined rather accurately given Taylor coefficients to sufficiently high order. Heuristically, the oblongated shape of the confidence contours can be understood to follow from the appearance of the pre-factors $h^{-2}\ell^{2n_i}$ in the exponent of equation (3.3.4). While the degeneracy $h \to \lambda h$, $\ell \to \lambda^{1/n_i}\ell$ certainly is broken in several ways (by the ℓ dependence of μ_{α_i}, the differentiation in equations (3.3.10)–(3.3.12), and by factors with different n_i), the hyperparameters are most strongly constrained when ℓ and h are not both increased or decreased from the best-fit value.

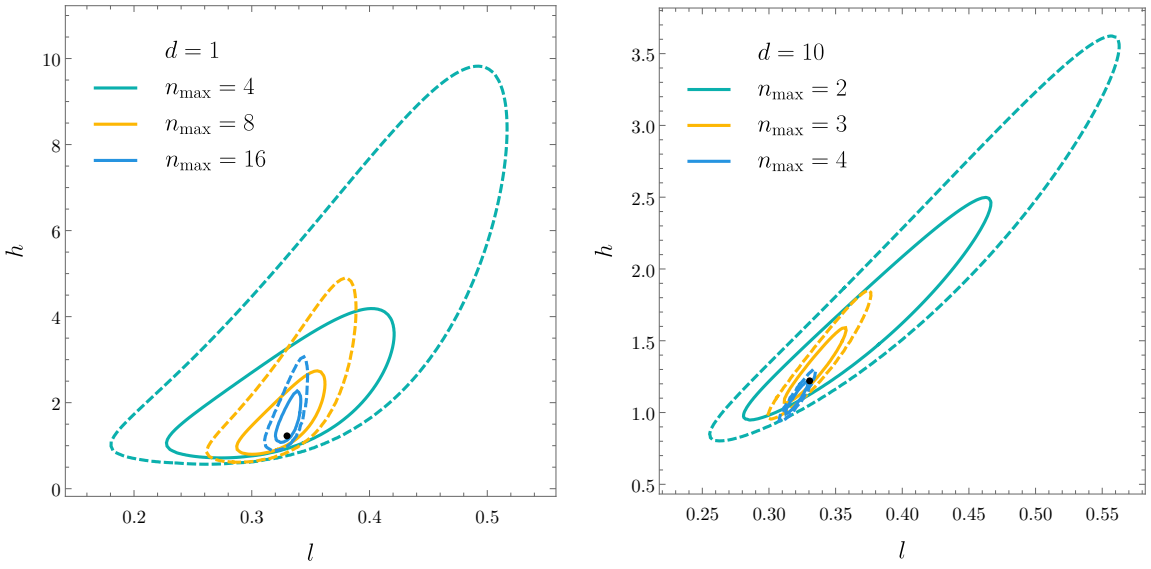

Fig. 3.2 Likelihood contours for the hyperparameters at the 68% and 95% confidence levels obtained from random realisations of the GRF. The true hyperparameter values are $(h, \ell) = (1.22, 0.33)$ as indicated by the black dot, and we have fixed $\bar{f} = 0$.

3.4 Conclusions

In this chapter, we have presented a new method for simplifying the PDF of the Taylor coefficients of GRFs with a Gaussian covariance function. By computing the PDF sequentially, we have shown that the covariance matrices for the Taylor coefficients at every step become diagonal. This result holds for any dimension and to any order in the Taylor coefficients. This simplification essentially trivialises the evaluation of the probability distribution of the Taylor coefficients, which depends on the inverse of the covariance matrix.

We have shown that this method can have several interesting applications. GRFs constructed this way can be used as models of complicated potential energy functions, and we have showed in Chapter 2 how this can be used to explicitly study cosmic inflation in theories with many interacting fields. Moreover, GRFs with Gaussian covariance functions appear very frequently in machine learning applications. We have demonstrated that our method can be used to simplify the regression problem of determining the hyperparameters, given a training data set that consists of the local Taylor coefficients of the GRF, although we expect this to be a rather niche application.

Accompanying this chapter, there is a Mathematica notebook containing the explicit examples of these applications.

Our method has several limitations. The algebraic simplifications that we have identified are only applicable to isotropic Gaussian covariance functions, which constitute a special, albeit commonly considered, class of GRFs. We know of no generalisations to more general classes of covariance functions, including those constructed as sums of independent Gaussian functions. Moreover, since our method is based on the local Taylor coefficients, it becomes cumbersome to use for describing the potential over field displacements of many ℓ. Finally, training data sets in machine learning applications are often noisy, which can make it challenging to determine the Taylor coefficients to a sufficiently high order.

Nevertheless, we expect this method to offer useful simplifications to a wide variety of practical applications of Gaussian random fields and Gaussian processes.

Chapter 4

Hyperinflation

4.1 Introduction

In the standard slow-roll paradigm involving a single canonically normalised scalar field ϕ, accelerated expansion is supported when ϕ evolves slowly in a scalar potential, $V(\phi)$, that is sufficiently flat, satisfying

$$\frac{|V_{,\phi}|}{V} < \frac{\sqrt{2}}{M_{\rm P}}\,. \tag{4.1.1}$$

However, this is not the only way inflation can be realised. Models of inflation involving multiple fields and non-trivial kinetic terms can also be consistent with observations, and recently, much effort has been devoted to elucidating the rich possibilities offered by inflationary theories with geometrically non-trivial field spaces (cf. e.g. [2, 3, 5, 33, 45, 46, 51, 52, 56, 57, 59, 65, 80, 82, 99, 104, 105, 114–122, 125–127, 149, 165, 166, 169]). The most well-studied class of such models, 'α-attractors', builds on the observation that if the coefficients of the kinetic terms become large, even highly featured potentials can support standard slow-roll inflation [2, 46, 51, 52, 99, 115–119, 121, 126, 169]. However, non-trivial field space geometries can also support conceptually new realisations of inflation, that do not rely on equation (4.1.1). In this chapter we will be investigating one of these models, 'hyperinflation' [45], in detail to understand how it works. The original proposal of this model left many questions unanswered about its dynamics - in particular, the solution relied on global symmetries of the field space, even though the equations of motions are local.

Hyperinflation is a particularly interesting mechanism for realising inflation when the field space is a hyperbolic plane with a constant curvature of $L \ll M_{\rm P}$. Reference

[45] showed that if the field initially has some (field space) angular momentum and the scalar potential is rotationally symmetric, the radial motion is slowed by an additional centrifugal force, which helps sustain inflation even in steep potentials.[1] In this scenario, equation (4.1.1) is replaced by the much more relaxed condition

$$\frac{3L}{M_{\rm P}^2} < \frac{|V_{,\phi}|}{V} < \frac{1}{L}\,, \tag{4.1.2}$$

for the canonically normalised radial field ϕ.

Reference [149] further developed the perturbation theory of these models, but the framework of hyperinflation is not yet fully developed. In this chapter we address the following important questions:

- The proposal of [45], which was further studied in [149], applies strictly to a restrictive set of two-field models in which the field space is the hyperbolic plane, the scalar potential is rotationally symmetric, and the field is initially displaced far from the origin (so that the initial angular momentum is large). *Are these assumptions required to realise hyperinflation? If not, how can they be relaxed, and hyperinflation generalised?*

- Models of inflation in steep potentials are potentially interesting because they may not require the same level of fine tuning as slow-roll models, and may be more easily compatible with ultraviolet completions of inflation, e.g. into string theory. Recently, much activity has been devoted to identifying 'swampland' criteria that supposedly delineate the low-energy effective field theories that can be consistently embedded in quantum gravity. In particular, the 'de Sitter' and 'distance' conjectures respectively state that $|V_{,\phi}| > \mathcal{O}(V/M_{\rm P})$ and the total field excursion is bounded from above, $\Delta\phi < \mathcal{O}(M_{\rm P})$. These conditions, if true, strongly constrain standard slow-roll inflation. *Can hyperinflation be realised in steep potentials with sub-Planckian field excursions? Is the theory compatible with the proposed 'swampland conjectures'?*

To address these questions, we identify a set of conditions on the scalar potential and its derivatives that must be satisfied by (generalised) models of hyperinflation. We express these conditions covariantly and show that they can be satisfied in a variety of models, including those without rotational symmetry, with random interactions, and with any number of fields ($N_f \geq 2$). Moreover, we demonstrate how (generalised) hyperinflation can be realised without any special conditions on the initial value

[1] This mechanism generalises the idea of 'spinflation' [86].

of the angular momentum (which is not a conserved quantity in the general case). For example, hyperinflation can follow a period of slow-roll inflation with small or vanishing angular momentum which then becomes 'geometrically destabilised' [165] by the negative curvature (cf. also [45]). This links hyperinflation to so-called 'side-tracked inflation' recently discussed in [105, 165]: we point out that while these setups share some similarities, the side-tracked model of [105] does not realise hyperinflation in either its original or here generalised forms.

We furthermore consider perturbations around the homogeneous solution and provide the first detailed proof of the attractor nature of hyperinflation, and its generalised versions. For models with $N_f > 2$ fields, we show that the dynamics of the perturbations decouples the adiabatic and first 'entropic' mode from the remaining $N_f - 2$ modes. We note that this makes the observational predictions rather independent of the number of fields.

Finally, we discuss the status of hyperinflation in relation to various conjectures regarding the general properties of effective field theories arising in low-energy limits of consistent theories of quantum gravity, a.k.a. the 'swampland program' [156, 157]. We show that hyperinflation can be consistent with either the 'de Sitter conjecture' or the 'distance conjecture', but struggles to satisfy both conditions simultaneously while also reheating the universe after inflation. Moreover, the simplest models of hyperinflation considered in [45] are in strong tension with the weak gravity conjecture [22], but generalisations can be unaffected by this condition.

4.2 Hyperbolic geometry and hyperinflation

In this section, we review the mechanism for hyperinflation proposed in [45]. To set our notation conventions, we begin with a brief reiew of inflation in curved field spaces.

The action governing inflation in curved field spaces is given by

$$\mathcal{S} = \frac{1}{2}\int d^4x\sqrt{-g}\left[R - G_{ab}g^{\mu\nu}\partial_\mu\phi^a\partial_\nu\phi^b - 2V\right], \tag{4.2.1}$$

where G_{ab} is the field space metric. In a Friedmann-Robertson-Walker background, the equations of motion for a homogeneous background field become

$$\mathcal{D}_t\dot{\phi}^a + 3H\dot{\phi}^a + G^{ab}V_{,b} = 0, \tag{4.2.2}$$

where the derivative $\mathcal{D}_t$ is defined by $\mathcal{D}_t X^a = \dot{X}^a + \Gamma^a_{bc}\dot{\phi}^b X^c$ for any field space vector X^a.

The dynamics of the perturbations around a homogeneous solution in spatially flat gauge is governed by the second-order action [107, 110, 172]:

$$\mathcal{S}_2 = \frac{1}{2}\int \frac{d^3k}{(2\pi)^3} dt a^3 \left[G_{ab}\mathcal{D}_t\delta\phi^a(\mathbf{k})\mathcal{D}_t\delta\phi^b(-\mathbf{k}) - \left(\frac{k^2}{a^2}G_{ab} + M_{ab}\right)\delta\phi^a(\mathbf{k})\delta\phi^b(-\mathbf{k})\right], \tag{4.2.3}$$

where M_{ab} is the effective mass matrix given by

$$M_{ab} = V_{;ab} - R_{acdb}\dot{\phi}^c\dot{\phi}^d + (3-\epsilon)\frac{\dot{\phi}_a\dot{\phi}_b}{M_{\rm P}^2} + \frac{\dot{\phi}_a V_{,b} + V_{,a}\dot{\phi}_b}{HM_{\rm P}^2} \tag{4.2.4}$$

where $V_{;ab} = V_{,ab} - V_{,c}\Gamma^c_{ab}$. The equations of motion for the perturbations are

$$\mathcal{D}_t\mathcal{D}_t\delta\phi^a + 3H\mathcal{D}_t\delta\phi^a + \frac{k^2}{a^2}\delta\phi^a + M^a{}_b\delta\phi^b = 0. \tag{4.2.5}$$

One of the novel aspects of inflation in negatively curved spaces is that the second term can induce a negative mass-squared, leading to geometric destabilisation of inflation attractors [165][2]. In two dimensions, the Riemann tensor always takes the form $R^a{}_{bcd} = R(\delta^a{}_c G_{bd} - \delta^a{}_d G_{bc})/2$, and hyperbolic geometry corresponds to constant $R = -2/L^2$.[3] More generally, for an $N_{\rm f}$-dimensional hyperbolic geometry, one can show that in an orthonormal basis (normal coordinates), the Riemann tensors takes the form $R^a{}_{bcd} = -(\delta^a{}_c\delta_{bd} - \delta^a{}_d\delta_{bc})/L^2$.

Commonly used representations of the metric of the hyperbolic plane include the Poincare disk model,

$$ds^2 = 4L^2\frac{dr^2 + r^2d\theta^2}{(1-r^2)^2}\,, \tag{4.2.6}$$

for $r < 1$, and the non-compact representation,

$$ds^2 = d\phi^2 + L^2\sinh^2(\phi/L)d\theta^2\,. \tag{4.2.7}$$

These are related by the change of radial coordinate $\phi = L\sinh^{-1}(2r/(1-r^2))$.

4.2.1 Hyperinflation

The action of a homogeneous background field in the hyperbolic plane can be written as

$$\mathcal{S} = \int d^4x a^3\left(\frac{1}{2}\dot{\phi}^2 + \frac{1}{2}L^2\sinh^2(\phi/L)\dot{\theta}^2 - V(\phi,\theta)\right). \tag{4.2.8}$$

[2]This destablisation, although very different in origin, is akin to hybrid inflation [101, 128]

[3]The curvature scale L is related to the eponymous parameter of α-attractors by $\alpha = 2L^2/3$.

If the scalar potential only depends on the radial coordinate, $V = V(\phi)$, the equations of motion are given by

$$\ddot{\phi} + 3H\dot{\phi} - L\sinh(\phi/L)\cosh(\phi/L)\dot{\theta}^2 = -V_{,\phi} \tag{4.2.9}$$

$$\ddot{\theta} + 3H\dot{\theta} + \frac{2}{L}\coth(\phi/L)\dot{\theta}\dot{\phi} = 0\,. \tag{4.2.10}$$

Following [45], we assume that $V(\phi)$ has a minimum at $\phi = 0$. For this rotationally symmetric system, equation (4.2.10) may also be derived as the conservation equation for field-space angular momentum, $dJ/dt = 0$, where

$$J \equiv a^3 L^2 \sinh^2(\phi/L)\dot{\theta}\,. \tag{4.2.11}$$

The conservation of J simplifies the radial equation to

$$\ddot{\phi} + 3H\dot{\phi} = \frac{J^2\cosh(\phi/L)}{a^6 L^3 \sinh^3(\phi/L)} - V_{,\phi}\,, \tag{4.2.12}$$

where the first term on the right-hand side may be regarded as a centrifugal force. One may search for solutions in which $\ddot{\phi}$ is negligible, and the two terms on the right-hand side balance to keep $3H\dot{\phi}$ slowly varying. For $\phi \gg L$, $\sinh(\phi/L) \simeq \cosh(\phi/L) \simeq e^{\phi/L}/2$, and such solutions must realise the scaling relation

$$a^6 e^{2\phi/L} V_{,\phi} = \text{const}\,. \tag{4.2.13}$$

Differentiating this condition with respect to time leads to a simple equation for the radial velocity:

$$\dot{\phi} = -\frac{3HL}{1 + \eta_L/2} \simeq -3HL\,, \tag{4.2.14}$$

where in the last step we have assumed that $|\eta_L| \ll 1$ for

$$\eta_L = \frac{LV_{,\phi\phi}}{V_{,\phi}}\,. \tag{4.2.15}$$

The speed in the angular direction may now be found from equation (4.2.9) and is given by

$$L\sinh(\phi/L)\dot{\theta} \simeq \sqrt{LV_{,\phi} - (3HL)^2}\,. \tag{4.2.16}$$

A consistent solution requires $LV_{,\phi} > (3HL)^2$.

Accelerated expansion is realised if the inflationary epsilon parameter is small:

$$\epsilon = -\frac{\dot{H}}{H^2} = \frac{\frac{1}{2}\dot{\phi}^2 + \frac{1}{2}L^2\sinh^2(\phi/L)\dot{\theta}^2}{H^2} \simeq 3\frac{\frac{1}{2}LV_{,\phi}}{\frac{1}{2}LV_{,\phi} + V} < 1\,. \tag{4.2.17}$$

Combining the consistency condition from (4.2.16) with the inequality (4.2.17) leads to equation (4.1.2). A sustained period of inflation then requires $\epsilon_L \ll 1$ for

$$\epsilon_L = \frac{LV_{,\phi}}{V}\,. \tag{4.2.18}$$

The number of e-folds of expansion is straightforwardly related to the radial field excursion by

$$N = \int H dt = -\frac{1}{3L}\int d\phi = \frac{\Delta\phi}{3L}. \tag{4.2.19}$$

Obtaining at least 60 e-folds of inflation requires $\Delta\phi \gtrsim 180L$. The total field excursion including both the radial and angular motion is given by

$$d\phi_{\rm tot} = \sqrt{LV_{,\phi}}\,dt = \sqrt{3\epsilon_L}\,dN\,. \tag{4.2.20}$$

For future reference we define the dimensionless parameter [45]

$$\bar{h} \equiv \frac{L\sinh(\phi/L)\dot{\theta}}{HL} = 3\sqrt{\frac{\epsilon_L}{3L^2} - 1} = \sqrt{\left(\frac{1}{L}\frac{d\phi_{\rm tot}}{dN}\right)^2 - 9}\,, \tag{4.2.21}$$

which closely approximates the turn-rate of the fields. We note that the above results come out easily because of the metric choice. In the Poincare disk model, the hyperinflation solution appears more complicated. The large radius condition $\phi \gg L$ clearly corresponds to $r \simeq 1$, but the condition $\ddot{\phi} \approx 0$ translates into the less clear condition

$$\frac{2L}{1-r^2}\left(\ddot{r} + \frac{2r\dot{r}^2}{1-r^2}\right) \approx 0. \tag{4.2.22}$$

To obtain a more general understanding of when and how hyperinflation arises, we will now reformulate the relevant conditions in a coordinate-independent way.

4.3 Generalising hyperinflation

In this section we generalise the notion of hyperinflation. As we have reviewed, hyperinflation can be supported in potentials that would be too steep to sustain slow-

roll inflation, but the construction of [45] required a number of assumptions. It applied only to two-field models for which the field space was given by the hyperbolic plane and the potential was rotationally symmetric, and it furthermore relied on the initial field being far from the origin with non-vanishing angular momentum, $J \neq 0$. There are good reasons to expect that these assumptions can be relaxed: the hyperinflation solution only probes a small region of the field space, and should not be sensitive to global properties of the potential. Moreover, with a general potential there is nothing special about the chosen origin of the hyperbolic plane, and the metric could equally well be expressed locally around a point on the inflationary trajectory.

We begin in section 4.3.1 by reviewing how the Klein-Gordon equation can be expressed covariantly using a local orthonormal basis, and we then show in section 4.3.2 how the conditions for hyperinflation can be expressed using only local and covariant properties of the potential. This setup then allows us to generalise hyperinflation to more general potentials in section 4.3.3, and to models with more than two fields in section 4.3.4.

4.3.1 Two-field covariant formulation

The starting assumptions of the hyperinflation solution of [45] – setting $\ddot{\phi}$ to zero and taking $H\dot{\phi}$ to be slowly varying – are not covariant. To generalise hyperinflation we here rephrase the mechanism using vielbeins. A convenient local orthonormal basis of the two-dimensional field space is defined by the unit vector in the potential gradient direction,

$$v^a = V^{,a}/\sqrt{V^{,b}V_{,b}} \equiv V^{,a}/V_{;v}\,, \tag{4.3.1}$$

and a second unit vector orthogonal to it, w^a. The reason for working with this basis, rather than say the commonly used 'kinematic basis' that takes $\dot{\phi}^a$ and $\ddot{\phi}^a$ to span the field space [161, 162], is that we know the directions of v^a and w^a without solving the equations of motions. This simplifies the analysis.

In terms of this basis for the tangent space, we expand the field-space velocity as

$$\dot{\phi}^a = v^a\dot{\phi}_v + w^a\dot{\phi}_w\,. \tag{4.3.2}$$

Here $\dot{\phi}_v = v_a\dot{\phi}^a$ and $\dot{\phi}_w = w_a\dot{\phi}^a$ are covariant scalars. As the field evolves, the basis vectors rotate. To take this into account, we note that

$$\mathcal{D}_t v_a = \frac{V_{;ab}\dot{\phi}^b}{V_{;v}} - v_a\frac{v^b V_{;bc}\dot{\phi}^c}{V_{;v}} = w_a\frac{w^b V_{;bc}\dot{\phi}^c}{V_{;v}}, \tag{4.3.3}$$

where in the last step we used the identity $v^a v_b + w^a w_b = \delta^a{}_b$. From the orthonormality condition, $v_a w^a = 0$, it also follows that

$$\mathcal{D}_t w_a = -v_a \frac{w^b V_{;bc} \dot{\phi}^c}{V_{;v}}. \tag{4.3.4}$$

In this vielbein basis, the Klein-Gordon equations are then given by

$$\begin{aligned} \ddot{\phi}_v &= v_a \mathcal{D}_t(\dot{\phi}^a) + \mathcal{D}_t(v_a)\dot{\phi}^a = -3H\dot{\phi}_v - V_{;v} + \dot{\phi}_w \frac{w^a V_{;ab}\dot{\phi}^b}{V_{;v}} \\ \ddot{\phi}_w &= w_a \mathcal{D}_t(\dot{\phi}^a) + \mathcal{D}_t(w_a)\dot{\phi}^a = -3H\dot{\phi}_w - \dot{\phi}_v \frac{w^a V_{;ab}\dot{\phi}^b}{V_{;v}}\,. \end{aligned} \tag{4.3.5}$$

These expressions hold in general for two-dimensional field spaces. To identify the local manifestation of the hyperinflation solution, we furthermore need information about the second covariant derivatives of the potential.

4.3.2 Generalised hyperinflation

We now reconsider the hyperinflation solution reviewed in section 4.2.1 and re-express it using our local orthonormal-basis. In the original polar coordinate system, the basis vectors are $v^a = (1,\ 0)$ and $w^a = (0,\ 1/L\sinh(\phi/L))$. Using these, it is straightforward to check that the potential in the original solution satisfies

$$V_{;v} = V_{,\phi}, \qquad V_{;vv} = V_{,\phi\phi}, \qquad V_{;vw} = 0, \qquad V_{;ww} = \frac{V_{,\phi}}{L}\,. \tag{4.3.6}$$

Here we have introduced the notation $v^a V_{;ab} w^b = V_{;vw}$, etc. and used the non-vanishing Christoffel symbols $\Gamma^v_{ww} = -\Gamma^w_{wv} = -\frac{1}{L}\cosh(\phi/L)/\sinh(\phi/L)$. The hyperinflation parameters ϵ_L and η_L clearly translate into

$$\epsilon_L \equiv \frac{LV_{,v}}{V}\,, \quad \text{and} \quad \eta_L \equiv \frac{LV_{;vv}}{V_{;v}}\,. \tag{4.3.7}$$

To generalise hyperinflation, we look for solutions of the equation of motion with

$$|\eta_L| \ll 1\,, \quad 3L < \epsilon_L < 1\,, \quad V_{;vw} \approx 0\,, \quad \text{and} \quad V_{;ww} = \frac{V_{;v}}{L}\,. \tag{4.3.8}$$

These conditions are all covariant statements, and can be easily evaluated for any potential and representation of the metric.

Using the conditions (4.3.8), the basis vector rotations simplify to

$$\mathcal{D}_t v_a = w_a \frac{\dot{\phi}_w}{L}, \qquad \mathcal{D}_t w_a = -v_a \frac{\dot{\phi}_w}{L}\,. \tag{4.3.9}$$

The equations of motion (4.3.5) are now simplified to

$$\ddot{\phi}_v = -3H\dot{\phi}_v - V_{;v} + \frac{\dot{\phi}_w^2}{L} \tag{4.3.10}$$

$$\ddot{\phi}_w = -3H\dot{\phi}_w - \frac{\dot{\phi}_v\dot{\phi}_w}{L}. \tag{4.3.11}$$

Setting $\ddot{\phi}_v = \ddot{\phi}_w = 0$ at some time t_p gives two possible solutions:

$$\left.\begin{aligned}\dot{\bar{\phi}}_v &= -V_v/3H\\ \dot{\bar{\phi}}_w &= 0\end{aligned}\right\}\ \text{slow roll}\,, \qquad \left.\begin{aligned}\dot{\bar{\phi}}_v &= -3HL\\ \dot{\bar{\phi}}_w &= \pm\sqrt{LV_{;v} - 9H^2L^2}\end{aligned}\right\}\ \text{hyperinflation} \tag{4.3.12}$$

We here focus on the hyperinflation solution, which again requires $LV_{;v} > 9H^2L^2$ (or equivalently, $\epsilon_L > 3L$ when ϵ_L is small). It remains to be shown is that these solutions can be consistently extended along the inflationary trajectory. Noting that the RHS can be expressed entirely as a function of ϕ (to a good approximation) during inflation, we look for a solution of the form $\dot{\phi} = \dot{\phi}(\phi(t))$, and expand the velocity variables as $\dot{\phi}_I = \dot{\bar{\phi}}_I + \delta\dot{\phi}_I$, where we need to show that $\delta\dot{\phi}_I(t) \sim \mathcal{O}(\epsilon\dot{\bar{\phi}}_I)$ along the inflationary solution.

When the equations (4.3.12) hold, the inflationary slow-roll parameters ϵ and η straightforwardly generalise to

$$\epsilon = \frac{\frac{1}{2}\dot{\bar{\phi}}^2}{H^2} = 3\frac{\epsilon_L}{\epsilon_L + 2}\,, \tag{4.3.13}$$

$$\eta = \frac{d\ln\epsilon}{Hdt} = \frac{1}{H\dot{\bar{\phi}}^2}\frac{d}{dt}\dot{\bar{\phi}}^2 + 2\epsilon = -3\eta_L + 2\epsilon\,. \tag{4.3.14}$$

The assumptions (4.3.8) imply that both ϵ and $|\eta|$ are small. Note that in equation (4.3.14), we take the time derivative of $\dot{\bar{\phi}}$ using the explicit expressions for the $\dot{\bar{\phi}}_I$ of equation (4.3.12), rather than the equations of motion (which remain to be solved for $\delta\dot{\phi}_I$). Explicitly,

$$\frac{d\dot{\bar{\phi}}_v}{dt} = 3H^2L\epsilon \quad \text{and} \quad \frac{d\dot{\bar{\phi}}_w}{dt} = \frac{3H(6H^2L^2\epsilon - LV_{;v}\eta_L)}{2\dot{\bar{\phi}}_w}, \tag{4.3.15}$$

where we emphasise that the right-hand sides can all be written as functions of ϕ^a only. The accelerations are both small, $d\dot{\bar{\phi}}_i/dt \sim \mathcal{O}(\epsilon H \dot{\bar{\phi}}_i)$, which justifies the expansion of the velocities. We may now use the full Klein-Gordon equation to solve for $\delta\dot{\phi}_i$,

$$\frac{d\dot{\bar{\phi}}_v}{dt} = -3H\delta\dot{\phi}_v + \frac{2\dot{\bar{\phi}}_w\delta\dot{\phi}_w}{L}, \qquad \frac{d\dot{\bar{\phi}}_w}{dt} = -3H\delta\dot{\phi}_w - \frac{\dot{\bar{\phi}}_w\delta\dot{\phi}_v + \dot{\bar{\phi}}_v\delta\dot{\phi}_w}{L}\,. \tag{4.3.16}$$

Defining, as in equation (4.2.21),

$$\bar{h} = \frac{\dot{\bar{\phi}}_w}{HL} \tag{4.3.17}$$

we find

$$\delta\dot{\phi}_v = \frac{HL(2\bar{h}^2\epsilon - (9+\bar{h}^2)\eta)}{2\bar{h}^2} \quad \text{and} \quad \delta\dot{\phi}_w = \frac{3HL(\bar{h}^2(4\epsilon-\eta) - 9\eta)}{4\bar{h}^3}\,. \tag{4.3.18}$$

We note that $\delta\dot{\phi}_I/\dot{\bar{\phi}}_I = \mathcal{O}(\epsilon)$, so that neglecting $d\delta\dot{\phi}_I/dt \sim \mathcal{O}(\epsilon^2\dot{\bar{\phi}}_I)$ is consistent. This explicitly demonstrates that equation (4.3.12) provides a self-consistent solution of the equations of motion to leading order in the slow-roll parameters.

As an aside, the equations of motion in hyperinflation resemble those of side-tracked inflation far away from the original axis. In side-tracked inflation [105], the field-space has negative curvature and much like in hyperinflation, slow-roll is destabilised and one ends up in a new attractor solution. However, the equations of motion are not exactly the same: in side-tracked inflation, when the fields have reached the second attractor solution, the Hessian of the potential is characterised by $V_{vv}/V_{ww} = \mathcal{O}(1)$ rather than $\mathcal{O}(\epsilon)$, and V_{vw} is no longer non-negligible, in contrast with hyperinflation. Consequently, $\dot{\phi}_v$ and $\dot{\phi}_w$ no longer satisfy equation 4.3.12, although there is some rough qualitative agreement. Moreover, in the second phase of side-tracked inflation, the fields must follow one of two specific trajectories in field space (which are mirrors of each other), whereas hyperinflation can happen anywhere in the hyperbolic plane where $LV_v > 9H^2L^2$. In Chapter 5 we will see exactly how the differences in the structure of the Hessian cause these differences in the dynamics. Nevertheless, as pointed out by [60], these two models behave very similarly in the vicinity of the initial slow-roll solution, in particular when they destabilise.

4.3.3 Hyperinflation in random potentials

The conditions on the derivatives of the potential in equation (4.3.8) are unusual, and may seem highly restrictive. In this section, we show that they are satisfied by broad classes of potentials, and do not rely on rotational symmetry.

For concreteness, we consider a random potential over $\mathbb{R}^2$ with derivatives $\partial_x V \sim \partial_y V$. In a polar coordinate system, this corresponds to

$$|V_{,\phi}| \sim |V_{,\theta}|/\phi, \qquad |V_{,\phi\phi}| \sim |V_{,\phi\theta}|/\phi \sim |V_{,\theta\theta}|/\phi^2 \,. \tag{4.3.19}$$

When considered as a potential over the hyperbolic plane with a metric of the form of equation (4.2.7), any angular gradients flatten exponentially when $\phi \gg L$. Despite the assumed randomness, $V_{;v} \approx V_\phi$ at large radius. The condition on the steepness of the potential from equation (4.3.8) (and the earlier equation (4.1.2)) forces the potential to be asymptotically intermediate between the two exponential functions,

$$\exp(3\phi L/M_{\rm Pl}^2) \quad \text{and} \quad \exp(\phi/L)\,, \tag{4.3.20}$$

where we for clarity have re-inserted factors of the reduced Planck mass. We note that over a field displacement of $\Delta\phi = 180L$, the potential may change by as little as $\exp((23L)^2)$ or as much as $\exp(180)$. We will return to this point in section 4.6.

At large radius, the Hessian of the random potentials also takes a simple form, with coefficients that satisfy equation (4.3.8):

$$V_{;vv} \simeq V_{,\phi\phi}, \quad V_{;vw} \simeq 0, \quad \text{and} \quad V_{;ww} \simeq \frac{V_{;v}}{L}\,. \tag{4.3.21}$$

Thus, hyperinflation draws heavily on the negative curvature of the hyperbolic plane, but is largely insensitive to the precise form of the potential.

4.3.4 Multifield generalisation

Our formalism also allows us to straightforwardly consider the case of hyperinflation in negatively curved field spaces with $N_{\rm f} > 2$ dimensions. With $N_{\rm f}$ fields, we solve the equations of motion in the vielbein orthonormal basis $e^I{}_a = \{v_a,\ w^1{}_a,\ w^2{}_a, ...\}$. We will be more specific on the definition of $w^1{}_a$ below. Following our discussion in section

4.3.2, we consider scalar potentials for which the Hessian in this local basis takes the diagonal form $V_{;ab} = \mathrm{diag}(V_{;vv},\ V_{;v}/L,\ V_{;v}/L, \dots)$.[4]

Here we study the evolution of $\dot{\phi}^a$ by looking at its component in the gradient-direction, $\dot{\phi}_v$, and its complement, $\dot{\phi}^a_\perp$. To proceed we first note that

$$\mathcal{D}_t v^a = (g^{ab} - v^a v^b)\frac{V_{;bc}\dot{\phi}^c}{V_{;v}} \equiv \perp^{ab} \frac{V_{;bc}\dot{\phi}^c}{V_{;v}}, \tag{4.3.22}$$

where $\perp^a{}_b$ is a projection tensor that removes the component in the gradient direction. The Klein-Gordon equation for the homogenous background field then implies that

$$\ddot{\phi}_v = \mathcal{D}_t(v_a\dot{\phi}^a) = -3H\dot{\phi}_v - V_{;v} + \frac{\dot{\phi}^a_\perp V_{;ab}\dot{\phi}^b}{V_{;v}} \tag{4.3.23}$$

$$\ddot{\phi}^a_\perp = \mathcal{D}_t(\perp^a{}_b\ \dot{\phi}^b) = -3H\dot{\phi}^a_\perp - \perp^{ab} \frac{V_{;bc}\dot{\phi}^c}{V_{;v}}\dot{\phi}_v - v^a\frac{\dot{\phi}^b_\perp V_{;bc}\dot{\phi}^c}{V_{;v}}\,. \tag{4.3.24}$$

The rate of change of the magnitude of $\dot{\phi}^a_\perp$ is then given by

$$\ddot{\phi}_\perp = \frac{1}{\dot{\phi}_\perp}\dot{\phi}_{\perp a}\mathcal{D}_t\dot{\phi}^a_\perp = -3H\dot{\phi}_\perp - \frac{\dot{\phi}^a_\perp V_{;ab}\dot{\phi}^b}{\dot{\phi}_\perp V_{;v}}. \tag{4.3.25}$$

Now, in the case of hyperinflation, we have $V_{;ab} = v_a v_b V_{;vv} + \perp_{ab} V_{;v}/L$, and hence

$$\ddot{\phi}_v = -3H\dot{\phi}_v - V_{;v} + \frac{\dot{\phi}^2_\perp}{L} \tag{4.3.26}$$

$$\ddot{\phi}^a_\perp = -3H\dot{\phi}^a_\perp - \frac{\dot{\phi}_v\dot{\phi}^a_\perp}{L} - v^a\frac{\dot{\phi}^2_\perp}{L}. \tag{4.3.27}$$

The acceleration $\ddot{\phi}^a_\perp$ is therefore in the plane spanned by v^a and $\dot{\phi}^a_\perp$, and the motion is planar. It therefore suffices to look at the evolution of the norm $\dot{\phi}_\perp$, which is governed by the equation:

$$\ddot{\phi}_\perp = -3H\dot{\phi}_\perp - \frac{\dot{\phi}_v\dot{\phi}_\perp}{L}. \tag{4.3.28}$$

We note that equations (4.3.26) and (4.3.28) are identical to the two-field equations (4.3.10) and (4.3.11) (with $\dot{\phi}_\perp \to \dot{\phi}_w$). Importantly, this means that the most important dynamics of the $N_{\rm f}$-dimensional system reduces to the standard two-field hyperinflation equations, with $N_{\rm f} - 2$ perpendicular directions decoupled.[5] We will now turn to

[4]This, for example, happens for if one takes a radial potential in $\mathbb{H}^3$, or at large ϕ for metrics of the form $ds^2_{N_{\rm f}} = d\phi^2 + L^2\sinh^2(\phi/L)d\Omega^2_{N_{\rm f}-1}$.

[5]In view of section 4.3.3, we expect that multifield hyperinflation can be realised in sufficiently steep random potentials. This could be tested explicitly by adapting the methods of e.g. [39, 40, 77, 78, 142].

the dynamics of long-wavelength perturbations around this system, where we will in particular show that this decoupling of modes persists.

4.4 Linear stability

In this short section, we provide the first detailed proof of the attractor nature of (generalised) hyperinflation by showing that small perturbations away from the solution decay. We begin by considering the two-field case, which then straightforwardly generalises to the general case with $N_{\rm f} \geq 2$ fields.

4.4.1 The two-field case

To prove the linear stability of this solution, we look at the equations for the $k = 0$ mode of linearised perturbations around the background solution:

$$\mathcal{D}_t\mathcal{D}_t\delta\phi^a + 3H\mathcal{D}_t\delta\phi^a + [(k^2/a^2H^2)\delta^a{}_b + M^a{}_b]\delta\phi^b = 0. \tag{4.4.1}$$

During hyperinflation, the parameters ϵ and η are small, and we here work to first order in these parameters. We will prove that $k = 0$ perturbations around the background solution decay unless they are in a phase-space direction that still satisfies the hyperinflation equation of motion.

To study the perturbations, it is convenient to use a kinematic basis with $n^a = \dot{\phi}/|\dot{\phi}|$ and $s^a = \mathcal{D}_t n^a/|\mathcal{D}_t n^b|$ [7, 8, 110, 161, 162] (cf. Appendix B.1 for more details). The turn-rate of the field is given by

$$a^a \equiv \mathcal{D}_N n^a = \frac{\dot{\phi}_w V_v}{H\dot{\phi}^2} s^a = \left(h - \frac{3\eta}{h}\right) s^a \equiv \omega s^a\,, \tag{4.4.2}$$

where $h = \dot{\phi}_w/HL$. In this basis, the equations of motion for the $k = 0$ mode are given by

$$\frac{d^2\delta\phi^n}{dN^2} + (3-\epsilon)\frac{d\delta\phi^n}{dN} - 2\omega\frac{d\delta\phi^s}{dN} - \frac{3\eta}{2}\delta\phi^n - \left[\omega(6-2\epsilon+\eta) + \frac{(9+\omega^2)\eta}{\omega}\right]\delta\phi^s = 0 \tag{4.4.3}$$

$$\frac{d^2\delta\phi^s}{dN^2} + (3-\epsilon)\frac{d\delta\phi^s}{dN} + 2\omega\frac{d\delta\phi^n}{dN} - \omega\eta\delta\phi^n - \left[\frac{1}{3}\omega^2(6-2\epsilon+\eta) + \frac{3(9+\omega^2)\eta}{\omega^2}\right]\delta\phi^s = 0\,. \tag{4.4.4}$$

Defining $\delta\pi^I \equiv d\delta\phi^I/dN$, we can rewrite this system as

$$\frac{d}{dN}\begin{pmatrix}\delta\phi_n\\ \delta\phi_s\\ \delta\pi_n\\ \delta\pi_s\end{pmatrix} = \begin{pmatrix} 0 & 0 & 1 & 0\\ 0 & 0 & 0 & 1\\ 3\eta/2, & \omega(6-2\epsilon+\eta)+\frac{(9+\omega^2)\eta}{\omega}, & -(3-\epsilon) & 2\omega\\ \omega\eta, & \frac{1}{3}\omega^2(6-2\epsilon+\eta)+\frac{3(9+\omega^2)\eta}{\omega^2}, & -2\omega & -(3-\epsilon)\end{pmatrix}\begin{pmatrix}\delta\phi_n\\ \delta\phi_s\\ \delta\pi_n\\ \delta\pi_s\end{pmatrix}. \tag{4.4.5}$$

We assume that ϵ and η vary slowly during inflation so that they can consistently be treated as constant to linear order. Local stability of the system can now be determined by computing the local Lyapunov exponents, i.e. the eigenvalues λ of the evolution matrix of equation (4.4.5). To leading order, they are given by

$$\lambda_1 = \eta/2 + \mathcal{O}(\epsilon^2)\,, \tag{4.4.6}$$

$$\lambda_2 = -3 + \mathcal{O}(\epsilon)\,, \tag{4.4.7}$$

$$\lambda_{3,4} = \frac{1}{2}\left(-3 \pm \sqrt{9-8\omega^2}\right) + \mathcal{O}(\epsilon)\,. \tag{4.4.8}$$

The latter three all have negative real parts and thus correspond to decaying modes. The first one is a near-constant mode corresponding to the direction $(1, 0, \eta/2, 0)^T$. In the (n^a, s^a)-basis, this mode is given by,

$$\delta\phi^I \propto (\sqrt{\epsilon}, 0)\,, \tag{4.4.9}$$

and is the regular superhorizon-scale adiabatic mode corresponding to shifts along the hyperinflation solution.[6] Since all other modes decay, we confirm that the general two-field hyperinflation solutions are stable.

We note in closing that, due to the high turning rate of the background-solution, the adiabatic mode is a little bit different from the standard slow-roll case. For a perturbation $\delta\phi_{\rm ad} = A(1,\ 0)$ with $dA/dN = \eta A/2$, the momentum perturbation is hyperinflation given by $\mathcal{D}_N\delta\phi_{\rm ad} = A(\eta/2,\ \bar{h})$, and is therefore of comparable size to the field perturbation, and in some limits much larger. By contrast, in standard slow-roll inflation, $\mathcal{D}_N\delta\phi_{\rm ad} = \eta\delta\phi_{\rm ad}/2$, which is suppressed relative the field perturbation.

[6]It follows from equation (4.4.9) that the curvature perturbation in constant density gauge freezes out on superhorizon scales.

4.4.2 Perturbations in the general multifield case

We now show that the decoupling we identified in the background equations of generalised hyperinflation with $N_{\rm f}$ fields (cf. section 4.3.4) applies to the perturbations as well. This enables us to reduce the general problem of the perturbations to the two-field case discussed above.

We can without loss of generality set ${w_1}^a \propto \perp^a{}_b\, \dot{\phi}^b$. It then follows that

$$\mathcal{D}_t v^a = \frac{\dot{\phi}_{w_1}}{L} {w_1}^a, \qquad \mathcal{D}_t {w_1}^a = -\frac{\dot{\phi}_{w_1}}{L} v^a. \tag{4.4.10}$$

These two vectors rotate in their own plane, meaning that the other basis vectors must rotate in the perpendicular subspace that they span. If we have only one more vector it follows automatically that its time derivative must vanish, but if we have more, it will be basis-dependent.

To proceed we now need to define a kinematic basis. We write it as $e^I_a = \{n_a,\ {s^1}_a, ...\}$, where we take $n^a = (\dot{\phi}_v v^a + \dot{\phi}_{w_1} {w_1}^a)/\dot{\phi}$ and ${s_1}^a = (-\dot{\phi}_{w_1} v^a + \dot{\phi}_v {w_1}^a)/\dot{\phi}$. The evolution equations for the perturbations in the n^a and ${s_1}^a$ directions are again given by equation (4.3.10) and (4.3.11), and the solution in this plane remains an attractor solution. We do not have explicit expressions for the remaining basis vectors, but since the mass matrix for these perturbations is proportional to the identity matrix, one can show (see Appendix B.1) that it is always possible to pick a basis for the perturbations where the equations of motion take the form

$$\frac{d^2\delta\phi^{s_I}}{dN^2} + (3-\epsilon)\frac{d\delta\phi^{s_I}}{dN} + \left[\frac{k^2}{a^2H^2} - \frac{3(9+\omega^2)\eta}{2\omega^2}\right]\delta\phi^{s_I} = 0\,. \tag{4.4.11}$$

These are all uncoupled near-massless modes that do not source the adiabatic perturbations. In section 4.6.2 we will argue that even if these entropic modes are numerous, the level of isocurvature is naturally suppressed.

4.5 Examples

In this section we provide several explicit examples of models of hyperinflation that in various ways generalise the simple models discussed in [45, 149]. In particular, our examples demonstrate that hyperinflation can proceed in highly asymmetric scalar potentials, and may follow a period of slow-roll inflation that becomes geometrically destabilised by the negative curvature. We furthermore present the first explicit models

with a sub-Planckian field excursion, and models with more than two fields. Throughout this section, we concentrate on the problem of realising inflation; we will turn to the observational predictions in section 4.6.

4.5.1 Example 1: hyperinflation in the Poincare patch

In section 4.2.1 we noted that the conditions under which hyperinflation is realised are non-trivial in the Poincare patch, cf. equation (4.2.22). The formalism we have developed in section 4.3 makes this issue much more clear. Assuming a radial potential, the vielbein are given by $v^a = ((1-r^2)/2L, 0)$ and $w^a = (0, (1-r^2)/2Lr)$, and the velocities in the hyperinflation solution are given by

$$\dot{\phi}_v = \frac{2L}{1-r^2}\dot{r}, \qquad \dot{\phi}_w = \frac{2Lr}{1-r^2}\dot{\theta}. \tag{4.5.1}$$

Differentiating the first equation of (4.5.1) and setting the acceleration to zero gives the condition (4.2.22).

The class of potentials that support hyperinflation in the Poincare patch need to be sufficiently steep close the boundary of the Poincare disk. In the original coordinates, the velocities are given by

$$\dot{r} = -\frac{3}{2}H(1-r^2), \qquad \dot{\theta} = \frac{1-r^2}{2Lr}\sqrt{\frac{1-r^2}{2}V_{,r} - 9H^2L^2}. \tag{4.5.2}$$

Near the boundary it is convenient to express $r \equiv 1-\delta$, and the condition $3L < \epsilon_L < 1$ translates into:

$$\frac{3L^2}{\delta} < \frac{V_{,r}}{V} < \frac{1}{\delta}\,. \tag{4.5.3}$$

Thus, hyperinflation is supported by a class of potentials that grow sufficiently rapidly towards the edge of the Poincare disk.[7]

4.5.2 Examples 2 & 3: the non-symmetric hyperinflation attractor and 'geometric destabilisation'

The original model of hyperinflation considered rotationally symmetric potentials so that the field space angular momentum (cf. equation (4.2.11)) is conserved. We now give two examples of hyperinflation realised in non-symmetric potentials, to show explicitly that this assumptions can be relaxed. These examples also demonstrate how

[7]For less rapidly growing potentials, α-attractor slow-roll inflation becomes possible.

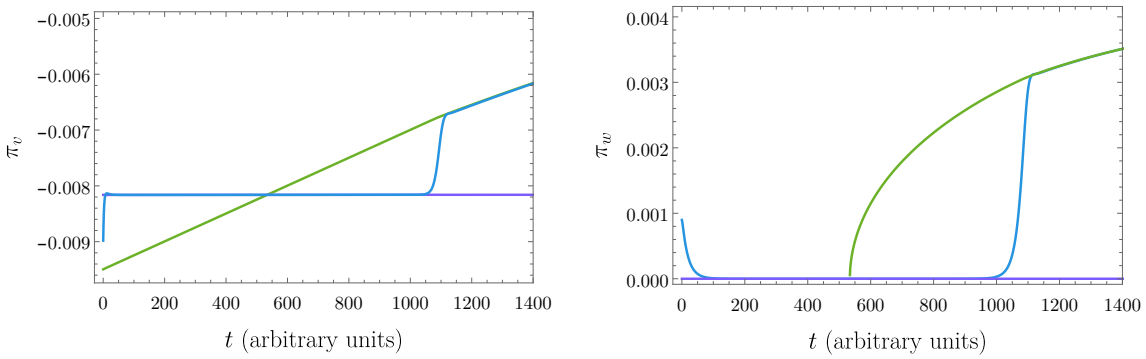

Fig. 4.1 The analytical predictions from hyperinflation (green) and slow-roll inflation (purple) together with a numerical realisation of Example 2 (blue). The momenta are quickly attracted to the slow-roll solution, but then destabilise and approach the hyperinflation attractor.

hyperinflation can follow 'geometric destabilisation' [165] of slow-roll inflation.

Example 2: As a first example of a non-symmetric hyperinflation, we consider the model

$$G_{ab} = \begin{pmatrix} \frac{2\cosh^2\left(\frac{\phi}{L}\right)\cosh^2\left(\frac{\chi}{L}\right)}{\cosh\left(\frac{2\phi}{L}\right)+\cosh\left(\frac{2\chi}{L}\right)} & -\frac{\sinh\left(\frac{2\phi}{L}\right)\sinh\left(\frac{2\chi}{L}\right)}{2\left(\cosh\left(\frac{2\phi}{L}\right)+\cosh\left(\frac{2\chi}{L}\right)\right)} \\ -\frac{\sinh\left(\frac{2\phi}{L}\right)\sinh\left(\frac{2\chi}{L}\right)}{2\left(\cosh\left(\frac{2\phi}{L}\right)+\cosh\left(\frac{2\chi}{L}\right)\right)} & \frac{2\cosh^2\left(\frac{\phi}{L}\right)\cosh^2\left(\frac{\chi}{L}\right)}{\cosh\left(\frac{2\phi}{L}\right)+\cosh\left(\frac{2\chi}{L}\right)} \end{pmatrix}, \qquad V = \frac{1}{2}m^2\phi^2. \tag{4.5.4}$$

This metric is constructed such that on the ϕ and χ axes, the metric becomes the identity matrix. The curvature is again negative and constant: $R = -2/L^2$. The quadratic Lagrangian for homogeneous perturbations around an assumed background solution on the ϕ-axis takes the form

$$\mathcal{L}\Big|_{\bar{\chi}=0} = \frac{1}{2}a^3\left[\delta\dot{\phi}^2 + \delta\dot{\chi}^2 - \left(V_{,\phi\phi} + \frac{2V_{,\phi}\dot{\phi}}{H} + (3-\epsilon)\dot{\phi}^2\right)\delta\phi^2 - \left(\frac{LV_{,\phi} - \dot{\phi}^2}{L^2}\right)\delta\chi^2\right]. \tag{4.5.5}$$

The negative term in the effective χ-mass, $-\dot{\phi}^2/L^2$, is identical to the term appearing in [165], where it was identified as the trigger of geometric destabilisation. The slow-roll solution, $\dot{\phi} = -V_{,\phi}/3H$ is stable as long as $V_{,\phi} < 9H^2L = 3VL$. Once the gradient exceeds this value, slow-roll undergoes geometric destabilisation, and the solution transitions into the hyperinflation attractor.

In our example, with $V = \frac{1}{2}m^2\phi^2$, the instability kicks in at $\phi = 2/(3L)$. Further out than this, slow-roll remains the attractor. In the case shown in Figure 4.1, which has $L = 0.05$, we start at $\phi = 31$ with initial momenta ($\pi_v \equiv \dot{\phi}_v$ and $\pi_w \equiv \dot{\phi}_w$)

perturbed away from the slow-roll solution. The figure shows how the momenta quickly converge back to the slow-roll solution, but eventually as the fields pass the instability point, they transition into the hyperinflation attractor.

A Planck-compatible model with this metric can easily be constructed with an exponential potential, $V_0 = V_0 e^{\phi/\lambda}$, and fields starting on the ϕ axis. Models with exponetial potentials can be shown to have $\eta \approx 0$, giving $n_s - 1 = -2\epsilon$ [149]. A Planck compatible spectral index is therefore obtained by setting $\lambda = 3L/(1 - n_s)$.

Example 3: We now consider the model defined by the metric and the non-rotationally symmetric potential,

$$G_{ab} = \mathrm{diag}\left(1, L^2 \sinh^2(\phi/L)\right), \qquad V = \frac{1}{2} m^2 \phi^2 \cos^2\theta \,. \tag{4.5.6}$$

At $\phi \gg L$, $V_{;v} = m^2 \phi \cos^2\theta = 2V/\phi$, so slow-roll undergoes geometric destabilisation at $\phi = 2/(3L)$ for all angles (except $\theta = \pi, 3\pi/2$). Hyperinflation is only possible inside of this radius, and until $\phi = \mathcal{O}(L)$. This metric is easy to work with everywhere in the hyperbolic plane, and here we explore more general initial conditions.

Figure 4.2 (which again have $L = 0.05$ and $m = 0.01$) displays several aspects of the hyperinflation attractor. The phase space plot (top), shows that for all sampled initial conditions (for ϕ_i, θ_i, $\dot{\phi}_i$, and $\dot{\theta}_i$), the momenta π_v and π_w consistently converge to the values predicted by the hyperinflation solution. The left plot shows how π_v (blue) and π_w (green) converge to the predicted values for one set of initial conditions. The final, right plot shows how trajectories that start in near slow roll (straight blue line) converge to hyperinflation (straight green line). The example shown are inflation models where the initial value for π_v is $-V_v/3H$ and $\pi_w = k\pi_v$ where k runs from 10^{-2} through 10^{-10}. As the figure illustrates, the slow-roll solution is exponentially unstable.

4.5.3 Example 4: small-field hyperinflation

So far we have only given examples of large-field models with $\Delta\phi_{\mathrm{tot}} > 1$. Small-field models of hyperinflation are more intricate to realise, in particular for steep potentials. This example foreshadows some of the issues discussed in the next section.

We consider the metric (4.2.7) and the scalar potential

$$V = V_\star \left[1 + \frac{2\tilde{\epsilon}}{\tilde{\eta}} \left(e^{\tilde{\eta}(\phi - \phi_\star)/3L} - 1\right)\right], \tag{4.5.7}$$

with positive parameters $\tilde{\epsilon}$ and $\tilde{\eta}$. This is a simple way of realising a small-field inflation model with a small ϵ and negative η. These are fixed by choosing the values for ϵ and

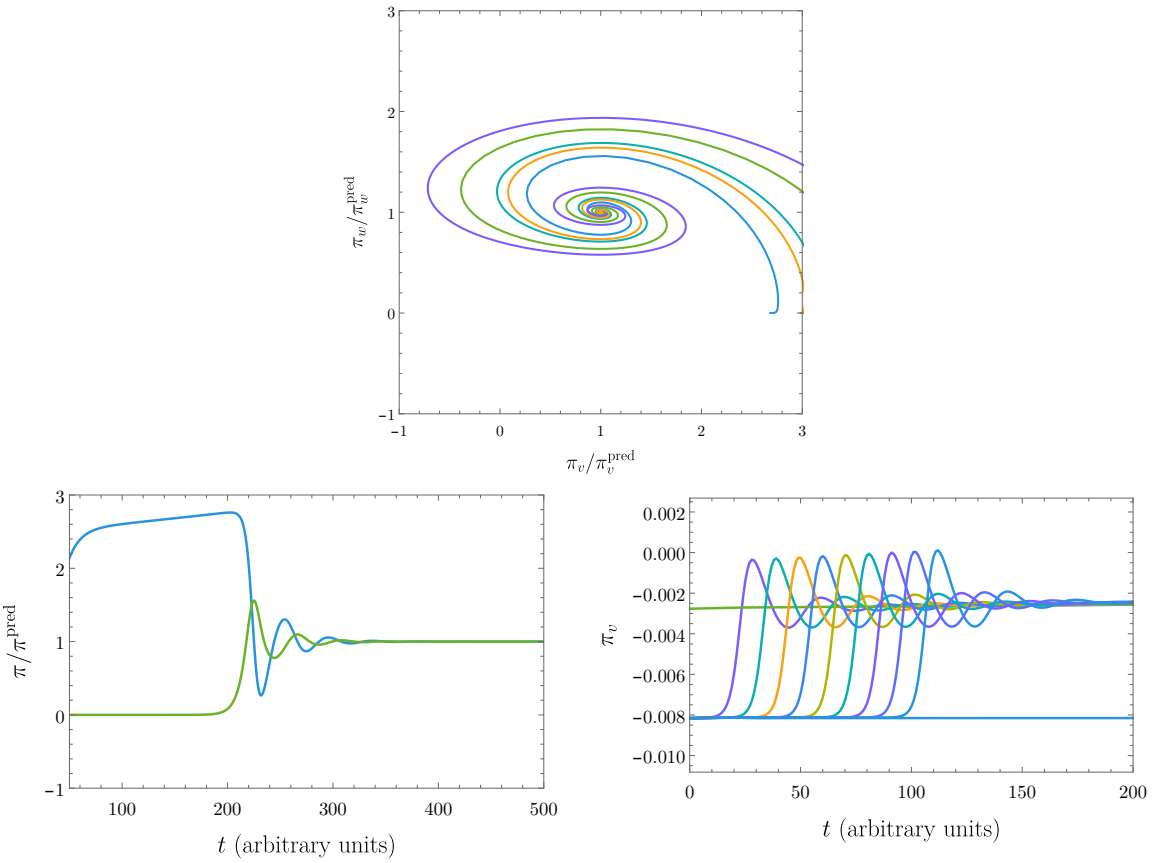

Fig. 4.2 Three graphs for the antisymmetric hyperinflation model of Example 3. The top figure shows five trajectories in field space converging to the hyperinflation attractor. The left figure shows how the momenta π_v and π_w converge to the correct values in one example. The right figure shows how slow-roll with a small velocity in the w-direction quickly becomes unstable for $\pi_{w,i}/\pi_{v,i} = 10^{-2}, \ldots, 10^{-10}$.

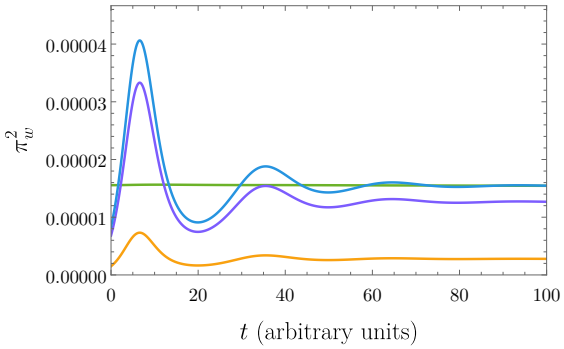

Fig. 4.3 The convergence of π_{w1}^2 (orange), π_{w2}^2 (purple) and their sum (blue) to the analytic hyperinflation solution (green) of Example 5 with $N_{\rm f} = 3$.

η at $\phi_\star$, giving, $\tilde{\epsilon} = \epsilon_\star$ and $\tilde{\eta} = 2\epsilon_\star - \eta_\star$, and we will take $\phi_\star$ to correspond to the value of ϕ when the CMB modes exited the horizon.

We would now like to construct a model with $\Delta\phi < 1$ and $V_{;v}/V$ as large as possible, that is, a small-field model with a steep gradient. To do this, we set $\epsilon_\star = 5.80 \times 10^{-6}$ and $\eta_\star = -4.28 \times 10^{-4}$, corresponding to the parameters $\tilde{\epsilon} = 5.80 \times 10^{-6}$ and $\tilde{\eta} = 4.40 \times 10^{-4}$, and fix $L = 3.87 \times 10^{-5}$. The model generates 60 e-folds of inflation over a distance $\Delta\phi = 0.2$. It also generates a correctly normalised power spectrum and spectral index ($n_s = 0.965$) [12, 14]. We note however that the maximal reheating temperature of this model is at the lower edge of what can possibly be compatible with Big Bang Nucleosynthesis: $T_{\rm rh} \lesssim 4\,{\rm MeV}$. We will return to this serious issue in section 4.6.

4.5.4 Example 5: multifield hyperinflation

Finally, we give an example of a hyperinflation model with more than two fields. This particular model has $N_{\rm f} = 3$, with a metric and a potential given by,

$$G_{ab} = {\rm diag}\left(1, L^2 \sinh^2(\phi/L), L^2 \sinh^2(\phi/L) \sin^2\theta\right), \qquad V = \frac{1}{2} m^2 \phi^2. \tag{4.5.8}$$

with the parameter values $L = 0.05$, $m = 0.01$. This is a straightforward generalisation of the original hyperinflation solution with a quadratic potential, and the numerical solution again agrees very well with the analytic predictions. Figure 4.3 shows how the square of the orthogonal momenta converge to the predicted values.

4.6 Hyperinflation and the swampland

Various conjectures have recently been proposed to delineate the effective theories that can arise from consistent theories of quantum gravity (the landscape), from those that cannot (the swampland) (see e.g. [13, 22, 67, 156] and references therein). Some of these conjectured conditions have strong implications for early universe cosmology, including models of inflation. For example, a simple form of the 'weak gravity conjecture' (WGC) applied to '0-form' gauge potentials [22] limits axion decay constants to $f_a \lesssim 1$ in natural units. If true, this would rule out 'natural inflation' in which the inflaton is an axion with a super-Planckian axion decay constant [96]. The 'swampland distance conjecture' (cf. e.g. [156, 157]) states that the maximal field space displacement over which an effective field theory is valid is bounded from above. In some version of this conjecture, the bound is taken to be close to the Planck scale, $\Delta\phi \lesssim 1$ [13]. If true, this conjecture would rule out all EFT descriptions of large-field inflation. Moreover, the 'swampland de Sitter conjecture' (in its second incarnation [106, 157]) states that the norm of the gradient of the potential is bounded from below: $|\nabla V| > \mathcal{O}(V)$, unless the Hessian matrix has a sufficiently tachyonic eigenvalue. If true, this conjecture would rule out standard single-field slow-roll inflation. The status of these conjectures remain highly uncertain and controversial (cf. e.g. [16, 62, 68, 73]), and in this section we simply explore their consequences for hyperinflation without suggesting their broad validity.

Multifield models with rapidly turning trajectories have been proposed to provide a possible way to circumvent the swampland criteria [3]. Hyperinflation provides a concrete and specific class of models of this type, and in this section we critically discuss hyperinflation in the light of the swampland conjectures. We show that while hyperinflation is less constrained by the swampland conditions than standard slow-roll inflation, it cannot simultaneously (1) satisfy the de Sitter conjecture, (2) satisfy the distance conjecture, and (3) manage to reheat the universe to $T \gtrsim 5\,\mathrm{GeV}$ at the end of inflation. We furthermore note that the simplest version of hyperinflation is in strong tension with the WGC, but generalised versions of hyperinflation may avoid this conjecture.

4.6.1 Hyperinflation and the weak gravity conjecture

The two-field system with a rotationally symmetric potential that we reviewed in section 4.2.1 admits an interpretation as a dilaton/modulus field (ϕ) coupled to an axion. An immediate consequence of this interpretation is that the axion decay constant

is exponentially large during inflation:

$$f_a \sim L \sinh(\phi/L) \sim \frac{L}{2} e^{180} \,. \tag{4.6.1}$$

On can show (e.g. by a slight adaptation of the arguments that we will give in section 4.6.3) that it is not possible to construct a simple hyperinflation model with only an axion and a modulus that is both observationally consistent and has $f_a \lesssim 1$. Consequently, the arguably most promising realisations of hyperinflation are of the generalised kind that we have presented in this chapter, which do not feature axions and for which the WGC does not apply.

4.6.2 Observational predictions for generalised hyperinflation

In this section, we briefly discuss the observational consistency of certain sub-classes of realisations of hyperinflation. The characteristic properties of the predictions follow directly from the exponential amplification of the adiabatic perturbations around horizon crossing [45]. According to [149], the power-spectrum of the (constant-density gauge) curvature perturbation, $\zeta = -\dot{\phi}_a \delta\phi^a / 2\epsilon H$ [82], is well approximated by

$$P_\zeta = \frac{H^2}{8\pi^2 \epsilon} \gamma(\bar{h})^2 \tag{4.6.2}$$

where the function $\gamma(\bar{h})^2$ parametrises the enhancement and is (for $\bar{h} \gtrsim 5$) given by

$$\gamma(\bar{h})^2 = \frac{9 + \bar{h}^2}{\bar{h}^2} e^{2p + 2q\bar{h}} \,, \tag{4.6.3}$$

with $p = 0.395$ and $q = 0.924$.

We begin by showing that models of hyperinflation with a small inflationary field excursion, $\Delta\phi < 1$, a monotonically increasing ϵ parameter, and with $\bar{h} \gtrsim 5$ are ruled out by observations. From equation (4.6.2), it follows that the spectral index is to leading order in the slow-roll parameters given by

$$n_s - 1 \simeq -2\epsilon + q\bar{h}\eta \,. \tag{4.6.4}$$

We first consider the case when ϵ grows monotonically during inflation ($\eta > 0$), and $\Delta\phi < 1$. In this case the field excursion is bounded by

$$1 > \Delta\phi > \sqrt{3\epsilon_L^\star} N_{\rm tot} \,, \tag{4.6.5}$$

where $\epsilon_L^\star$ is evaluated at the horizon crossing of the pivot scale. Clearly $\epsilon_L^\star < 1/(3N_{\rm tot}^2)$ and the negative 2ϵ contribution to the spectral index is too small to explain the observed deviation from scale invariance. To be compatible with the observed red spectral tilt, the second term ($q\bar{h}\eta$) needs to be negative. However, this requires $\eta < 0$, so that ϵ is not monotonously increasing, contrary to our assumption. Thus, rapidly turning small-field models of hyperinflation cannot explain the spectral tilt if the first slow-roll parameter is monotonically increasing during inflation, and any viable models with large $\bar{h}$ must therefore have $\eta < 0$.

Finally, we briefly comment on the perturbations in the general hyperinflation case with $N_{\rm f} > 2$ fields. From equation (4.4.11), we see that on superhorizon scales for $\bar{h} \approx \omega \gg 1$, the (spatially flat-gauge) amplitudes of these fields grow as $\sqrt{\epsilon}$, just as the adiabatic mode. The superhorizon evolution therefore does not suppress the entropic modes relative the adiabatic perturbations, and one might expect these models to produce large amounts of power in the isocurvature modes. This is not the case. The exponential amplification of the adiabatic perturbations reflected in equation (4.6.2) has no counterpart for the entropic perturbations, which emerge relatively suppressed on superhorizon scales. The isocurvature to curvature ratio is given by

$$\frac{P_{\mathcal{S}}}{P_\zeta} = (N_{\rm f}-2)\frac{h^2}{9+h^2}e^{-2p-2qh}\,, \tag{4.6.6}$$

where we made use of results in [149].

4.6.3 Small-field hyperinflation in steep potentials and reheating

Small-field models of hyperinflation satisfy $\Delta\phi < 1$ and are compatible with the 'swampland distance conjecture'. In this section, we consider the implications of small-field models of hyperinflation in steep potentials satisfying $V_{;v}/V > c$ where c is assumed to be an $\mathcal{O}(1)$ number.

Given $\epsilon_L > cL$, the limit on the total field excursion during inflation implies that,

$$1 > \Delta\phi_{\rm tot} = \int \sqrt{3\epsilon_L}dN > \sqrt{3cL}\,N_{\rm tot}\,. \tag{4.6.7}$$

We may cast this as an upper limit on the curvature scale: $L < 1/(3cN_{\rm tot}^2)$. The turning rate parameter $\bar{h}$ is related to ϵ_L and L by

$$\bar{h}^2 = 3\left(\frac{\epsilon_L}{L^2}-3\right) = 3\left(\frac{c}{L}-3\right) > 9\left(c^2N_{\rm tot}^2-1\right) \approx 9c^2N_{\rm tot}^2 \gg 1\,. \tag{4.6.8}$$

From equation (4.6.8) we see that the exponent of the enhancement factor is bounded from below by a rather large number, and the amplification of the perturbations is enormous. Still, the amplitude of the primordial curvature perturbation at the 'pivot scale' of $k_\star = 0.05$ Mpc^{-1} is fixed by observations of the cosmic microwave background to $P_\zeta(k_\star) = P_\star = 2.2 \times 10^{-9}$. As we will now argue, it is challenging to match the amplitude of the primordial power spectrum in models of hyperinflation with $\Delta\phi < 1$ and $V_{;v}/V > 1$.

Obtaining the right amplitude of the power spectrum requires,

$$e^{2q\bar{h}} = \epsilon_\star e^{-2p} \frac{24\pi^2 P_\star}{V_\star} < e^{-2p} \frac{24\pi^2 P_\star}{V_\star} \,, \tag{4.6.9}$$

which may be combined with equation (4.6.8) to give,

$$N_{\rm tot} < \frac{1}{6qc} \ln\left(\frac{24\pi^2 P_\star}{V_\star} e^{-2p}\right) = 24.6 \times \frac{1}{c}\left(1 + 0.0074 \ln\left(\frac{(100\,{\rm GeV})^4}{V_\star}\right)\right) . \tag{4.6.10}$$

Thus, these models cannot generate an arbitrarily large number of e-folds of expansion and a consistently normalised power spectrum. Indeed, as we will now show, for $c = 1$ and inflationary energy scales $V_\star^{1/4} \gtrsim 4.6\,{\rm GeV}$, these models cannot solve the horizon and flatness problems.

The inequality (4.6.10) rules out most of the possible parameter space for small-field hyperinflation in steep potentials. We here note that a small remaining window in principle exists, albeit at the expense of fine-tuning.

The inflationary epoch must be followed by a hot big bang cosmology that, in particular, can explain big bang nucleosynthesis and the thermalisation of the neutrinos. This puts a lower limit on the reheating temperature of the universe to $T \geq T_{\rm min} \approx 4$ MeV [70]. Additional requirements, such as the generation of the baryon asymmetry, may require a much higher reheating temperature, but are model dependent. Assuming (conservatively) instant reheating at the end of inflation, and that all the energy of the inflaton is transferred into the thermal plasma, we express the limit on T as a limit on the inflationary potential: $V_\star > V_{\rm end} \geq V_{\rm min} = \frac{\pi^2}{30} g_\star(T_{\rm min}) T_{\rm min}^4$, where $g_\star(T_{\rm min}) = 10.75$. This gives $3H^2 \approx V_\star > V_{\rm min} = (6\,{\rm MeV})^4$. We note that achieving rapid reheating requires a strong coupling of the inflaton to the Standard Model, which makes such models highly sensitive to loop corrections. We will not discuss this issue further here, but simply note that models with inflationary energies close to $V_{\rm min}^{1/4}$ are subject to multiple additional challenges.

Solving the flatness and horizon problems requires $N_{\rm tot} \gtrsim 62 - \ln(10^{16}\,{\rm GeV}/V_{\rm end}^{1/4})$ e-folds of expansion if the reheating is instantaneous. Small-field hyperinflation in steep potentials ($c = 1$) provides a solution to these classical problems of big bang cosmology only if

$$(6\,{\rm MeV})^4 < V_\star \approx V_{\rm end} < (4.6\ {\rm GeV})^4\,. \tag{4.6.11}$$

In other words, the enormous enhancement of the adiabatic perturbations during inflation forces the energy scale of inflation to be very low, pushing it into tension with reheating. The inequality (4.6.11) is a severe, general constraint on these models, and we expect that constructing explicit, realistic realisations will be very challenging, though not necessarily impossible.[8]

To avoid these constraints altogether in hyperinflation, one must relax either of the conditions $\Delta\phi < 1$ or $V_{;v}/V > c$. Our example in section 4.3.4 demonstrates that observationally consistent small-field models are possible, for example with $V_{;v}/V = 0.1$.

4.7 Conclusions

We have generalised the mechanism of hyperinflation to incorporate broad classes of theories in $N_{\rm f} \geq 2$ dimensional field spaces with constant negative curvature. In particular, we have shown that hyperinflation does not rely on rotationally symmetric scalar potentials, and can even be realised in theories with randomly interacting fields and without special initial conditions. In some models, hyperinflation can follow a period of slow-roll inflation that becomes 'geometrically destabilised' by the negative curvature; however, hyperinflation differs from the realisations of 'side-tracked inflation' studied in [105].

We have provided the first explicit proof of the attractor nature of hyperinflation and its generalisation, and provided a set of non-trivial explicit examples of the mechanism. These include the first explicit examples without rotational symmetry, with more than two fields, and a small-field model with an observationally consistent power spectrum.

We have furthermore shown that hyperinflation is in some tension with various 'swampland conjectures'. The simplest models are in stark conflict with the weak gravity conjecture, but more general realisations need not be. Moreover, hyperinflation can be realised in steep potentials but is hard pressed to satisfy both $\Delta\phi < 1$ and $|\nabla V|/V > 1$: these models give an enormous exponential enhancement of the primordial density perturbations, and can only be realised in models with an extremely low energy-scale of

[8] For example, baryogenesis may be achieved through the Affleck-Dine mechanism and dark matter may be non-thermally produced, e.g. as axions.

inflation ($6\,\mathrm{MeV} \lesssim V^{1/4} \lesssim 5\,\mathrm{GeV}$). However, we have also shown that slightly relaxing these conditions, e.g. by allowing $|\nabla V|/V = 0.1$, may permit for the construction of observationally viable models.

The mathematical techniques developed here will be of great use to us when we study rapid-turn two-field models in the next chapter. There we will find that hyperinflation is in fact just one particular example of a much more general solution, which also includes side-tracked inflation, among others.

Chapter 5

The rapid-turn attractor

5.1 Introduction

There has been much interest recently in multifield models of inflation with strongly non-geodesic motion [4, 7–9, 41, 45, 53, 56, 57, 59, 61, 65, 86, 98, 104, 105, 109, 112, 149, 165, 166]. Such models can be realised in potentials that are far too steep for slow-roll, and have furthermore been shown to arise as natural attractor solutions in hyperbolic field-spaces [41, 45, 59, 98, 104, 105, 109, 149, 165, 166], although they are by no means restricted to such geometries. In this chapter we show that two-field models of inflation with a high turn rate can collectively be described by a single attractor solution, and that several notable examples of strongly turning inflation models are in fact examples of this attractor.

To find this attractor solution, we look for a general solution to the background equations of motion with $\epsilon, |\eta| \ll 1$ and a large, slowly varying turn rate ω, meaning $\omega^2 \gg \mathcal{O}(\epsilon)$ and $\nu \equiv \mathcal{D}_N \ln \omega \ll 1$, since we want a stable, sustained phase of inflation. We can do this without specifying any metric or potential by projecting the equations of motion onto a suitable vielbein basis, and the results are consequently completely general. Examples of rapid-turn attractors include hyperinflation, side-tracked inflation, angular inflation, and the flat field-space turning inflation model of [4], a diverse collection of models which demonstrates the universality of the solution. These solutions can straightforwardly be recovered from the general solution, illustrating the power of this approach.

With the background solution determined, one immediately finds that two of the three independent components of the effective mass matrix of the perturbations are completely fixed (up to $\mathcal{O}(\epsilon)$ corrections). The equations of motion for the perturbations then only depend on two parameters, vastly simplifying the analysis. We will use this

result to discuss the stability of the solution and the observables of these theories, in particular the non-Gaussianities and growth of the power spectrum in theories with an imaginary speed of sound. We find that even though the power spectrum grows exponentially, non-Gaussianities in higher-order correlation functions remain moderate and compatible with current observational bounds.

We will also be interested in the behaviour of the solution in the limit $\omega \gtrsim 180$, when it is compatible with the recently proposed (and controversial) swampland conjectures [3, 13, 22, 67, 106, 123, 156, 157]. The solution simplifies in this limit, and the result may facilitate future studies of swampland-compatible inflation models.

5.2 Rapid-turn inflation

To solve the background evolution we want to find the (geometric scalar) field velocities $\dot{\phi}_v \equiv v_a\dot{\phi}^a$ and $\dot{\phi}_w \equiv w_a\dot{\phi}^a$ where like in Chapter 4 $v_a = V_{;a}/\|V_{;b}\|$ and w_a is a (co)vector field orthonormal to v^a. The equations of motion for these velocities, given earlier in equation 4.3.5, are

$$\ddot{\phi}_v = -3H\dot{\phi}_v - V_v + \Omega_v\dot{\phi}_w \tag{5.2.1}$$

$$\ddot{\phi}_w = -3H\dot{\phi}_w - \Omega_v\dot{\phi}_v\,, \tag{5.2.2}$$

where we now define $V_v = v^aV_{;a}$, $V_{vw} = v^aw^bV_{;ab}$ etc and $\Omega_v \equiv w_a\mathcal{D}_tv^a = (V_{vw}\dot{\phi}_v + V_{ww}\dot{\phi}_w)/V_v$. Ω_v is the (dimensionful) turn rate of the gradient basis vectors, which will play an important role shortly.

The reason for using the gradient basis $e^a_I = (v^a, w^a)$ above is that unlike in the kinematic basis $e^a_I = (n^a, s^a)$, where $n^a = \dot{\phi}^a/\dot{\phi}$ and $s^a = (-\dot{\phi}_wv^a + \dot{\phi}_vw^a)/\dot{\phi}$, we already know the directions of v^a and w^a before we have the full solution, making them much easier to work with. In this chapter we are looking at inflation models with a significant turn rate, meaning $\omega^2 \gg \mathcal{O}(\epsilon)$. The turn rate $\omega \equiv s_a\mathcal{D}_Nn^a$ will be a crucial quantity to our analysis, and using the gradient basis it may be expressed as

$$\omega = \dot{\phi}_wV_v/H\dot{\phi}^2, \tag{5.2.3}$$

which is obtained using the Klein-Gordon equation [41].

However, while the gradient basis is very useful for solving the background equations of motion, when dealing with perturbations the kinematic basis has significant advantages. This is because we can automatically see which perturbations are adiabatic and which correspond to isocurvature modes. For compactness denoting d/dN by $'$s,

the equations of motion for the perturbations can be written [7, 110, 172]

$$\delta\phi''^I + [(3-\epsilon)\delta^I_J - 2\omega\epsilon^I_J]\delta\phi'^J + C(k)^I_J\delta\phi^J = 0 \tag{5.2.4}$$

where $\epsilon^1_2 = -\epsilon^2_1 = 1$ and $C(k)^I_J$ is given by

$$C(k)^I_J = \begin{pmatrix} \mu_n - \omega^2 + \frac{k^2}{a^2H^2} & \mu_\times - \omega(3-\epsilon+\nu) \\ \mu_\times + \omega(3-\epsilon+\nu) & \mu_s - \omega^2 + \frac{k^2}{a^2H^2} \end{pmatrix}, \tag{5.2.5}$$

where we further defined $\mu_n = n^a n^b M_{ab}/H^2$, $\mu_\times = n^a s^b M_{ab}/H^2$, and $\mu_s = s^a s^b M_{ab}/H^2$ as projections of the dimensionless mass matrix. These are given by

$$\begin{aligned} \mu_n &= \frac{V_{vv}\dot\phi_v^2 + 2V_{vw}\dot\phi_v\dot\phi_w + V_{ww}\dot\phi_w^2}{H^2\dot\phi^2} - 2\epsilon(3-\epsilon+\eta) \\ \mu_\times &= \frac{(V_{ww}-V_{vv})\dot\phi_v\dot\phi_w + V_{vw}(\dot\phi_v^2 - \dot\phi_w^2)}{H^2\dot\phi^2} - 2\omega\epsilon \\ \mu_s &= \frac{V_{ww}\dot\phi_v^2 - 2V_{vw}\dot\phi_v\dot\phi_w + V_{vv}\dot\phi_w^2 + R\dot\phi^4/2}{H^2\dot\phi^2}, \end{aligned} \tag{5.2.6}$$

where in the middle line we used the definition of the turning rate to tidy up the expression.

5.2.1 Finding the attractor solution

During inflation we need our field velocities $\dot\phi_v$ and $\dot\phi_w$ to satisfy $\ddot\phi_I \sim \mathcal{O}(\epsilon)H\dot\phi_I$, which is necessary for ϵ and η to be small. The same goes for the total field velocity, $\mathcal{D}_t\dot\phi^2 = \mathcal{O}(\epsilon)H\dot\phi^2$, and so the equations of motion for $\dot\phi_v$ and $\dot\phi_w$ together give (c.f. equation 1.1.23)

$$\dot\phi_v V_v/H\dot\phi^2 = -3 + \mathcal{O}(\epsilon). \tag{5.2.7}$$

With our expression for ω in equation 5.2.3 this immediately implies

$$\frac{\dot\phi_v}{\dot\phi} = \frac{-3}{\sqrt{9+\omega^2}}, \quad \frac{\dot\phi_w}{\dot\phi} = \frac{\omega}{\sqrt{9+\omega^2}}, \tag{5.2.8}$$

which is accurate when $\omega^2 \gg \mathcal{O}(\epsilon)$. Furthermore, using the above expression for $\dot\phi_v/\dot\phi$, equation 5.2.7 immediately tells us

$$\dot\phi = \frac{V_v}{H\sqrt{\omega^2+9}}. \tag{5.2.9}$$

The individual field velocities are therefore

$$\dot{\phi}_v = \frac{-3V_v}{H(\omega^2+9)}, \qquad \dot{\phi}_v = \frac{\omega V_v}{H(\omega^2+9)} \tag{5.2.10}$$

As we can see, in this vielbein basis, the field velocities are automatically fixed by the turn rate ω. The turn rate is still unknown, but ensuring that the field equations of motion are statisfied individually and that ω varies slowly will allow us to fix it, and thus find a complete solution. As a brief aside, we also note that the above equation implies $\epsilon_V = \epsilon(1+\omega^2/9)$ [3, 112], which is why rapid turn inflation can be realised in potentials that are too steep for slow-roll.

Looking at the equation of motion for $\dot{\phi}_v$ in 5.2.1 alone, demanding $\ddot{\phi}_v = H\dot{\phi}_v\mathcal{O}(\epsilon)$, and using the results in equations 5.2.8 and 5.2.9, we find that the solution requires

$$\Omega_v/H = \omega + \mathcal{O}(\epsilon/\omega), \tag{5.2.11}$$

i.e. the gradient basis vectors must turn at the same rate as the fields along the solution trajectory. From this one can show

$$\frac{V_{ww}}{H^2} - \frac{3}{\omega}\frac{V_{vw}}{H^2} = \omega^2 + 9 + \mathcal{O}(\epsilon). \tag{5.2.12}$$

The equation of motion for $\dot{\phi}_w$ requires $\Omega_v/H = \omega + \mathcal{O}(\epsilon)$, which is compatible with the former (but less stringent). Intuitively, requiring $\Omega_v/H \simeq \omega$ makes sense: equation 5.2.8 fixes what fractions of the field velocity are parallel and orthogonal to the gradient direction, and if this is to be maintained as the fields turn, the basis vectors need to turn at the same rate.

Finally, we want this solution to have a slowly varying turn rate. The next step is therefore to compute $\nu = \mathcal{D}_N \ln\omega$, and to do so we will use the expression for ω in equation 5.2.3. From this we see that $\nu = \mathcal{O}(\epsilon)$ requires $\mathcal{D}_N \ln V_v = \mathcal{O}(\epsilon)$, which implies

$$\frac{V_{vw}}{H^2} - \frac{3}{\omega}\frac{V_{vv}}{H^2} = \mathcal{O}(\omega\epsilon), \tag{5.2.13}$$

where we used equations 5.2.8 and 5.2.9. These two equations can also be combined into the convenient form

$$\frac{V_{ww}}{H^2} - \frac{9}{\omega^2}\frac{V_{vv}}{H^2} = \omega^2 + 9 + \mathcal{O}(\epsilon). \tag{5.2.14}$$

When $V_{vv}/H^2 \lesssim \mathcal{O}(\omega^2\epsilon)$ and $V_{vw}/H^2 \lesssim \mathcal{O}(\omega\epsilon)$, one straightforwardly finds that the turn rate is given by $\omega^2 \simeq V_{ww}/H^2 - 9$. However, when V_{vv} and V_{vw} are non-negligible,

the situation is a little bit more complicated. The direction of motion must now be chosen so that $\dot{V}_v = V_{vv}\dot{\phi}_v + V_{vw}\dot{\phi}_w \approx 0$, imposing a second constraint on the turn rate beyond ensuring that the equations of motion are satisfied. In this scenario one can find two particularly convenient expressions for ω,

$$\omega = \frac{3V_{vv}}{V_{vw}}, \quad \omega^2 = \frac{V_{ww}}{H^2} - \frac{V_{vw}^2}{V_{vv}^2}\frac{V_{vv}}{H^2} - 9, \tag{5.2.15}$$

which must be matched if rapid-turn inflation is to take place. This is generally not possible everywhere in the target space, and will restrict where rapid-turn inflation may happen. Examples of this will be given later.

A technical detail that should be mentioned is that what we have really done, much like in Chapter 4, is to find the leading order parts of the solutions $\dot{\phi}_v = \dot{\bar{\phi}}_v + \delta\dot{\phi}_v$ and $\dot{\phi}_w = \dot{\bar{\phi}}_w + \delta\dot{\phi}_w$ that we take to be functions of field-space position only. This gives us an approximate solution, which is valid as long as the necessary corrections are small, i.e. $\delta\dot{\phi}_I \sim \mathcal{O}(H\dot{\bar{\phi}}_I\epsilon)$. For this to be the case, the explicit time derivatives of the field velocities must satisfy $d\dot{\bar{\phi}}_I/dt \sim O(H\dot{\bar{\phi}}_I\epsilon)$, which requires the terms V_v, V_{vw}, etc to vary slowly along the trajectory. This is a very much consistent with our assumption of $\nu = \mathcal{O}(\epsilon)$.

5.2.2 Perturbations and stability

Now we would like to look at the behaviour of perturbations in these models. We first need to verify that the background solution is stable, a necessary condition for it to be an attractor. To begin, we note that (after some tedious algebra) the Klein-Gordon equation gives

$$\mathcal{D}_N\omega = s_a\mathcal{D}_N\mathcal{D}_N n^a = -\mu_\times + \omega(-3 + \epsilon - \eta) \tag{5.2.16}$$

Demanding $\nu = \mathcal{D}_N \ln\omega \sim \mathcal{O}(\epsilon)$ therefore requires

$$\mu_\times = -3\omega + \mathcal{O}(\omega\epsilon), \tag{5.2.17}$$

and we have fixed one element of the effective mass matrix. One can also show that equations 5.2.13 and 5.2.14 imply

$$\mu_n = \omega^2 + \mathcal{O}(\epsilon). \tag{5.2.18}$$

We now define $\delta\pi_I \equiv \delta\phi_I'$, and find that the equations of motion for the perturbations can be written

$$\begin{pmatrix} \delta\phi_n' \\ \delta\phi_s' \\ \delta\pi_n' \\ \delta\pi_s' \end{pmatrix} = \begin{pmatrix} 0 & 0 & 1 & 0 \\ 0 & 0 & 0 & 1 \\ -\kappa^2 & 6\omega & -3 & 2\omega \\ 0 & \omega^2 - \mu_s - \kappa^2 & -2\omega & -3 \end{pmatrix} \begin{pmatrix} \delta\phi_n \\ \delta\phi_s \\ \delta\pi_n \\ \delta\pi_s \end{pmatrix} \tag{5.2.19}$$

where $\kappa \equiv k/aH$ and we have ignored $\mathcal{O}(\epsilon)$ corrections.

To see whether the background solution is stable, we look at the eigenvalues of the evolution matrix (the local Lyapunov exponents) when $k = 0$. They are given by

$$\lambda = -3, \quad 0, \quad \frac{1}{2}\left(-3 \pm \sqrt{9 - 4\mu_s - 12\omega^2}\right). \tag{5.2.20}$$

As long as the dimensionless entropic mass satisfies $\mu_s > -3\omega^2$, the system has one (near) constant mode (the adiabatic one) and three decaying ones, and is thus stable. Using equations 5.2.6 and 5.2.12 one can show that the entropic mass can be written in the convenient form

$$\mu_s = \frac{9V_{ww}}{H^2(\omega^2 + 9)} + \frac{V_{vv}}{H^2} + \frac{R\dot{\phi}^2}{2H^2} + \mathcal{O}(\epsilon) \tag{5.2.21}$$

which must satisfy the above condition.

5.2.3 Rapid-turn inflation and the swampland

For inflation to be compatible with the swampland conjectures [13, 22, 67, 106, 156, 157], the field excursion must be bounded, $\Delta\phi \leq M_{\rm P} \equiv (8\pi G)^{-1/2}$, which implies $\epsilon \leq 1/2N^2$ (where N is the number of e-folds of inflation), and either the gradient satisfies $M_{\rm P}V_v/V \geq c$ or the minimum eigenvalue of the Hessian satisfies $M_{\rm P}^2 \min(V_{;ab})/V \leq -c'$, where c and c' are $\mathcal{O}(1)$ coefficients.

If we want to satisfy the swampland conjectures by having a large gradient, the turn rate will satisfy $\omega \gtrsim 180$ [3]. In this limit, the rapid-turn attractor solution drastically simplifies, assuming that V_{vv} is not parametrically larger than V_{ww}, and we find

$$\omega^2 \simeq \frac{V_{ww}}{H^2}, \quad \dot{\phi}_v \simeq -\frac{3HV_v}{V_{ww}}, \quad \dot{\phi}^2 \simeq \frac{V_v^2}{V_{ww}}. \tag{5.2.22}$$

The two conditions can then be reformulated as

$$M_{\rm P}V_v/V \geq c, \quad M_{\rm P}V_{ww}/V_v \geq 3cN^2, \tag{5.2.23}$$

which are straightforward to check.

If instead we want to satisfy the condition on the Hessian, there are fewer simplifications that can be made, since the turn rate is no longer necessarily very large.

For a given model, we do not have full freedom in choosing which of these conditions we want to satisfy, and there are pitfalls that need to be avoided. The spectral index of the power spectrum needs to be matched with obserervations, which constrains the background solution, potentially ruling out one or both of these options (c.f. [41]). Moreover, in very rapidly turning models ($\omega \geq \mathcal{O}(100)$), entropic masses $\mu_s < \omega^2$ can cause such large growth of the power spectrum that it becomes hard to reheat the universe after inflation (c.f. Chapter 4). This is especially problematic for models realised in hyperbolic field-spaces, where $R < 0$. From equations 5.2.21 and 5.2.22 one can deduce that these models need at least $V_{vv} \gtrsim V_{ww}$ to avoid this problem, which in turn implies that these models will be of the type where both the constraints in equations 5.2.13 and 5.2.14 are important.

5.3 Examples of rapid-turn attractors

In this section we show that several non-standard two-field inflation models are examples of rapid-turn attractors, and use the relations derived above to straightforwardly find the form of the solutions. Hyperinflation and the turning inflation model of [4] present two algebraically simple models where we can easily derive the form of the full solution, and for the latter we also give some numerical examples of the agreement between the attractor model predictions and numerical simulation. Side-tracked inflation and angular inflation, however, are algebraically messy. In the former case we present more numerical examples of the agreement between the attractor predictions and simulations, and in the latter case we show how we can straightforwardly recover the parametric equation for the field trajectory.

The point of this section is not to delve into the details of these models; it is instead to show what a broad class of models can be described by this attractor solution, and to demonstrate how powerful these techniques can be for finding explicit solutions given a metric and potential. In models where V_{vv} and V_{vw} are negligible (e.g. hyperinflation), rapid-turn inflation can occur anywhere in the target space, and equations 5.2.9 and

5.2.14 immediately give the full solution (i.e. $\dot{\phi}_v$ and $\dot{\phi}_w$) which is valid everywhere. In models where V_{vv} and V_{vw} are non-negligible, however, the expressions for ω in equations 5.2.13 and 5.2.14 must be matched, and solving these two equations will tell us where in field-space this phase may occur.

5.3.1 Hyperinflation

This model, which was first introduced by [45], and then further studied in [41, 149], provides a very clean example of a rapid-turn attractor. The usual metric and potential used for this model are

$$ds^2 = d\phi^2 + L^2 \sinh(\phi/L)^2 d\theta^2, \quad V = V(\phi), \tag{5.3.1}$$

although more generally it just requires $V_{ww} = V_v/L$, $V_{vw} \simeq 0$ and $V_{vv} \ll V_{ww}$. Hyperinflation refers to a new phase of inflation that occurs when the potential becomes sufficiently steep for slow-roll to be geometrically destabilised [45, 165]. Using the results derived earlier in this chapter and the above covariant derivatives of the potential, one immediately finds

$$\dot{\phi}_v = -3HL, \quad \dot{\phi}^2 = LV_v, \tag{5.3.2}$$

which is only a consistent solution if $LV_v > 9H^2L^2$, which is precisely the condition for slow-roll to become unstable [45, 165]. Its entropic mass, given by $\mu_s = -\omega^2 + \mathcal{O}(\epsilon)$, is very tachyonic in the $\omega \gg 1$ limit, but the background evolution is nevertheless stable.

5.3.2 A flat field-space model

This example, first introduced in [4], is very different from hyperinflation, especially since the field space is not hyperbolic. Here we have the metric and potential

$$ds^2 = d\rho^2 + \rho^2 d\theta^2, \; V = V_0 - \alpha\theta + \frac{1}{2}m^2(\rho - \rho_0)^2. \tag{5.3.3}$$

In this model, the rapid-turn regime appears at $\rho \gg \rho_0$, where the gradient of the potential is dominated by the ρ-direction, but where the θ-term nevertheless plays an important role. Here we have $V_v \simeq m^2\rho$, $V_{vv} \simeq V_{ww} \simeq m^2$, and $V_{vw} \simeq \alpha/\rho^2$. Equations 5.2.13 and 5.2.14 thus give us two expressions for ω:

$$\omega \simeq 3\rho^2 m^2/\alpha, \quad \omega \simeq \sqrt{3} M_{\rm P} m/\sqrt{V_0}. \tag{5.3.4}$$

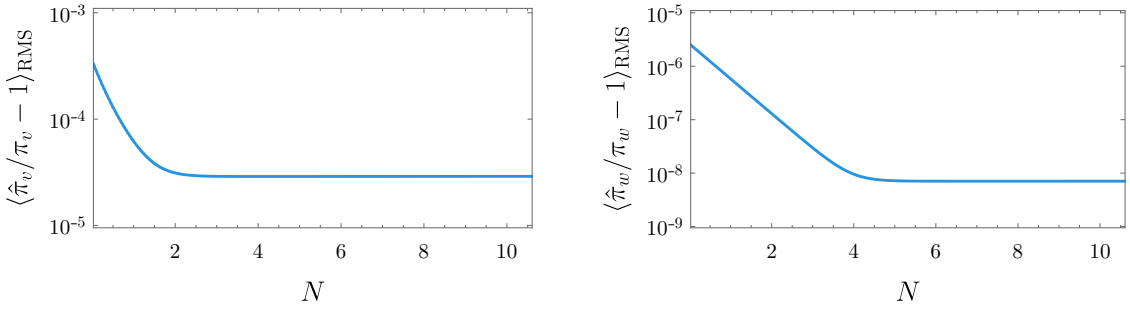

Fig. 5.1 RMS fractional differences over a few oscillation cycles between the predicted $\hat{\pi}_v$ (left), $\hat{\pi}_w$ (right) and numerically calculated field momenta π_v, π_w in the flat field-space model as the solutions converge.

These must match (up to a sign), telling us that this type of inflation can only happen at

$$\rho^2 = M_{\rm P}\alpha/\sqrt{3V_0}m, \quad \Rightarrow \quad \dot{\theta} = \dot{\phi}_w/\rho \simeq m, \tag{5.3.5}$$

in agreement with [4]. Moreover, to illustrate the accuracy of the rapid-turn attractor predictions, Figure 5.1 shows the agreement between predictions and simulations for a swampland compatible model with $\alpha = 5.0\times10^{-16}$, $m = 2.5\times10^{-3}$ and $V_0 = 3.4\times10^{-10}$, giving $\omega \approx 230$.

5.3.3 Side-tracked inflation

Side-tracked inflation is another example of a rapid-turn attractor in hyperbolic geometry, which like hyperinflation can arise after geometric destabilisation of slow-roll [105, 165]. Looking at the side-tracked inflation model with the so called 'minimal geometry', we have

$$ds^2 = \left(1 + \frac{2\chi^2}{M^2}\right) d\phi^2 + d\chi^2, \; V = U(\phi) + \frac{m_h^2}{2}\chi^2. \tag{5.3.6}$$

In this model, m_h is the mass of a heavy field with $m_h \gg H$, but despite the size of this mass, slow-roll is destabilised by the negative curvature, and we end up in a 'side-tracked' phase of inflation, which is another example of a rapid-turn attractor. V_{vv} and V_{vw} are non-negligible in this model, so we can use equations 5.2.13 and 5.2.14 to find where in field-space side-tracked inflation may happen. Assuming $MU_{,\phi\phi} \ll U_{,\phi}$

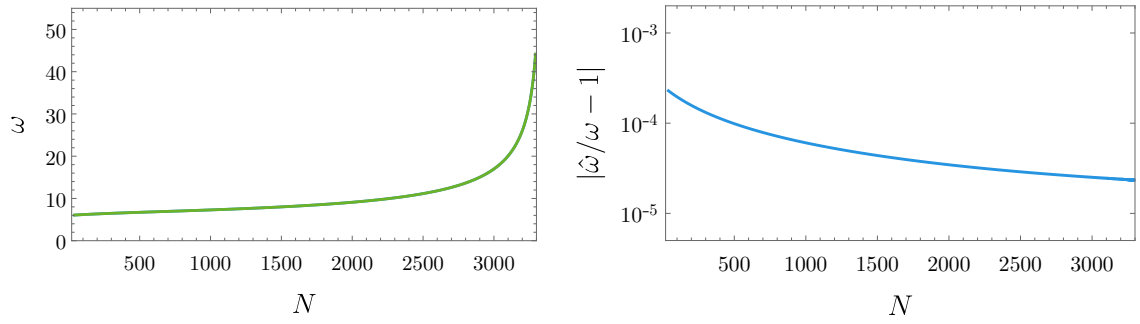

Fig. 5.2 The turn rate ω in the side-tracked example (green), and the fractional difference between the numerical and predicted values (blue).

[105] and that U dominates the potential energy, we find that this happens at

$$\frac{2\chi^2}{M^2} = \sqrt{\frac{2}{3}}\frac{M_{\rm P}|U_{,\phi}|}{m_h M\sqrt{U}} - 1, \tag{5.3.7}$$

recovering the expression found in [105]. Figure 5.2 also illustrates the agreement between the rapid-turn attractor predictions and numerical simulations for a model with a natural inflation potential $U(\phi)$ with $M = 0.001M_{\rm P}$ and $m_h/H = 10$.

5.3.4 Angular inflation

An additional attractor model was found recently by [59], in the context of α-attractor models [2, 51, 52, 116, 118, 118–120, 125], where the geometry again is hyperbolic. Here we work with a metric and potential of the form

$$ds^2 = \frac{6\alpha(d\phi^2 + d\chi^2)}{(1-\phi^2-\chi^2)^2}, \quad V = \frac{\alpha}{6}\left(m_\phi^2\phi^2 + m_\chi^2\chi^2\right). \tag{5.3.8}$$

Reparametrising this as $\phi = r\cos\theta$, $\chi = r\sin\theta$, and defining $R = m_\chi^2/m_\phi^2$, they found a new angular attractor solution at $1 - r \ll 1$ when the parameters α and R satisfied $\alpha \ll 1$ and $R \gtrsim 10$. Defining $\delta \equiv 1 - r^2$, one can then solve equations 5.2.13 and 5.2.14 (eliminating ω) to leading order in δ, to find its parametrisation by θ as written in [59][1]:

$$\delta(\theta) = 1 - r(\theta)^2 = \frac{9\alpha(\cot\theta + R\tan\theta)^2}{2(R-1)^2}. \tag{5.3.9}$$

[1]The current arXiv version (v1) has a typo in equation (2.14), where cot and tan appear with squares. If (2.13) is expanded in α, however, these squares do not appear.

5.4 Primordial perturbations

The first-order equations of motion satisfied by the perturbations, given in equation 5.2.19, notably only depend on two free paramters, ω and μ_s, which have a significant impact on the primordial perturbations generated by these models. If $\xi \equiv \mu_s/\omega^2 > 1$, the perturbations can be analysed using a single-field EFT with a reduced speed of sound, which has been studied extensively in the literature (see e.g. [4, 7–9, 53]). Observationally, these models are generally characterised by large equilateral non-Gaussianity ($\propto c_s^{-2}$), and a suppressed tensor-scalar ratio ($\propto c_s$). If $\xi < 1$, the situation is rather different. The speed of sound of the single-field EFT is now imaginary, and one can see very large growth of the power spectrum at horizon crossing. These are the theories we shall focus on in the remainder of this chapter.

It will be convenient for us to work with the curvature perturbation $\zeta = \delta\phi_n/\sqrt{2\epsilon}$ and with the entropic perturbation $\sigma = \delta\phi_s$, with which the action takes the following form:

$$\mathcal{S} = \frac{1}{2}\int dt \frac{d^3k}{(2\pi)^3} a^3 \Bigg[2\epsilon \left(\dot{\zeta}^2 - \frac{k^2}{a^2}\zeta^2 \right) + \dot{\sigma}^2 - \frac{k^2}{a^2}\sigma \\ - H^2\omega^2(\xi - 1)\sigma^2 - 4\sqrt{2\epsilon}\omega H \sigma \dot{\zeta} \Bigg]. \tag{5.4.1}$$

The aim here is to compute the mode function of ζ analytically (neglecting Hubble friction, similarly to references [4, 53]) using a WKB approach, and thus compute the growth of the power spectrum in general. The equations of motion resulting from equation (5.4.1) are

$$\ddot{\zeta} + 3H\dot{\zeta} + \frac{k^2}{a^2}\zeta = \frac{2\omega H}{\sqrt{2\epsilon}}(\dot{\sigma} + 3H\sigma) \tag{5.4.2}$$

$$\ddot{\sigma} + 3H\dot{\sigma} + \frac{k^2}{a^2}\sigma + H^2\omega^2(\xi - 1)\sigma^2 = -2\omega H\sqrt{2\epsilon}\dot{\zeta}, \tag{5.4.3}$$

and the goal of this section is to find and understand their solutions. To make progress we assume that we are in a phase where Hubble friction can be neglected (which given the exponential growth and $\omega \gg 1$ is a fair assumption), and make the ansatz

$$\zeta = \zeta_+ e^{i\lambda_+ t} + \zeta_- e^{i\lambda_- t}, \qquad \sigma = \sigma_+ e^{i\lambda_+ t} + \sigma_- e^{i\lambda_- t}. \tag{5.4.4}$$

Both of these frequencies should of course appear twice, with different signs, but for notational convenience we ignore this at the moment. We then find that the frequencies $\lambda_\pm$ are given by

$$\lambda_\pm^2/H^2 \equiv \tilde{\lambda}_\pm^2 = \kappa^2 + \frac{3+\xi}{2}\omega^2 \pm \frac{1}{2}\sqrt{16\kappa^2\omega^2 + (3+\xi)^2\omega^4}, \tag{5.4.5}$$

where we have introduced the notation $\kappa \equiv k/aH$. It will shortly be useful for us to work with e-folds as a time coordinate, and when ignoring $\mathcal{O}(\epsilon)$ corrections we are free to shift it (for each k-mode) such that $\kappa = e^{-N}$, meaning that horizon exit happens at $N = 0$.

The first thing we note is that for $\xi < 1$, λ_- becomes imaginary for sufficiently small κ. This happens at

$$\kappa^2 + \frac{3+\xi}{2}\omega^2 = \frac{1}{2}\sqrt{16\kappa^2\omega^2 + (3+\xi)^2\omega^4} \quad \Rightarrow \quad \kappa = \sqrt{1-\xi}\omega, \tag{5.4.6}$$

and therefore from $N = -\ln(\sqrt{1-\xi}\omega)$ e-folds before horizon crossing and onwards, λ_- is imaginary. This means that during this phase the mode functions will grow exponentially, which is exactly what one finds numerically. In hyperinflation, $\xi = -1$, and we recover Brown's result that the growth starts at $\ln(\sqrt{2}\omega)$ e-folds before horizon crossing [45].

We are now in a position to compute an analytic approximation for the mode functions for ζ without an EFT. This can be done by integrating $|\tilde{\lambda}_-|$ from $N = -\ln(\sqrt{1-\xi}\omega)$ to up to some arbitrary N (in effect, we are using the WKB method), and it is more accurate than one might initially expect, since the contributions from Hubble friction are negligible on superhorizon scales. Here we let $\zeta_\pm$ refer to the positive and negative frequency solutions of the low frequency modes, and they can be written as

$$\zeta_\pm \propto \exp\left[\pm\mathcal{I}(N)\right], \tag{5.4.7}$$

where the integral $\mathcal{I}(N)$ is given by

$$\mathcal{I}(N) = \int_{-\ln(\sqrt{1-\xi}\omega)}^{N} \sqrt{-\kappa^2 - \frac{3+\xi}{2}\omega^2 + \frac{1}{2}\sqrt{16\kappa^2\omega^2 + (3+\xi)^2\omega^4}}dN. \tag{5.4.8}$$

One can show after tedious algebra (see Appendix B.4) that this integral can be evaluated to

$$\mathcal{I}(N) = F(b-1) - F(\sqrt{1 + 16\kappa^2/(3+\xi)^2\omega^2}), \tag{5.4.9}$$

where the function F is given by,

$$F(y) = \frac{2\omega}{b}\sqrt{(y-1)(b-1-y)} - \omega \arctan\left[\frac{b-2y}{2\sqrt{(y-1)(b-1-y)}}\right] - \omega\sqrt{\frac{2}{b}}\arctan\left[\frac{\sqrt{2}(2-3b+2y+by)}{4\sqrt{b(y-1)(b-1-y)}}\right], \tag{5.4.10}$$

and we have defined $b = 8/(3+\xi)$. While this is not an easy expression to work with, it is accurate. Of particular interest to us is the behaviour of the mode functions in the regime of validity of the EFT, when κ^2/ω^2 is small. Here we find that they simplify to (see appendix B.4)

$$\zeta_\pm \propto \exp\left[\pm(2-\sqrt{3+\xi})\frac{\pi\omega}{2} \mp |c_s|\kappa\right], \tag{5.4.11}$$

where $|c_s| = \sqrt{(1-\xi)/(3+\xi)}$.

With the above expressions, we can also give an analytic expression for the growth of the power spectrum before horizon crossing, denoted by $\gamma^2 = \gamma^2(\omega,\xi) = P_\zeta(\omega,\xi)/P_\zeta(0)$. We assume that once we are on superhorizon scales, ζ_+ is dominant, and that ζ_+ and ζ_- had roughly equal power at $N = -\ln(\sqrt{1-\xi}\omega)$. Then, for consistency also neglecting the Hubble friction for the single-field ζ, we find that the relative growth of the power spectrum is given by

$$\ln(\gamma^2) \approx (2-\sqrt{3+\xi})\pi\omega, \tag{5.4.12}$$

which is obtained by letting $\kappa \to 0$ in equation (5.4.11). In hyperinflation, we then find that $\ln(\gamma) \propto 0.920\,\omega$, similar to the numerical result of Mizuno et al. that $\ln(\gamma) \propto 0.924\,\omega$ [149].

The expression for the ζ mode function we derived here is an approximation, but it is remarkably accurate. As shown in Figure 5.3, the formula for the growth of the power spectrum given in equation (5.4.12) agrees very well with numerics.

Equation (5.4.12) also allows us to determine the maximal turn rate that can be realised in an observationally compatible inflationary model. Sometime after inflation has ended, the universe is reheated to create the conditions for the hot Big Bang cosmology. To ensure the success of Big Bang Nucleosynthesis (and the thermalisation of the neutrinos), reheating must happen at $T_{\text{reheat}} > T_{\text{min}} \approx 4$ MeV. Enforcing (very conservatively) that the Hubble parameter at horizon crossing, H_*, is larger than the

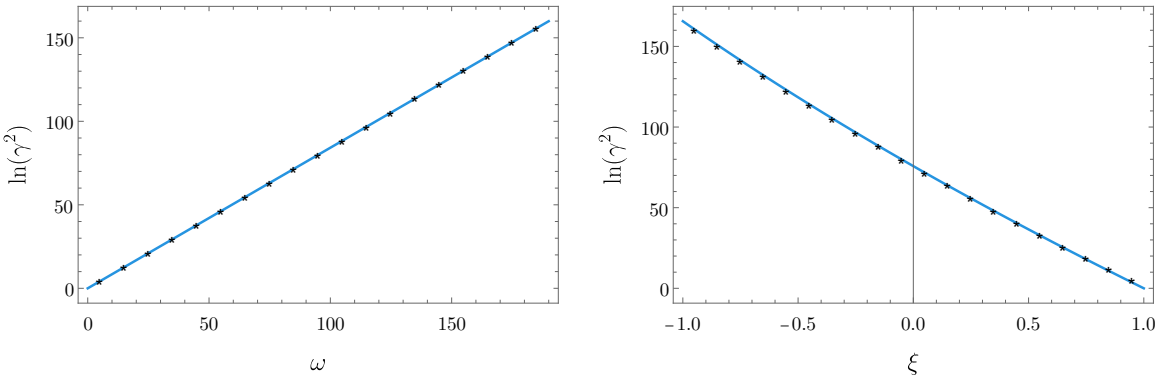

Fig. 5.3 Comparison between predicted growth and numerically calculated values, computed using the methods of appendix B.3. The graph on the left has $\xi = 0$ fixed and the one on the right has $\omega = 90$.

.

minimal value $H_{\min}$, that $\epsilon_* < 1$, and that P_ζ has the correct amplitude then gives

$$\ln \gamma^2 \lesssim \ln\left(8\pi^2 P_{\rm obs}\left(\frac{M_{\rm Pl}}{T_{\min}}\right)^4\right) \approx 176\,. \tag{5.4.13}$$

This bound then constrains ω and ξ through equation (5.4.12). For example, in hyperinflation with $\xi = -1$ the turn rate is bounded by $\omega \lesssim 96$.

5.5 Non-Gaussianity and perturbativity

In the single-field EFT with an imaginary speed of sound, the mode function of the curvature perturbation can be written as [98, 104]

$$\zeta_k(\tau) = \left(\frac{2\pi^2}{k^3}\right)^{1/2} \alpha\left(e^{k|c_s|\tau+x}(k|c_s|\tau - 1) - \rho e^{i\psi} e^{-(k|c_s|\tau+x)}(k|c_s|\tau + 1)\right)\,. \tag{5.5.1}$$

The coefficients α, ρ and ψ are all assumed to have a mild k-dependence, although quantisation fixes $\alpha^2 \sim H^2/\epsilon M_{\rm P}^2$. This EFT is expected to be valid for $-x/|c_s| < k\tau$. Most important here is x, which parametrises the magnitude of the power spectrum at horizon crossing (i.e at the end of the transient growth), and which is expected to be large when the turning rate is large: $x \sim \omega$ [98]. The resulting power spectrum can be written

$$P_\zeta \approx \alpha^2 e^{2x}, \tag{5.5.2}$$

assuming that $\rho \lesssim \mathcal{O}(1)$.

Encouragingly, the form of the above mode function agrees well with with the two-field result in equation 5.4.11 (the additional factors $k|c_s|\tau \pm 1$ arise from Hubble friction, which we ignored in the two-field calculation). We can therefore match the EFT-result with its 'UV completion' to find

$$x(\omega, \xi) = \left(2 - \sqrt{3+\xi}\right) \frac{\pi\omega}{2}. \tag{5.5.3}$$

What makes the EFT treatment of [98] particularly interesting is that it allowed for the first discussion and calculations of non-Gaussianities in these models. Specifically, the bispectrum was found to peak for flattened configurations (for which $k_2 = k_3 = k_1/2$) with an amplitude of $f_{\rm NL}^{\rm flat} = \mathcal{O}(50)$ for one example of hyperinflation. Most importantly however, some contributions to the (non-Gaussian) connected n-point correlation functions for $n \geq 4$ were analytically found to be *exponentially large*, leading to an apparent loss of perturbative control.

Key to this discussion is the expansion of the curvature perturbation ζ in terms of a Gaussian field ζ_g:

$$\zeta = \zeta_g \left(1 + f_{\rm NL}^{(1)} \zeta_g + f_{\rm NL}^{(2)} \zeta_g^2 + \dots\right), \tag{5.5.4}$$

where the coefficients $f_{\rm NL}^{(n-2)}$ are given by

$$f_{\rm NL}^{(n-2)} = \frac{\langle \zeta^n \rangle_c}{\langle \zeta^{2n-2} \rangle}, \tag{5.5.5}$$

and the subscript c denotes a connected correlation function. For the expansion to be well-defined, we require (heuristically)

$$f_{\rm NL}^{(n-2)} |\zeta_g|^{n-2} \sim f_{\rm NL}^{(n-2)} \langle \zeta^2 \rangle^{(n-2)/2} \lesssim 1. \tag{5.5.6}$$

Thus, as argued in Reference [98], we retain perturbative control as long as

$$\frac{\langle \zeta^n \rangle_c}{\langle \zeta^2 \rangle^{n-1}} \lesssim \langle \zeta^2 \rangle^{-(n-2)/2}. \tag{5.5.7}$$

Some contributions to $\langle \zeta^n \rangle_c$ were shown to be harmless in [98]: contact interactions lead to no exponential enhancement in the non-Gaussian parameters. This explains why, in particular, the connected three-point function is not very large. However, other contributions that involve the tree-level exchange of (a scalar) ζ, were found to be dangerous. The starting point for this argument is the expansion of the correlators in

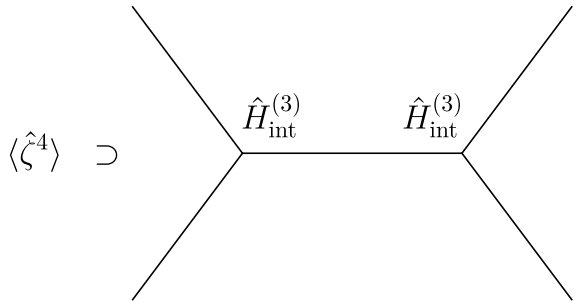

Fig. 5.4 The four-point correlation function gets a contribution from a scalar exchange diagram, corresponding to two insertions of the cubic interaction Hamiltonian.

.

the in-in formalism

$$\langle\hat{\zeta}^n(\tau)\rangle = \sum_{k=0}^{\infty} i^k \int_{-\infty}^{\tau} d\tau_1 \ldots \int_{-\infty}^{\tau_{k-1}} d\tau_k \langle[\hat{H}_{\rm int}(\tau_k), \ldots [\hat{H}_{\rm int}(\tau_1), \hat{\zeta}^n(\tau)]\ldots]\rangle, \qquad (5.5.8)$$

where the operators on the right-hand side are in the interaction picture. To evaluate these correlators, one uses the mode functions of the (free) quadratic theory, and incorporates cubic and higher-order interaction terms through $\hat{H}_{\rm int}$.

The simplest example of an arguably dangerous contribution to the four-point function is shown in Figure 5.4. The corresponding contribution to the connected 4-point function is in the in-in formalism given by

$$\langle\hat{\zeta}^4(\tau)\rangle_c \supset -\int_{-\infty}^{\tau} d\tau_1 \int_{-\infty}^{\tau_1} d\tau_2 \langle[\hat{H}_{\rm int}(\tau_2), [\hat{H}_{\rm int}(\tau_1), \hat{\zeta}^4(\tau)]]\rangle, \qquad (5.5.9)$$

with cubic interactions $\hat{H}_{\rm int} \sim \frac{1}{\alpha^2}\hat{\zeta}^3$. The actual interactions involve derivatives of ζ, but these do not affect the exponential scaling or the general argument. Moreover, the important factor of α^{-2} comes from the factor of $\epsilon M_{\rm P}^2/H^2$ in the cubic vertex. We will explain both these points in more detail later on in this section.

The integrand of this contribution to (5.5.9) then involves 10 powers of $\hat{\zeta}$ (three respectively at τ_1 and τ_2, and four at τ), which should all be appropriately contracted using Wick's theorem. The naive scaling of this diagram is therefore:

$$\langle\hat{\zeta}^4(\tau)\rangle_c \sim \alpha^6 e^{10x} \qquad \text{(naive)} \qquad (5.5.10)$$

It then follows from equation 5.5.2 that $g_{\rm NL}$ scales like

$$g_{\rm NL} = \frac{\langle\zeta^4\rangle_c}{\langle\zeta^2\rangle^3} \sim e^{4x}\,, \qquad \text{(naive)} \qquad (5.5.11)$$

which is exponentially large and will even be larger than P_ζ^{-1} for $x \gtrsim 5$.

Thus, it would seem that hyperinflation and other rapidly turning models are severely constrained by limits on non-Gaussianity, currently at the level $g_{\rm NL} \lesssim \mathcal{O}(10^4 - 10^6)$ [15, 148], and even the requirement of perturbativity. However, as we will now show, such a conclusion would be too quick and, in fact, inaccurate. The estimates (5.5.10) and (5.5.11) do not account for subtle yet exact cancellations within the relevant correlation functions, and the actual non-Gaussian parameters of these models are merely $\sim \mathcal{O}(1)$ – far from observational constraints or tensions with perturbativity. The terms which one naively would expect to be dominant instead cancel out, and the dominant terms will be products of exponentially growing and decaying modes, limiting the overall growth. These results are analagous to those for gauge fields axially coupled to the inflaton during inflation [93]. Reference [98] noted that this was the case for the the bispectra of rapid-turn models, and here we will show that this is in fact also the case for the trispectra and higher-order correlation functions.

5.5.1 The 4-point correlator

Before we consider the general n-point correlator, we will for simplicitly consider the specific case of the 4-point correlation function, and show that $g_{\rm NL}$ is not outside of observational bounds. We will in particular show why the term in the correlator arising from two insertions of cubic Hamiltonians must be proportional to e^{6x} (instead of e^{10x} as in equation (5.5.10)), and gives $g_{\rm NL} \sim 1$ (instead of $g_{\rm NL} \sim e^{4x}$ as in equation (5.5.11)).

The correlator inside the integral in equation (5.5.9) can be expanded as

$$\begin{aligned}\langle[\hat{H}_{\rm int}(\tau_1),[\hat{H}_{\rm int}(\tau_2),\hat{\zeta}^4(\tau)]]\rangle &= \langle\hat{H}_{\rm int}(\tau_1)\hat{H}_{\rm int}(\tau_2)\hat{\zeta}^4(\tau)\rangle - \langle\hat{H}_{\rm int}(\tau_1)\hat{\zeta}^4(\tau)\hat{H}_{\rm int}(\tau_2)\rangle \\ &\quad + \langle\hat{\zeta}^4(\tau)\hat{H}_{\rm int}(\tau_2)\hat{H}_{\rm int}(\tau_1)\rangle - \langle\hat{H}_{\rm int}(\tau_2)\hat{\zeta}^4(\tau)\hat{H}_{\rm int}(\tau_1)\rangle \\ &= 2\,{\rm Re}\left(\langle\hat{H}_{\rm int}(\tau_1)\hat{H}_{\rm int}(\tau_2)\hat{\zeta}^4(\tau)\rangle\right) \\ &\quad - 2\,{\rm Re}\left(\langle\hat{H}_{\rm int}(\tau_1)\hat{\zeta}^4(\tau)\hat{H}_{\rm int}(\tau_2)\rangle\right) \end{aligned} \tag{5.5.12}$$

where in the second line we used the fact that the Hamiltonians and observable n-point correlators are Hermitian. Within each of these correlators, we now have Wick contractions turning them into all products of five pairs of $\zeta_1\zeta_2^*$. Writing the generic mode functions from the single-field EFT as(cf. equation (5.5.1))

$$\zeta_i(\tau) = f_i(\tau)e^x + ig_i(\tau)e^{-x}, \tag{5.5.13}$$

we see that the terms proportional to e^{10x} in *both* terms will be

$$e^{10x}\prod_i f_i, \tag{5.5.14}$$

and they will hence cancel out after we contract all combinations. Any term proportional to e^{8x} must be imaginary, and hence does not contribute either. Only at e^{6x} do we expect the terms not to cancel out. Another way to see this is to note that a Wick contraction between real mode functions is a symmetric operator. Since the e^{10x} term comes from only the real part of the mode functions, the order of the operators inside the correlator does not matter and the two terms will cancel out.

To make the discussion a bit more precise, the interaction Hamiltonian contains terms of the form [98, 103, 104]

$$\begin{aligned}\hat{H}_{\rm int} &\sim \int d^3x \frac{a\epsilon M_{\rm P}^2}{H}\left(\frac{1}{c_s^2}-1\right)(\partial\hat{\zeta})^3 \sim \int d^3x \frac{-1}{\tau}\frac{\epsilon M_{\rm P}^2}{H^2}\left(\frac{1}{c_s^2}-1\right)(\partial\hat{\zeta})^3 \\ &\sim \int d^3x \frac{-1}{\tau}\alpha^{-2}\left(\frac{1}{c_s^2}-1\right)(\partial\hat{\zeta})^3.\end{aligned}$$

The conservation of ζ on superhorizon scales then implies that the time integrals in equation (5.5.9) peak around the horizon crossing time of the modes. The presence of derivatives does affect the argument so we can neglect them. Therefore, the contribution to $\langle\zeta^4\rangle$ from two insertions of this operator then scales as

$$\left(\frac{1}{c_s^2}-1\right)^2 \alpha^6 e^{6x} \tag{5.5.15}$$

and it follows that $g_{\rm NL}$ will satisfy

$$g_{\rm NL} \sim \frac{\langle\zeta^4\rangle}{\langle\zeta^2\rangle^3} \sim \left(\frac{1}{c_s^2}-1\right)^2 \frac{\alpha^6 e^{6x}}{\alpha^6 e^{6x}} \sim 1. \tag{5.5.16}$$

At $n = 4$, we retain perturbative control as long as

$$g_{\rm NL} \lesssim P_\zeta^{-1}, \tag{5.5.17}$$

which is satisfied with a very good margin for theories with $P_\zeta \sim 10^{-9}$.

5.5.2 The general n-point correlator

To show that the same holds for all higher n-point correlation functions, we need to take a different approach, as the previous one does not generalise easily to higher orders.

As a starting point, we consider the commutator of some (at least cubic) interaction Hamiltonian $\hat{H}_{\rm int}$ with some product of operators $\hat{A}$:

$$\langle[\hat{H}_{\rm int}, \hat{A}]\rangle = \langle\hat{H}_{\rm int}\hat{A}\rangle - \langle\hat{A}\hat{H}_{\rm int}\rangle. \tag{5.5.18}$$

If $\hat{H}_{\rm int}$ contains an odd number of operators, at least one of them must be contracted with some operator(s) in $\hat{A}$. If $\hat{H}_{\rm int}$ contains an even number of operators, the terms with all operators contracted internally will cancel out (see RHS), and hence at least two must be contracted with operators in $\hat{A}$. Therefore, any surviving terms will have contractions between some of the operators in $\hat{H}_{\rm int}$ and some of those in $\hat{A}$.

This has important consequences. As we shall see below, this always gives the imaginary part of the products of the mode functions, and we will show that the only non-zero terms from the expectation of nested commutators involve contractions between terms on the LHS and RHS of each commutator. Every time we do this, we will pick up a factor of the imaginary part of the product of some number of mode functions. Since the imaginary parts of the mode functions scale as αe^{-x}, this limits the size of the connected n-point correlators arising from the cubic scalar exchange vertex.

To see why we get the imaginary part of the product of the mode functions, consider the terms containing contractions of some operators $\hat{\zeta}_{1a}, \hat{\zeta}_{1b}...$ on the left hand side of the commutator with $\hat{\zeta}_{2a}, \hat{\zeta}_{2b}...$ on the right hand side. These operators are either the curvature perturbation or various derivatives of it, but have the same annihilation and creation operators. We thus have

$$\begin{aligned}&\langle\dots[\dots\zeta_{1a}\dots\zeta_{1b}\dots,\dots\zeta_{2b}\dots\zeta_{2a}\dots]\dots\rangle\\ &\propto \zeta_{1a}\zeta^*_{2a}\zeta_{1b}\zeta^*_{2b}\dots - \zeta_{2a}\zeta^*_{1a}\zeta_{2b}\zeta^*_{1b}\dots = 2i\,\mathrm{Im}\left(\zeta_{1a}\zeta^*_{2a}\zeta_{1b}\zeta^*_{2b}\dots\right),\end{aligned}$$

which will give us terms where we pick up an odd number of imaginary parts of the mode functions. It is important to note that these contractions do not depend on the relative positions of the operators $\hat{\zeta}_{2a}, \hat{\zeta}_{2b}...$ on the RHS. It does not matter if commutators inside the RHS shuffle these around or if some other operators inside the commutator are contracted with operators outside of it – it always gives the same

factor. Therefore, terms with Wick contractions across n commutators, whether they are nested or not, are proportional to the product of n factors of imaginary parts of products of mode functions.

The mode functions in the EFT we consider can be written as in equation (5.5.13). Hence, the dominant term in $\mathrm{Im}(\zeta_1 \dots \zeta_n^*)$ does not scale as e^{nx}, as one might naively expect, but instead as

$$\mathrm{Im}(\zeta_1 \dots \zeta_n^*) \propto e^{(n-1)x} e^{-x} = e^{(n-2)x}. \tag{5.5.19}$$

In fact, every time we have a commutator we will see this relative suppression of the expectation value by e^{-2x} compared to the naively expected one, drastically limiting the size of certain diagrams. The reason for this is that when we have nested commutators all non-zero terms will have contractions across each commutator, giving us factors of imaginary parts of products of mode functions. We will argue why this is the case below.

To proceed, we want to consider a nested commutator with operators $\hat{H}_1 \equiv \hat{H}_{\mathrm{int}}(\tau_1)$, $\hat{H}_2 \equiv \hat{H}_{\mathrm{int}}(\tau_2)$ and so forth. We begin by looking at the case with two nested commutators:

$$\langle [\hat{H}_1, [\hat{H}_2, \hat{A}]] \rangle. \tag{5.5.20}$$

As we saw above, non-zero terms must have contractions of operators in $\hat{H}_1$ with operators in $[\hat{H}_2, \hat{A}]$. Expanding the above, we have

$$\langle [\hat{H}_1, [\hat{H}_2, \hat{A}]] \rangle = \langle \hat{H}_1 [\hat{H}_2, \hat{A}] \rangle - \langle [\hat{H}_2, \hat{A}] \hat{H}_1 \rangle. \tag{5.5.21}$$

The crucial point is that terms in $\langle \hat{H}_1 [\hat{H}_2, \hat{A}] \rangle$ or $\langle [\hat{H}_2, \hat{A}] \hat{H}_1 \rangle$ with no operators in $\hat{H}_2$ contracted with any in $\hat{A}$ must necessarily vanish. To see this, we note that for these terms, operators in $\hat{A}$ are contracted either internally or with those in $\hat{H}_1$, and the same goes for $\hat{H}_2$. Terms with all operators contracted internally within $\hat{A}$ vanish due to the commutator, hence at least some operators must be contracted with those in $\hat{H}_1$. But these terms vanish too, because (schematically)

$$\langle \overbrace{H_1 [H_2, A]} \rangle = \langle \overbrace{H_1 H_2 A} \rangle - \langle \overbrace{H_1 A} H_2 \rangle = 0, \tag{5.5.22}$$

as a consequence of no operators in $\hat{A}$ being contracted with any in $\hat{H}_2$. None of the terms above depend on the relative position of $\hat{H}_2$ and $\hat{A}$, and so they cancel out exactly. It is therefore only if some operators in $\hat{H}_2$ are contracted with operators in $\hat{A}$ that these expressions can be non-zero.

We are now free to replace $\hat{A}$ with $[\hat{H}_3, \hat{B}]$, giving

$$\begin{aligned}\langle[\hat{H}_1,[\hat{H}_2,[\hat{H}_3,\hat{B}]]]\rangle = \langle\hat{H}_1\hat{H}_2[\hat{H}_3,\hat{B}]\rangle - \langle\hat{H}_1[\hat{H}_3,\hat{B}]\hat{H}_2\rangle \\ - \langle\hat{H}_2[\hat{H}_3,\hat{B}]\hat{H}_1\rangle + \langle[\hat{H}_3,\hat{B}]\hat{H}_2\hat{H}_1\rangle,\end{aligned} \tag{5.5.23}$$

and again, each term will vanish unless some operators in $\hat{H}_3$ are contracted with some in $\hat{B}$. We can repeat this argument indefinitely, and the result can be summarised as: *In evaluating the expectation of n nested commutators, all non-zero terms will include at least one operator on the LHS of each commutator contracted with operators on the RHS.*

Putting it all together, we therefore see that with $n-2$ insertions of a cubic interaction Hamiltonian $\hat{H}_{\rm int}$, the dominant contribution to the n-point correlator therefore scales as

$$\begin{aligned}\langle[\hat{H}_{\rm int}(\tau_1),\ldots,[\hat{H}_{\rm int}(\tau_{n-2}),\hat{\zeta}^n]\ldots]\rangle &\propto \alpha^{-2(n-2)}\alpha^{4n-6}e^{(4n-6)x}e^{-2(n-2)x} \\ &\propto \alpha^{2n-2}e^{(2n-2)x}\end{aligned}$$

instead of the naive $\alpha^{2n-2}e^{(4n-6)x}$. We then find

$$\frac{\langle\zeta^n\rangle}{\langle\zeta^2\rangle^{n-1}} \sim \frac{\alpha^{2n-2}e^{(2n-2)x}}{\alpha^{2n-2}e^{(2n-2)x}} = 1, \tag{5.5.24}$$

causing no issues with perturbative control.

Do we expect these result hold even when we include loop corrections? Yes, because for every insertion of the cubic interaction Hamiltonian we pick an overall factor of $\alpha e^x = P_\zeta^{1/2} \ll 1$. The more of these we insert (and we need two for every loop correction), the greater the suppression is (prior to integration). There is therefore a priori no reason to expect that loop corrections will change these results.

5.6 Conclusions

In this chapter, we have shown that there exists a completely general rapidly turning attractor solution in two-field inflation. The attractor is not restricted to any particular background geometry or form of the potential, and we have shown how several recently studied non-standard inflationary attractors are in fact examples of this rapid-turn attractor.

Having a large, slowly varying turn rate was sufficient to allow the equations of motion to be solved in generality. Moreover, we showed that these solutions have two out of three elements in the effective mass matrix constrained up to $\mathcal{O}(\epsilon)$ corrections. Only the turn rate and entropic mass remain unconstrained degrees of freedom, which will control the primordial perturbations generated by these theories. The primordial perturbations of these models fall into two classes, one with a reduced speed of sound and one with an imagniary speed of sound. The former has already been studied extensively in the literature, but here we contribute to the understanding of the latter by computing the growth of the power spectrum and showing that the higher-order non-Gaussian correlation functions are well-behaved.

The analysis has been restricted to two fields, but we expect it to generalise to models with more than two fields. Such solutions have been explicitly shown to exist in the context of hyperinflation [41], but a general analysis is rather non-trivial and has yet to be completed.

Chapter 6

Conclusions

In this thesis we have looked at multifield inflation, trying to understand both the observables that these theories generate and the background behaviour of non-slow-roll, slow-turn solutions. In Chapter 2 we looked at multifield inflation with as many as 100 fields in random potentials generated using Gaussian random field techniques, which emulate generic effective field theory potentials. Since the potentials generated this way have well-defined third derivatives, unlike those generated using DBM techniques, we were able to look at non-Gaussianity in random many-field theories, which had never been done before. We found that even though we introduced millions of interaction terms, the behaviour of the resulting inflation models was remarkably simple. The field momenta almost immediately aligned themselves with the (locally) most tachyonic direction of the field space, giving very smooth trajectories that did not change in character as the number of fields was increased. As a result, the power spectra produced were as smooth and simple as in single-inflation, and the local non-Gaussianity was small, even though the superhorizon growth of the power spectrum often was substantial. The rare exceptions to this were however also characterised by surviving isocurvature modes, meaning that the observables may change through reheating.

These results have a clear implication: very complicated many-field slow-roll solutions can produce observables that are almost completely indistinguishable from single-field inflation. While the GRF potentials do not capture all possible types of inflation models (e.g. potentials with sharp features), it is a rather minimalistic prior. The potentials were constructed so as to allow interesting multifield effects to happen on superhorizon scales, as they did, but even though the power spectra evolved on superhorizon scales, they remained very simple, and in all but a very small number of cases, no large local non-Gaussianity was produced. Future LSS experiments hope to be able to determine whether $f_{\rm NL}^{\rm local}$ is smaller or greater than 1. As we have shown

here, if $f_{\rm NL}^{\rm local}$ were constrained to be smaller than 1, an enormous class of multifield models would still be observationally viable, but if it were found to be larger than 1, not only would single-field inflation can be ruled out, but it would also point towards some unusual properties of either the potential or field-space metric. If we find that $f_{\rm NL}^{\rm local} < 1$, attempts at distinguishing between single- and multifield inflation will on the other hand require a study of the complete bispectrum. Computationally, this is more challenging but very much doable. Several codes capable of computing the bispectra of any given inflation model already exist (c.f. [154, 170, 173]), but a more specialised approach may be necessary for potentials as complicated as the GRF potentials.

In Chapter 3 we developed the mathematical machinery necessary for generating the random potentials used in Chapter 2. We proved that for a Gaussian random field with a Gaussian covariance function, if the Taylor coefficients are generated order by order (separately for even and odd derivatives), the covariance matrices in the conditional (marginal) distributions are always diagonal. This almost completely removes the barrier to generating many-dimensional GRFs with this covariance function, which was previously limited by inverting the covariance matrices, the size of which grows super-exponentially with dimension and order in the Taylor series. With this new approach, the covariance matrices can be treated with much more numerically effective methods than before, since they are diagonal. The computational bottleneck now lies in the matrices that are needed to shift the expectation values, but these are generally sparse, and never need to be inverted or decomposed, so this bottleneck is much less restrictive than the previous one.

Beyond generating potentials for large numbers of fields, this method can be used to generate analytic potentials for large landscapes with small numbers of fields, and it can even be applied to Gaussian process regression. These random potentials could also have applications beyond inflation; an obvious use for them would be to study reheating in random vacua, and it is also possible that they would have applications in condensed matter physics. However, as powerful as the technique is, it is also rather niche, and it is unlikely that it will ever see any use in statistical or machine learning applications, although one can never know what the future holds.

The second part of the thesis was concerned with rapid-turn inflation models. In Chapter 4 we studied hyperinflation, trying to obtain a better understanding of this non-slow roll, slow-turn solution. By introducing a new vielbein basis on the target space, based on the gradient of the potential, we were able to understand the solution in a field-space local way, and found that the solution was more general than originially thought. The original solution was derived in a rotationally symmetric potential on the

hyperbolic plane, but this global symmetry is not necessary, and using insights from the vielbein approach we were able to realise hyperinflation in new set-ups. We also studied the primordial perturbations of this theory, and found that even though it can give inflation in very steep potentials, there are complications with the perturbations if the potential is too steep and the field trajectory too short. The steeper the potential is, and the shorter the field trajectory is, the greater the turn rate becomes, and since the power spectrum grows exponentially in the turn rate, this gives an enormous amplification of the power spectrum when the turn rate is large. To give the correct amplitude for the power spectrum when the turn rate is very large ($\omega \gtrsim \mathcal{O}(100)$), the value of the potential energy becomes too small for the universe to be reheated afterwards.

Following on from the work on hyperinflation, in Chapter 5 we showed that there exists a general rapidly turning two-field inflation attractor solution, of which hyperinflation is only a specific example. In the gradient vielbein basis, we were able to show that by looking for a rapidly turning solution with a slowly varying turn rate, the equations of motion can be solved completely without even specifying a target space geometry. The resulting solution gives the field velocity as a function of position in field space, much like slow-roll, slow-turn, and from the general solution we were able to recover several previously known turning solutions in various target space geometries, such as sidetracked inflation, angular inflation, and a flat field space model, highlighting how general the solution is. Up to $\mathcal{O}(\epsilon)$ corrections, the evolution equations for perturbations in rapid-turn inflation only depend on two parameters, and using this we proved the (linear) stability of the general solution. Moreover, we were able to compute an analytic expression for the growth of the power spectrum in imaginary speed of sound theories, which had previously only been computed numerically.

Rapidly turning inflation models are one of the more exciting developments in modern inflationary cosmology. Over the last ten years or so, we have come to realise that slow-roll, slow-turn is not the only type of inflationary cosmology with scalar fields minimally coupled to gravity, and that other solutions can be realised in potentials that one naively thought were too steep for inflation. These rapid-turn solutions have also been shown to arise as global attractors in hyperbolic field spaces, and given that the latter occur frequently in string compactifications and other models for high energy physics, they are very interesting from a phenomenological point of view. The primordial power spectra and non-Gaussianities of these models are becoming increasingly better understood, and they exhibit some very interesting behaviours compared to slow-roll, slow-turn. The transient instability of the mode functions before

horizon crossing gives an exponential amplification of the power spectrum yet still only leads to moderate amounts of non-Gaussianity. Finally, it would also be interesting to see how this solution generalises to the case of more than two fields, when the solution might no longer be planar. This is of particular interest as string compactifications and extensions of the Standard Model frequently feature large numbers of scalar fields.

References

[1] Aazami, A. and Easther, R. (2006). Cosmology from random multifield potentials. *JCAP*, 0603:013.

[2] Achúcarro, A., Kallosh, R., Linde, A., Wang, D.-G., and Welling, Y. (2018). Universality of multi-field α-attractors. *JCAP*, 1804(04):028.

[3] Achúcarro, A. and Palma, G. A. (2018). The string swampland constraints require multi-field inflation.

[4] Achucarro, A., Atal, V., Cespedes, S., Gong, J.-O., Palma, G. A., and Patil, S. P. (2012a). Heavy fields, reduced speeds of sound and decoupling during inflation. *Phys. Rev.*, D86:121301.

[5] Achucarro, A., Atal, V., Germani, C., and Palma, G. A. (2017). Cumulative effects in inflation with ultra-light entropy modes. *JCAP*, 1702(02):013.

[6] Achucarro, A., de Carlos, B., Casas, J. A., and Doplicher, L. (2006). De Sitter vacua from uplifting D-terms in effective supergravities from realistic strings. *JHEP*, 06:014.

[7] Achucarro, A., Gong, J.-O., Hardeman, S., Palma, G. A., and Patil, S. P. (2011a). Features of heavy physics in the CMB power spectrum. *JCAP*, 1101:030.

[8] Achucarro, A., Gong, J.-O., Hardeman, S., Palma, G. A., and Patil, S. P. (2011b). Mass hierarchies and non-decoupling in multi-scalar field dynamics. *Phys. Rev.*, D84:043502.

[9] Achucarro, A., Gong, J.-O., Hardeman, S., Palma, G. A., and Patil, S. P. (2012b). Effective theories of single field inflation when heavy fields matter. *JHEP*, 05:066.

[10] Ade, P. A. R. et al. (2016). Planck 2015 results. XX. Constraints on inflation. *Astron. Astrophys.*, 594:A20.

[11] Agarwal, N., Bean, R., McAllister, L., and Xu, G. (2011). Universality in D-brane Inflation. *JCAP*, 1109:002.

[12] Aghanim, N. et al. (2018). Planck 2018 results. VI. Cosmological parameters.

[13] Agrawal, P., Obied, G., Steinhardt, P. J., and Vafa, C. (2018). On the Cosmological Implications of the String Swampland. *Phys. Lett.*, B784:271–276.

[14] Akrami, Y. et al. (2018a). Planck 2018 results. X. Constraints on inflation.

[15] Akrami, Y. et al. (2019). Planck 2018 results. IX. Constraints on primordial non-Gaussianity.

[16] Akrami, Y., Kallosh, R., Linde, A., and Vardanyan, V. (2018b). The landscape, the swampland and the era of precision cosmology. *Fortsch. Phys.*, 2018:1800075.

[17] Alvarez, M. et al. (2014). Testing Inflation with Large Scale Structure: Connecting Hopes with Reality.

[18] Amendola, L., Gordon, C., Wands, D., and Sasaki, M. (2002). Correlated perturbations from inflation and the cosmic microwave background. *Phys. Rev. Lett.*, 88:211302.

[19] Amin, M. A. and Baumann, D. (2016). From Wires to Cosmology. *JCAP*, 1602(02):045.

[20] Amin, M. A., Garcia, M. A. G., Xie, H.-Y., and Wen, O. (2017). Multifield Stochastic Particle Production: Beyond a Maximum Entropy Ansatz.

[21] Anderson, G. J., Mulryne, D. J., and Seery, D. (2012). Transport equations for the inflationary trispectrum. *JCAP*, 1210:019.

[22] Arkani-Hamed, N., Motl, L., Nicolis, A., and Vafa, C. (2007). The String landscape, black holes and gravity as the weakest force. *JHEP*, 06:060.

[23] Bachlechner, T. C. (2014). On Gaussian Random Supergravity. *JHEP*, 04:054.

[24] Bachlechner, T. C., Eckerle, K., Janssen, O., and Kleban, M. (2017). Systematics of Aligned Axions.

[25] Bachlechner, T. C., Marsh, D., McAllister, L., and Wrase, T. (2013). Supersymmetric Vacua in Random Supergravity. *JHEP*, 01:136.

[26] Baldauf, T., Mirbabayi, M., Simonovic, M., and Zaldarriaga, M. (2016). LSS constraints with controlled theoretical uncertainties.

[27] Bardeen, J. M., Bond, J. R., Kaiser, N., and Szalay, A. S. (1986). The Statistics of Peaks of Gaussian Random Fields. *Astrophys. J.*, 304:15–61.

[28] Bartolo, N., Matarrese, S., and Riotto, A. (2002). Nongaussianity from inflation. *Phys. Rev.*, D65:103505.

[29] Battefeld, D. and Battefeld, T. (2013). A Smooth Landscape: Ending Saddle Point Inflation Requires Features to be Shallow. *JCAP*, 1307:038.

[30] Battefeld, D., Battefeld, T., and Schulz, S. (2012). On the Unlikeliness of Multi-Field Inflation: Bounded Random Potentials and our Vacuum. *JCAP*, 1206:034.

[31] Battefeld, T. and Easther, R. (2007). Non-Gaussianities in Multi-field Inflation. *JCAP*, 0703:020.

[32] Battefeld, T. and Modi, C. (2015). Local random potentials of high differentiability to model the Landscape. *JCAP*, 1503(03):010.

[33] Baumann, D. and McAllister, L. (2015). *Inflation and String Theory*. Cambridge University Press.

[34] Berera, A. (1996). Thermal properties of an inflationary universe. *Phys. Rev.*, D54:2519–2534.

[35] Bernardeau, F. and Uzan, J.-P. (2002). NonGaussianity in multifield inflation. *Phys. Rev.*, D66:103506.

[36] Bernardeau, F. and Uzan, J.-P. (2003). Inflationary models inducing non-Gaussian metric fluctuations. *Phys. Rev.*, D67:121301.

[37] Bjorkmo, T. (2019). Rapid-Turn Inflationary Attractors. *Phys. Rev. Lett.*, 122(25):251301.

[38] Bjorkmo, T., Ferreira, R. Z., and Marsh, M. C. D. (2019). Mild Non-Gaussianities under Perturbative Control from Rapid-Turn Inflation Models. *JCAP*, 1912(12):036.

[39] Bjorkmo, T. and Marsh, M. C. D. (2018a). Local, algebraic simplifications of Gaussian random fields. *JCAP*, 1812(12):022.

[40] Bjorkmo, T. and Marsh, M. C. D. (2018b). Manyfield Inflation in Random Potentials. *JCAP*, 1802(02):037.

[41] Bjorkmo, T. and Marsh, M. C. D. (2019). Hyperinflation generalised: from its attractor mechanism to its tension with the 'swampland conditions'. *JHEP*, 04:172.

[42] Blaback, J., Danielsson, U. H., Dibitetto, G., and Vargas, S. C. (2015). Universal dS vacua in STU-models. *JHEP*, 10:069.

[43] Blanco-Pillado, J. J., Vilenkin, A., and Yamada, M. (2018). Inflation in Random Landscapes with two energy scales. *JHEP*, 02:130.

[44] Bray, A. J. and Dean, D. S. (2007). Statistics of critical points of Gaussian fields on large-dimensional spaces. *Phys. Rev. Lett.*, 98:150201.

[45] Brown, A. R. (2018). Hyperbolic Inflation. *Phys. Rev. Lett.*, 121(25):251601.

[46] Broy, B. J., Galante, M., Roest, D., and Westphal, A. (2015). Pole inflation – Shift symmetry and universal corrections. *JHEP*, 12:149.

[47] Byrnes, C. T. and Choi, K.-Y. (2010). Review of local non-Gaussianity from multi-field inflation. *Adv. Astron.*, 2010:724525.

[48] Byrnes, C. T., Choi, K.-Y., and Hall, L. M. H. (2008). Conditions for large non-Gaussianity in two-field slow-roll inflation. *JCAP*, 0810:008.

[49] Byrnes, C. T., Choi, K.-Y., and Hall, L. M. H. (2009). Large non-Gaussianity from two-component hybrid inflation. *JCAP*, 0902:017.

[50] Byrnes, C. T. and Wands, D. (2006). Curvature and isocurvature perturbations from two-field inflation in a slow-roll expansion. *Phys. Rev.*, D74:043529.

[51] Carrasco, J. J. M., Kallosh, R., and Linde, A. (2015a). Cosmological Attractors and Initial Conditions for Inflation. *Phys. Rev.*, D92(6):063519.

[52] Carrasco, J. J. M., Kallosh, R., Linde, A., and Roest, D. (2015b). Hyperbolic geometry of cosmological attractors. *Phys. Rev.*, D92(4):041301.

[53] Cespedes, S., Atal, V., and Palma, G. A. (2012). On the importance of heavy fields during inflation. *JCAP*, 1205:008.

[54] Chen, X. (2012). Primordial Features as Evidence for Inflation. *JCAP*, 1201:038.

[55] Chen, X., Firouzjahi, H., Namjoo, M. H., and Sasaki, M. (2013). A Single Field Inflation Model with Large Local Non-Gaussianity. *EPL*, 102(5):59001.

[56] Chen, X., Palma, G. A., Riquelme, W., Scheihing Hitschfeld, B., and Sypsas, S. (2018a). Landscape tomography through primordial non-Gaussianity. *Phys. Rev.*, D98(8):083528.

[57] Chen, X., Palma, G. A., Scheihing Hitschfeld, B., and Sypsas, S. (2018b). Reconstructing the Inflationary Landscape with Cosmological Data. *Phys. Rev. Lett.*, 121(16):161302.

[58] Chen, X. and Wang, Y. (2010). Quasi-Single Field Inflation and Non-Gaussianities. *JCAP*, 1004:027.

[59] Christodoulidis, P., Roest, D., and Sfakianakis, E. I. (2018). Angular inflation in multi-field α-attractors.

[60] Christodoulidis, P., Roest, D., and Sfakianakis, E. I. (2019a). Attractors, Bifurcations and Curvature in Multi-field Inflation.

[61] Christodoulidis, P., Roest, D., and Sfakianakis, E. I. (2019b). Scaling attractors in multi-field inflation.

[62] Cicoli, M., De Alwis, S., Maharana, A., Muia, F., and Quevedo, F. (2018). De Sitter vs Quintessence in String Theory. *Fortsch. Phys.*, 2018:1800079.

[63] Cicoli, M., Quevedo, F., and Valandro, R. (2016). De Sitter from T-branes. *JHEP*, 03:141.

[64] Creminelli, P. and Zaldarriaga, M. (2004). Single field consistency relation for the 3-point function. *JCAP*, 0410:006.

[65] Cremonini, S., Lalak, Z., and Turzynski, K. (2011). Strongly Coupled Perturbations in Two-Field Inflationary Models. *JCAP*, 1103:016.

[66] Dalal, N., Dore, O., Huterer, D., and Shirokov, A. (2008). The imprints of primordial non-gaussianities on large-scale structure: scale dependent bias and abundance of virialized objects. *Phys. Rev.*, D77:123514.

[67] Danielsson, U. H. and Van Riet, T. (2018). What if string theory has no de Sitter vacua? *Int. J. Mod. Phys.*, D27(12):1830007.

[68] David Marsh, M. C. (2019). The Swampland, Quintessence and the Vacuum Energy. *Phys. Lett.*, B789:639–642.

[69] de Putter, R., Gleyzes, J., and Doré, O. (2016). The next non-Gaussianity frontier: what can a measurement with $\sigma(f_{\rm NL}) \lesssim 1$ tell us about multifield inflation?

[70] de Salas, P. F., Lattanzi, M., Mangano, G., Miele, G., Pastor, S., and Pisanti, O. (2015). Bounds on very low reheating scenarios after Planck. *Phys. Rev.*, D92(12):123534.

[71] Dean, D. S. and Majumdar, S. N. (2006). Large deviations of extreme eigenvalues of random matrices. *Phys. Rev. Lett.*, 97:160201.

[72] Deift, P. (2006). Universality for mathematical and physical systems. *ArXiv Mathematical Physics e-prints*.

[73] Denef, F., Hebecker, A., and Wrase, T. (2018). de Sitter swampland conjecture and the Higgs potential. *Phys. Rev.*, D98(8):086004.

[74] Desjacques, V. and Seljak, U. (2010). Primordial non-Gaussianity from the large scale structure. *Class. Quant. Grav.*, 27:124011.

[75] Dias, M., Elliston, J., Frazer, J., Mulryne, D., and Seery, D. (2015a). The curvature perturbation at second order. *JCAP*, 1502(02):040.

[76] Dias, M., Frazer, J., and Liddle, A. R. (2012). Multifield consequences for D-brane inflation. *JCAP*, 1206:020. [Erratum: JCAP1303,E01(2013)].

[77] Dias, M., Frazer, J., and Marsh, M. C. D. (2016a). Simple emergent power spectra from complex inflationary physics. *Phys. Rev. Lett.*, 117(14):141303.

[78] Dias, M., Frazer, J., and Marsh, M. C. D. (2018a). Seven Lessons from Manyfield Inflation in Random Potentials. *JCAP*, 1801(01):036.

[79] Dias, M., Frazer, J., Mulryne, D. J., and Seery, D. (2016b). Numerical evaluation of the bispectrum in multiple field inflation – the transport approach with code. *JCAP*, 1612(12):033.

[80] Dias, M., Frazer, J., Retolaza, A., Scalisi, M., and Westphal, A. (2018b). Pole N-flation.

[81] Dias, M., Frazer, J., and Seery, D. (2015b). Computing observables in curved multifield models of inflation — A guide (with code) to the transport method. *JCAP*, 1512(12):030.

[82] Dias, M., Frazer, J., and Seery, D. (2015c). Computing observables in curved multifield models of inflation—A guide (with code) to the transport method. *JCAP*, 1512(12):030.

[83] Dias, M. and Seery, D. (2012). Transport equations for the inflationary spectral index. *Phys. Rev.*, D85:043519.

[84] Dudas, E. and Mambrini, Y. (2006). Moduli stabilization with positive vacuum energy. *JHEP*, 10:044.

[85] Dyson, F. J. (1962). A Brownian-Motion Model for the Eigenvalues of a Random Matrix. *Journal of Mathematical Physics*, 3(Nov.):1191 – 1198.

[86] Easson, D. A., Gregory, R., Mota, D. F., Tasinato, G., and Zavala, I. (2008). Spinflation. *JCAP*, 0802:010.

[87] Easther, R., Frazer, J., Peiris, H. V., and Price, L. C. (2014). Simple predictions from multifield inflationary models. *Phys. Rev. Lett.*, 112:161302.

[88] Easther, R., Guth, A. H., and Masoumi, A. (2016). Counting Vacua in Random Landscapes.

[89] Easther, R. and McAllister, L. (2006). Random matrices and the spectrum of N-flation. *JCAP*, 0605:018.

[90] Erdos, L. (2012). Universality for random matrices and log-gases. *ArXiv e-prints*.

[91] Ferrara, S., Kallosh, R., and Linde, A. (2014). Cosmology with Nilpotent Superfields. *JHEP*, 10:143.

[92] Ferraro, S. and Smith, K. M. (2015). Using large scale structure to measure f_{NL}, g_{NL} and τ_{NL}. *Phys. Rev.*, D91(4):043506.

[93] Ferreira, R. Z., Ganc, J., Noreña, J., and Sloth, M. S. (2016). On the validity of the perturbative description of axions during inflation. *JCAP*, 1604(04):039. [Erratum: JCAP1610,no.10,E01(2016)].

[94] Frazer, J. and Liddle, A. R. (2011). Exploring a string-like landscape. *JCAP*, 1102:026.

[95] Frazer, J. and Liddle, A. R. (2012). Multi-field inflation with random potentials: field dimension, feature scale and non-Gaussianity. *JCAP*, 1202:039.

[96] Freese, K., Frieman, J. A., and Olinto, A. V. (1990). Natural inflation with pseudo - Nambu-Goldstone bosons. *Phys. Rev. Lett.*, 65:3233–3236.

[97] Freivogel, B., Gobbetti, R., Pajer, E., and Yang, I.-S. (2016). Inflation on a Slippery Slope.

[98] Fumagalli, J., Garcia-Saenz, S., Pinol, L., Renaux-Petel, S., and Ronayne, J. (2019). Hyper non-Gaussianities in inflation with strongly non-geodesic motion.

[99] Galante, M., Kallosh, R., Linde, A., and Roest, D. (2015). Unity of Cosmological Inflation Attractors. *Phys. Rev. Lett.*, 114(14):141302.

[100] Gallego, D., Marsh, M. C. D., Vercnocke, B., and Wrase, T. (2017). A New Class of de Sitter Vacua in Type IIB Large Volume Compactifications.

[101] Garcia-Bellido, J., Linde, A. D., and Wands, D. (1996). Density perturbations and black hole formation in hybrid inflation. *Phys. Rev.*, D54:6040–6058.

[102] Garcia-Bellido, J. and Wands, D. (1996). Metric perturbations in two field inflation. *Phys. Rev.*, D53:5437–5445.

[103] Garcia-Saenz, S., Pinol, L., and Renaux-Petel, S. (2019). Revisiting non-Gaussianity in multifield inflation with curved field space.

[104] Garcia-Saenz, S. and Renaux-Petel, S. (2018). Flattened non-Gaussianities from the effective field theory of inflation with imaginary speed of sound. *JCAP*, 1811(11):005.

[105] Garcia-Saenz, S., Renaux-Petel, S., and Ronayne, J. (2018). Primordial fluctuations and non-Gaussianities in sidetracked inflation. *JCAP*, 1807(07):057.

[106] Garg, S. K. and Krishnan, C. (2018). Bounds on Slow Roll and the de Sitter Swampland.

[107] Gordon, C., Wands, D., Bassett, B. A., and Maartens, R. (2001). Adiabatic and entropy perturbations from inflation. *Phys. Rev.*, D63:023506.

[108] Green, D. (2015). Disorder in the Early Universe. *JCAP*, 1503(03):020.

[109] Grocholski, O., Kalinowski, M., Kolanowski, M., Renaux-Petel, S., Turzyński, K., and Vennin, V. (2019). On backreaction effects in geometrical destabilisation of inflation.

[110] Groot Nibbelink, S. and van Tent, B. J. W. (2002). Scalar perturbations during multiple field slow-roll inflation. *Class. Quant. Grav.*, 19:613–640.

[111] He, Y.-H., Jejjala, V., Pontiggia, L., Xiao, Y., and Zhou, D. (2017). Flatness of Minima in Random Inflationary Landscapes.

[112] Hetz, A. and Palma, G. A. (2016). Sound Speed of Primordial Fluctuations in Supergravity Inflation. *Phys. Rev. Lett.*, 117(10):101301.

[113] Kachru, S., Kallosh, R., Linde, A. D., and Trivedi, S. P. (2003). De Sitter vacua in string theory. *Phys. Rev.*, D68:046005.

[114] Kaiser, D. I. and Sfakianakis, E. I. (2014). Multifield Inflation after Planck: The Case for Nonminimal Couplings. *Phys. Rev. Lett.*, 112(1):011302.

[115] Kallosh, R. and Linde, A. (2013a). Multi-field Conformal Cosmological Attractors. *JCAP*, 1312:006.

[116] Kallosh, R. and Linde, A. (2013b). Universality Class in Conformal Inflation. *JCAP*, 1307:002.

[117] Kallosh, R. and Linde, A. (2016). Cosmological Attractors and Asymptotic Freedom of the Inflaton Field. *JCAP*, 1606(06):047.

[118] Kallosh, R., Linde, A., and Roest, D. (2013). Superconformal Inflationary α-Attractors. *JHEP*, 11:198.

[119] Kallosh, R., Linde, A., and Roest, D. (2014). Large field inflation and double α-attractors. *JHEP*, 08:052.

[120] Kallosh, R., Linde, A., Roest, D., Westphal, A., and Yamada, Y. (2018). Fibre Inflation and α-attractors. *JHEP*, 02:117.

[121] Kallosh, R., Linde, A., Roest, D., and Wrase, T. (2016). Sneutrino inflation with α-attractors. *JCAP*, 1611:046.

[122] Karananas, G. K. and Rubio, J. (2016). On the geometrical interpretation of scale-invariant models of inflation. *Phys. Lett.*, B761:223–228.

[123] Kinney, W. H., Vagnozzi, S., and Visinelli, L. (2018). The Zoo Plot Meets the Swampland: Mutual (In)Consistency of Single-Field Inflation, String Conjectures, and Cosmological Data.

[124] Kuijlaars, A. B. J. (2011). Universality. *The Oxford Handbook on Random Matrix Theory, (G. Akemann, J. Baik, and P. Di Francesco, eds.), Oxford University Press*, pages 103–134.

[125] Linde, A. (2015). Single-field α-attractors. *JCAP*, 1505:003.

[126] Linde, A. (2017). Random Potentials and Cosmological Attractors. *JCAP*, 1702(02):028.

[127] Linde, A., Wang, D.-G., Welling, Y., Yamada, Y., and Achúcarro, A. (2018). Hypernatural inflation. *JCAP*, 1807(07):035.

[128] Linde, A. D. (1994). Hybrid inflation. *Phys. Rev.*, D49:748–754.

[129] Linde, A. D. and Mukhanov, V. F. (1997). Nongaussian isocurvature perturbations from inflation. *Phys. Rev.*, D56:R535–R539.

[130] Liu, J. (2017). Artificial Neural Network in Cosmic Landscape.

[131] Liu, J., Wang, Y., and Zhou, S. (2015). Nonuniqueness of classical inflationary trajectories on a high-dimensional landscape. *Phys. Rev.*, D91(10):103525.

[132] Lyth, D. H. (1985). Large Scale Energy Density Perturbations and Inflation. *Phys. Rev.*, D31:1792–1798.

[133] Lyth, D. H. (1997). What would we learn by detecting a gravitational wave signal in the cosmic microwave background anisotropy? *Phys. Rev. Lett.*, 78:1861–1863.

[134] Lyth, D. H. and Riotto, A. (1999). Particle physics models of inflation and the cosmological density perturbation. *Phys. Rept.*, 314:1–146.

[135] Lyth, D. H. and Rodriguez, Y. (2005a). The Inflationary prediction for primordial non-Gaussianity. *Phys. Rev. Lett.*, 95:121302.

[136] Lyth, D. H. and Rodriguez, Y. (2005b). The Inflationary prediction for primordial non-Gaussianity. *Phys. Rev. Lett.*, 95:121302.

[137] Lyth, D. H., Ungarelli, C., and Wands, D. (2003). Primordial density perturbation in the curvaton scenario. *Phys. Rev. D*, 67:023503.

[138] Lyth, D. H. and Wands, D. (2002). Generating the curvature perturbation without an inflaton. *Phys. Lett.*, B524:5–14.

[139] Maldacena, J. M. (2003). Non-Gaussian features of primordial fluctuations in single field inflationary models. *JHEP*, 05:013.

[140] March-Russell, J. and Riva, F. (2006). Signals of Inflation in a Friendly String Landscape. *JHEP*, 07:033.

[141] Marsh, D., McAllister, L., and Wrase, T. (2012). The Wasteland of Random Supergravities. *JHEP*, 03:102.

[142] Marsh, M. C. D., McAllister, L., Pajer, E., and Wrase, T. (2013). Charting an Inflationary Landscape with Random Matrix Theory. *JCAP*, 1311:040.

[143] Marsh, M. C. D., Vercnocke, B., and Wrase, T. (2015). Decoupling and de Sitter Vacua in Approximate No-Scale Supergravities. *JHEP*, 05:081.

[144] Masoumi, A., Vilenkin, A., and Yamada, M. (2017a). Inflation in multi-field random Gaussian landscapes.

[145] Masoumi, A., Vilenkin, A., and Yamada, M. (2017b). Inflation in random Gaussian landscapes. *JCAP*, 1705(05):053.

[146] Matarrese, S. and Verde, L. (2008). The effect of primordial non-Gaussianity on halo bias. *Astrophys. J.*, 677:L77–L80.

[147] McAllister, L., Renaux-Petel, S., and Xu, G. (2012). A Statistical Approach to Multifield Inflation: Many-field Perturbations Beyond Slow Roll. *JCAP*, 1210:046.

[148] Meerburg, P. D. et al. (2019). Primordial Non-Gaussianity.

[149] Mizuno, S. and Mukohyama, S. (2017). Primordial perturbations from inflation with a hyperbolic field-space. *Phys. Rev.*, D96(10):103533.

[150] Mooij, S. and Palma, G. A. (2015). Consistently violating the non-Gaussian consistency relation. *JCAP*, 1511(11):025.

[151] Moroi, T. and Takahashi, T. (2002). Cosmic density perturbations from late decaying scalar condensations. *Phys. Rev.*, D66:063501.

[152] Mulryne, D., Seery, D., and Wesley, D. (2009). Non-Gaussianity constrains hybrid inflation.

[153] Mulryne, D. J. (2013). Transporting non-Gaussianity from sub to super-horizon scales. *JCAP*, 1309:010.

[154] Mulryne, D. J. and Ronayne, J. W. (2016). PyTransport: A Python package for the calculation of inflationary correlation functions.

[155] Mulryne, D. J., Seery, D., and Wesley, D. (2010). Moment transport equations for non-Gaussianity. *JCAP*, 1001:024.

[156] Obied, G., Ooguri, H., Spodyneiko, L., and Vafa, C. (2018). De Sitter Space and the Swampland.

[157] Ooguri, H., Palti, E., Shiu, G., and Vafa, C. (2019). Distance and de Sitter Conjectures on the Swampland. *Phys. Lett.*, B788:180–184.

[158] Pedro, F. G. and Westphal, A. (2014). The Scale of Inflation in the Landscape. *Phys. Lett.*, B739:439–444.

[159] Pedro, F. G. and Westphal, A. (2017). Inflation with a graceful exit in a random landscape. *JHEP*, 03:163.

[160] Peterson, C. M. and Tegmark, M. (2011a). Non-Gaussianity in Two-Field Inflation. *Phys. Rev.*, D84:023520.

[161] Peterson, C. M. and Tegmark, M. (2011b). Testing Two-Field Inflation. *Phys. Rev.*, D83:023522.

[162] Peterson, C. M. and Tegmark, M. (2013). Testing multifield inflation: A geometric approach. *Phys. Rev.*, D87(10):103507.

[163] Pourtsidou, A. (2016). Synergistic tests of inflation.

[164] Price, L. C., Peiris, H. V., Frazer, J., and Easther, R. (2016). Designing and testing inflationary models with Bayesian networks. *JCAP*, 1602(02):049.

[165] Renaux-Petel, S. and Turzynski, K. (2016). Geometrical Destabilization of Inflation. *Phys. Rev. Lett.*, 117(14):141301.

[166] Renaux-Petel, S., Turzynski, K., and Vennin, V. (2017). Geometrical destabilization, premature end of inflation and Bayesian model selection.

[167] Rigopoulos, G. I., Shellard, E. P. S., and van Tent, B. J. W. (2006). Large non-Gaussianity in multiple-field inflation. *Phys. Rev.*, D73:083522.

[168] Rigopoulos, G. I., Shellard, E. P. S., and van Tent, B. J. W. (2007). Quantitative bispectra from multifield inflation. *Phys. Rev.*, D76:083512.

[169] Roest, D. and Scalisi, M. (2015). Cosmological attractors from α-scale supergravity. *Phys. Rev.*, D92:043525.

[170] Ronayne, J. W. and Mulryne, D. J. (2017). Numerically evaluating the bispectrum in curved field-space - with PyTransport 2.0.

[171] Rummel, M. and Sumitomo, Y. (2015). De Sitter Vacua from a D-term Generated Racetrack Uplift. *JHEP*, 01:015.

[172] Sasaki, M. and Stewart, E. D. (1996). A General analytic formula for the spectral index of the density perturbations produced during inflation. *Prog. Theor. Phys.*, 95:71–78.

[173] Seery, D. (2016). CppTransport: a platform to automate calculation of inflationary correlation functions.

[174] Seery, D., Mulryne, D. J., Frazer, J., and Ribeiro, R. H. (2012). Inflationary perturbation theory is geometrical optics in phase space. *JCAP*, 1209:010.

[175] Senatore, L. and Zaldarriaga, M. (2012). The Effective Field Theory of Multifield Inflation. *JHEP*, 04:024.

[176] Slosar, A., Hirata, C., Seljak, U., Ho, S., and Padmanabhan, N. (2008). Constraints on local primordial non-Gaussianity from large scale structure. *JCAP*, 0808:031.

[177] Starobinsky, A. A. (1985). Multicomponent de Sitter (Inflationary) Stages and the Generation of Perturbations. *JETP Lett.*, 42:152–155. [Pisma Zh. Eksp. Teor. Fiz.42,124(1985)].

[178] Tanaka, T., Suyama, T., and Yokoyama, S. (2010). Use of delta N formalism - Difficulties in generating large local-type non-Gaussianity during inflation -. *Class. Quant. Grav.*, 27:124003.

[179] Tegmark, M. (2005). What does inflation really predict? *JCAP*, 0504:001.

[180] Tye, S. H. H. and Xu, J. (2010). A Meandering Inflaton. *Phys. Lett.*, B683:326–330.

[181] Tye, S. H. H., Xu, J., and Zhang, Y. (2009). Multi-field Inflation with a Random Potential. *JCAP*, 0904:018.

[182] Uhlenbeck, G. and Ornstein, L. (1930). On the Theory of the Brownian Motion. *Phys.Rev.*, 36:823 – 841.

[183] Vernizzi, F. and Wands, D. (2006). Non-gaussianities in two-field inflation. *JCAP*, 0605:019.

[184] Wands, D., Bartolo, N., Matarrese, S., and Riotto, A. (2002). An Observational test of two-field inflation. *Phys. Rev.*, D66:043520.

[185] Wands, D., Malik, K. A., Lyth, D. H., and Liddle, A. R. (2000). A New approach to the evolution of cosmological perturbations on large scales. *Phys. Rev.*, D62:043527.

[186] Wang, G. and Battefeld, T. (2016). Random Functions via Dyson Brownian Motion: Progress and Problems. *JCAP*, 1609(09):008.

[187] Wang, T. (2010). Note on Non-Gaussianities in Two-field Inflation. *Phys. Rev.*, D82:123515.

[188] Westphal, A. (2007). de Sitter string vacua from Kahler uplifting. *JHEP*, 03:102.

[189] Wigner, E. P. (1951). On the statistical distribution of the widths and spacings of nuclear resonance levels. *Mathematical Proceedings of the Cambridge Philosophical Society*, 47(04):790 – 798.

Appendix A

Extra material for Chapter 2

A.1 Numerical method

Background evolution

Equation (2.2.47) comprises a set of $N_{\rm f}$ coupled, non-linear first-order ordinary differential equations, and its general solution is not known. For large $N_{\rm f}$, solving it numerically can also be challenging: the right hand side may involve many of millions of terms encoding the various interactions between the fields. We now discuss our method for evolving the fields.

To solve equation (2.2.47), we approximate the full potential in very small regions around the trajectory to quadratic order, and solve the evolution of the background in a step-by-step manner with a multiderivative method. More precisely, for some small e-fold step ΔN, we write the solution as

$$\Delta\phi_a(\Delta N) = \Delta\phi_a^{(1)}\Delta N + \frac{1}{2}\Delta\phi_a^{(2)}\Delta N^2 + \mathcal{O}(\Delta N^3)\,. \tag{A.1.1}$$

Substituting this Ansatz into the slow-roll equations and matching order-by-order in ΔN, we find

$$\Delta\phi_a^{(1)} = -\frac{V_a}{V}\,, \tag{A.1.2}$$

$$\Delta\phi_a^{(2)} = \frac{V_{ab}V_b}{V^2} - \frac{V_aV_bV_b}{V^3}\,. \tag{A.1.3}$$

When implementing this solution, it is important to make sure that the second order term in the solution is much smaller than the first-order term; otherwise the series is not a good approximation to the solution. The number of small patches needed

depends on the individual realisation, and on hyperparameters such as the initial spectrum, and the number of fields. For 50 fields, we typically find that breaking up the inflationary trajectory to around 2000 small patches suffices to keep the step-size small enough for this method to be numerically accurate.

When working with potentials with many millions of interaction terms, finding the local values of the Taylor coefficients in each patch can be come computationally intensive. To ameliorate this problem, we approximate the fifth order Taylor expanded potential in moderately small regions by lower order Taylor series involving fewer terms. For 50 fields, we may approximate the potential to fourth order in around 60 such moderately small regions for each inflationary realisation. We then use this lower order potential to compute the second order Taylor coefficients in the very small local patches used in the solution of equation (2.2.47). We note however that the calculations of non-Gaussianity are very sensitive to numerical errors, so care is needed to ensure that the computation is sufficiently accurate.

Perturbations

As first pointed out in [77, 78], the transport method is easily implemented in a patch-by-patch manner. The propagator $\Gamma^a{}_b$ transports the perturbation between spatially flat hypersurfaces and satisfies the chain rule

$$\Gamma^a{}_b(N_3, N_1) = \Gamma^a{}_c(N_3, N_2)\Gamma^c{}_b(N_2, N_1)\,. \tag{A.1.4}$$

In a sufficiently small patch, say $N_2 - N_1 = \Delta N \ll 1$ the propagator (2.2.53) simplifies to

$$\Gamma^a{}_b(N_2, N_1) = \exp\left(\Delta N\, u^a{}_b\right)\,, \tag{A.1.5}$$

where $u^a{}_b = u^a{}_b(N_1 + \Delta N/2) \approx u^a{}_b(N_1) \approx u^a{}_b(N_2)$. The full propagator from horizon crossing to the end of inflation is then obtained by left-multiplication of all subsequent propagators [77, 78], i.e.

$$\Gamma^a{}_b(N_{\rm end}, N^\star) = \Gamma^a{}_{c_p}(N_{\rm end}, N_p)\,\Gamma^{c_p}{}_{c_{p-1}}(N_p, N_{p-1})\ldots\Gamma^{c_2}{}_{c_1}(N_2, N_1)\,\Gamma^{c_1}{}_b(N_1, N^\star)\,. \tag{A.1.6}$$

Similarly, Γ_{abc} can be simplified by splitting up the integral (2.2.54) into many parts,

$$\Gamma^{d}{}_{ef}(N_{i+1}, N_i) = \int_{N^i}^{N^{i+1}} dN' \Gamma^{d}{}_{\mu}(N_{i+1}, N') u^{\mu}{}_{\nu\rho}(N') \Gamma^{\nu}{}_{e}(N', N_i) \Gamma^{\rho}{}_{f}(N', N_i)\,, \quad \text{(A.1.7)}$$

$$\Gamma^{a}{}_{bc}(N, N^\star) = \sum_{i=0}^{p} \Gamma^{a}{}_{d}(N, N_{i+1}) \Gamma^{d}{}_{ef}(N_{i+1}, N_i) \Gamma^{e}{}_{b}(N_i, N^\star) \Gamma^{f}{}_{c}(N_i, N^\star)\,, \quad \text{(A.1.8)}$$

where $N_0 = N^\star$ and $N_{p+1} = N$. Assuming the step size is sufficiently small, we can with good accuracy evaluate $\Gamma_{def}(N_{i+1}, N_i)$ as

$$\Gamma^{d}{}_{ef}(N_{i+1}, N_i) \simeq \int_{N^i}^{N^{i+1}} dN'\, e^{\left[(N^{i+1}-N')u^{d}{}_{\mu}\right]}\, u^{\mu}{}_{\nu\rho}(N')\, e^{\left[(N'-N^{i})u^{\nu}{}_{e}\right]}\, e^{\left[(N'-N^{i})u^{\rho}{}_{f}\right]}\,, \quad \text{(A.1.9)}$$

which is easily evaluated numerically. Once the $\Gamma^{a}{}_{b}(N_{i+1}, N_i)$ and $\Gamma^{d}{}_{ef}(N_{i+1}, N_i)$ have been calculated for all steps, they can be used to calculate power spectrum and $f_{\rm NL}$ modes crossing the horizon at any point during inflation. Moreover, by doing the gauge transformation to a constant energy density surface (cf. equations (2.2.56), and (2.2.57)) at any point during inflation, we can follow the evolution of the power spectrum and $f_{\rm NL}$ on superhorizon scales.

A.2 Ensembles of models

For each of the initial conditions below we ran 2,000 simulations, giving us more than 1,000 successful inflation models ($N \geq 60$) for all ICs except near certain fringes of the parameter space (e.g. very small $\Lambda_{\rm h}$ or large $\epsilon_{\rm i}$). The analysis of the perturbations was only done for the models which gave at least 60 e-folds of inflation.

Varying $N_{\rm f}$

$\Lambda_{\rm h}$	Mass spectrum	Gradient direction	$\epsilon_{\rm i}$	$\eta_{\rm i}$	$N_{\rm f}$
0.4	Uniform	Random	$2 \cdot 10^{-9}$	-10^{-4}	5, 10, 15, 20, 25, 30, 35, 40, 45, 50
0.4	Compressed	Random	$1 \cdot 10^{-10}$	-10^{-4}	5, 10, 15, 20, 25
0.4	Uniform	Aligned	$5 \cdot 10^{-10}$	-10^{-4}	5, 10, 15, 20, 25, 30
0.4	Uniform, uplifted	Random	$2 \cdot 10^{-9}$	-10^{-4}	5, 10, 15, 20, 25
0.4	Compressed, uplifted	Random	$1 \cdot 10^{-10}$	-10^{-4}	5, 10, 15, 20

Varying Λ_h

N_f	Mass spectrum	Gradient direction	ϵ_i	η_i	Λ_h
10	Uniform	Random	$2 \cdot 10^{-9}$	-10^{-4}	0.1, 0.2, 0.3, 0.4, 0.5, 0.6, 0.7, 0.8, 0.9, 1.0
10	Compressed	Random	$1 \cdot 10^{-10}$	-10^{-4}	0.1, 0.2, 0.3, 0.4, 0.5, 0.6, 0.7, 0.8, 0.9, 1.0
10	Uniform	Aligned	$5 \cdot 10^{-10}$	-10^{-4}	0.1, 0.2, 0.3, 0.4, 0.5, 0.6, 0.7, 0.8, 0.9, 1.0

50-field runs

N_f	Λ_h	Mass spectrum	Gradient direction	ϵ_i	η_i
50	0.4	Uniform	Random	$2 \cdot 10^{-9}$	-10^{-4}
50	0.4	Compressed	Random	$2 \cdot 10^{-11}$	-10^{-4}
50	0.4	Uniform	Aligned	$1 \cdot 10^{-10}$	-10^{-4}

Varying ϵ_i

N_f	Λ_h	Mass spectrum	Gradient direction	η_i	ϵ_i
10	0.4	Uniform	Random	-10^{-4}	$2 \cdot 10^{-10}$, $5 \cdot 10^{-10}$, $1 \cdot 10^{-9}$, $2 \cdot 10^{-9}$, $5 \cdot 10^{-9}$, $1 \cdot 10^{-8}$, $2 \cdot 10^{-8}$
10	0.4	Compressed	Random	-10^{-4}	$1 \cdot 10^{-11}$, $2 \cdot 10^{-11}$, $5 \cdot 10^{-11}$, $1 \cdot 10^{-10}$, $2 \cdot 10^{-10}$, $5 \cdot 10^{-10}$, $1 \cdot 10^{-9}$

Varying η_i

N_f	Λ_h	Mass spectrum	Gradient direction	ϵ_i	η_i
10	0.4	Uniform	Random	$2 \cdot 10^{-9}$	-10^{-4}, -10^{-3}, -10^{-2},$-5 \cdot 10^{-2}$, -10^{-1}
10	0.4	Compressed	Random	$2 \cdot 10^{-11}$	-10^{-4}, -10^{-3}, -10^{-2},$-5 \cdot 10^{-2}$, -10^{-1}

A.3 A single-field toy model

We have seen in section 2.3.3 that the observational predictions of manyfield models of inflation coincide with some of the 'generic predictions' of single-field slow-roll inflation:

an approximately scale-invariant power spectrum over observable scales, with a small running of the spectral index. While we have also seen in section 2.3.4 that multifield are typically important in the full manyfield models, it is interesting to investigate the extent to which our results can be understood through simpler single-field models. Such models may capture the most important aspects of the more complicated manyfield models, but are simple enough to admit an analytic treatment. In this section, we construct such simple class of single-field models, and discuss how its predictions compare against our numerical simulations of the full manyfield models.

We expand the single-field potential to cubic order around the approximate critical point at $\phi = 0$,

$$V(\phi) = V_0 \left(1 - c_1\phi - \frac{c_3}{3!}\phi^3\right) . \tag{A.3.1}$$

where the c_i all are positive. We have here set the second order term at $\phi = 0$ to zero, since, as we will justify below, this term is overwhelmed by the third order term already for small field displacements. We furthermore assume that the potential remain approximately constant during inflation, $V \approx V_0$, which simplifies the analytic expressions for the slow-roll parameters in this model:

$$\epsilon_V \simeq M_{\rm P}^2 \frac{(c_1 + c_3\phi^2/2)^2}{2} , \qquad \eta_V \simeq -M_{\rm P}^2 c_3 \phi . \tag{A.3.2}$$

We will now use this model to compute the expected total number of e-folds generated during inflation and the predictions for the spectral index and its running. We first note that inflation ends when $\epsilon_V \approx -\dot{H}/H^2 = 1$, which happens when the value of the field is

$$\phi^{\rm end} \equiv \frac{2^{3/4}}{\sqrt{(c_3 M_{\rm P})}} . \tag{A.3.3}$$

The number of e-folds generated as the field travel from $\phi = 0$ to some value ϕ is given by,

$$N(\phi) = \int_0^\phi \frac{d\phi'}{M_{\rm P}\sqrt{2\epsilon_V}} = \frac{\tan^{-1}(\sqrt{c_3/2c_1}\phi)}{M_{\rm P}^2\sqrt{c_1 c_3/2}} . \tag{A.3.4}$$

Upon evaluating equation (A.3.4) for $\phi = \phi^{\rm end}$, we see that the argument of the inverse tangent function becomes very large so that $\tan^{-1}(\sqrt{c_3/2c_1}\phi^{\rm end}) \approx \pi/2$, and the total number of e-folds is approximately given by

$$N^{\rm end} \approx N^{\rm max} \equiv \frac{\pi}{M_{\rm P}^2\sqrt{2c_1 c_3}} . \tag{A.3.5}$$

Inflation ends before N becomes exactly $N^{\max}$, but for the initial conditions we are interested in, it is a good approximation.

We can of course also invert equation (A.3.4) to give ϕ as a function of N:

$$\phi(N) = \sqrt{\frac{2c_1}{c_3}} \tan\left(\frac{\pi N}{2N^{\max}}\right), \tag{A.3.6}$$

which is valid for $N \leq N^{\rm end} < N^{\max}$. Using equation (A.3.6), it is straightforward to compute the spectral index and its running analytically for this toy model. For the models we are interested in, $|\eta_V| \gg \epsilon_V$, and the spectral index is given by

$$n_s - 1 = 2\eta_V - 6\epsilon_V \simeq -2M_{\rm P}^2 c_3 \phi_\star = -\frac{2\pi}{N^{\max}} \cot\left(\frac{\pi \Delta N}{2N^{\max}}\right), \tag{A.3.7}$$

where we defined $\Delta N = N^{\max} - N_\star$ (in our multifield simulations, we take $\Delta N = 55$). For $N^{\max} \geq \Delta N$, the spectrum is red and n_s has the limit $1 - 4/\Delta N$ as $N^{\max} \to \infty$, and it is easy to see that this is a lower bound. Using $\mathrm{d}\ln k \simeq \mathrm{d}N_\star$, we find that the running is given by

$$\alpha_s = \frac{dn_s}{dN_\star} = -\left(\frac{\pi}{N^{\max}}\right)^2 \csc^2\left(\frac{\pi \Delta N}{2N^{\max}}\right), \tag{A.3.8}$$

which is manifestly negative and has the limit $-4/\Delta N^2$ as $N^{\max} \to \infty$, which is an upper limit.

We are now interested in comparing this class of single-field models to the full multifield models with potential (2.2.7). To do so, we identify $V_0 = \Lambda_{\rm v}^4$ and $c_1 = \sqrt{2\epsilon_{\rm i}} M_{\rm P}^{-1}$. A non-vanshing second-order term could be identified with $c_2 = |\eta_{\rm i}| M_{\rm P}^{-2}$. The coefficient c_3 then corresponds to a randomly generated third-order derivative, which, as we will detail below, we take to be of $\mathcal{O}(\Lambda_{\rm h}^{-3})$. Already for small field displacements, $\Delta\phi/\Lambda_{\rm h} \gtrsim |\eta_{\rm i}|(\Lambda_{\rm h}/M_{\rm P})^2$, the third derivative comes to dominate over the second order term. This justifies dropping the second order term from the potential. To see roughly how $N^{\rm end}$ scales with the various parameters, we fix c_3 to

$$c_3 = \frac{\sqrt{\sum_a \langle V_{a11}^2 \rangle}}{\Lambda_{\rm v}^4} \approx \sqrt{2N_{\rm f}} \frac{1}{\Lambda_{\rm h}^3}, \tag{A.3.9}$$

where we have denoted the initial gradient direction by '1'.[1] Since we are using the RMS value of the third order coefficients in the multifield model to fix c_3, we expect that predictions made from the single-field model may capture the mean values of $N^{\rm end}$ (up to some $\mathcal{O}(1)$ coefficient), which in turn tells us how the mean values of n_s and α_s will scale.[2]

Plugging our expressions for c_1 and c_3 into equation (A.3.4), we see that the total number of e-folds of the single field model is is given by

$$N^{\rm end} \approx \frac{\pi}{2}\frac{1}{(N_{\rm f}\epsilon_{\rm i})^{1/4}}\left(\frac{\Lambda_{\rm h}}{M_{\rm P}}\right)^{3/2} . \tag{A.3.10}$$

By comparing equation (A.3.10) to the results of the numerical simulations plotted in Figure 2.5, we see that the scaling of $N^{\rm end}$ with $\Lambda_{\rm h}$, $N_{\rm f}$ and $\epsilon_{\rm i}$ are not followed very closely. However, in the more special cases when we start with the gradient aligned with the smallest eigenvalue or when we use the compressed spectrum, these scalings are reasonably accurate (but the $\mathcal{O}(1)$ coefficient is incorrect).

Figure 2.9 shows the single-field prediction of equation (A.3.7) together with the numerical simulations from the full GRF models. Qualitatively, the single-field model is in good agreement, and captures both the decrease of n_s for $N^{\rm end}$ not too large, and its asymptotical constancy for $N^{\rm end} \gg 60$. However, the precise predictions for n_s are inaccurate. The single-field limit for α_s is quite close to value we observe for the multi-field models. For $\Delta N = 55$, the value is $\alpha_s = -0.00132$, which agrees with the baseline model prediction, $\alpha_s = -0.00143 \pm 0.00034$.

Altogether, we see that the single-field toy model captures several of the qualitative features of the multifield models, but does not produce quantitatively accurate predictions. This is not surprising, since the single-field model neither takes into account turns of the trajectory nor the superhorizon evolution of the power spectra. To make accurate predictions, the full multifield treatment is needed.

[1] The approximation comes from taking the contribution from $a = 1$, $\langle (V^i_{111})^2\rangle = 6\Lambda_{\rm v}^8\Lambda_{\rm v}^{-6}$, to be the same as for $a \neq 1$, $\langle (V^i_{a11})^2\rangle = 2\Lambda_{\rm v}^8\Lambda_{\rm v}^{-6}$. Note that since V_a is already fixed to be very small, the (conditional) mean of V_{abc} is zero to a very good approximation.

[2] Of course, to find the mean values of all these quantities, one should write them as funtions of the V_{a11} and integrate over the PDF. Since our single-field model makes several approximations, however, there is no need to work with such precision (but we did check that for $N^{\rm end}$ the answer is very close).

A.4 The DBM construction of random manyfield potentials

In this subsection, we briefly review the construction of random scalar field potentials using non-equilibrium random matrix theory, and we discuss the most relevant properties and predictions of these models.

A key motivation for the construction of [142] is that inflation is only sensitive to the scalar potential in the vicinity of the field trajectory, while being independent of its properties elsewhere in field space. One may take advantage of this fact by generating the scalar potential only along the dynamically determined field trajectory by gluing together nearby patches in which the potential is locally defined up to some fixed, low order. This method avoids the steep computational cost that limited early studies of multifield inflation in GRF potentials to only involving a few fields, with structure only over super-Planckian field-space distances [95].

The starting point of the 'DBM construction' is the scalar potential defined up to quadratic order around the point p_0,

$$V = (\Lambda_{\rm v}^{\rm DBM})^4 \sqrt{N_{\rm f}} \left(v_0 + v_a \frac{\phi^a}{\Lambda_{\rm h}^{\rm DBM}} + \frac{1}{2} v_{ab} \frac{\phi^a}{\Lambda_{\rm h}^{\rm DBM}} \frac{\phi^b}{\Lambda_{\rm h}^{\rm DBM}} \right) . \tag{A.4.1}$$

Here, $\Lambda_{\rm v}^{\rm DBM}$ sets the vertical scale of the potential, the convention for the prefactor $\sqrt{N_{\rm f}}$ is explained in [78, 142], and $\Lambda_{\rm h}^{\rm DBM}$ sets the horizontal scale of the potential (we will shortly return to the interpretation of this parameter). At a nearby point in field space, say p_1 separated from p_0 by $\delta\phi^a$, the potential admits a local Taylor expansion in which the coefficients v_0, v_a, and v_{ab} only differ from those at p_0 by a small amount:

$$\begin{aligned} v_0\Big|_{p_1} &= v_0\Big|_{p_0} + v_a\Big|_{p_0} \frac{\delta\phi^a}{\Lambda_{\rm h}^{\rm DBM}} , \qquad v_a\Big|_{p_1} = v_a\Big|_{p_0} + v_{ab}\Big|_{p_0} \frac{\delta\phi^b}{\Lambda_{\rm h}^{\rm DBM}} , \\ v_{ab}\Big|_{p_1} &= v_{ab}\Big|_{p_0} + \delta v_{ab}\Big|_{p_0 \to p_1} . \end{aligned} \tag{A.4.2}$$

Here δv_{ab} captures the effects of cubic (and higher-order) terms on the second derivatives of the potential. Clearly, by stipulating the rules for how δv_{ab} is generated, any potential may be locally generated in this fashion. In a given small patch, the slow-roll equations for the background and the evolution equations for the perturbations are easily solved, making it possible to follow the evolution of the system along a string of points, p_0, p_1, p_2, etcetera, on the dynamically determined inflationary trajectory. By repeating the procedure of (A.4.2), the potential is 'charted' as the field evolves.

The prescription for constructing δv_{ab} determines the generated potential. To study multifield inflation with randomly interacting fields, reference [142] considered a stochastic evolution law for δv_{ab}, leading to an ensemble of random scalar potentials for each initial choice of parameters. In [142], the law governing the generation of δv_{ab} was then chosen so that, over large distances, v_{ab} samples the Gaussian Orthogonal Ensemble of random symmetric matrices. A simple example of such a law is to take the independent matrix elements of v_{ab} evolve with the Brownian motion of independent harmonic oscillators. More precisely, the independent elements of δv_{ab} are generated as Gaussian random numbers with the first two moments given by

$$\begin{aligned} \mathbb{E}[\delta v_{ab}\big|_{p_i\to p_{i+1}}] &= -v_{ab}\big|_{p_i}\frac{|\delta\phi^a|}{\Lambda_{\rm h}^{\rm DBM}}\,, \\ \mathrm{Var}[\delta v_{ab}^2\big|_{p_i\to p_{i+1}}] &= \sigma^2\,(1+\delta_{ab})\,\frac{|\delta\phi^a|}{\Lambda_{\rm h}^{\rm DBM}}\,. \end{aligned} \tag{A.4.3}$$

This is 'Dyson Brownian motion' (DBM), originally proposed as an out-of-equilibrium extension of the 'Coulomb gas' statistical picture of random matrix theory. Given any initial configuration of $v_{ab}(0)$ at p_0, the DBM evolution continuously relaxes the Hessian matrix to a random sample of the GOE. The probability distribution of v_{ab} then becomes a function of the path length, s, in units of $\Lambda_{\rm h}^{\rm DBM}$ [85, 182],

$$P(v_{ab}(s)) \sim \exp\left[-\frac{\mathrm{tr}\left((v_{ab}(s)-qv_{ab}(0))^2\right)}{2\sigma^2(1-q^2)}\right] \xrightarrow[s\gg 1]{} \exp\left[-\frac{\mathrm{tr}(v_{ab}(s)^2)}{2\sigma^2}\right]\,, \tag{A.4.4}$$

where $q=\exp(-s)$. Thus, $\Lambda_{\rm h}^{\rm DBM}$ has the interpretation of the coherence length over which the Hessian randomises, the corresponding eigenvectors 'delocalise', and the potential exhibit significant random structure.

In [142], the DBM construction was used to gain access to inflation in scalar potentials with multiple interacting fields, and in [77, 78], these were used to, for the first time, study the observational predictions of manyfield models of inflation. Some modifications and extensions of this prescription were discussed in [32, 159, 186], and in [97] the predictions of a single-field approximation to the large-$N_{\rm f}$ DBM models was elaborated on. (Note however that the observational predictions of this single-field model were already falsified in [77], as subsequently discussed in [78].)

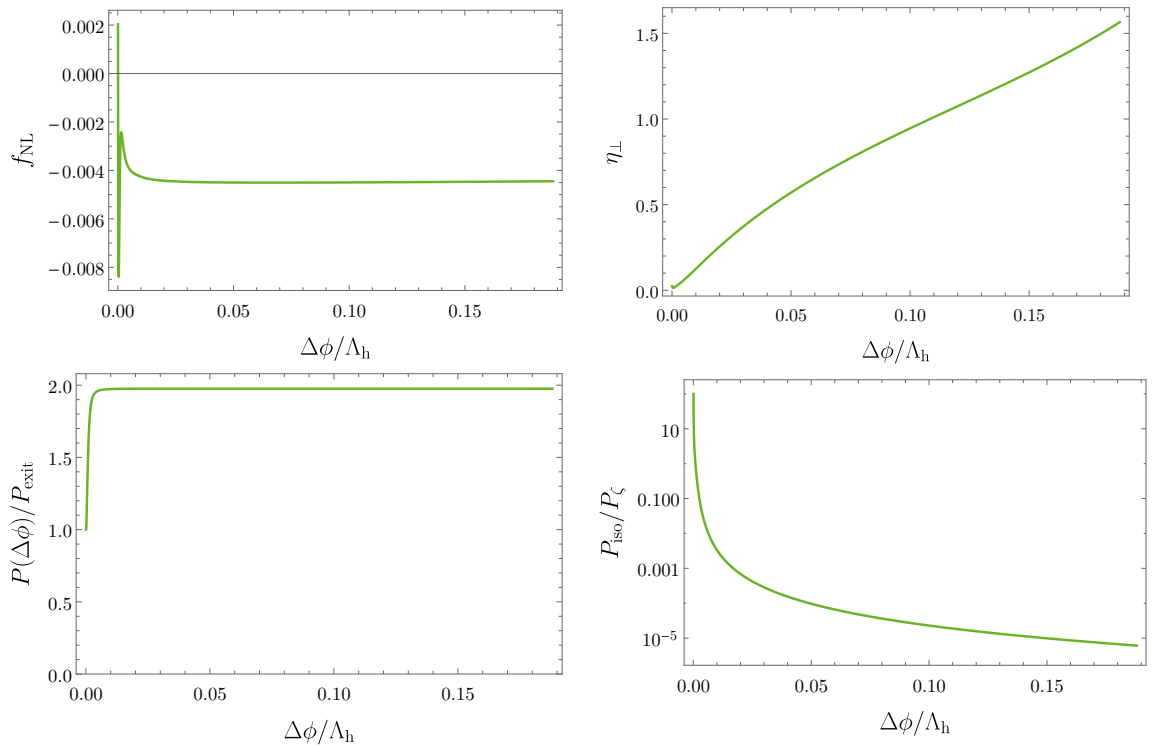

Fig. A.1 Multifield aspects of the 100-field example.

A.5 Case studies and a modified GRF potential

In the main body of this chapter, we focussed on the statistical predictions of ensembles of manyfield models. In this appendix, we discuss two particular examples of randomly generated inflation models that highlight the general results discussed in this chapter. We furthermore discuss the case of 'uplifted' potentials mentioned in section 2.4.1.

The first inflation model we look at is a 100-field model which, despite significant superhorizon evolution of the power spectrum, gives little non-Gaussianity. The second case is a 25-field model which is one of the rare examples with significant non-Gaussianity at the end of inflation. It is in fact the only model with the uniform mass spectrum that we found to produce large non-Gaussianity, and we will highlight what distinguishes this model from the others.

A.5.1 A 100-field model

The spectrum of the random 100-field models that we discuss in this section is shown in Figure 2.4, and its background evolution if further illustrated by Figure 2.3. Recall

that the initial conditions for this model are $\Lambda_{\rm h} = 0.4$, $\epsilon_{\rm i} = 5 \times 10^{-10}$, mass-squareds evenly distributed between $\eta_{\rm i} V_0 M_{\rm P}^{-2}$ and $(3H/2)^2$ with $\eta_{\rm i} = -10^{-4}$.

The spectral index of this model is $n_s = 0.978$, and its running is given by $\alpha_s = -0.0018$. The amplitude of local non-Gaussianity at the end of inflation is given by $f_{\rm NL} = -0.004$.

While the observables produced by this model are simple, the superhorizon dynamics of the perturbations is not. Figure A.1 shows that the scalar power at the pivot scale doubles after horizon crossing, and that for several e-folds, the isocurvature-to-curvature ratio is greater than one (recall that almost all the field-space movement happens towards the end of inflation). Nevertheless, by the end of inflation the isocurvature becomes heavily suppressed, the power spectrum freezes out, and $f_{\rm NL}$ remains small.

To further understand the multifield aspects of this model, we define the vector

$$\eta_{\perp\, i} = \frac{n^a V_{ab} w_i^b}{V}\,, \tag{A.5.1}$$

so that, according to equation (2.2.64), $\zeta' = 2\eta_{\perp\, i}\mathcal{S}^i$. Thus, the norm $\eta_\perp \equiv |\eta_{\perp i}|$ determines the strength of the isocurvature-to-curvature sourcing. Figure A.1 shows that $\eta_\perp$ increases during inflation in the 100 field model, and becomes $\mathcal{O}(1)$ towards the end of inflation. However, at this point the isocurvature has decayed exponentially, so that ζ remains essentially constant.

A.5.2 A 25-field model giving large non-Gaussianity

In rare cases, we found randomly generated manyfield models with substantially non-Gaussian perturbations. A particular example of this is a 25-field model with the uniform initial mass spectrum, $\Lambda_{\rm h} = 0.4$, $\epsilon_{\rm i} = 2 \times 10^{-9}$ and $\eta_{\rm i} = -10^{-4}$. The final spectral index is $n_s = 0.978$ with running $\alpha_s = -0.0014$. The fractional increase of the power spectrum is 2.15, and the final ratio of the isocurvature and curvature power spectra is 0.015. The amplitude of local non-Gaussianities is given by $f_{\rm NL} = 1.42$, far above the typical values encountered.

What sets this model apart from other models is that the two smallest eigenvalues of the Hessian remain close to each other throughout most of the trajectory, and even 'bounce off' each other relatively early on during inflation. The evolution of the spectrum of the Hessian is given by the top panel of Figure A.2. When the two eigenvalues are near each other there is significant power in the isocurvature modes and we see a drastic increase in $f_{\rm NL}$. The generation of $f_{\rm NL}$ in this model is consistent with equation (2.5.1): as the two eigenvalues of the Hessian come very close to each other,

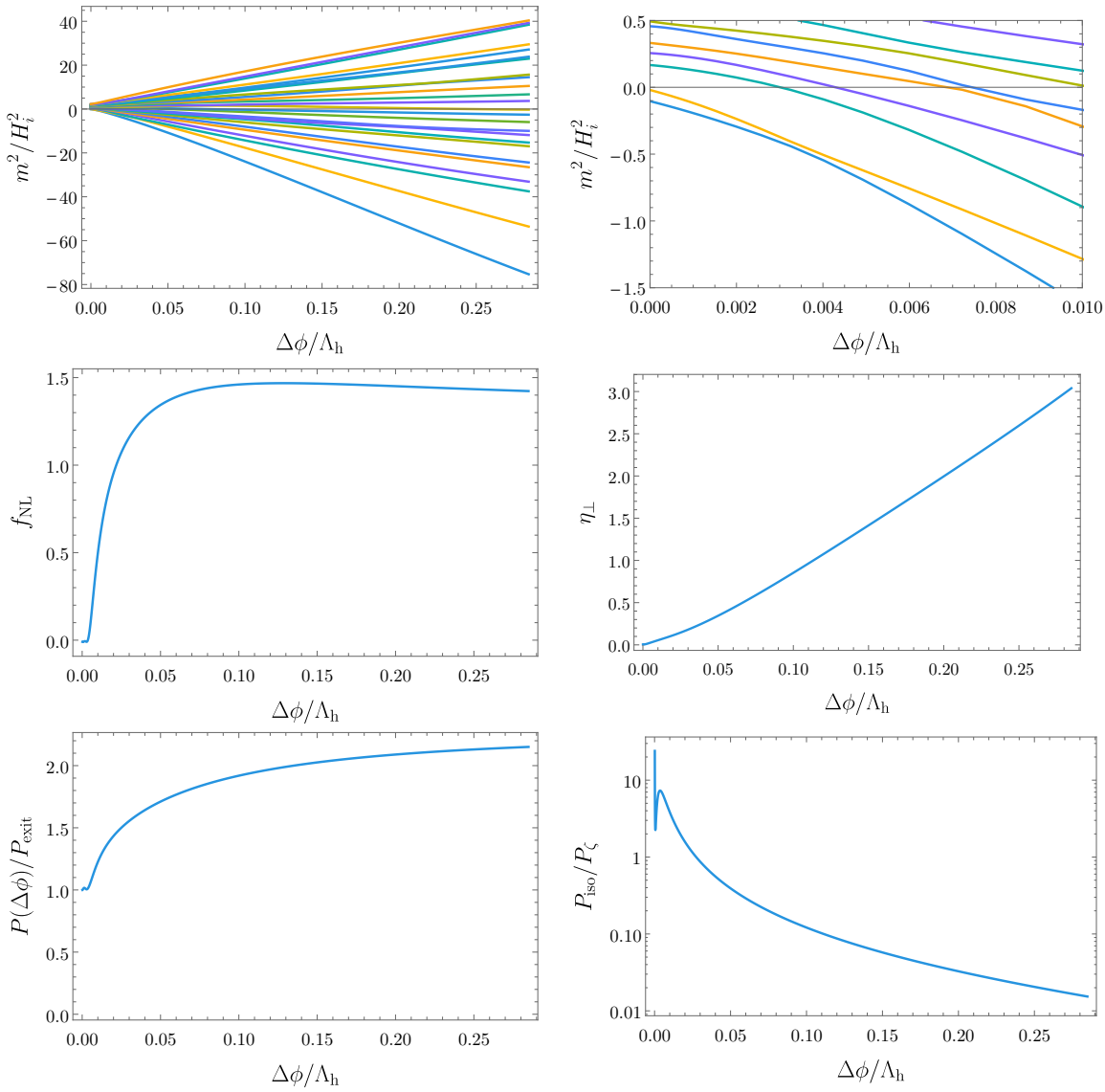

Fig. A.2 Multifield effects in the 25-field model with large non-Gaussianity.

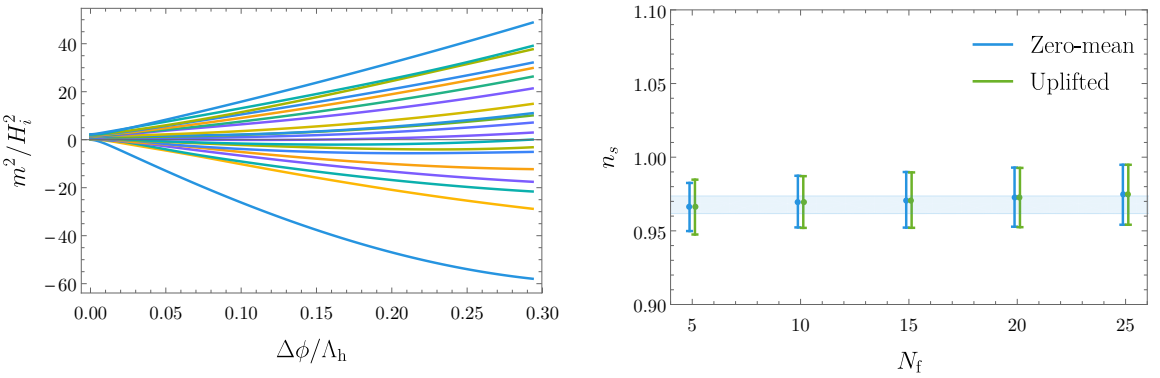

Fig. A.3 Eigenvalue evolution for a 20-field model with uplifted potential (left) and comparison of predictions for spectral index computed from ensembles of 1000 models (right).

slightly perturbed classical trajectories can become widely separated and experience drastically different levels of superhorizon evolution. We note that $\eta_\perp$ grows during inflation and the isocurvature decays rather slowly. The predictions of this model are likely to be sensitive to the physics of the post-inflationary era.

A.5.3 Manyfield inflation in uplifted potentials

For Gaussian random fields with zero mean, the minima of the potential typically appear at lower and lower values as the number of fields is increased, and the radius of the Wigner semi-circle grows. As we live in a vacuum with a small, positive cosmological constant, it may therefore be interesting to consider GRF potentials which have been uplifted so that minima typically occur around $V = 0$, cf. our discussion in section 2.4.1. From equation (2.2.29), we see that the lower edge of the semi-circle will be at zero at $V = 0$ if we lift the potential by $\sqrt{2}N_f\Lambda_v^4$.

The typical spectrum of these models is still too broad to make them useful tools to study multifield inflation, and we again consider the uniform initial spectrum of equation (2.2.42). The evolution of the eigenvalues of the Hessian of these models behave somewhat differently from those of the simplest, mean-zero GRFs. An example of this is shown in Figure A.3: while the dominant effect for small field values is still the eigenvalue repulsion and roughly conical spread of the eigenvalues, for larger values of the field, the smallest eigenvalue tends upwards, towards the lower edge of the equilibrium spectrum.

The upturning behaviour is most clearly visible for small N_f, which is as expected, as for large N_f, eigenvalue repulsion dominates. The predictions of these models for n_s do

not differ appreciably from the mean-zero GRF models with similar initial spectra, as shown in Figure A.3. The uplifted models were generated with the same random seeds as the zero-mean ones, and have identical odd-order Taylor coefficients (the even-order Taylor coefficients differ however). The striking similarities in the predictions of these models can be understood as a consequence of the dominance of the cubic terms in the potential during a large fraction of the inflationary evolution.

Clearly, there are many ways to use GRFs to construct inflationary models. We expect that the findings of this chapter will extend also to other constructions of small-field, saddle-point inflation in which the spectrum relaxes during inflation (with some eigenvalues taking tachyonic values). However, other, substantially different constructions (e.g. large-field models or other variants of uplifted models) can certainly lead to different predictions.

Appendix B

Perturbations in rapid-turn inflation models

B.1 Linear perturbations

In this Appendix we look at linear perturbations around two-field rapid-turn inflaton models, first generally and then more specifically at the case of hyperinflation. We do this using the mathematical framework of vielbeins, in the manner of Achucarro et al. [7], and begin by looking at the two-field case. For our purposes it is convenient to write the equations of motion using e-folds as the time-variable, giving

$$\mathcal{D}_N\mathcal{D}_N\delta\phi^a + (3-\epsilon)\mathcal{D}_N\delta\phi^a + [\kappa^2\delta^a{}_b + \tilde{M}^a{}_b]\delta\phi^b = 0, \tag{B.1.1}$$

where $\tilde{M}^a{}_b \equiv M^a{}_b/H^2$ and $\kappa \equiv k/aH$.

It is convenient to work with perturbations in a vielbein basis, definied by

$$\delta\phi^I \equiv e^I_a\delta\phi^a \quad \Leftrightarrow \quad \delta\phi^a = e^a_I\delta\phi^I. \tag{B.1.2}$$

Our basis vectors satisfy $e^I_a e^J_b G^{ab} = \delta^{IJ}$ and $e^I_a e^J_b \delta_{IJ} = G_{ab}$. The $I,\ J$ indices are raised with deltas. From these identities it also follows that

$$e^I_a\mathcal{D}_N e^a_J = -e^a_J\mathcal{D}_N e^I_a, \qquad e^I_a\mathcal{D}_N e^b_I = -e^b_I\mathcal{D}_N e^I_a. \tag{B.1.3}$$

One can introduce a covariant derivative for these perturbations, given by

$$\mathcal{D}_N X^I \equiv \frac{dX^I}{dN} + Y^I{}_J\, X^J, \tag{B.1.4}$$

where the antisymmetric matrix $Y^I{}_J$ is defined by

$$Y^I{}_J \equiv e^I_a \mathcal{D}_N e^a_J. \tag{B.1.5}$$

With this definition this covariant derivative satisfies $e^I_a \mathcal{D}_N X^a = \mathcal{D}_N X^I$, from which it follows that we can write the equations of motions as

$$\mathcal{D}_N \mathcal{D}_N \delta\phi^I + (3-\epsilon)\mathcal{D}_N \delta\phi^I + [\kappa^2 \delta^I{}_J + \tilde{M}^I{}_J]\delta\phi^I = 0, \tag{B.1.6}$$

where we further defined $\tilde{M}^I{}_J \equiv e^J_a \tilde{M}^a{}_b e^b_J$.

The perturbations are best analysed in the kinematic basis, consisting of the adiabatic and entropic unit vectors,

$$e^I_a = (n_a,\ s_a)^T, \qquad e^a_I = (n^a,\ s^a), \tag{B.1.7}$$

where

$$n^a = (\dot{\phi}_v v^a + \dot{\phi}_w w^a)/\dot{\phi}, \qquad s^a = (-\dot{\phi}_w v^a + \dot{\phi}_v w^a)/\dot{\phi}. \tag{B.1.8}$$

One could also work in the gradient basis defined earlier in this thesis, which was very useful in solving the background equations of motion, but for the perturbations the kinematic basis makes the results much more clear. The matrix $Y^I{}_J$ is by definition given by

$$Y^I{}_J = \omega \begin{pmatrix} 0 & -1 \\ 1 & 0 \end{pmatrix}, \tag{B.1.9}$$

and as explained in Chapter 5, in this basis the mass matrix can be written

$$\tilde{M}^I{}_J = \begin{pmatrix} \omega^2 & -3\omega \\ -3\omega & \mu_s \end{pmatrix}, \tag{B.1.10}$$

up to $\mathcal{O}(\epsilon)$ corrections (recall from Chapter 5 that $\tilde{M}_{nn} = \mu_n$, $\tilde{M}_{ns} = \mu_\times$, and $\tilde{M}_{ss} = \mu_s$). To go further than this, we can use the fact that

$$\mathcal{D}_N \omega \equiv \omega\nu = -\mu_\times + \omega(-3 + \epsilon - \eta), \tag{B.1.11}$$

and demand that there should exist a conserved adiabatic mode on superhorizon scales, which implies

$$\mu_s = \omega^2 - 3\eta/2 + \mathcal{O}(\epsilon^2), \tag{B.1.12}$$

to find that generally, the equations of motion may be written

$$\begin{pmatrix}\delta\phi_n'\\ \delta\phi_s'\\ \delta\pi_n'\\ \delta\pi_s'\end{pmatrix} = \begin{pmatrix}0 & 0 & 1 & 0\\ 0 & 0 & 0 & 1\\ \kappa^2+3\eta/2, & \omega(6-2\epsilon+2\nu-\eta), & -(3-\epsilon) & 2\omega\\ \omega\eta, & \kappa^2-\mu_s+\omega^2, & -2\omega & -(3-\epsilon)\end{pmatrix}\begin{pmatrix}\delta\phi_n\\ \delta\phi_s\\ \delta\pi_n\\ \delta\pi_s\end{pmatrix} \quad \text{(B.1.13)}$$

with $\delta\pi^I \equiv d\delta\phi^I/dN$ and $' = d/dN$.

B.2 Hyperinflation

In hyperinflation we have $R = -2/L^2$, so we can straightforwardly find that the effective mass matrix is given by

$$\tilde{M}^I{}_J = \begin{pmatrix}\omega^2-\frac{3}{2}\eta & -\omega(3-\epsilon+\frac{3}{2}\eta)-\frac{9}{2}\eta/\omega\\ -\omega(3-\epsilon+\frac{3}{2}\eta)-\frac{9}{2}\eta/\omega & -\omega^2(1-\frac{2}{3}\epsilon+\frac{1}{3}\eta)-3\eta-\frac{27}{2}\eta/\omega^2\end{pmatrix}. \quad \text{(B.2.1)}$$

The rate of change of the turn rate can be found to be given by $d\omega/dN = (9+\omega^2)\eta/2\omega + \mathcal{O}(\epsilon^2)$, and using this we find the complete equations of motion

$$\begin{pmatrix}\delta\phi_n'\\ \delta\phi_s'\\ \delta\pi_n'\\ \delta\pi_s'\end{pmatrix} = \begin{pmatrix}0 & 0 & 1 & 0\\ 0 & 0 & 0 & 1\\ \kappa^2+\frac{3}{2}\eta, & \omega(6-2\epsilon+\eta)+\frac{(9+\omega^2)\eta}{\omega}, & \epsilon-3 & 2\omega\\ \omega\eta, & \kappa^2+\frac{1}{3}\omega^2(6-2\epsilon+\eta)+\frac{3(9+\omega^2)\eta}{\omega^2}, & -2\omega & \epsilon-3\end{pmatrix}\begin{pmatrix}\delta\phi_n\\ \delta\phi_s\\ \delta\pi_n\\ \delta\pi_s\end{pmatrix}. \quad \text{(B.2.2)}$$

In this formulation, we can infer whether the system is locally stable by computing the local Lyapunov exponents, i.e. the eigenvalues λ of the evolution matrix, for $k = 0$. To first order, they are given by

$$\lambda = \eta/2 + \mathcal{O}(\epsilon^2),\ \ -3 + \mathcal{O}(\epsilon),\ \ \frac{1}{2}\left(-3 \pm \sqrt{9-8\omega^2}\right) + \mathcal{O}(\epsilon). \quad \text{(B.2.3)}$$

The latter three all have negative real parts, and thus correspond to decaying modes. The first one is a slowly growing mode corresponding to the direction $(1, 0, \eta/2, 0)^T$. This of course is just our regular superhorizon scale adiabatic perturbation, $\delta\phi^I \propto (\sqrt{\epsilon},\ 0)$, and corresponds to a shift along the trajectory. All other solutions decaying, we see that the system indeed is stable.

B.2.1 Multifield extension to hyperinflation

The extension to more than two fields is reasonably straightforward. From equation 4.4.10, we see that the matrix ${Y^I}_J$ is block diagonal,

$$ {Y^I}_J = \begin{pmatrix} Y_{(2)} & 0 \\ 0 & Y_{(N_\mathrm{f}-2)} \end{pmatrix}, \tag{B.2.4} $$

where $Y_{(2)}$ is our previous Y matrix. We cannot know the form of $Y_{(N_\mathrm{f}-2)}$ without specifying the other basis vectors, however as we shall see, we will not need to make an explicit choice for this. Recalling that in an orthonormal basis ${R^I}_{JKL} = -({\delta^I}_K\delta_{JL} - {\delta^I}_L\delta_{JK})/L^2$, we see that the mass matrix is also block diagonal,

$$ {M^I}_J = \begin{pmatrix} M_{(2)} & 0 \\ 0 & M_{(N_\mathrm{f}-2)} \end{pmatrix}, \tag{B.2.5} $$

where $M_{(2)}$ is our old mass matrix. $M_{(N_\mathrm{f}-2)}$ is a diagonal matrix given by

$$ M_{(N_\mathrm{f}-2)} = \left(\frac{V_{;v}}{L} - \frac{\dot\phi^2}{L^2} \right) I_{(N_\mathrm{f}-2)}. \tag{B.2.6} $$

Since both the Y and M matrices are block-diagonal, the additional $N_\mathrm{f}-2$ perturbations decouple from the first two at quadratic order. We can therefore solve for their evolution independently of the first two.

We now define a new set of fields $\delta\phi'^I$ (for $I > 2$) through $\delta\phi^I = {R^I}_J\delta\phi'^J$, where the rotation matrix ${R^I}_J$ satisfies $d{R^I}_J/dt = -HY_{(N_\mathrm{f}-2)}{}^I{}_K\,{R^K}_J$. These fields satisfy [7]

$$ \mathcal{D}_t\delta\phi^I = {R^I}_J\frac{d\delta\phi'^J}{dt}, \qquad \mathcal{D}_t\mathcal{D}_t\delta\phi^I = {R^I}_J\frac{d^2\delta\phi'^J}{dt^2}, \tag{B.2.7} $$

giving the equations of motion

$$ \frac{d^2\delta\phi'^I}{dN^2} + (3-\epsilon)\frac{d\delta\phi'^I}{dt} + \left[\kappa^2{\delta^I}_J + (R^T M_{(N_\mathrm{f}-2)}R)^I{}_J\right]\delta\phi'^J = 0, \tag{B.2.8} $$

but since the mass matrix is diagonal this just reduces to

$$ \frac{d^2\delta\phi'^I}{dN^2} + (3-\epsilon)\frac{d\delta\phi'^I}{dt} + \left[\kappa^2{\delta^I}_J + M_{(N_\mathrm{f}-2)}{}^I{}_J\right]\delta\phi'^J = 0. \tag{B.2.9} $$

These are just $N_\mathrm{f}-2$ uncoupled modes (with indices s_i), each satisfying

$$\frac{d^2\delta\phi^{s_i}}{dN^2}+(3-\epsilon)\frac{d\delta\phi^{s_i}}{dN}+\left[\kappa^2-\frac{3(9+\omega^2)\eta}{2\omega^2}\right]\delta\phi^{s_i}=0. \tag{B.2.10}$$

These modes do not decay, but also do not see the growth that the adiabatic one does before horizon crossing, and hence are relatively suppressed. Moreover, since their mass is $\mathcal{O}(\epsilon)$, they do not affect the stability of the solution.

B.3 Primordial perturbations

To study the observables of rapid-turn inflation models, we need to calculate the mode functions. Excluding ϵ corrections, but keeping the k-dependence and defining $v^I=a\delta\phi^I$, the action for the perturbations can be written

$$\begin{aligned}\mathcal{S}=\frac{1}{2}\int\frac{d^3k}{(2\pi)^3}d\tau\Bigg[&(v_n')^2+(v_s')^2+\frac{2\omega}{\tau}(v_sv_n'-v_nv_s')+\frac{6\omega}{\tau^2}v_nv_s\\&+\left(\frac{2}{\tau^2}-k^2\right)v_n^2+\left(\frac{2+(1-\xi)\omega^2}{\tau^2}-k^2\right)v_s^2\Bigg].\end{aligned} \tag{B.3.1}$$

The equations of motion can then be written

$$v_n''+\left(k^2-\frac{2}{\tau^2}\right)v_n+\frac{2\omega}{\tau}v_s'-\frac{4\omega}{\tau^2}v_s=0 \tag{B.3.2}$$

$$v_s''+\left(k^2-\frac{2+(1-\xi)\omega^2}{\tau^2}\right)v_s-\frac{2\omega}{\tau}v_n'-\frac{2\omega}{\tau^2}v_n=0. \tag{B.3.3}$$

We will not be able to integrate these equations exactly analytically, but they are straightforward to solve numerically and we will still be able to say a lot about them with analytic methods.

To start, we need to understand their initial conditions. Deep inside the horizon, $x\equiv k\tau\ll-1$, and here the equations become

$$\frac{d^2v_n}{dx^2}+v_n+\frac{2\omega}{x}\frac{dv_s}{dx}=0 \tag{B.3.4}$$

$$\frac{d^2v_s}{dx^2}+v_s-\frac{2\omega}{x}\frac{dv_n}{dx}=0, \tag{B.3.5}$$

which for large x have the solutions

$$v_n = C_1(-x)^{i\omega}e^{ix} + C_2(-x)^{-i\omega}e^{ix} + C_3(-x)^{i\omega}e^{-ix} + C_4(-x)^{-i\omega}e^{-ix} \tag{B.3.6}$$

$$v_s = -iC_1(-x)^{i\omega}e^{ix} + iC_2(-x)^{-i\omega}e^{ix} - iC_3(-x)^{i\omega}e^{-ix} + iC_4(-x)^{-i\omega}e^{-ix}. \tag{B.3.7}$$

We would now like fix these with Bunch-Davies initial conditions, but to do so we need to proceed carefully. The perturbations in the action B.3.1 do not have canonical kinetic terms, since our frame is rotating. We now define a new set of fields u^I through $v^I = R^I{}_J u^J$, where the matrix $R^I{}_J$ satisfies $dR^I{}_J/d\tau = -\mathcal{H}Y^I{}_K\, R^K{}_J$, then the fields satisfy [7]

$$\mathcal{D}_\tau v^I = R^I{}_J \frac{du^J}{d\tau}, \qquad \mathcal{D}_\tau\mathcal{D}_\tau v^I = R^I{}_J \frac{d^2u^J}{d\tau^2}. \tag{B.3.8}$$

The u^I fields have canonical kinetic terms, and on subhorizon scales their equations simplify to simple harmonic oscillators. *These* are the fields which must satisfy our normal Bunch-Davies initial conditions:

$$\lim_{\tau\to-\infty} u^I = \frac{1}{\sqrt{2k}}e^{-ik\tau}. \tag{B.3.9}$$

The good news here is that we now only need to find the matrix $R^I{}_J$:

$$R^I{}_J = \exp\left[-\begin{pmatrix}0 & -1\\ 1 & 0\end{pmatrix}\int_{\tau_i}^{\tau} d\tau\omega\mathcal{H}\right] = \begin{pmatrix}\cos(\omega\ln\frac{-\tau}{-\tau_i}) & -\sin(\omega\ln\frac{-\tau}{-\tau_i})\\ \sin(\omega\ln\frac{-\tau}{-\tau_i}) & \cos(\omega\ln\frac{-\tau}{-\tau_i})\end{pmatrix}. \tag{B.3.10}$$

We are free to set our initial time here to whatever we want. This is just the time when we have $R^I{}_J = \delta^I{}_J$. We therefore set it to $\tau_i = -1/k$ for our own convenience. This gives us

$$\begin{aligned}\lim_{\tau\to-\infty}\begin{pmatrix}v_n\\ v_s\end{pmatrix} &= \begin{pmatrix}\cos(\omega\ln -k\tau) & -\sin(\omega\ln -k\tau)\\ \sin(\omega\ln -k\tau) & \cos(\omega\ln -k\tau)\end{pmatrix}\begin{pmatrix}1\\ e^{i\alpha}\end{pmatrix}\frac{1}{\sqrt{2k}}e^{-ik\tau}\\ &= \frac{e^{-ik\tau}}{2\sqrt{2k}}\begin{pmatrix}(1-ie^{i\alpha})(-k\tau)^{-i\omega} + (1+ie^{i\alpha})(-k\tau)^{i\omega}\\ i(1-ie^{i\alpha})(-k\tau)^{-i\omega} - i(1+ie^{i\alpha})(-k\tau)^{i\omega}\end{pmatrix}.\end{aligned} \tag{B.3.11}$$

This precisely matches the solution we derived earlier, and we have now fixed the constants C_3 and C_4. Note that these depend on the phase difference between the two independent oscillators. This is because the v_n and v_s modes are in fact correlated, due to the rotation.

Following [149], we make the equations dimensionless by introducing a scale k_0 and defining $\tilde{u} = \sqrt{k_0}u$, $\tilde{k} = k/k_0$, $\tilde{\tau} = k_0\tau$, and $\tilde{\pi} = d\tilde{u}/d\tilde{\tau}$. The equations then take the form

$$\frac{d}{d\tilde{\tau}}\begin{pmatrix}\tilde{v}_n\\ \tilde{v}_s\\ \tilde{\pi}_n\\ \tilde{\pi}_s\end{pmatrix} = \begin{pmatrix} 0 & 0 & 1 & 0\\ 0 & 0 & 0 & 1\\ \frac{2}{\tilde{\tau}^2} - \tilde{k}^2 & \frac{4\omega}{\tilde{\tau}^2} & 0 & -\frac{2\omega}{\tilde{\tau}}\\ \frac{2\omega}{\tilde{\tau}^2} & \frac{2+(1+\xi)\omega^2}{\tilde{\tau}^2} - \tilde{k}^2 & \frac{2\omega}{\tilde{\tau}} & 0\end{pmatrix}\begin{pmatrix}\tilde{v}_n\\ \tilde{v}_s\\ \tilde{\pi}_n\\ \tilde{\pi}_s\end{pmatrix} \equiv U^{\mathrm{I}}{}_{\mathrm{J}}\, X^{\mathrm{J}}. \tag{B.3.12}$$

This has the solution

$$X^{\mathrm{I}}(\tilde{\tau}) = \Gamma^{\mathrm{I}}{}_{\mathrm{J}}(\tilde{\tau}, \tilde{\tau}_i)X^{\mathrm{J}}(\tilde{\tau}_i), \tag{B.3.13}$$

where

$$\Gamma^{\mathrm{I}}{}_{\mathrm{J}}(\tau, \tau_i) = \mathcal{T}\exp\left[\int_{\tilde{\tau}_i}^{\tilde{\tau}} U^{\mathrm{I}}{}_{\mathrm{J}}(\tilde{\tau})d\tilde{\tau}\right], \tag{B.3.14}$$

where $\mathcal{T}$ is the time-ordering operator. The late time mode-function is then given by

$$\tilde{v}_n(\tilde{\tau}) = \Gamma^{\tilde{v}_n}{}_I(\tilde{\tau}, \tilde{\tau}_i)X^I(\tilde{\tau}_i), \tag{B.3.15}$$

and its modulus squared by

$$|\tilde{v}_n(\tilde{\tau})|^2 = \Gamma^{\tilde{v}_n}{}_I(\tilde{\tau}, \tilde{\tau}_i)\Gamma^{\tilde{v}_n}{}_J(\tilde{\tau}, \tilde{\tau}_i)X^I(\tilde{\tau}_i)(X^*)^J(\tilde{\tau}_i) \equiv \Gamma^{\tilde{v}_n}{}_I(\tilde{\tau}, \tilde{\tau}_i)\Gamma^{\tilde{v}_n}{}_J(\tilde{\tau}, \tilde{\tau}_i)\Sigma^{IJ}(\tilde{\tau}_i). \tag{B.3.16}$$

The Γ matrices are real, since it is just a product of matrix exponents of real matrices, but since the initial values of the mode functions are complex, the mode functions will stay complex.

The curvature perturbation is given by

$$\zeta = -\frac{1}{\sqrt{2\epsilon}}\frac{\delta\phi_n}{M_{\mathrm{P}}} = -\frac{1}{\sqrt{2\epsilon}}\frac{v_n}{a}, \tag{B.3.17}$$

and the power spectrum is thus

$$P_\zeta = \frac{1}{2\epsilon}\frac{P_{v_n}}{a^2} = \frac{1}{2\epsilon}\frac{P_{v_n}}{a^2} = \left.\frac{k^3|v_n|^2}{4\pi^2\epsilon a^2}\right|_{k=aH}. \tag{B.3.18}$$

If $\omega = 0$, we are dealing with two uncoupled harmonic oscillators, and we know that [149]

$$|v_n|^2 \simeq \frac{1}{2k^3\tau^2} \Rightarrow P_\zeta(\omega = 0) = \left.\frac{1}{8\pi^2\epsilon(a\tau)^2}\right|_{k=aH} = \left.\frac{H^2}{8\pi^2\epsilon}\right|_{k=aH}. \tag{B.3.19}$$

To compute the power spectrum for $\omega \neq 0$ we then use [149]

$$\frac{P_\zeta(\omega,\xi)}{P_\zeta(0)} \equiv \gamma^2(\omega,\xi) = \frac{|v_n(\omega,\xi)|^2}{|v_n(0)|^2} = \frac{\tilde{\tau}^2|\tilde{v}_n(\omega,\xi)|^2}{\tilde{\tau}^2|\tilde{v}_n(0)|^2}, \tag{B.3.20}$$

evaluated at some point after horizon crossing when the adiabatic mode has frozen out. We followed [149] and reintroduced a factor of $\tilde{\tau}^2$ both in the numerator and denominator to get rid of the time-dependence of the latter.

We now need to find the Σ matrix. To begin, we define $\theta(\tau) = \omega \ln -k\tau$, cleaning up the algebra, and note

$$\begin{aligned} |v_n|^2 &= \frac{1 - 2\cos\alpha\sin\theta\cos\theta}{2k} \qquad & |v_s|^2 &= \frac{1 + 2\cos\alpha\sin\theta\cos\theta}{2k} \\ v_n v_s^* &= \frac{e^{-i\alpha} - 2\cos\alpha\sin^2\theta}{2k}. \end{aligned} \tag{B.3.21}$$

It is moreover easy to show that initially,

$$\begin{pmatrix} \pi_n \\ \pi_s \end{pmatrix} = -ik \begin{pmatrix} v_n \\ v_s \end{pmatrix} + \frac{\omega}{\tau} \begin{pmatrix} -v_s \\ v_n \end{pmatrix}, \tag{B.3.22}$$

from which it follows that

$$\begin{aligned} |\pi_n|^2 &= \frac{k^2\tau^2 + \omega^2 + 2\omega k\tau\sin\alpha - 2(k^2\tau^2 - \omega^2)\cos\alpha\sin\theta\cos\theta}{2k\tau^2} \\ |\pi_s|^2 &= \frac{k^2\tau^2 + \omega^2 + 2\omega k\tau\sin\alpha + 2(k^2\tau^2 - \omega^2)\cos\alpha\sin\theta\cos\theta}{2k\tau^2} \\ \pi_n\pi_s^* &= \frac{e^{-i\alpha}k^2\tau^2 - 2ik\tau\omega - e^{i\alpha}\omega^2 - 2(k^2\tau^2 - \omega^2)\cos\alpha\sin^2\theta}{2k\tau^2} \end{aligned} \tag{B.3.23}$$

and

$$\begin{aligned} v_n\pi_n^* &= \frac{ik\tau(1 - 2\cos\alpha\cos\theta\sin\theta) - \omega(e^{-i\alpha} - 2\cos\alpha\sin^2\theta)}{2k\tau} \\ v_n\pi_s^* &= \frac{\omega(1 - 2\cos\alpha\cos\theta\sin\theta) + ik\tau(e^{-i\alpha} - 2\cos\alpha\sin^2\theta)}{2k\tau} \\ v_s\pi_n^* &= \frac{-\omega(1 + 2\cos\alpha\cos\theta\sin\theta) + ik\tau(e^{i\alpha} - 2\cos\alpha\sin^2\theta)}{2k\tau} \\ v_s\pi_s^* &= \frac{ik\tau(1 + 2\cos\alpha\cos\theta\sin\theta) + \omega(e^{i\alpha} - 2\cos\alpha\sin^2\theta)}{2k\tau}. \end{aligned} \tag{B.3.24}$$

Now, deep inside the horizon, where these equations are valid, $|x| \gg |\omega|$. If this limit is applied, most expressions above simplify considerably. If we moreover average over

the phase, the expressions become

$$|v_n|^2 = |v_s|^2 = \frac{1}{2k} \qquad v_n v_s^* = 0 \qquad |\pi_n|^2 = |\pi_s|^2 = \frac{k^2\tau^2 + \omega^2}{2k\tau^2}$$
$$\pi_n \pi_s^* = -i\frac{\omega}{\tau} \qquad v_n \pi_n^* = v_s \pi_s^* = \frac{i}{2} \qquad v_n \pi_s^* = \pi_s v_n^* = 0. \tag{B.3.25}$$

With these initial conditions, it is then straightforward to numerically compute the power spectra.

B.4 Power spectra and mode functions in $c_s^2 < 0$ theories

The integral that computes the ζ mode function, and consequently the approximate growth of the power spectrum, in rapid-turn inflation with $\xi < 1$, is given by

$$\mathcal{I}(N) = \int_{-\ln(\sqrt{1-\xi}\omega)}^{N} \sqrt{-\kappa^2 - \frac{3+\xi}{2}\omega^2 + \frac{1}{2}\sqrt{16\kappa^2\omega^2 + (3+\xi)^2\omega^4}}\, dN. \tag{B.4.1}$$

where $\kappa = e^{-N}$. We now define

$$(3+\xi)^2\omega^4 + 16\omega^2\kappa^2 \equiv \omega^4(3+\xi)^2 y^2 \quad \Leftrightarrow \quad y^2 = 1 + \frac{16\kappa^2}{(3+\xi)^2\omega^2}, \tag{B.4.2}$$

giving (after changing integration limits)

$$\mathcal{I}(N) = \frac{2\omega}{b}\int_{\sqrt{1+\frac{16\kappa^2}{\omega^2(3+\xi)^2}}}^{b-1} \Big(b(y-1) - (y^2-1)\Big)^{1/2} \frac{y\,dy}{y^2-1}, \tag{B.4.3}$$

with $b \equiv 8/(3+\xi)$. One can show that the primitive function of the above is given by

$$F(y) = \frac{2\omega}{b}\sqrt{(y-1)(b-1-y)} - \omega \arctan\left[\frac{b-2y}{2\sqrt{(y-1)(b-1-y)}}\right]$$
$$- \omega\sqrt{\frac{2}{b}} \arctan\left[\frac{\sqrt{2}(2-3b+2y+by)}{4\sqrt{b(y-1)(b-1-y)}}\right], \tag{B.4.4}$$

and hence the integral is given by

$$\mathcal{I}(N) = F(b-1) - F(\sqrt{1 + 16\kappa^2/(3+\xi)^2\omega^2}). \tag{B.4.5}$$

To compute the overall growth, we need to evaluate $F(1)$ and $F(b-1)$. The first term contributes nothing in this limit, but the other two terms are somewhat non-trivial. Both the arguments of the arctan functions diverge in these limits, but noting that since $\xi < 1$ implies $b > 2$, one finds (with $y = 1+\delta$ and $y = b-1-\delta$ respectively)

$$\begin{aligned} F(1) &= \lim_{\delta\to 0^+}\left(-\omega \arctan\left[\frac{\sqrt{b-2}}{2\sqrt{\delta}}\right] - \omega\sqrt{\frac{2}{b}}\arctan\left[\frac{-\sqrt{b-2}}{\sqrt{2b\delta}}\right]\right) \\ &= -\frac{\pi\omega}{2} + \sqrt{\frac{2}{b}}\frac{\pi\omega}{2} = -(2-\sqrt{3+\xi})\frac{\pi\omega}{4} \end{aligned} \tag{B.4.6}$$

$$\begin{aligned} F(b-1) &= \lim_{\delta\to 0^+}\left(-\omega \arctan\left[\frac{-\sqrt{b-2}}{2\sqrt{\delta}}\right] - \omega\sqrt{\frac{2}{b}}\arctan\left[\frac{\sqrt{2b(b-2)}}{4\sqrt{\delta}}\right]\right) \\ &= \frac{\pi\omega}{2} - \sqrt{\frac{2}{b}}\frac{\pi\omega}{2} = (2-\sqrt{3+\xi})\frac{\pi\omega}{4}. \end{aligned} \tag{B.4.7}$$

We therefore find that the total growth is given by

$$\ln(\gamma^2) = \lim_{N\to\infty} 2\mathcal{I}(N) \approx (2-\sqrt{3+\xi})\pi\omega. \tag{B.4.8}$$

To get mode functions in the regime of validity of the EFT, we want to evaluate

$$\zeta \propto \exp\left[\pm(2-\sqrt{3+\xi})\frac{\pi\omega}{4} \mp F\left(\sqrt{1+\frac{16}{\omega^2(3+\xi)^2}\kappa^2}\right)\right], \tag{B.4.9}$$

in the limit $\kappa^2/\omega^2 \ll 1$. To do so, we need to compute $F(1+\delta)$ with $\delta = 8\kappa^2/(3+\xi)^2\omega^2$ to the first non-trivial order in κ. Upon doing this, one finds

$$\begin{aligned} F(1+\delta) &\simeq F(1) + \frac{2\omega\sqrt{b-2}}{b}\sqrt{\delta} + \omega\frac{2\sqrt{\delta}}{\sqrt{b-2}} - \omega\frac{2\sqrt{\delta}}{\sqrt{b-2}} \\ &= F(1) + |c_s|\kappa \end{aligned}$$

where in the first line we used $\arctan(1/x) = \pi/2 - \arctan(x)$ for $x > 0$ and $\arctan(1/x) = -\pi/2 - \arctan(x)$ for $x < 0$, and in the second line we used $|c_s| = \sqrt{(1-\xi)/(3+\xi)}$ and the definition of b. We therefore find the mode functions

$$\zeta \propto \exp\left[\pm(2-\sqrt{3+\xi})\frac{\pi\omega}{2} \mp |c_s|\kappa\right]. \tag{B.4.10}$$